

CONTACT METAMORPHISM OF CALCAREOUS CONCRETIONS IN THE  
BLUESTONE FORMATION, HALIFAX GROUP, HALIFAX, NOVA SCOTIA

Glenn G. Chapman

Submitted in partial fulfillment of the requirements  
for the degree of Bachelor of Science, Honours  
Department of Earth Science  
Dalhousie University, Halifax, Nova Scotia  
April 2011



**Department of Earth Sciences**  
Halifax, Nova Scotia  
Canada B3H 4J1  
(902) 494-2358  
FAX (902) 494-6889

DATE: April 25, 2011

AUTHOR: Glenn G. Chapman

TITLE: Contact Metamorphism of Calcareous Concretions  
in the Bluestone Formation, Halifax Group, Halifax,  
Nova Scotia

Degree: B.Sc Convocation: May Year: 2011

Permission is herewith granted to Dalhousie University to circulate and to have copied for non-commercial purposes, at its discretion, the above title upon the request of individuals or institutions.

Signature of Author

THE AUTHOR RESERVES OTHER PUBLICATION RIGHTS, AND NEITHER THE THESIS NOR EXTENSIVE EXTRACTS FROM IT MAY BE PRINTED OR OTHERWISE REPRODUCED WITHOUT THE AUTHOR'S WRITTEN PERMISSION.

THE AUTHOR ATTESTS THAT PERMISSION HAS BEEN OBTAINED FOR THE USE OF ANY COPYRIGHTED MATERIAL APPEARING IN THIS THESIS (OTHER THAN BRIEF EXCERPTS REQUIRING ONLY PROPER ACKNOWLEDGEMENT IN SCHOLARLY WRITING) AND THAT ALL SUCH USE IS CLEARLY ACKNOWLEDGED.

## Contact metamorphism of calcareous concretions in the Bluestone formation, Halifax Group, Halifax, Nova Scotia

Glenn G. Chapman

Department of Earth Science, Dalhousie University, Halifax, N.S., B3H 4J1  
gchapman@dal.ca

The Bluestone formation represents the uppermost unit of the Halifax Group in the Halifax area. It is an early Ordovician turbidite sequence, interpreted to have been deposited on the continental margin of Gondwana. The formation comprises a coarsening-up sequence of interbedded grey-blue slate, silt, and fine sandstone. A characteristic feature is the presence of abundant calcareous concretions concentrated within sandstone and siltstone layers. In outcrop the concretions generally form regularly spaced, discrete, oblate bodies from ~5 mm to 1 m across, and from 50 mm to several metres long. They locally form thin, continuous horizons, distinguishable by their distinctive green to buff colour and recessive weathering. Concentric colour banding in some concretions reflects systematic changes from Ca-rich cores to Ca-poor margins adjacent to the host rock. Compositional banding overprints cross-bedding and sedimentary laminations, and the concretions were deformed with their host rocks, indicating that they formed after deposition but before regional deformation, probably during diagenesis.

Samples for this study were collected throughout the Bluestone formation including Point Pleasant Park, Bluestone Quarry and the Williams Lake area. The concretions and their host rocks lie within the contact aureole of the South Mountain Batholith (SMB), with metamorphic grade increasing from east to west toward the intrusive contact. Mineral assemblages vary from calcite + grossular + anorthite + diopside-hedenbergite in low-grade examples, to grossular + vesuvianite + prehnite + quartz in high-grade (proximal) outcrops. The transition between concretion rims and host rocks is marked by radiating sprays of tabular chlorite intergrown with minor biotite. The groundmass in this zone is dominated by detrital quartz with intergranular plagioclase that is Ca-rich in low-grade samples, and Na-rich at high grade. Detrital quartz and feldspar, ubiquitous in distal concretions and their host rocks, are virtually absent in the highest-grade assemblage, proximal to the contact. The presence of vesuvianite indicates  $X_{CO_2} \leq 0.11$  at peak metamorphic grade near the contact. Retrogression is common in assemblages near the contact, where it is inferred to result from fluid-rock interaction during cooling of the SMB.

Keywords: Bluestone formation, calcareous, calc-silicate, contact metamorphism, concretions, metamorphic, petrology, Halifax Group, Meguma, anorthite, garnet, vesuvianite, prehnite, mineral assemblage

## Table of Contents

	Page
<b>Abstract</b>	<b>ii</b>
<b>Table of Contents</b>	<b>iii</b>
<b>List of Figures &amp; Tables</b>	<b>v</b>
<b>Acknowledgments</b>	<b>viii</b>
<b>Chapter 1 : Introduction</b>	
1.1 Statement of Problem	1
1.2 Calcareous Concretions and Halifax Group Stratigraphy	2
1.3 Calcareous Concretions and Halifax Group Metamorphism	3
1.4 Previous Studies of Calcareous Concretions in the Goldenville Group	4
1.5 Objectives and Methods	5
<b>Chapter 2 : Regional Geology and Field Relations</b>	
2.1 Introduction	7
2.2 Meguma Supergroup	10
2.2.1 Goldenville Group	10
2.2.2 Halifax Group	10
2.2.3 Bluestone Formation	11
2.3 Regional Structure	16
2.4 The South Mountain Batholith	16
2.5 Lithological Descriptions	18
2.5.1 Point Pleasant Park (PPP)	18
2.5.1.1 Black Rock Beach : PPP-30	18
2.5.1.2 Battery Point : PPP04-6,7	20
2.5.1.3 Battery Point Hillside : PPP09-5c	22
2.5.1.4 Purcells Landing : PPP04-4	22
2.5.1.5 Chain Rock : PPP04-17a,b	23
2.5.2 Purcells Cove	
2.5.2.1 Purcells Cove : PCR04-7	25
2.5.2.2 Upper Bluestone Quarry : PCR07-23	25
2.5.2.3 Royal Nova Scotia Yacht Squadron : PCR07-11	26
2.5.3 Williams Lake	27
2.6 Summary	28
<b>Chapter 3 : Petrography</b>	
3.1 Introduction	29
3.2 Low-Grade Mineral Assemblage	30
3.3 Medium-Grade Mineral Assemblage	31
3.4 High-grade Mineral Assemblage	33
3.5 Summary	36

<b>Chapter 4 : Geochemistry</b>	
4.1 Introduction	37
4.2 Mineral Chemistry	37
4.2.1 Garnet	38
4.2.2 Clinopyroxene	39
4.2.3 Feldspar	40
4.2.4 Chlorite	42
4.2.5 Prehnite	43
4.2.6 Vesuvianite	43
4.3 Whole Rock an Trace Element Geochemistry	44
4.4 Summary	46
<b>Chapter 5 : Petrology</b>	
5.1 Introduction	55
5.2 Metamorphic Conditions	55
5.3 Progressive Metamorphism	57
5.3.1 Low-Grade	57
5.3.2 Medium-Grade	58
5.3.3 High-Grade	60
5.4 Retrograde Metamorphism	63
5.5 Metasomatism and Mineralogical Zonation	63
5.6 Summary	64
<b>Chapter 6 : Summary and Conclusions</b>	
6.1 Discussion	66
6.2 Conclusions	67
6.3 Suggestions for further work	69
<b>References</b>	70
<b>Appendices</b>	
<b>Appendix I : Microprobe Data</b>	I. 73
<b>Appendix II : Microprobe BSE with mineral index</b>	II. 102
<b>Appendix III : UTM coordinates of analyzed outcrop</b>	III. 132
<b>Appendix IV : Raw XRF data (ppm)</b>	IV. 133

## Table of Figures

	Page
<b>Fig. 1.1:</b> Mineral isograd map of the study area (south-end Halifax, Purcells Cove, and Williams Lake) showing outcrop locations sampled/analyzed for this study. Modified after Jamieson (personal communication)	5
<b>Fig. 2.1:</b> Simplified geological map of mainland Nova Scotia showing groups of the Meguma Supergroup and the South Mountain Batholith (White, et al., 2008)	8
<b>Fig. 2.2:</b> Bedrock geology map of Halifax Regional Municipality (White et al. 2008)	9
<b>Fig. 2.3:</b> Map and cross section of the Bluestone formation superimposed on shaded LiDAR topography. J.W. Waldron, by permission.	15
<b>Fig. 2.4:</b> Outcrop photo of Calcareous Horizon, with early concretion, Black Rock Beach member.	19
<b>Fig. 2.5:</b> Outcrop photo, Battery Point, Point Pleasant member	19
<b>Fig. 2.6:</b> Outcrop photo, detail of a concretion margin, Battery Point, Point Pleasant member	21
<b>Fig. 2.7:</b> Colour banding, weathering rind on a concretion, Battery Point hillside	24
<b>Fig. 2.8:</b> Outcrop photo, Chain Rock, showing disaggregated clast (colour-banded concretion) and discontinuous disrupted layers	24
<b>Fig. 3.1:</b> Photomicrograph (PPL) of wheat-sheaf aggregates of radial tabular chlorite in concretion core, PPP-5c	34
<b>Fig. 3.2:</b> Photomicrograph (XPL) of WL-16b core assemblage	34
<b>Fig. 4.1:</b> Representative concretion traverse XRF data plots	45
<b>Fig. 4.1:</b> Thin section scan showing EMP analysis areas and ternary plots of major solid solution phases present. (PPP-30)	47
<b>Fig. 4.2:</b> Thin section scan showing EMP analysis areas and ternary plots of major solid solution phases present. (PPP-7c)	48
<b>Fig. 4.3:</b> Thin section scan showing EMP analysis areas and ternary plots of major solid solution phases present. (PPP-5c)	49

<b>Fig. 4.4:</b> Polished section scan showing EMP analysis areas and ternary plots of major solid solution phases present. (PCR-26b)	50
<b>Fig. 4.5:</b> Polished section scan showing EMP analysis areas and ternary plots of major solid solution phases present. (PCR-23a)	51
<b>Fig. 4.6:</b> Polished section scan showing EMP analysis areas and ternary plots of major solid solution phases present. (PCR-11b)	52
<b>Fig. 4.7:</b> Polished section scan showing EMP analysis areas and ternary plots of major solid solution phases present. (WL-18b)	53
<b>Fig. 4.8:</b> Polished section scan showing EMP analysis areas and ternary plots of major solid solution phases present. (WL-16b)	54
<b>Fig. 5.1:</b> Metamorphic isograd map of the study area with Raman spectroscopy derived isotherms. (Jamieson et al., 2011)	57
<b>Fig. 5.2:</b> T-X stability plot of garnet at 3kb with inferred T for low-grade assemblage	58
<b>Fig. 5.3:</b> T-X plot of stable reactions for grossular, anorthite, diopside, calcite, zoisite, qtz, at 3kb	59
<b>Fig. 5.4:</b> T-X plot of equilibria in the CaO-MgO-Al <sub>2</sub> O-SiO <sub>2</sub> -CO <sub>2</sub> -H <sub>2</sub> O system	62
<b>Fig. 5.5:</b> Crystallization sequence diagram of metamorphic minerals in concretion-core assemblages	65

## List of Tables

	<b>Page</b>
<b>Table A:</b> EMP analysis data, concretion-core assemblage	I. 73
A.1: Garnet	I. 73
A.2: Clinopyroxene	I. 79
A.3: Feldspar	I. 83
A.4: Chlorite	I. 86
A.5: Vesuvianite	I. 89
A.6: Prehnite	I. 90
<b>Table B:</b> EMP analysis data, concretion-rim assemblage	I. 91
B1: Garnet	I. 91
B2: Clinopyroxene	I. 94
B3: Feldspar	I. 96
B4: Chlorite	I. 101
<b>Table C.1:</b> UTM coordinates of concretion bearing outcrops analyzed	III. 132
<b>Table D:</b> XRF data	IV. 133

## Acknowledgements

My deep gratitude extends to the faculty, staff, and denizens of Dalhousie's Earth Science department whose instruction and support have made this project possible. In particular, to Gordon Brown with the Dalhousie thin section preparation lab, and EMP guru Dan MacDonald with the Robert MacKay Electron Microprobe laboratory for his patience and expertise. To John Waldron for sharing ongoing research, and Chris White for the generous offer of time and access to the DNR XRF spectrometer. To Becky Jamieson, for allowing me to become involved in her work, and whose attention, expertise, encouragement and generosity enabled me to get to know a little piece of home a whole lot more, I am deeply indebted. To the Dawson society and members of the honours class of 2011, mahalo!

## Chapter 1

# INTRODUCTION

### **1.1 Statement of Problem**

The Bluestone formation is the uppermost unit of the Halifax Group in Halifax, Nova Scotia. It is an early Ordovician turbidite sequence, interpreted to have been deposited on the continental margin of Gondwana. First recognized as a distinct unit by Jamieson et al. (2005), and since adopted by the Department of Natural Resources (White et al., 2008; White, 2010) the formation is composed of inter-bedded blue-grey slates, fine-grained sandstone, and siltstone. The presence of calcareous concretions in the Bluestone formation is consistent with a change in oxidizing conditions from highly anoxic to oxidizing. They are interpreted to have formed during early diagenesis (Jamieson et al., 2011; Waldron et al., 2011). Though calcareous concretions are commonly found in the underlying Goldenville Group, the occurrence of similar bodies within the Halifax Group is unique to the Bluestone formation. Their presence in every member of the Bluestone formation, and absence from the underlying Cunard formation, makes them a diagnostic feature of the former.

This purpose of this thesis is two-fold: to examine and characterize the mineral assemblages associated with these anomalous diagenetic structures, and to constrain P-T-X (composition) metamorphic conditions affecting these calcareous concretions in the Bluestone formation by tracking textural and mineral chemical variations across the contact aureole. A clear and thorough account of the nature of these features, their

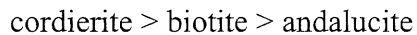
distribution, and metamorphic assemblages is required to further our understanding of both the Halifax Group stratigraphy and contact metamorphism.

## **1.2      Calcareous Concretions and Halifax Group Stratigraphy**

Peninsular Halifax is entirely underlain by Cambrian-Ordovician Meguma Supergroup deep-water turbidites, deposited on the continental margin of Gondwana (Schenk, 1982). Goldenville Group rocks contact the Halifax Group along NE-SW striking limbs of regional scale folds. Conformably overlying the Goldenville Group is the early Ordovician graphitic black slate of the Cunard formation, which forms the bedrock for most of peninsular Halifax. Originally undifferentiated, the Cunard Fm is now recognized as two distinct and conformable lithological units, of which the Bluestone formation is the upper. The Bluestone - Cunard formation transition in Halifax's south-end occurs along a contact roughly perpendicular to the Halifax waterfront from Pier 21 to the old Dingle Tower in Sir Stanford Fleming Park west of the Northwest Arm, sub-parallel to the axial trace of the Point Pleasant Syncline (fig. 2.2, 5.1). Locally, the Bluestone formation forms bedrock for the remaining portion of peninsular Halifax south of the described transition, as well as the Williams Lake and Purcells Cove areas west and southwest of Point Pleasant Park, respectively.

### **1.3 Halifax Group Metamorphism**

Regional greenschist facies metamorphism of the Halifax Group produced regional km-scale SW-NE trending tight to open folds and a strongly developed axial planar cleavage (Horne and Culshaw, 2006). This is overprinted by a narrow contact aureole associated with the eastern margin of the South Mountain Batholith, producing the isograd sequence in the Bluestone formation (Hart, 2006):



Annealing of the Bluestone formation rocks proximal to the contact has obscured some fine sedimentary structures and obliterated the cleavage preserved in distal rocks, yet both calcareous concretions and semi-continuous horizons are preserved at the highest metamorphic grades. Applying a geothermometer calibrated for graphite, Hilchie and Jamieson (2008) inferred temperatures ranging from 350°C at the outer limits to 570°C at the contact across the contact aureole in Halifax. Mahoney (1996) studied the geochemistry and isograd structure of the SMB contact aureole more generally, determining P-T conditions that describe intrusion pressures corresponding to depths ranging from 7-10 km, and with ~ 1-2 km difference in depth between the eastern and western extents of the batholith. Dalhousie and Saint Mary's universities have long used Point Pleasant Park as an accessible location for various field based undergraduate projects and studies. A detailed survey of previous work in the study area is given in chapter 2.

#### **1.4 Previous Studies of Calcareous Concretions in the Goldenville Group**

M.F. Purves (1974) examined calcareous concretions in the Goldenville Group, and was the first to document internal compositional variations, increasing in intensity with increasing metamorphic grade, from chlorite to sillimanite grade regional metamorphism. He also noted distinct colour zones reflecting concentric ‘discrete mineralogical assemblages’ in concretions, and proposed a model of non-volatile diffusion metasomatism across chemical potential gradients between the originally calcite-rich concretion and the Al, Fe, Mg, Mn rich semi-peltic host. This conclusion follows the tendency for two lithologies juxtaposed in mutual chemical disequilibrium to exchange mobile components across a contact boundary, forming contact-parallel zones of localized equilibrium. A follow-up study by Mitchell (2006) examined compositional zoning in Goldenville Group-hosted calcareous concretions to assess P-T-X conditions of regional metamorphism in southwestern Nova Scotia. However, neither Purves (1974), nor Mitchell (2004) included samples of Halifax Group hosted concretions, or concretions found within the South Mountain Batholith contact aureole.

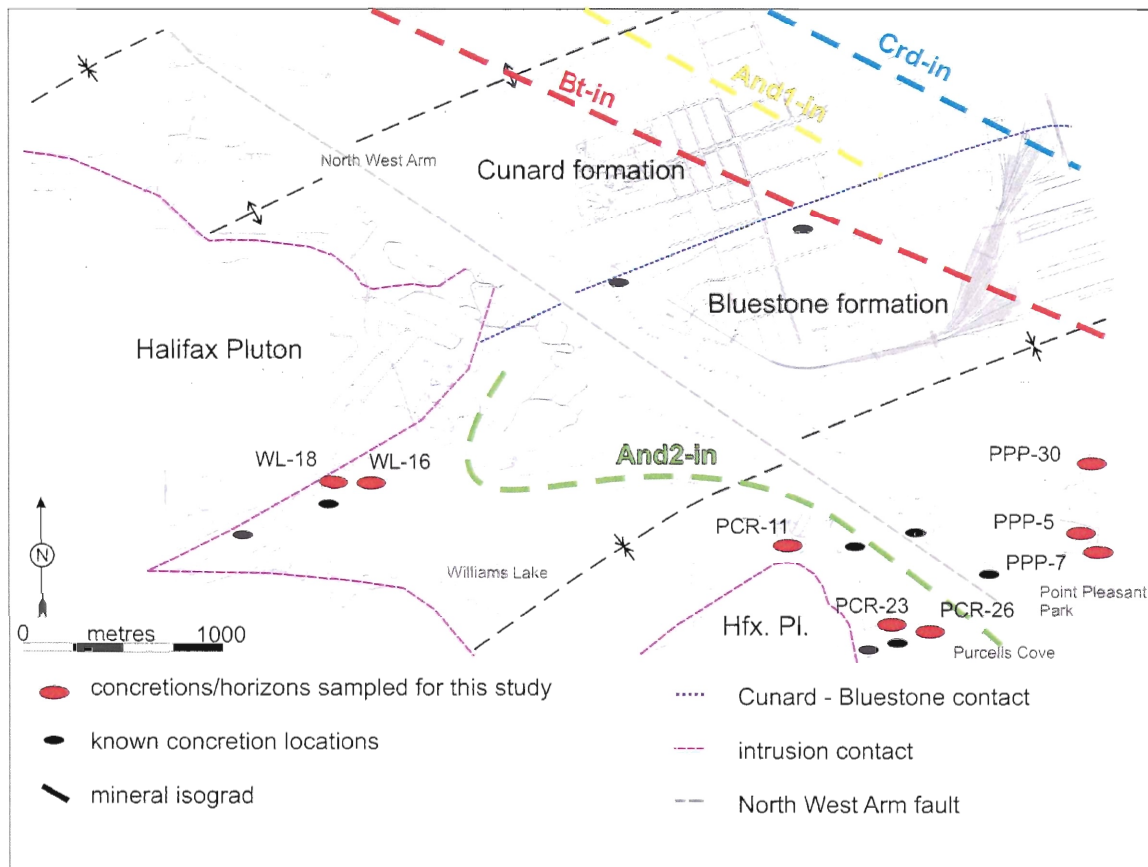


**Figure 1.1** Mineral isograd map of the study area (modified after Jamieson et al., 2005) showing sample locations for this study. Locations marked in red were sampled for detailed EMP analysis.

## 1.5 Objectives and Methods

Samples for this study were collected from concretions within several permanent outcrops along the shoreline and hillsides of Point Pleasant Park, Purcells Cove, Williams Lake, and the old Bluestone quarry. Together, they represent a transect through the SMB contact aureole in the area underlain by the Bluestone formation. Lowest-grade representatives were taken from the slate and sandy siltstone outcrops at Point Pleasant Park's Black Rock Beach in the eastern most margin of the study area. High-grade representatives, by contrast, were collected from outcrops of indurated deep black-purple hornfels behind the Royal Nova Scotian Yacht Squadron on the Northwest Arm, and

from new (2007) development sites in Ravenscraig Subdivision, both within 250 m from the Halifax pluton contact.

Fieldwork was undertaken to establish the structural and stratigraphic context of calcareous concretion formation, and assess the relationship of these features to the host lithologies in all members of the Bluestone formation at outcrop scale. Microscope petrography was used to investigate textural and mineralogical variations and relationships to the host lithology, and as reconnaissance for detailed Microprobe analyses. Electron microprobe analyses (EMP), secondary electron backscatter (BSE) imaging and electron dispersive spectrometry (EDS) mapping were undertaken to investigate sub-microscopic textural relationships, mineral assemblages, and variations in mineral composition both as a function of internal mineralogical zones within concretions, and as a function of metamorphic grade across the SMB contact aureole. X-ray diffraction spectrometry of selected samples provided an independently derived dataset to compare trends in chemical variation observed in the EMP data. WinTWQ v. 2.36 (Berman, 2007) was used to calculate possible equilibration reactions in P-T and T-X(composition) space for observed mineral assemblages. Thermodynamic properties from the internally-consistent thermodynamic dataset (Holland and Powell, 1998) were used to incorporate vesuvianite into the WinTWQ mineral database.

## Chapter 2

### GEOLOGICAL SETTING AND FIELD RELATIONS

#### 2.1 Introduction

The Meguma terrane of southern Nova Scotia is underlain mainly by Neoproterozoic to Ordovician rocks of the Meguma Supergroup that were intruded by Devonian granitoid plutons. Over the past few decades, numerous studies have documented the geology, stratigraphy, and provenance of the Meguma Supergroup (e.g., Schenk 1970, 1997; O'Brien 1988; Waldron 1992; White et al. 2008; Waldron et al. 2009, 2011; White, 2010) as well as the petrology and geochemistry of the South Mountain Batholith and other peraluminous intrusions (e.g., Clarke et al. 1988, 2004; MacDonald & Clarke 1985; MacDonald & Horne, 1988; MacDonald 2001; Erdmann et al. 2009). By comparison, relatively few studies have addressed either the regional or contact metamorphism of the Meguma Supergroup (e.g., Mahoney 1996, Hicks et al 1999; Jamieson et al. 2005, 2011; Tobey, 2006; Hart, 2006; Scallion et al. 2011).

Recent work on the Halifax Group in the city of Halifax by R.A. Jamieson and colleagues (Jamieson et al. 2005, 2011; Hart, 2006; Tobey, 2006; Waldron et al. 2011) has led to the recognition of the Bluestone formation as a lithostratigraphic unit distinct from and conformably overlying the Cunard formation. One of its most characteristic features is the presence of the calcareous concretions that are the subject of this thesis. This chapter reviews the regional geology and specific characteristics of the Bluestone formation, and describes Bluestone formation outcrops in Point Pleasant Park, Bluestone Quarry, and the Williams Lake area. Concretion abundance, distribution, geometry, mineralogy, and weathering properties observed in hand sample and outcrop are

described, with particular attention to metamorphic grade as a function of distance from the SMB contact. The stratigraphic nomenclature used throughout this thesis is that proposed by White (2010) and Jamieson et al. (2011).

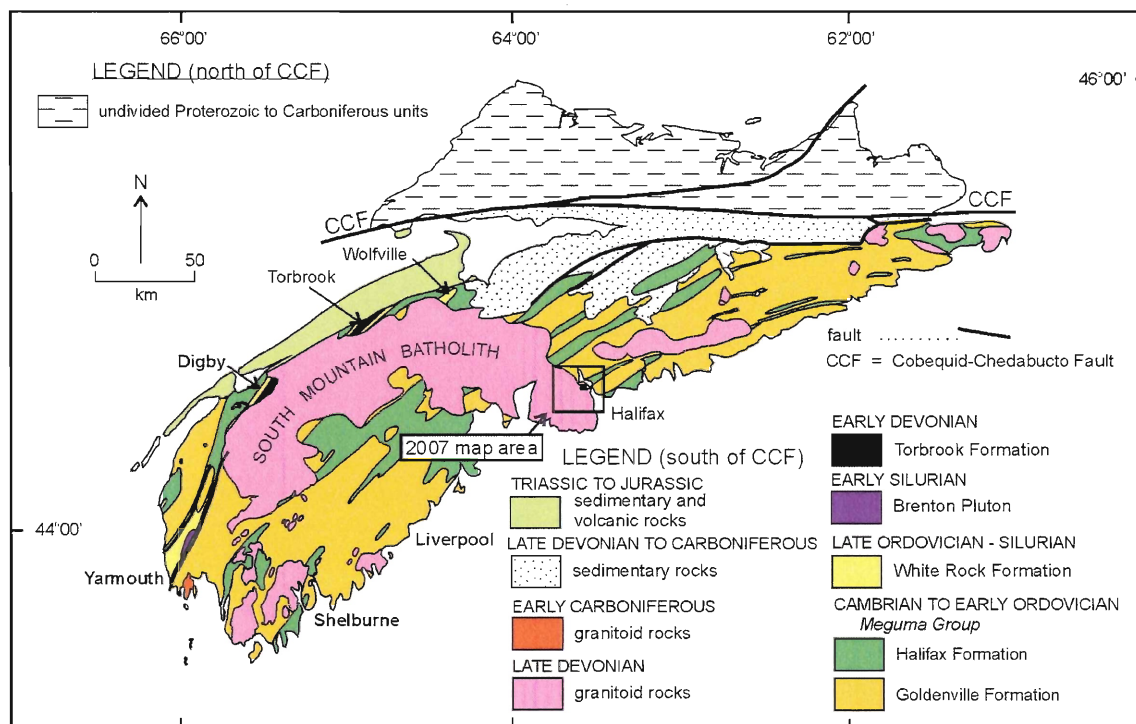
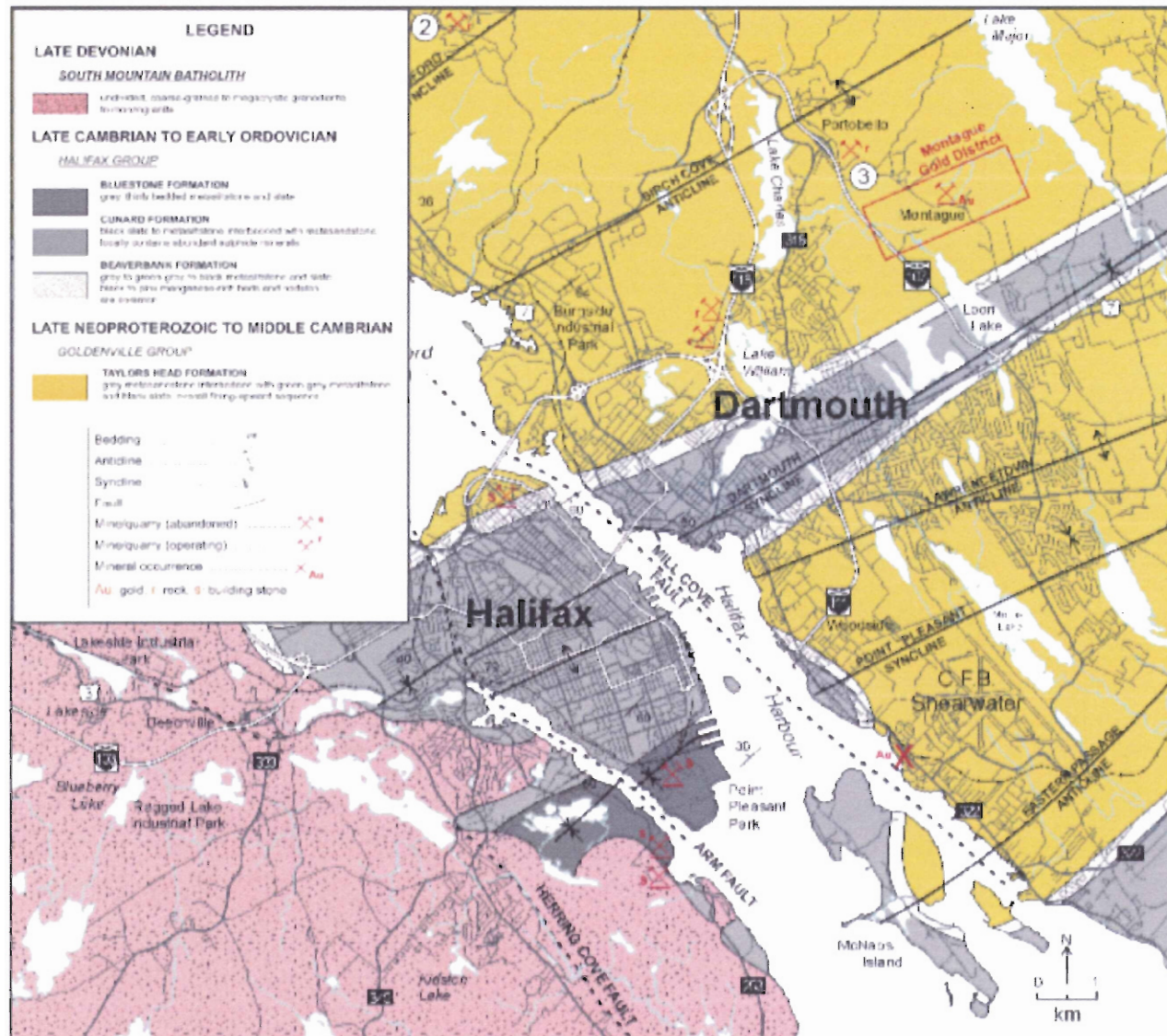


Figure 2.1 Simplified geological map of mainland Nova Scotia showing the position of the following map (fig. 2.2) and study area from White et al. (2008) Meguma Group has since been upgraded to Supergroup. Halifax and Goldenville Formations have been upgraded to Groups.

Figure 2.2 Bedrock geology of the central part of HRM (White et al., 2008). New data collected since this map was published (Jamieson et al., 2001; Waldron et al., 2011) have led to some revisions, including placement of the Cunard – Bluestone contact and apparent displacement on the Northwest Arm Fault (fig. 1.1, 2.2, 5.1)



## **2.2 Meguma Supergroup**

### **2.2.1 Goldenville Group**

Halifax is underlain by the Meguma Supergroup, represented locally by the late Neoproterozoic Cambrian Goldenville Group, and overlying early Ordovician Halifax Group. The Goldenville Group is composed primarily of quartzo-feldspathic greywacke and indurated, thickly bedded, and massive feldspathic sandstone deposited as deep water turbidites on the slope and rise of Gondwanaland (Schenk, 1982; White 2010). With an estimated minimum thickness of 7 km, the base of the Goldenville is not exposed, and underlying units remain unknown (Schenk, 1997). Locally, Goldenville Group rocks (Beaverbank and Taylor Head formations; White et al. 2008) crop out at the northern tip of peninsular Halifax, and along the shores of Bedford Basin. Sandstone horizons within the Goldenville Group locally contain calcareous concretions (e.g., Purves, 1974; Mitchell, 2004). These are not included within the scope of this study, which focuses exclusively on calcareous concretions and horizons in the Bluestone formation, the uppermost unit of the Halifax Group.

### **2.2.2 The Halifax Group**

The Halifax Group, which conformably overlies the Goldenville Group, forms the bedrock underlying most of peninsular Halifax and the western shore of the Northwest Arm. It comprises a sequence of late Cambrian - early Ordovician grey to black slates and siltstones. In the Mahone Bay area, it comprises the Cunard and Feltzen formations (e.g., O'Brien et al. 1988), with the underlying Mosher's Island formation recently re-assigned to the Goldenville Group (White, 2010). In Halifax, the dominant unit is the

Cunard formation (500-8000 m), composed of graphitic and sulphidic black slate and grey siltstone (Horne et al., 2006; White et al. 2008). Until recently, the Cunard formation in Halifax was considered a single, undifferentiated unit with a transitional upper lithology consisting of inter-bedded blue-black slate with silt and fine sandstone, locally containing calcareous nodules (Horne and Culshaw, 2001). The work of undergraduate students Neil Tobey (2006) and Glenn Hart (2006), and research by R.A. Jamieson (2004 to present) and J.W.F. Waldron (2010-11), has distinguished this upper unit as the Bluestone formation, a stratigraphic correlative of the Feltzen formation of the Mahone Bay area, the Glen Brook formation of central Meguma area and the Eastern Shore, and the Bear River formation exposed in the Digby area (White et al. 2007, 2008; White 2010).

### **2.2.3 The Bluestone Formation**

The Bluestone formation is distinguished from the underlying Cunard formation on the basis of stratigraphy, sedimentary structures, and contrasting metamorphic isograd sequence, the latter reflecting its distinctive geochemical signature (Jamieson et al. 2005; Hart, 2006). The name comes from the Bluestone Quarry near Purcell's Cove on the west side of the Northwest Arm, and the unit also underlies southern peninsular Halifax between Point Pleasant Park and Gorsebrook Field. Recent mapping in Halifax has led to subdivision of the Bluestone formation into four distinctive members (Jamieson et al. 2011; Waldron et al. 2011). Bluestone formation member descriptions follow Jamieson et al. (2011), Waldron et al. (2011), and new observations from this study.

The Bluestone formation takes its name from Bluestone Quarry in Purcell's Cove, so named for the characteristic blue-grey building stone collected from this formation in the nineteenth and early-mid twentieth centuries. These materials are still visible in some of the oldest stone structures throughout the city of Halifax, including several buildings on Dalhousie Campus.

### **Point Pleasant member**

The Point Pleasant Park member is the lowest stratigraphic unit of the Bluestone formation and conformably overlies the black, graphic slate of the Cunard formation. Inter bedded fine sand and siltstone layers are expressed as fine laminations, climbing ripples, starved and truncated ripples, and thick, graded beds consistent with Bouma sequence turbidite facies easily recognizable in outcrop (Fraser, 2010). Calcareous concretions are abundant in the Point Pleasant member and readily visible at Battery Point and outcrops on the adjacent hillside.

### **Black Rock Beach member**

The Black Rock Beach member overlies the Point Pleasant member and is distinguished from the former by the lack of thick sandy layers. Silt and sandstone layers are laminated and cross-laminated throughout. Cleavage developed during regional deformation is well preserved in mudstone layers in the type section at Black Rock Beach. Calcareous horizons and abundant concretions are present at this location where they form recessively weathering, greenish horizons and pods.

### **Chain Rock member**

The Chain Rock member overlies the Black Rock Beach member, and consists of disrupted and discordantly folded beds in a fine-grained featureless matrix. Laminations, cross laminations, and ripples are preserved in folded layers, and calcareous concretions are visible throughout glacially scoured exposures of the unit, which has been interpreted to be a down-slope mass transport deposit. The irregular deformation of primary structures has indurated the unit, resulting in a prominent ridge topography exploited for fortifications by the British in the 19<sup>th</sup> century (Waldron et al., 2011).

### **Quarry Pond member**

The Quarry Pond member is the uppermost unit of the Bluestone formation named for the classic field instruction location at Quarry Pond in Point Pleasant Park. The unit is similar to the Black Rock Beach member with laminated and cross-laminated, thinly bedded silt and sandstone layers. However, concretions are less abundant than in the lower unit. Relative timing of the underlying mass-transport deformation event to the deposition of the Quarry Pond member remains ambiguous. Bedding orientations indicate little deviation from the Point Pleasant syncline, however this does not rule out the possibility of intact transportation of an overlying block above a plastic substrate (Waldron et al., 2011).

## **Calcareous Concretions and Horizons**

Calcareous concretions and horizons within the Bluestone formation are superbly exposed in outcrops in Point Pleasant Park, Purcell's Cove, and north of Williams Lake. Similar structures are found within the Feltzen formation, further supporting correlation of the two formations (Hart, 2006). Concretions observed in the Bluestone formation typically form near the base of sandy beds, directly above scoured tops or sharp contacts with underlying mudstone (now slate). Semi continuous, coarse-grained horizons containing abundant calcareous material are found throughout the Bluestone formation as well, and can span several metres in length. Outcrop size and distribution however, limits comprehensive measurements of the continuity of these horizons.

The presence of carbonate in the Bluestone formation indicates the boundary between the Bluestone fm. and the Cunard formation marks a change in oxidizing conditions. Graphite, abundant in the Cunard formation, is virtually absent from the Bluestone Formation, characterized by the precipitation of carbonate along discrete sedimentary layers. The formation of individual concretions follows the diffusion of carbonate ions through permeable lithologies to a concentrated nuclei. Precipitation of carbonate during diagenesis follows a chemical activity potential gradient. Consequently, concretion size is a function of rates of diffusion, duration of ionic mobility, and composition of the host/source lithology. Concretions have been interpreted to be diagenetic (Waldron et al., 2011), though detailed explanation of the diagenetic formation mechanisms responsible for these structures lies outside the scope of this project.

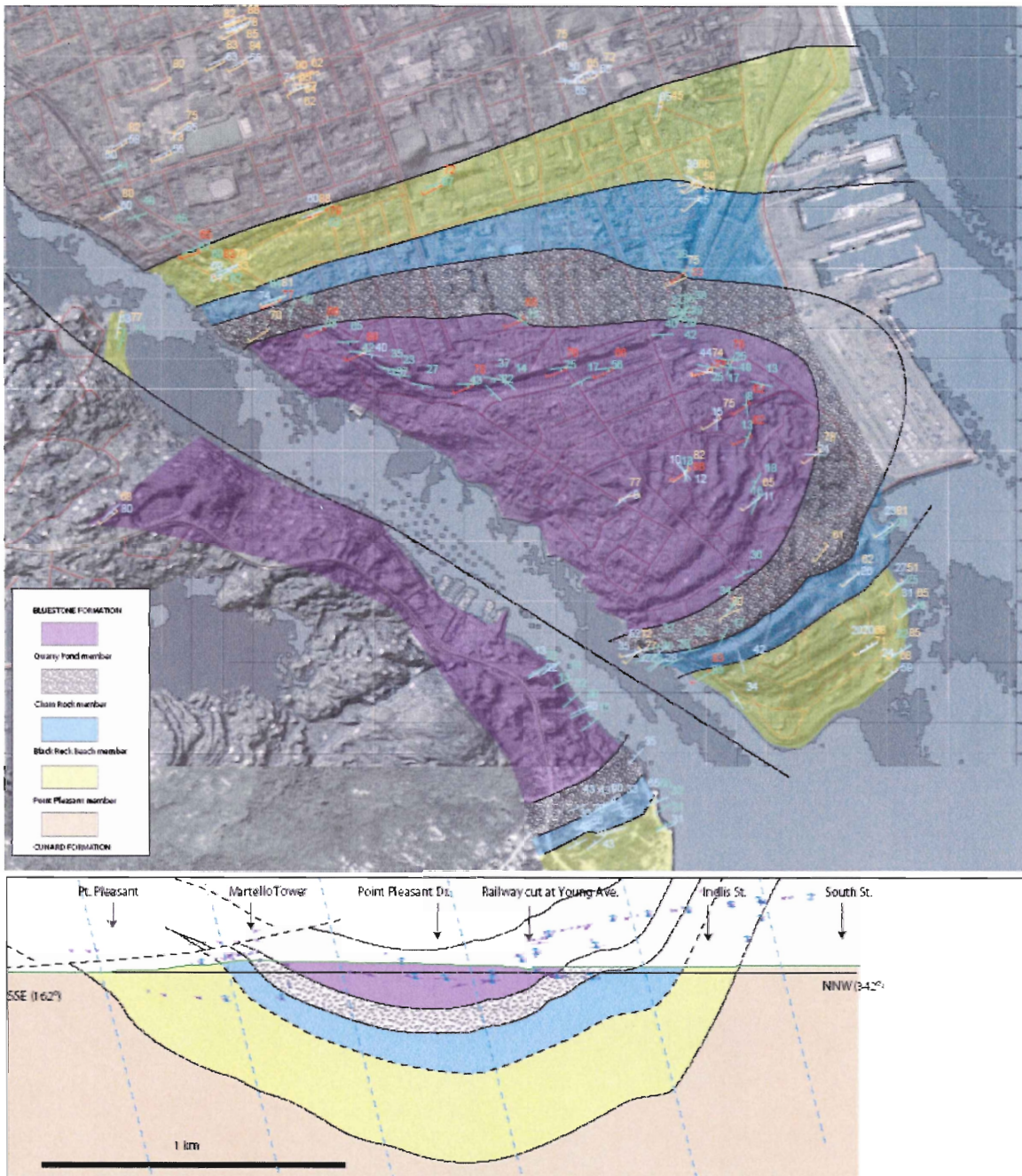


Figure 2.3 Map and cross section superimposed on shaded LiDAR topography showing the members of the Bluestone formation and structural measurements. Cross section is perpendicular to the axial trace of the Point Pleasant Syncline. Map and stratigraphy by J.W. Waldron, used by permission.

### **2.3 Regional Structure**

The metasediments of the Meguma Supergroup have been folded into a series of tight to open synclines and anticlines gently plunging southwest to northeast (eg. Horne and Culshaw, 2001). The axes of three major folds cross peninsular Halifax. The Dartmouth Syncline to the north and the Point Pleasant Syncline to the south are separated by the Lawrencetown Anticline. The axial plane of the Point Pleasant Syncline strikes roughly 020, dipping ~ 80°. The syncline plunges gently to the SW, resulting in an arcuate surface exposure of Bluestone stratigraphy (White et al., 2008; Waldron et al., 2011; Jamieson et al., 2011; Figure 2.3). Axial planar cleavage associated with the Point Pleasant syncline is well developed in pelitic lithologies of the Bluestone formation, less well defined in psammitic lithologies, and is well preserved in low grade outcrops in the study area (Horne and Culshaw, 2001). Sinistral strike-slip displacement along the Northwest Arm fault offsets the Bluestone formation stratigraphy (fig. 2.3).

### **2.4. The South Mountain Batholith**

The middle to late Devonian Acadian Orogeny saw the accretion and regional deformation and greenschist facies metamorphism of the Meguma Supergroup sediments with the closing of the Iapetus during the formation of Pangea (Schenk, 1997; White et al., 2008). Numerous late syn-tectonic peraluminous granitic intrusions were emplaced, ca. 370-380 Ma, into the Meguma terrane (MacDonald, 2001). At roughly 200 km in length and with a maximum width of 50 km, the South Mountain Batholith (SMB) represents the largest continuous intrusive complex in the Appalachians. The Halifax pluton forms the easternmost extent of the SMB, with virtually unbroken granitic

coastline outcrop extending from Purcell's Cove in Halifax to the town of Mahone Bay, including the scenic communities of Sambro Head and Peggy's Cove. The petrology, mineralogy, and geochemistry of the South Mountain Batholith have been investigated in detail (e.g. MacDonald & Clarke, 1985; Clarke et al., 1988; MacDonald & Horne, 1988; MacDonald, 2001; Clarke et al., 2004; Erdmann et al., 2009); a comprehensive summary is beyond the scope of this thesis.

Intrusion of the South Mountain Batholith into the Meguma Supergroup produced a contact aureole ranging in width from 500 m to 3 km (Mahoney 1996; Jamieson et al. 2005). Based on a regional study of the entire SMB contact aureole, Mahoney (1996) concluded that depths of intrusion in the east correspond to pressures ranging between 3.5 to 3.8 kb (Hart, 2006). The study area lies entirely within the contact aureole produced by intrusion of the Halifax Pluton into the Halifax Group in what is now the southern part of the city of Halifax. The closest approach of the pluton to peninsular Halifax is a narrow protrusion exposed at the Dingle Park on the west side of the Northwest Arm opposite the foot of South Street; no granite bodies of any size have yet been found on the peninsula. The outer limit of the contact aureole in Halifax is defined by the first appearance of cordierite (Jamieson et al., 2005; Hart, 2006) at a temperature of ca. 400°C (Hilchie and Jamieson, 2008). At the contact, the assemblage andalusite + K-feldspar, with rare sillimanite and only retrograde muscovite, suggests temperatures of ca. 600°C and pressures of 2.5-3 kbar (Jamieson et al., 2005; Hilchie and Jamieson; Jamieson, unpublished data), corresponding to a depth of intrusion in the study area of ca. 7-10 km.

## **2.5      Lithological Descriptions**

Fieldwork was undertaken in the fall of 2010 to establish the lithological, structural, and stratigraphic context of calcareous concretion and horizon formation in the Bluestone formation. For more detailed descriptions of host lithologies in Point Pleasant Park, refer to Tobey, (2006); Hart, (2006); and Fraser, (2010). Numerous observations by R.A. Jamieson are included here, including observations pertaining to Williams Lake. Fieldwork in the Williams Lake area (samples denoted WL) was undertaken during construction of the Ravenscraig subdivision in 2007.

### **2.5.1    Point Pleasant Park (PPP)**

#### **2.5.1.1 Black Rock Beach: PPP04-30**

Concretion samples representing the lowest grade of metamorphism (PPP-30) included in this study were collected from Black Rock Beach at the northeast corner of Point Pleasant Park (Fig. 1.1). Consistent with NW-SE trending isograds described by Hart (2006), metamorphic grade within the park increases to the SW. Samples collected from the William's Lake and Purcell's Cove areas all come from outcrops within ~300 m of the SMB contact. The Black Rock Beach member is named for the superb type locality outcrop adjacent Black Rock Beach at Point Pleasant Park's lower parking lot.



Figure 2.4 Bluestone Formation, Black Rock Beach, showing calcareous horizon with early concretion forming at center. Truncated ripples, and laminated pitted siltstone and slate visible above. Overprinted laminations are clearly visible

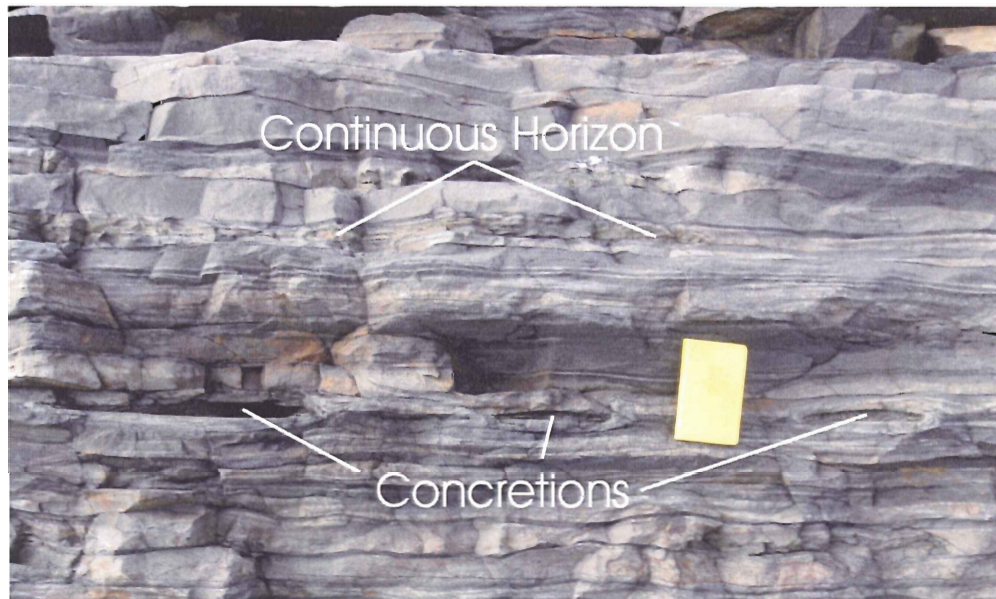


Figure 2.5 Battery Point, PPP04-6 & 7. Calcareous concretions preferentially weather, forming oblate cavities (lower three). The semi-continuous horizon at top show abundant pitting from weathered sulfides. (notebook is 18 cm tall)

### **2.5.1.2 Battery Point: PPP04-6,7**

Battery Point in Point Pleasant Park contains the most numerous exposures of calcareous concretions within the study area. Concretions and, less commonly, semi-continuous horizons, form within sand- and silt-rich beds and are typically limited to particular layers (Fig. 2.3). Up to five individual nodules were noted within a single layer, three of which can be seen in figure 2.5. A semi-continuous, coarse-grained calcareous horizon <5 cm thick can be seen in figure 2.5, though thicker, more continuous horizons are found elsewhere.

Preferentially weathered cordierite is responsible for the characteristic pitting seen throughout Bluestone formation slates, with increasing concentration toward the SW in Point Pleasant Park. Sulphides are commonly found within coarser psammitic layers and concretions that recessively weather to form sparse pitting in calcareous layers and concretions. Concretions at Battery Point are mantled by margins ~1-2 cm thick of smooth, cordierite-free slate and silt. Despite the near-complete weathering of nodule cores here, a radiating pattern or inward growth of acicular material is faintly visible with a hand lens, within the white-grey nodule boundary (fig. 2.6).



Figure 2.6 Detail of a concretion margin showing both smooth, cordierite-free host (center-right) and pitted, cordirite bearing host (at bottom). Recessive weathering core visible (at left), and faint radial texture is seen (at center).

### **2.5.1.3      Battery Point Hillside: PPP09-5c**

The arrival of Hurricane Juan in Halifax during September of 2003 leveled over 10,000 trees in PPP, revealing new, previously heavily vegetated Bluestone formation outcrops. One of these is an escarpment, several metres long and roughly 2 m high, located directly above Battery Point. Laminations, climbing and truncated ripples corresponding to Bouma sequence Tabcde and Tae are clearly visible here (Fraser, 2010), along with numerous large concretions similar to those in the upper portions of the Battery Point shoreline outcrop. Exposed portions of concretions here are roughly 1 m in length and 10 cm thick, have coarse-grained interiors, and show abundant pitting from weathered sulphides. Additionally, a distinct red and white-banded weathering rind (Fig. 2.7) is visible on an old fracture face cross cutting the lateral terminus of a particular concretion. This is interpreted to have formed prior to exposure in 2003, and indicates a transition in chemical and mineral composition within the concretion as a function of distance from core to boundary.

### **2.5.1.4 Purcell's Landing: PPP04-4**

The degree of annealing associated with the contact aureole increases markedly from Battery Point to the SW shore of Point Pleasant Park. Cleavage plainly visible in Black Rock Beach slates is virtually non-existent here, and most sedimentary structures in fine-grained layers are obscured by abundant cordierite porphyroblasts. However, sedimentary structures (e.g. ripples, cross laminations) in meta-siltstone and sandstone layers are very well preserved. Thick, massive meta-sandstone beds are present along much of the Northwest Arm.

The east shore on the Northwest Arm suffered significant erosion during Hurricane Juan. Subsequent park restoration work included the armouring of beaches below unstable slopes with heaps of fresh boulders from the Goldenville Group. Luckily, the characteristic pink weathering rinds of annealed Bluestone formation rocks makes Point Pleasant member outcrop relatively easy to distinguish, given that beach armour itself is now being eroded. Concretions are less prevalent here, though continuous coarse-grained pink and green calcareous horizons are readily visible among bedded light grey – brown, given relatively rough weathering texture (Fraser, 2010).

### **2.5.1.5 Chain Rock: PPP04-17a,b**

The enigmatic structure at Chain Rock has eluded simple classification for years (eg. Tobey, 2006). The outcrop, after which the Chain Rock member is named, preserves discontinuous bedding folded in numerous, discordant orientations. Up-slope, where Martello Tower stands on a glacially scoured level plane, the same discordant folding is expressed as sigmoidal bedding traces. Rounded, oblate clasts representing disaggregated concretions (Fig. 2.8) are found at Chain Rock. These tend to be sulphide-rich, and display white and red banded weathering rinds similar to those on the Battery Point hillside (PPP09-5c). Recent work by Waldron (personal communication 2011; Waldron et al., 2011) suggests this unit represents mass transport or slump deposit predating lithification of the Bluestone formation. If so, the presence of these concretions as competent clasts in unconsolidated sediments requires the early diagenetic formation of these concretions, predating final lithification of the Bluestone host.



Figure 2.7 PPP-5c, Battery Point hillside, detail of a concretion displaying colour banded weathering rinds with finger for scale.



Figure 2.8 Discontinuous disrupted and folded layers (left) at Chain Rock. An oblate concretion (right) in relatively massive host with colour bands corresponding to those seen at PPP-5 (fig. 2.6). Scale card in centimetres (top) and inches (bottom).

## **2.5.2 Purcell's Cove (PCR)**

### **2.5.2.1 Purcell's Cove: PCR04-7**

This site outcrops near a small pier just below Bluestone Quarry and north of Purcell's Cove proper. The outcrop is dominated by pink-weathering sandstones, with typical parallel laminae and faint ripple marks, similar to PPP04-4 located directly across the Northwest Arm, indicating this is an outcrop of the Point Pleasant member. Large concretions (~1 m by 10 cm) contain large, unidentified equant white crystals up to 5mm in diameter. Minor slate layers, <10 cm thick, are also present.

### **2.5.2.2 Upper Bluestone Quarry: PCR07-23**

Bluestone Quarry ceased commercial operations in the mid-twentieth century, after which the geology program at Dalhousie University made use of the site's excellent exposures for introductory field classes. Field station numbers can still be seen from field classes dating back to the seventies although the site has since suffered decades of clandestine dumping and graffiti.

Bluestone formation rocks within the quarry are hornfels with massive layers and totally annealed cleavage. Clearly preserved siltstone-sandstone layers and associated sedimentary structures and numerous calcareous concretions are present throughout. A prominent quartzo-feldspathic layer ~80 cm thick outcrops south of the quarry aside Bluestone Rd. It represents the thickest meta-sandstone horizon observed in this study, and lies near the top of the Point Pleasant member. Numerous granitic veins intrude the

Bluestone rocks, presumably derived from the nearby (~100 m) SMB. One to five centimeter thick intrusions appear to exploit structural weaknesses and are both concordant and discordant to bedding planes. Within the quarry, concretions ranging from 3-4 cm up to 60 cm thick are present.

Irregular to oblate clasts with distorted bedding are found above the quarry, similar to clasts observed at Chain Rock. Numerous shear zones are also found in the uppermost bedding-perpendicular outcrop faces of the quarry, with undisturbed sedimentary layers above and below the shear plane. Small, centimeter-scale drag folds indicate normal-sense ductile deformation.

The presence of thick, massive sandstone layers to the south of the quarry and shear zones with distorted bedding to the north of the quarry provides ideal constraints for the extension of mappable Bluestone formation members across the Northwest Arm to the Bluestone Quarry area near Purcells Cove. The Point Pleasant member lies to the south of the quarry, the Chain Rock member lies north of the quarry, and the Black Rock Beach member runs through the middle, comprising the building material for which the formation is named.

#### **2.5.2.3 Royal Nova Scotia Yacht Squadron: PCR07-11**

A large block of deep purple-black, freshly blasted hornfels outcrops within the winter storage lot directly across Purcells Cove Road from the RNSYS club dockyards. Continuity with bedrock cannot be demonstrated, but as the outcrop measures several metres across, the likelihood that this material represents a foreign erratic is slim. In

addition, this hornfels lithology is to be expected given the proximity (< 100 m) of the SMB contact to the southwest.

Quartz-feldspathic material forms white to grey horizons up to ~ 10 cm thick, in which faint, dark laminations can be seen. Grain size reversals can be seen, where micas have crystallized from clay-rich sediments concentrated toward to top of fining-up sequences, subsequently grown larger than the underlying silt and sand. No distinct mineral phases could be discerned within the horizon in hand sample. Site PCR07-11 lies well within the Quarry Pond member of the Bluestone formation.

### **2.5.3 Williams Lake (WL)**

Outcrops within 150 m of the SMB contact northwest of Williams Lake were sampled in 2007 during construction of the Ravenscraig subdivision. Most of these outcrops are now buried under homes or landscaping. The rocks consist mainly of interlayered psammitic and pelitic hornfels, with well preserved sedimentary structures in originally coarser-grained layers. Cleavage is totally annealed. Pelitic layers are mottled, with abundant cordierite and andalusite porphyroblasts; one outcrop within 10 m of the granite contact contains fibrolitic sillimanite. A massive metasandstone layer near the western edge of the area suggests that the rocks should be assigned to the Point Pleasant member of the Bluestone formation, consistent with the presence of numerous calc-silicate concretions. These are generally small (< 30 cm long) and variably zoned from buff-coloured cores to darker rims that locally appear to grade into the host rock. Samples WL07-18 and WL07-16 were collected within 50 and 100 m, respectively, of the inferred position of the contact.

## **2.6 Summary**

The Bluestone formation is subdivided into four distinct and mappable stratigraphic units underlying southern peninsular Halifax, Purcells Cove, and Williams Lake. Calcareous concretions and horizons are present in all four members, and are easily distinguishable in outcrop. Intrusion of the South Mountain Batholith produced a contact metamorphic aureole, affecting the texture and mineralogy of both the calcareous features and the Bluestone formation host rocks.

## Chapter 3 PETROGRAPHY

### 3.1 Introduction

This study focuses on distinctive, originally diagenetic structures in a host rock of varying lithology and texture. Textures, mineral assemblages, and chemistry of the host Bluestone formation reflect contact metamorphic overprinting of regional greenschist facies metamorphism. Typical mineral isograd sequences observed by Hart (2006) developed in the host pelite. However, no mineral assemblage for concretions entirely unaffected by some degree of contact metamorphism has been identified or documented to date. Electron dispersive spectroscopic (EDS) elemental maps and secondary electron backscatter (BSE) images were used to identify and track minerals too fine-grained to detect or identify optically.

Samples from Point Pleasant Park contain the low-grade contact metamorphic mineral assemblages included in this study, comprising cal + qtz + grt + pl + cpx + chl + ttn. “High-grade” metamorphic assemblages, for the purposes of this study, reach epidote-hornfels to hornblende-hornfels zones on the west side of the Northwest Arm < 250 m from the SMB contact (Fig. 1.1).

Concretions examined in this study contain distinct and continuous mineralogical zones 5 - 8 mm thick demarking an outer rim or boundary with the surrounding host. Weathering at outcrop PPP-5 produces ~ 10mm thick white bands corresponding to this zone, reflecting an anorthite-dominated concretion rim separating the Ca-rich core from the surrounding Fe-rich silty sandstone. Radiating sprays or bundles of tabular chlorite demark ~2.5 mm of this transition zone at low grades, and can be identified in all

samples, despite textural modification and/or replacement by hornblende at higher metamorphic grades. Deep orange-red weathering of concretions at PPP-5c (fig. 2.4) appears to be an alteration product of Ca+Fe – rich clinopyroxene. Similar orange-red banding in samples from site PPP-7c show some association with Ca-rich garnet in addition to clinopyroxene. Concretions are more abundant along the base of medium to fine sandy layers. Modal abundance of detrital quartz varies little between concretion interiors and the surrounding pelite in low-grade samples, though grain size increases slightly in the former.

Modal quartz abundance decreases with proximity to the SMB contact, with the notable exception of PCR-23a. Detrital quartz dominates the groundmass of this concretion, with large poikiloblastic clinopyroxene becoming a major phase. Anomalously, concretions sampled from this site contain no garnet, suggesting a contrast in bulk composition between this and other concretions studied.

### 3.2 Low-Grade Mineral Assemblage

The lowest grade concretions found in the Bluestone formation, at Black Rock Beach, provided a bulk chemistry for interpretation of incrementally higher metamorphic grades. Despite variations in modal abundance, outcrops PPP-30, 5, and 7 show minimal variation in mineralogy and have been grouped for reference as the low-grade assemblage.

The core region is dominated by equant, coarse-grained poikiloblastic calcite (< 0.5 mm) and Ca-rich garnet up to 0.5 mm in diameter. The latter forms elongate, diffuse

aggregates up to 6 mm long and 1.5 mm wide, that overprint relict sedimentary layering in the concretion core. Angular, equigranular detrital quartz (0.05 - 0.15 mm) is ubiquitous, varying in modal abundance ~ 40 – 80 % depending on the abundance of garnet and calcite. Average quartz grain size increases from ~ 0.05 mm in the host to ~ 0.08 – 0.10 mm in the concretion core. Minor xenoblastic titanite, epidote, clinozoisite, ilmenite and apatite found at this grade are generally too fine-grained to discern without EDS maps or BSE images.

Ovoid to wheat-sheaf shaped bundles of tabular radiating chlorite are found within a ~ 2 - 5 mm thick zone along concretion rims. The first appearance of this chlorite coincides with the virtual absence of biotite within the concretion core. Minor intergrowths of biotite in chlorite occur within the outermost 2 mm of the concretion rim, but are not found inside this zone. The distinct and consistent morphology of these chlorite bundles coupled with their restriction to concretion rims make them key tracers for identifying concretion boundaries across metamorphic grade.

### **3.3 Medium-Grade Mineral Assemblage**

All concretions sampled west of the Northwest Arm occur within the second andalusite-in isograd of contact aureole in the Bluestone formation (Hart, 2006; fig 1.1, 5.1) Samples PCR-23 and -26 contain no calcite in the core region, but otherwise differ greatly from each other in terms of core assemblage and texture. For this reason, it is useful to describe each sample independently.

The core zone of sample PCR-23 is dominated by sub-angular, equigranular, detrital quartz (30 – 50 modal %), in an anorthite matrix with minor muscovite

intergrowths. Clinopyroxene forms the dominant porphyroblast phase (~ 5 %), with irregular, poikiloblastic porphyroblasts < 1 mm in diameter. Inclusions in clinopyroxene include anorthite, titanite, chlorite and rare quartz. Xenoblastic clinopyroxene within the concretion-rim zone appears to be pseudomorphs after chlorite, preserving radial inclusion fabrics. Minor inclusions of chlorite in clinopyroxene support this hypothesis. Samples at site PCR-23 are both anomalous and conspicuous for their complete lack of garnet.

Samples examined from the shoreline of Purcells Cove mark a dramatic shift in core mineralogy. Calcite is replaced or consumed entirely by muscovite, apatite, chlorite, and garnet. Sample PCR-26b is texturally complex, particularly in the chlorite-boundary transition zone, not seen in any other concretion in the study area. Furthermore, sample PCR-26b contains anomalous biotite porphyroblasts inboard of the chlorite rim, forming large (~5mm) herringbone-shaped or skeletal aggregates extending at high angles from the base of the chlorite-bundle boundary zone toward the concretion core. The matrix of the core and the chlorite-rim zone is dominated by micro-granular muscovite and white mica. The concretion rim zone contains distinct wheat-sheaf morphology or radiating bundles of tabular chlorite. Micro-granular quartz comprises roughly 2 – 5 % of the matrix, with minor apatite, rutile, and Mn-rich ilmenite, comprising < 5 % of the mode.

The core of PCR-26b, by contrast, contains virtually no quartz (< 1% modal abundance), observed only where biotite aggregates inter-layer with concretion-rim matrix material (< 0.05 mm in diameter) that appears to spall or peal back toward the concretion-core. Micro-granular white mica dominates the concretion core, constituting ~70 % of the matrix. Garnet porphyroblasts, up to 0.8 mm across, within the core and rim

zones comprise up to 8 % of the mode, though typically less than 5 %. Minor anorthite and alkali feldspar are present as inclusions in garnet. Heavily embayed apatite rimmed by intergranular chlorite, in clear disequilibrium with the mica-dominated matrix, completes the core mineral assemblage.

Sample PCR-26b contains a boundary zone demarcated by radiating bundles of tabular chlorite and highly calcic plagioclase characteristic of calcareous concretions. The current mineral assemblage of the core-region suggests the sampled structure, a continuous layer as opposed to an isolated discreetly bounded concretion, is the remnant of a significantly altered calc-silicate lithology.

### **3.4 High-Grade Mineral Assemblage**

Samples collected from concretions found within ~ 250 m of the Halifax Pluton contact are grouped, for convenience, as the high-grade metamorphic assemblage in this study. Six known concretion-bearing locations fall within this range, including samples PCR-11b, WL-16b, and WL-18b. The mineralogy in this region is dominated by low-to-moderately high temperature hydrous phases including prehnite, epidote, vesuvianite, amphibole, and muscovite. These phases are not present in all high-grade samples, possibly reflecting lateral variations in fluid-rock interaction, variations in the local thermal gradient of the aureole, and/or variations in bulk composition. Despite lateral heterogeneities, concretion rim and core mineralogical zones are distinguishable in all samples.

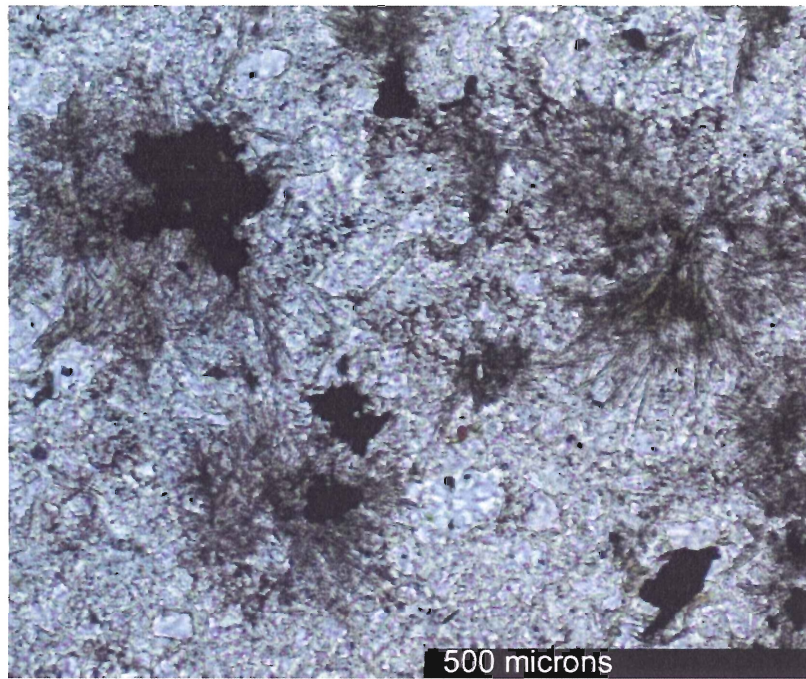


Figure 3.1 Wheat-sheaf aggregates of tabular chlorite the concretion-rim mineralogical zone in sample PPP-5c. This morphology is maintained across all metamorphic grades, with chorite coarsening somewhat in high-grade samples.

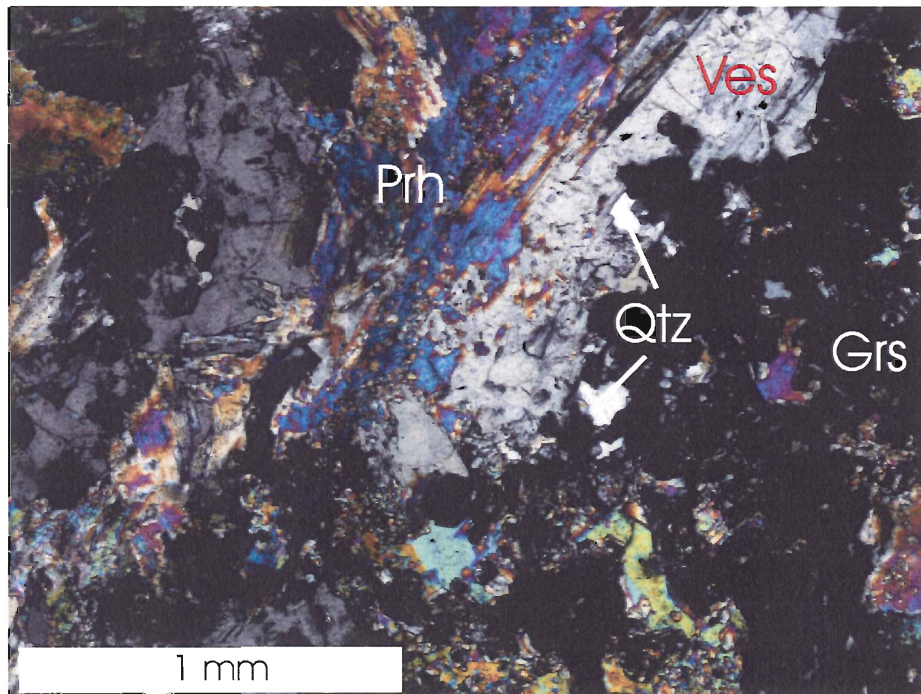


Figure 3.2 Photo-micrograph of the core assemblage from WL-16b showing alteration of vesuvianite to prehnite and idiomictic granular grossular in cross-polarized light.

Deep green hornblende first appears as a significant phase in samples PCR-11b and WL-18b, where it replaces chlorite bundles in concretion rims. Clinopyroxene remains the dominant porphyroblast in the cores of these concretions, forming elongate poikiloblastic crystals up to 2.5 mm long. Prehnite first appears in samples PCR-11b and WL-16b as an inter-granular matrix phase, though characteristic ‘bow-tie’ or ‘hour-glass’ shaped aggregates are rare.

Sample WL-16b is unique in the study area for its relatively coarse and limited mineral assemblage. Vesuvianite porphyroblasts up to 10mm long constitute ~ 25 % of the concretion-core assemblage, a mineral not observed elsewhere in the study area. Idioblastic granular garnet and rounded quartz are present as inclusions within coarse vesuvianite crystals, in addition to pervasive, tight intergrowths of xenoblastic prehnite. Equigranular, idioblastic garnets, ~ 0.1 mm in diameter, form aggregates and partial coronae around vesuvianite, comprising ~ 40 % of the core assemblage. Sub-idioblastic prehnite prophyroblasts, inter-growths, and veins comprise roughly ~ 35 % of the core assemblage. Prehnite-filled veins cut a number of vesuvianite pophyroblasts (Figure #), suggesting the prehnite may be a retrograde alteration product of the latter, formed during cooling and fluid infiltration following intrusion of the SMB.

### **3.5 Summary**

Calcareous concretions can be divided broadly into low, medium, and high-grade mineral assemblages. The presence of significant calcite defines low-grade assemblage, with successive grades based loosely on progressively higher T, texturally well-equilibrated calc-silicate minerals. Medium-grade assemblages are anomalous, possibly reflecting different bulk compositions. High T, hydrous Ca-rich phases and retrograde metamorphic-metasomatic phases are characteristic of the high-grade assemblage. Distinct core and rim mineralogical zones are distinguishable across all metamorphic grades.

## Chapter 4 MINERAL CHEMISTRY

### 4.1 Introduction

Petrologic studies of the Cunard formation and the Bluestone formation have focused on mineral assemblages and associated reactions in the pelitic-psammitic meta-sediments (Jamieson et al. 2005; Hart, 2006; Tobey, 2006), in order to determine isograds and P-T conditions in the contact aureole. To infer possible metamorphic and metasomatic reactions in calcareous concretions under these P-T conditions, electron microprobe and trace element analysis were employed to examine the mineral assemblages and to track variations in concretion composition across the contact aureole.

### 4.2 Mineral Chemistry

Eight sample locations were selected, representing a transect across the South Mountain Batholith contact aureole roughly perpendicular to the isograd contours. Polished sections from seven of the eight selected locations were analyzed at the Robert MacKay Electron Microprobe Laboratory at Dalhousie University. The instrument is a JEOL JXA-8200 scanning electron microprobe. Operating conditions were an accelerating voltage of 15 kV, minimum spot size of 2  $\mu\text{m}$ , and a beam current of ca. 20 nA, calibrated for silicate analysis. R.A. Jamieson analyzed the eighth sample (WL-18b) in February 2009 at the University of Calgary Laboratory for Electron Microprobe Analysis (UCLEMA). The UCLEMA also has a JEOL JXA-8200 microprobe, operated under similar conditions. Data from the 2009 analyses are incorporated into this study with permission of R.A. Jamieson.

#### 4.2.1 Garnet

Ternary plots for the grossular-spessartine-almandine solid solution demonstrate systematic variations in garnet composition as a function of distance from the concretion rim (Fig. 4.1-8). Mg is negligible in garnets in the study area (predominantly < 0.01 cations pfu) and the pyrope component is disregarded. Using the idealized formula  $(\text{Ca},\text{Fe},\text{Mn})_3\text{Al}_2\text{Si}_3\text{O}_{12}$  for garnet (Deer et al., 1992), end-members are reported as mole %  $\text{Grs}_x\text{Sps}_x\text{Alm}_x$ .

Garnets in low-grade assemblages are minor, intergranular phases with high diversity of end-member components. The average composition at the concretion outer-rim for PPP-5c is  $\text{Grs}_{10}\text{Sps}_{50}\text{Alm}_{40}$ . By contrast, average composition for garnet in the core of the same concretion is  $\text{Grs}_{60}\text{Sps}_{20}\text{Alm}_{20}$ . Average garnet compositions in the core of PPP-30, the lowest-grade sample in this study, are identical to the core of PPP-5c with  $\text{Grs}_{60}\text{Sps}_{20}\text{Alm}_{20}$ . Sigmoidal mineralogical zones in sample PPP-7c (fig. 4.2) yield average compositions ranging from  $\text{Grs}_{50}\text{Sps}_{30}\text{Alm}_{20}$  to  $\text{Grs}_{70}\text{Sps}_{10}\text{Alm}_{20}$ .

Garnet analyses associated with medium-grade assemblages are limited to the concretion core and inner-rim region of sample PCR-26b (Fig. 4.4). No garnet was found in PCR-23a (Fig. 4.5). Sample PCR-26b presents numerous textural and compositional anomalies as described in section 3.3. Analyses of idioblastic garnet in the muscovite-dominated core show compositional abundances typical of phases within or adjacent to the Fe-rich pelitic host. Average garnet composition in the core of PCR-26b is  $\text{Grs}_6\text{Sps}_{37}\text{Alm}_{57}$ .

Analyses of numerous core regions in high-grade samples show no evidence for variation in component abundances as a function of distance from the concretion boundary (Fig. 4.6-8). The average composition of garnet in the core assemblage at high-grade is consistently  $\text{Grs}_{90}\text{Sps}_0\text{Alm}_{10}$ . This degree of compositional homogeneity between sample locations suggests prolonged, highly efficient ionic diffusion consistent with proximity to the Halifax Pluton contact. For comparison, relatively large ( $\leq 0.5$  mm in diameter) garnet porphyroblasts in pelitic host rock  $< 1$  mm from the concretion boundary in samples WL-16b and WL18b yielded average compositions of  $\text{Grs}_{10}\text{Sps}_{30}\text{Alm}_{60}$ .

#### 4.2.2 Clinopyroxene

Samples PPP-30 (Fig. 4.1) and PPP-5c (Fig. 4.3) have similar clinopyroxene compositions as expressed by the diopside-hedenbergite (Di - Hd) solid solution series,  $\text{Ca}(\text{Mg},\text{Fe})\text{Si}_2\text{O}_6$ . No clinopyroxene is found in sample PPP-07 (Fig. 4.2), and clinopyroxene was only found within the concretion-pelite boundary in sample PPP-30. Using the idealized formula  $\text{Ca}(\text{Mg},\text{Fe})\text{Si}_2\text{O}_6$ , the average composition for clinopyroxene in the concretion boundary of PPP-30 is  $\text{Di}_{50}\text{Hd}_{50}$ . The average compositions of core-region clinopyroxene in this sample and PPP-5c are  $\text{Di}_{30}\text{Hd}_{70}$  and  $\text{Di}_{20}\text{Hd}_{80}$  respectively.

The presence of clinopyroxene in the medium grade-assemblage is limited to sample PCR-23a (Fig. 4.5), where it represents a significant proportion of this concretion (~5%). Composition varies greatly in this sample with no clear correlation between composition and position relative to the concretion margin. Clinopyroxene in the concretion core shows the greatest intra-grain compositional variability, ranging from

$\text{Di}_{10}\text{Hd}_{90}$  to  $\text{Di}_{60}\text{Hd}_{40}$ , giving an average idealized formula of  $\text{Ca}(\text{Fe}_{0.6}\text{Mg}_{0.4})\text{Si}_2\text{O}_6$ .

Analyses near the outer-core region and the concretion rim in PCR-23a show identical average composition of  $\text{Ca}(\text{Mg}_{0.5}\text{Fe}_{0.5})\text{Si}_2\text{O}_6$ , with  $X_{\text{Di}}X_{\text{Hd}}$  varying < 0.2 from the mean.

Clinopyroxene analyses in high – grade samples yield  $X_{\text{Di}}X_{\text{Hd}}$  ratios that are broadly similar to  $X_{\text{Di}}X_{\text{Hd}}$  ratios in medium and low – grade samples, with the exception of a core-region population in sample area PCR11b-4 (fig. 4.6). Clinopyroxene composition for this area averages  $(\text{Ca}_{0.6}\text{Mg}_{0.8}\text{Fe}_{0.6})\text{Si}_2\text{O}_6$ , containing roughly 50% of the Ca cations necessary for the Di-Hd solid solution. The composition is characteristic of augite, possibly forming as the product of exsolution during cooling of the SMB. Sample WL-18b shows marked (Fig. 4.7), returning average composition ratios between  $\text{Di}_{38}\text{Hd}_{62}$  for the concretion rim and  $\text{Di}_{27}\text{Hd}_{73}$  for the concretion core. Analyses of sample PCR-11b (Fig. 4.6), by contrast, yield average values of  $\text{Di}_{30}\text{Hd}_{70}$  for the outer core, and a bimodal population of  $\text{Di}_{50}\text{Hd}_{50}$  and augite with an average composition described above. No clinopyroxene has been found in the vesuvianite-bearing sample, WL-16b.

#### 4.2.3 Feldspar

All feldspar found in low-grade samples PPP-30, 5c, and 7c is albite – anorthite solid solutions of plagioclase. With the exception of sample PPP-5c, virtually every feldspar analysis at this grade yields  $\text{Ca}/(\text{Ca}+\text{Na}+\text{K}) > 0.9$ , indicating virtually pure anorthite regardless of distance from the concretion margin. Feldspar through all regions of sample PPP-30 averages An<sub>97</sub>, and average compositions range between An<sub>96</sub> - An<sub>98</sub> throughout sample PPP-5c. Sample PPP-7c, by contrast, shows systematic variation in

An content with proximity to the margin. Core compositions for PPP-7c correlate directly to PPP-30 and -5c with An<sub>99</sub>. The anorthite component in PPP-7c drops to An<sub>85</sub> in the inner concretion-rim region (Fig. 4.3), and analyses at the margin yield values ranging from An<sub>30</sub> to An<sub>83</sub>. By comparison, plagioclase in the host pelite is albite (Hart, 2006; Tobey, 2006)

The feldspar composition in medium-grade assemblages correlates broadly with low-grade compositions. Feldspar in sample PCR-23a yields anorthite components in excess of 95 % regardless of distance from the margin. Composition of feldspar in sample PCR-26b reflects both the textural complexity of the margin, and the anomalous mineralogy of the core (Fig. 4.4). Three feldspar analyses from two core regions in PCR-26b yield two plagioclases with An<sub>95</sub> and a single anorthoclase with Or<sub>28</sub>Ab<sub>72</sub>. Feldspars in the texturally complex outer margin are plagioclase, showing increasing sodium content with increased distance from the concretion core. These regions lie outside of the chlorite bundle zone described in chapter 3. Compositions from the innermost of these two regions average An<sub>34</sub>. The outermost region is the host pelite, and contains oligoclase.

Feldspar in high – grade core – assemblages is restricted to samples PCR-11b and WL-18b. Feldspar in sample WL-16b is found only in the inner rim. Composition in high – grade assemblages is characterized by bimodal, relatively pure end members and homogenous distribution of these end-members throughout the core and rim regions with little correlation to distance from margin (Fig. 4.7). Anorthite, albite, and orthoclase rich end-members, > 90 % in each case, comprise feldspar compositions in the core and concretion rim region of sample WL-18b. Analyses of feldspars in the outer core region

yield both  $\text{An}_{98}$  and  $\text{Or}_{98}\text{Ab}_2$ . The outer margin, 10 mm from the host lithology, contains both plagioclase and potassium-feldspar averaging  $\text{An}_{92}$  and  $\text{Or}_{98}\text{Ab}_2$  respectively.

#### 4.2.4 Chlorite

As described in chapter 3, concretion margins are demarcated by distinct radiating bundles or wheat-sheaf aggregates of tabular chlorite that are distinguishable at all metamorphic grades. Where this distinct morphology of chlorite is not present, replacement textures after chorite indicate progressive metamorphic overprinting. Clinopyroxene porphyroblasts in the chlorite – rim region of sample PCR-23a contain radial inclusion trails of chlorite. WL-18b is the only sample to contain radial bundles of coarser tabular Fe and Mg - rich amphibole in the concretion rim region, morphologically equivalent to chlorite bundles observed at lower metamorphic grade.

The solid solution of chlorite can be described by mol % clinochlore - chamosite ( $\text{Clc}_x\text{Chm}_x$ ) in the Mg – Fe solid solution series. Low-grade chlorite composition varies little with average values ranging from  $\text{Clc}_{40}\text{Chm}_{60}$  to  $\text{Clc}_{60}\text{Chm}_{40}$ . Sample PPP-5c is a notable exception with core region chlorite compositions averaging  $\text{Clc}_{25}\text{Chm}_{75}$ .

Chlorite in medium-grade assemblages has significantly lower Mg-content , ranging from  $\text{Clc}_{37}\text{Chm}_{63}$  to  $\text{Clc}_{40}\text{Chm}_{60}$  for sample PCR-26b with lower Mg compositions occurring nearest the concretion core. Chlorite in the core of sample PCR-23a averages even lower Mg, with  $\text{Clc}_{26}\text{Chm}_{74}$ .

Chlorite does not form a significant portion of the concretion-core assemblage in high-grade samples. Sample WL-18b is the only high-grade sample containing chlorite in the core region, yielding a single compositional analysis of  $\text{Clc}_{70}\text{Chm}_{70}$ . Chlorite in the

concretion – rim regions of WL-16b and PCR-11b yield compositions of  $\text{Clc}_{56}\text{Chm}_{44}$  and  $\text{Clc}_{48}\text{Chm}_{52}$  respectively. Chlorite in sample WL-16b is rare and likely retrograde.

#### 4.2.5 Prehnite

Prehnite is observed in the concretion – core mineralogical zone of samples PCR-11b and WL-16b, with virtually identical chemical compositions. The general chemical formula  $\text{Ca}_2(\text{Al},\text{Fe}^{3+})(\text{AlSi}_3\text{O}_{10})(\text{OH})_2$  shows the substitution of ferric iron and aluminum. In spite of this, analyses of prehnite in the study area yield negligible Fe content, and sufficient Al cations pfu to satisfy the ideal chemical formula  $\text{Ca}_2\text{Al}(\text{AlSi}_3\text{O}_{10})(\text{OH})_2$ .

#### 4.2.6 Vesuvianite

Among the studied samples, vesuvianite is restricted to a single outcrop from Ravenscraig subdivision in the Williams Lake area from which sample WL-16b was collected. The general chemical formula for vesuvianite,  $\text{Ca}_{19}(\text{Al},\text{Fe})_{10}(\text{Mg},\text{Fe})_3[\text{Si}_2\text{O}_7]_4[\text{SiO}_4]_{10}(\text{O},\text{OH},\text{F})_{10}$ , involves the substitution of  $\text{Fe}^{3+}$  for Al, in addition to  $\text{Fe}^{2+}$  for Mg. Despite this, analyses of vesuvianite from WL-16b yield an average total Fe content of only 1.54 cations pfu (74 oxygens). Mg content is similarly low with 1.18 cations pfu. Calculations were based on 74 oxygens to approximate fixed number of Ca and Si cations. No samples included in this study were analyzed for fluorine.

#### **4.3 Whole Rock and Trace Element Geochemistry**

X-ray fluorescence spectrometry was performed on a number of concretion samples from each region of the study area to assess variations in bulk composition REE concentration. Raw data (appendix 4) indicate elevated levels of both Ca and Mn in concretion cores, relative to the surrounding pelite. Core depletions in S, K, Ti, Sr, Rb, and Zr, relative to the host, are also noted. Surprisingly, Fe content, relative to the host rock, varies between sample locations, and shows trends of enrichment and depletion in the cores of different samples. Sample PCR-11 shows strong Fe-depletion in the core. However, Fe-concentration in the cores of samples PPP-7c, PCR-18, and WL-20b show varying degrees of enrichment relative to their host rocks.

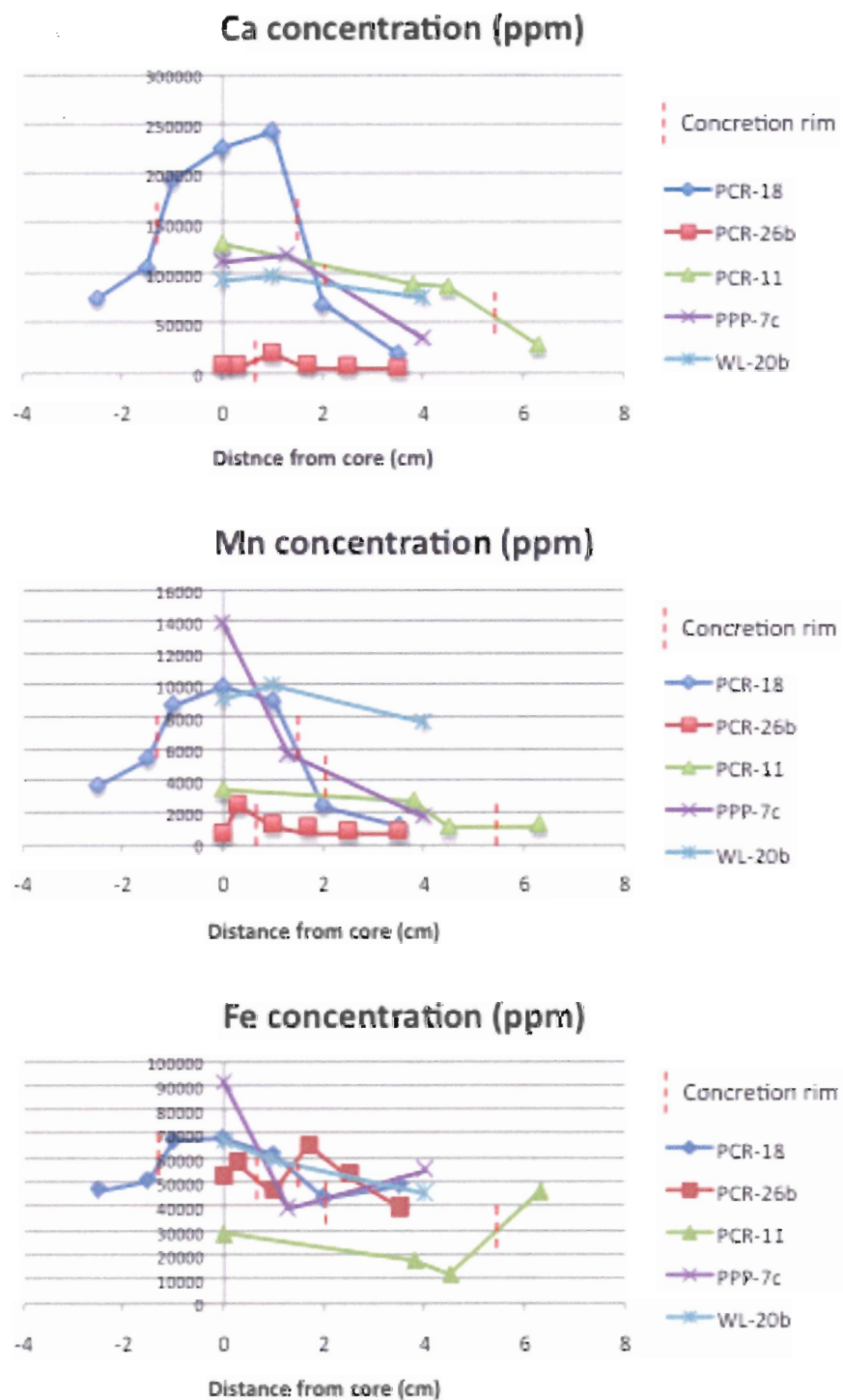


Figure 4.1 XRF data plots of Ca, Mn, and Fe concentration (ppm) relative to distance from concretion core (0 cm)

#### **4.4 Summary**

Variations in relative composition of major solid solution phases reflect equilibration at varying T-X conditions and, possibly, varying bulk compositions. Low-grade garnet shows a great deal of compositional heterogeneity, primary as a function of distance from the concretion margins. Low-grade core-assemblage plagioclase is, exclusively, almost pure anorthite. Core-region garnet compositions homogenize with increasing grade, becoming increasing Ca-rich. Feldspar, by contrast, develops bi- and tri-modal pure end-member populations with increasing grade, suggesting exsolution. Core-assemblage clinopyroxene in medium and low-grade samples predominantly yield  $X_{\text{Hd}} > X_{\text{Di}}$ , consistent with the Fe-enrichment trends shown in independent XRF analyses.

**Figure 4.2 PPP-30**

Standard thin section (30 µm thick) showing relative analysis locations on corresponding polished section. EMP data for garnet, clinopyroxene, and feldspar are colour-coded to analysis locations (coloured boxes) shown below. Area label corresponds to EMP data-point numbering scheme. (Appendix 1)

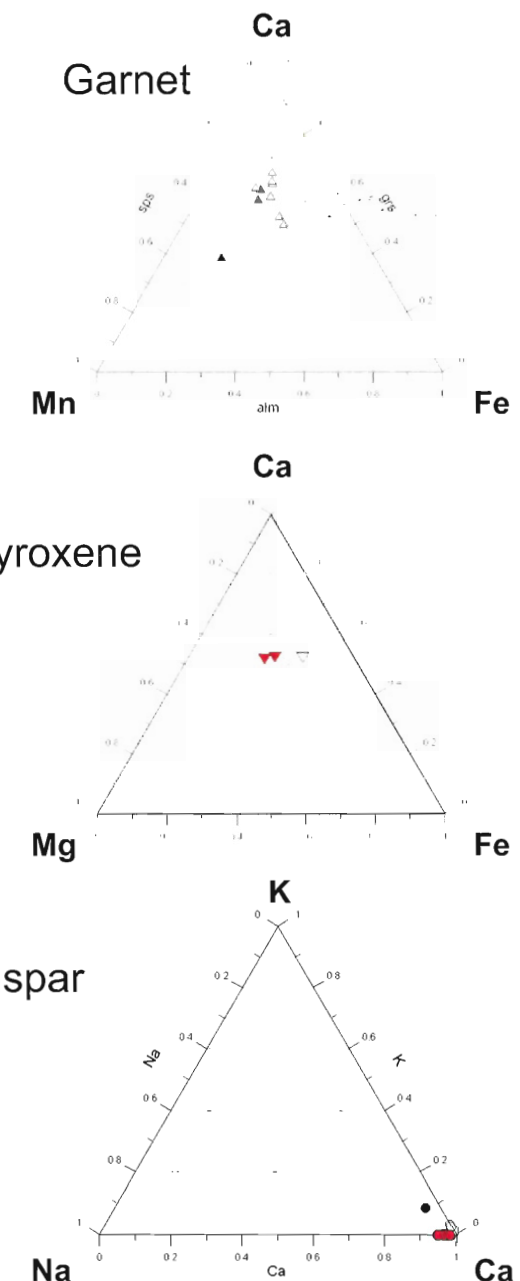
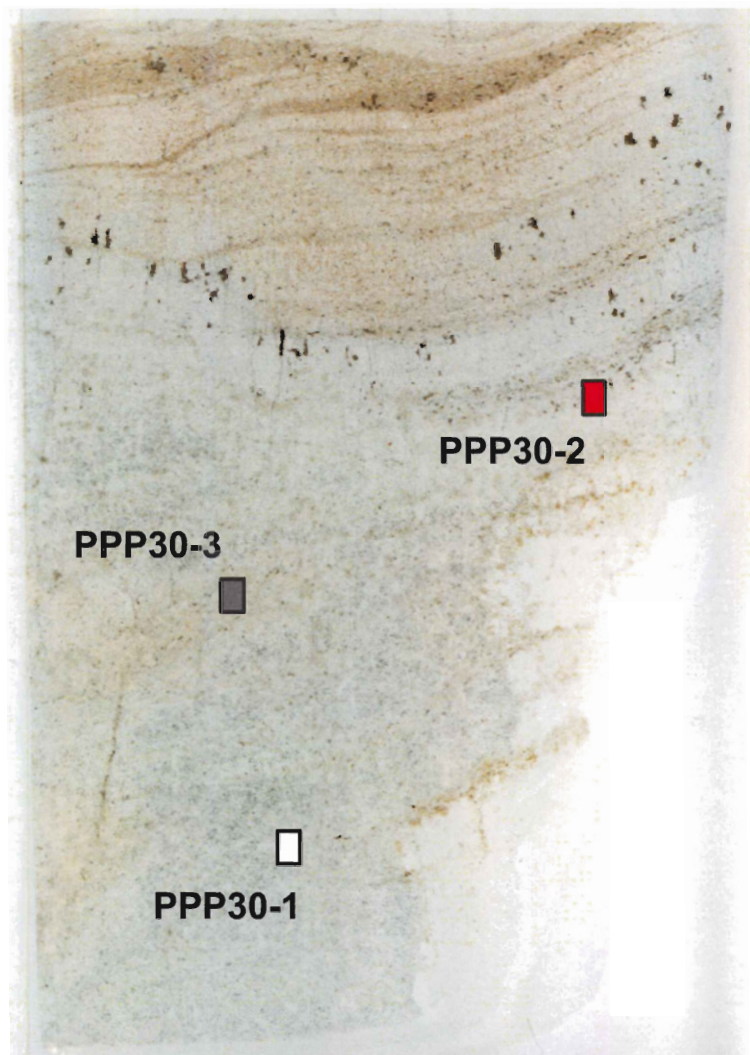
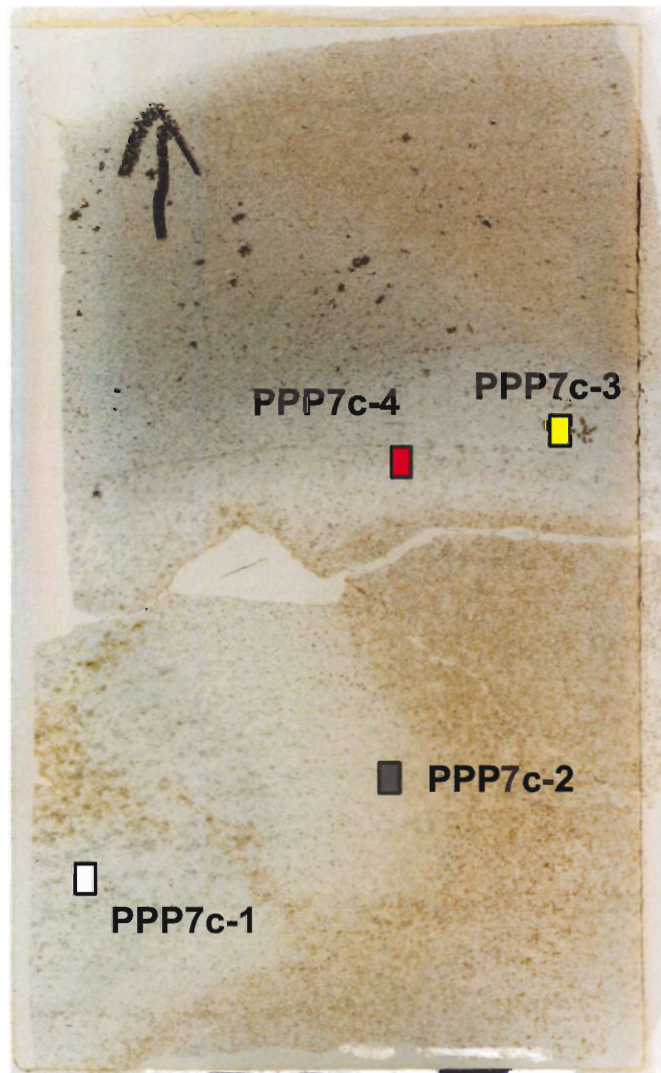


**Figure 4.3 PPP-7c**

Standard thin section (30 µm thick) showing relative analysis locations on corresponding polished section. EMP data for garnet and feldspar are colour-coded to analysis locations (coloured boxes) shown below. Area label corresponds to EMP data-point numbering scheme. (Appendix 1)



48

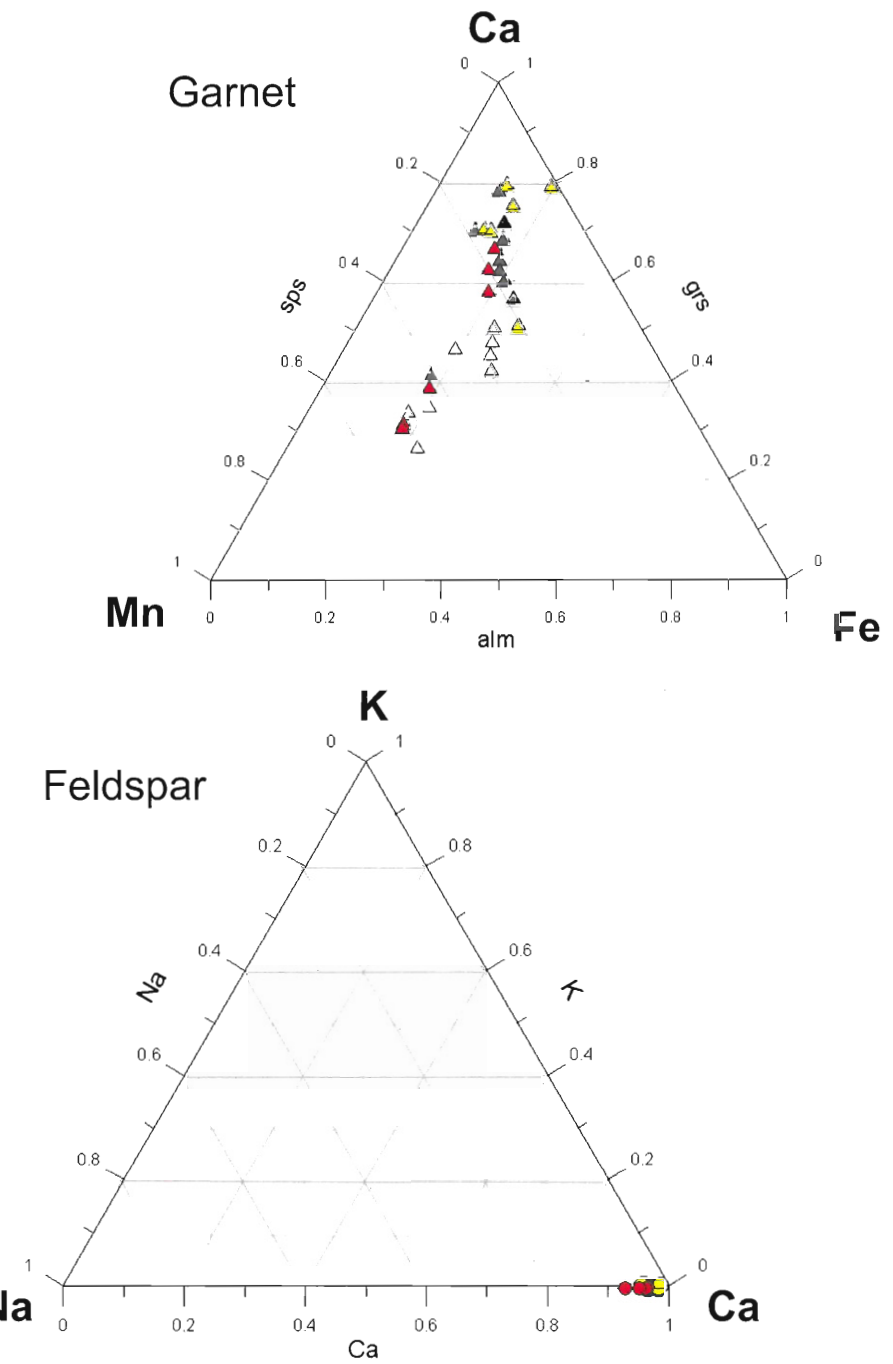


**Figure 4.4 PPP-5c**

Standard thin section (30 µm thick) showing relative analysis locations on corresponding polished section. EMP data for garnet, clinopyroxene, and feldspar are colour-coded to analysis locations (coloured boxes) shown below. Area label corresponds to EMP data-point numbering scheme. (Appendix 1)

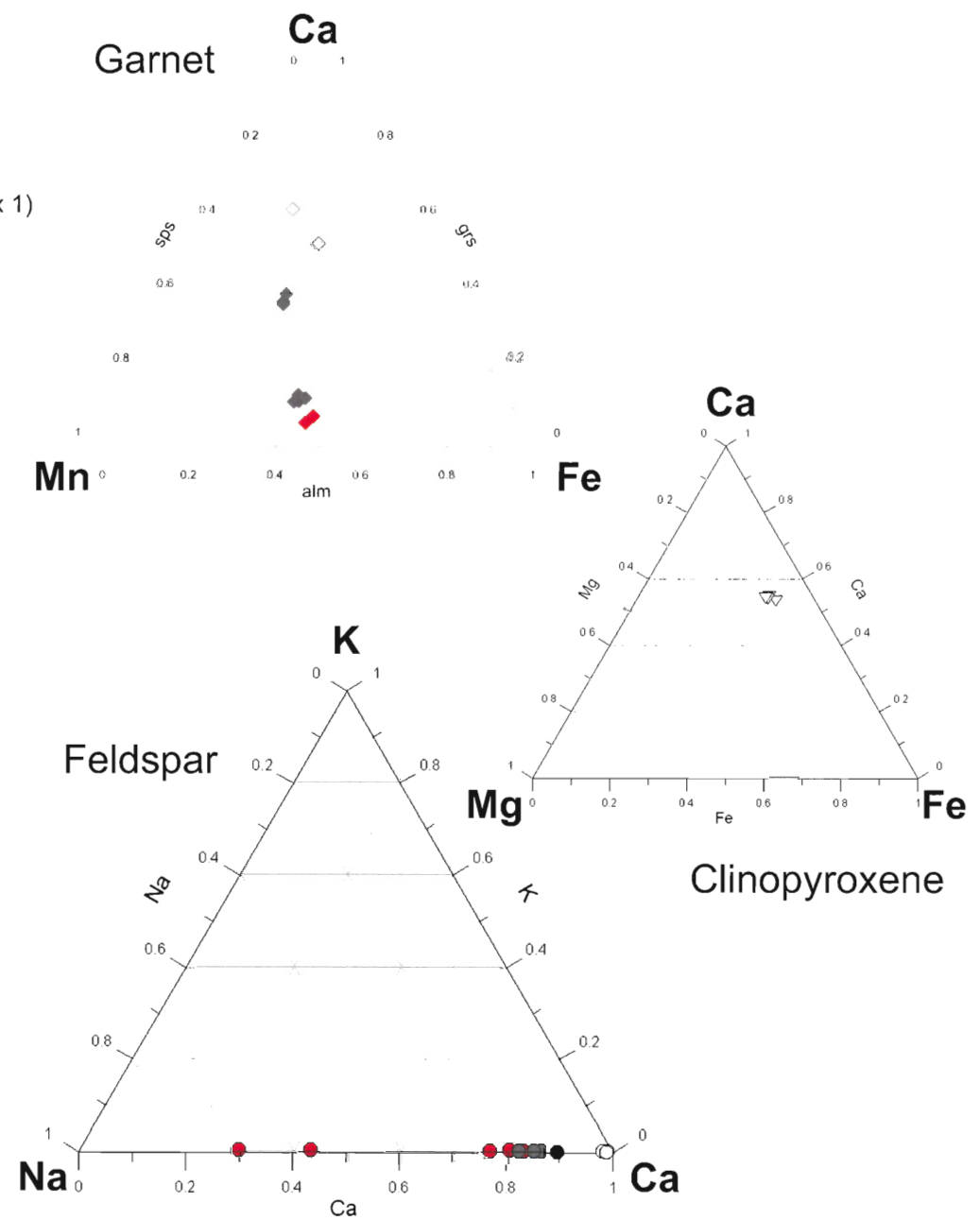
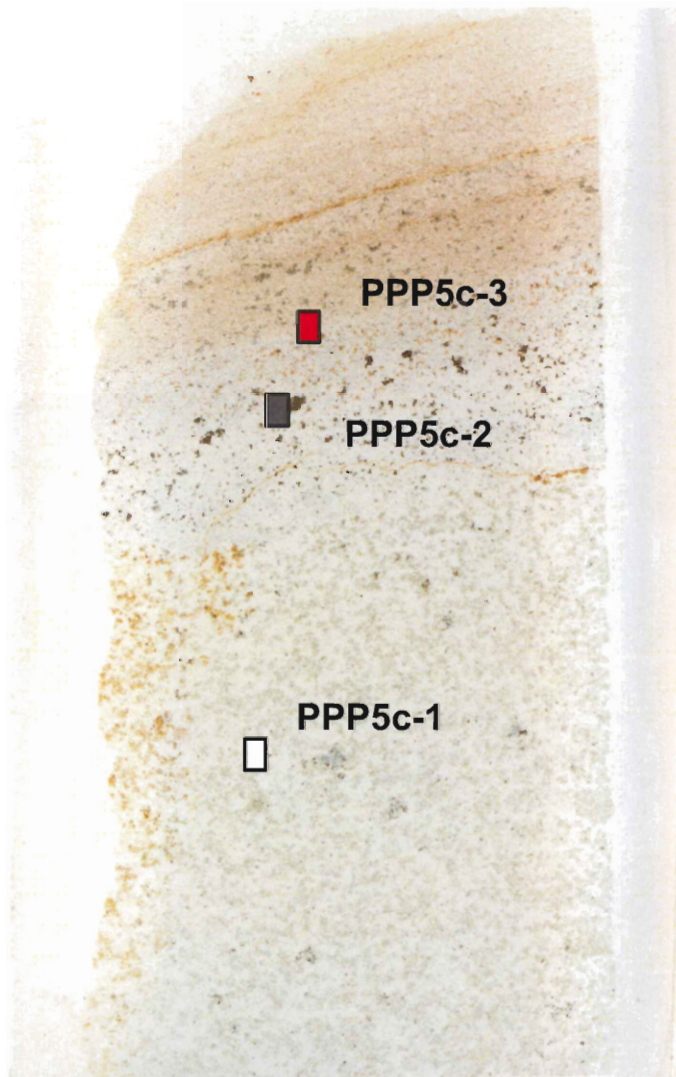


**Figure 4.5 PCR-26b**

Standard polished section showing analysis locations. EMP data for garnet and feldspar are colour-coded to locations (coloured boxes) shown below. Data from the hollow red box are not applicable to ternary plots. Area label corresponds to EMP data-point numbering scheme. (Appendix 1)

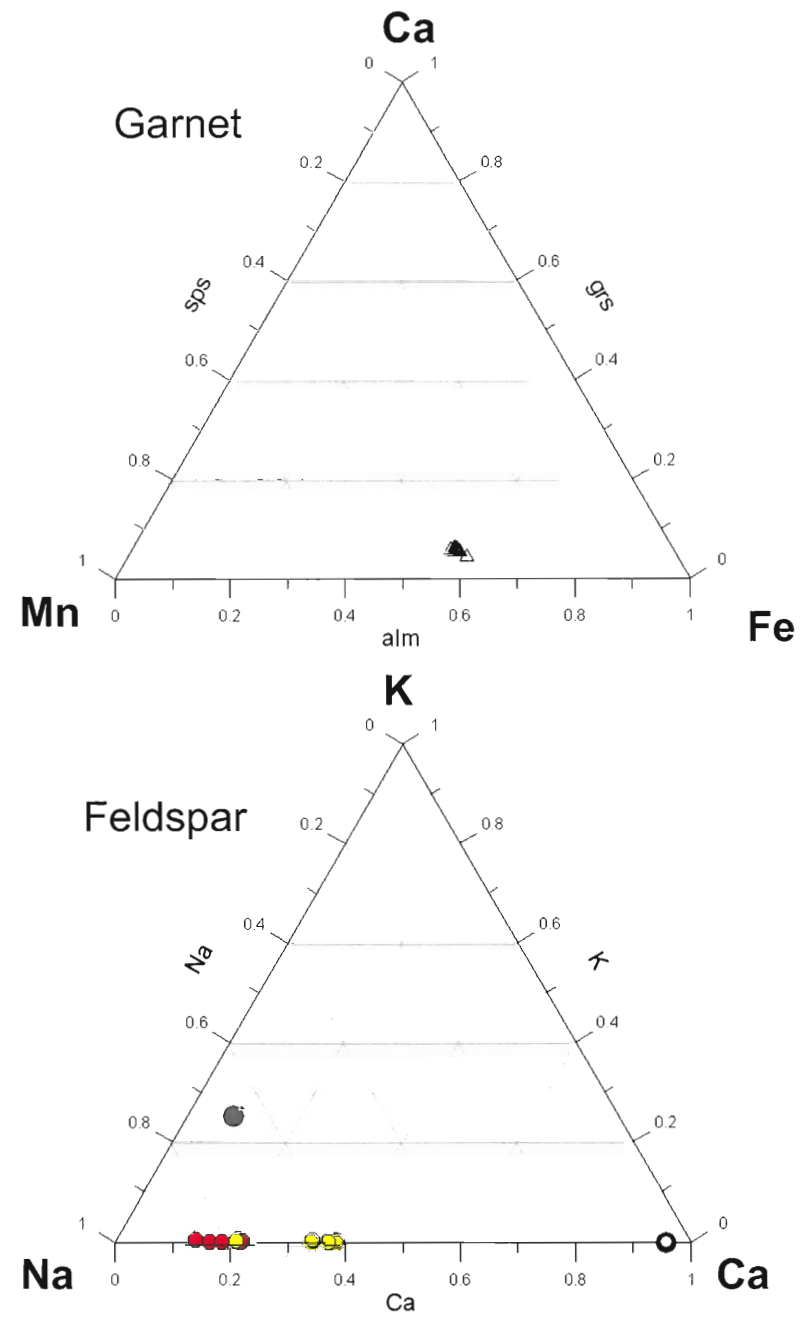
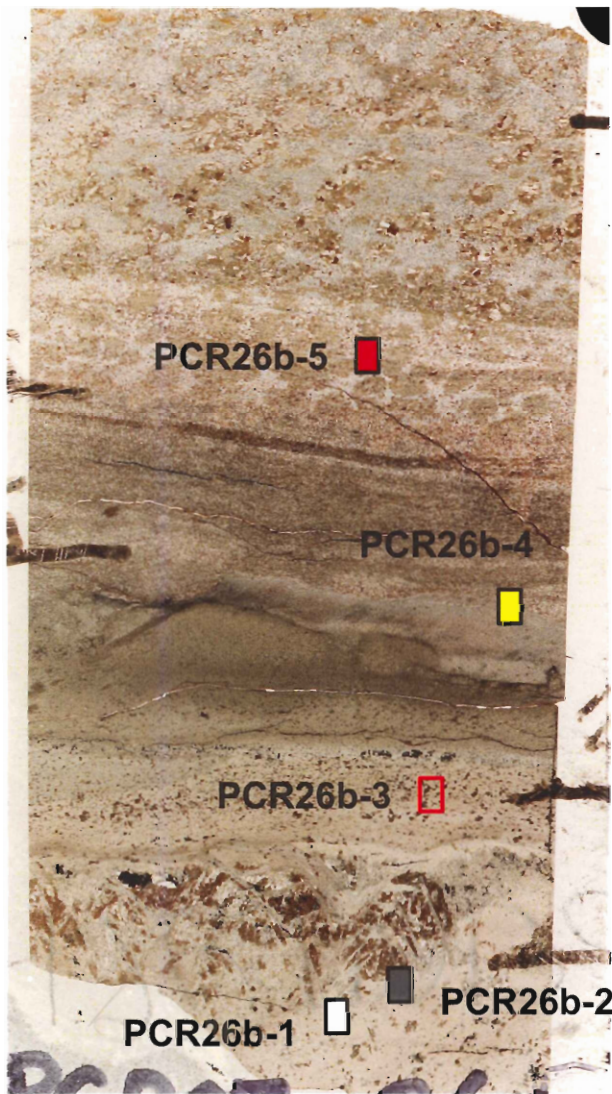


**Figure 4.6 PCR-23a**

Standard polished showing analysis locations. EMP data for clinopyroxene and feldspar are colour-coded to locations (coloured boxes) shown below. Area label corresponds to EMP data-point numbering scheme. (Appendix 1)

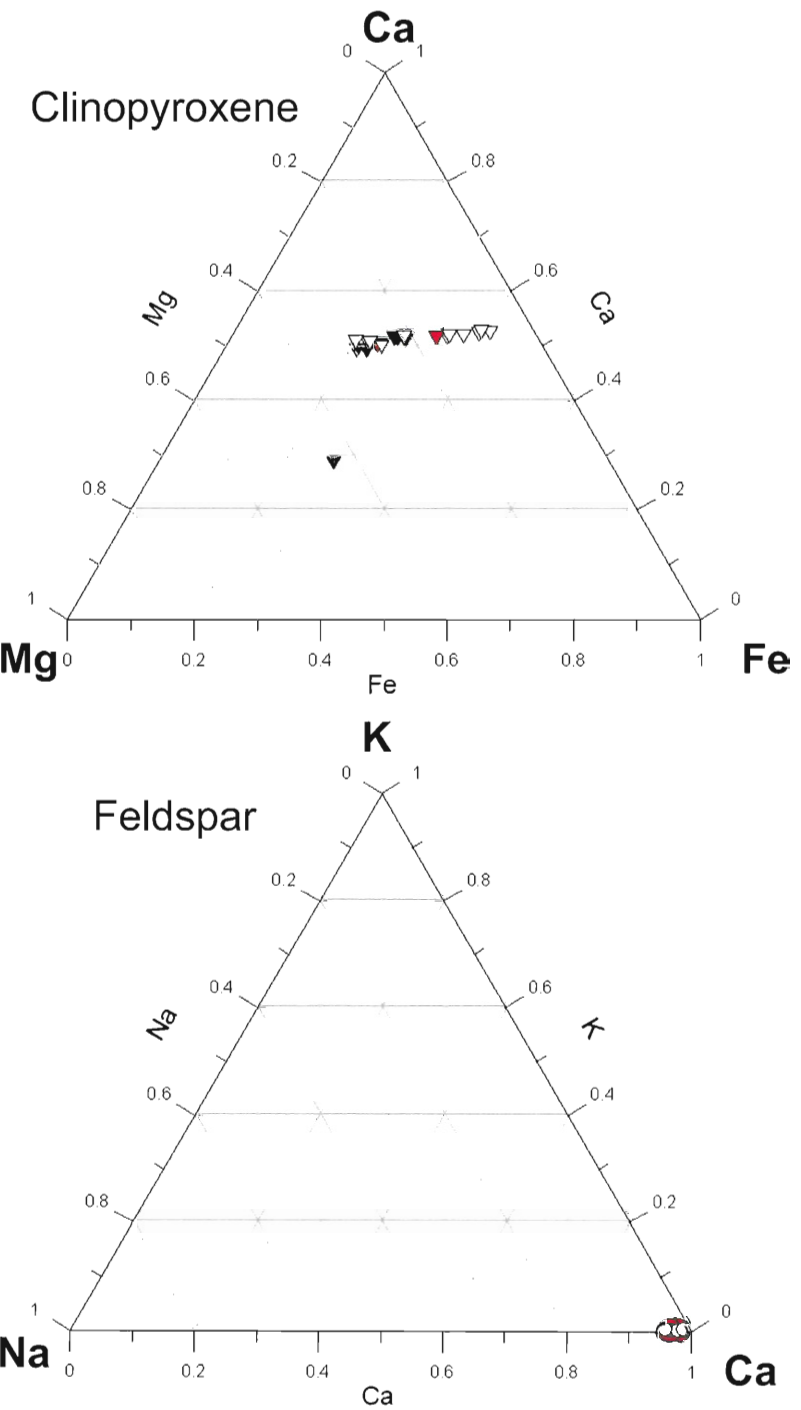
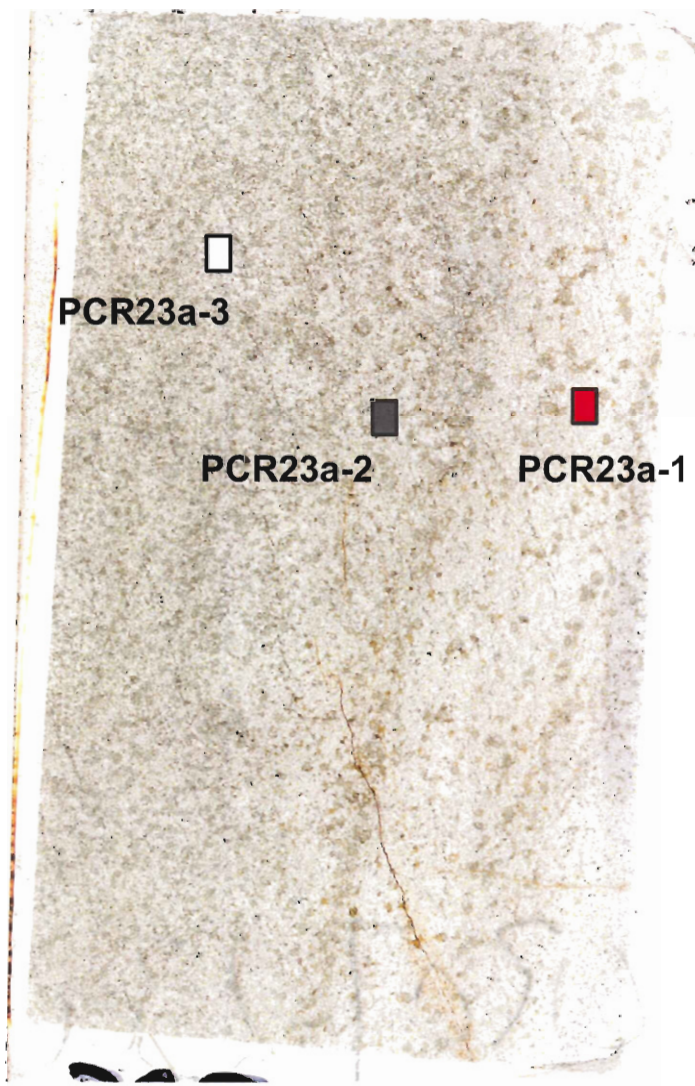


**Figure 4.7 PCR-11b**

Standard polished showing analysis locations. EMP data for garnet, clinopyroxene, and feldspar are colour-coded to locations (coloured boxes) shown below. Area label corresponds to EMP data-point numbering scheme. (Appendix 1)

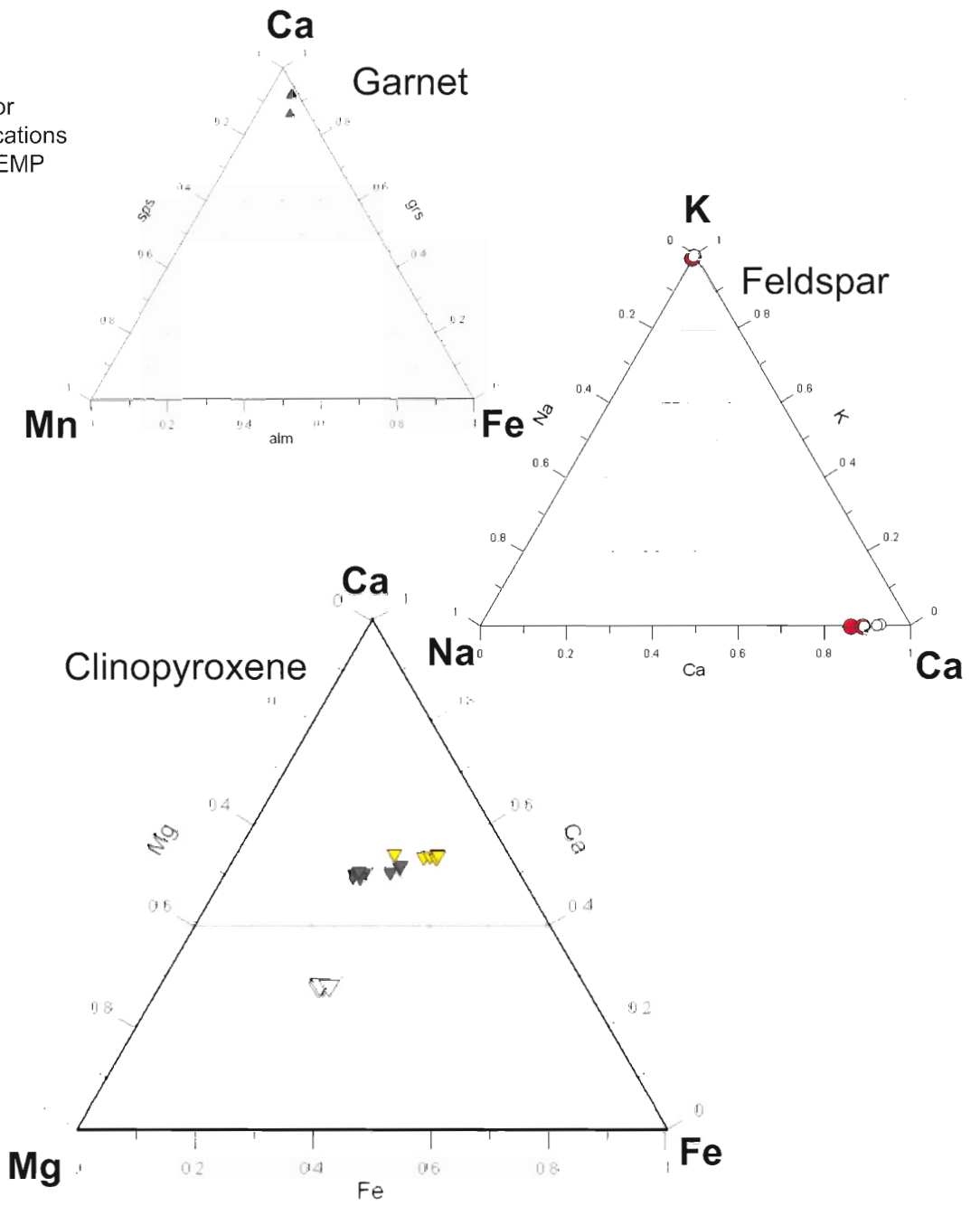
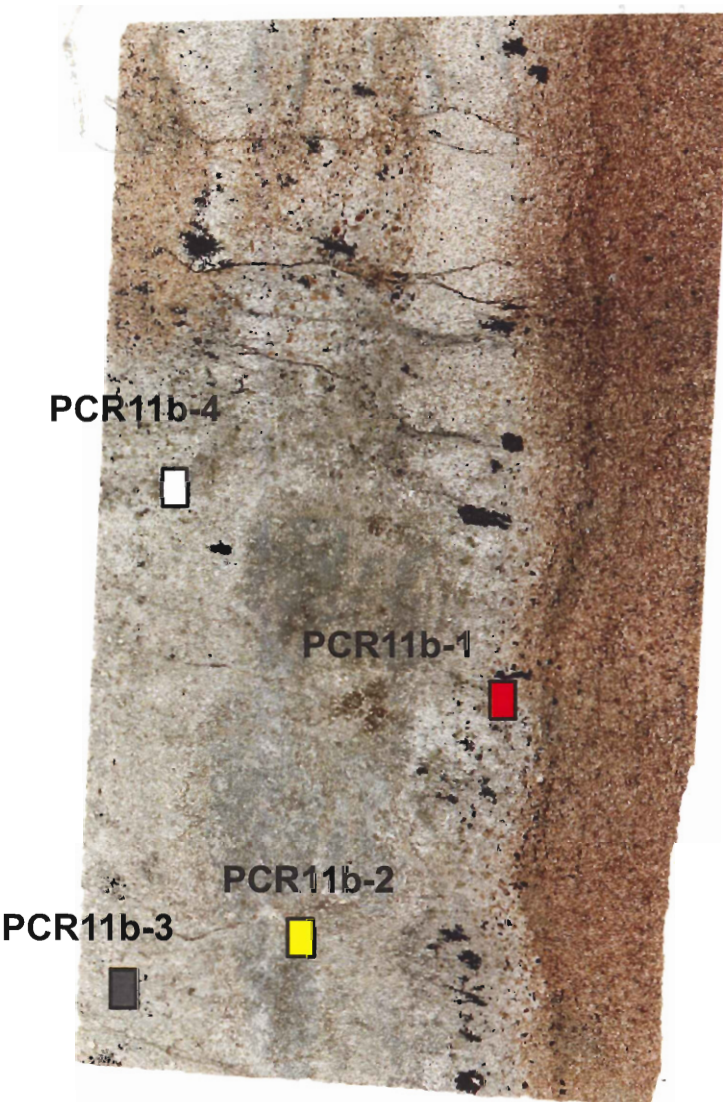


**Figure 4.8 WL-18b**

Standard polished section showing approximate analysis locations. EMP data for garnet, clinopyroxene, and feldspar are colour-coded to locations (coloured boxes) shown below. Area label corresponds to EMP data-point numbering scheme. (Appendix 1)

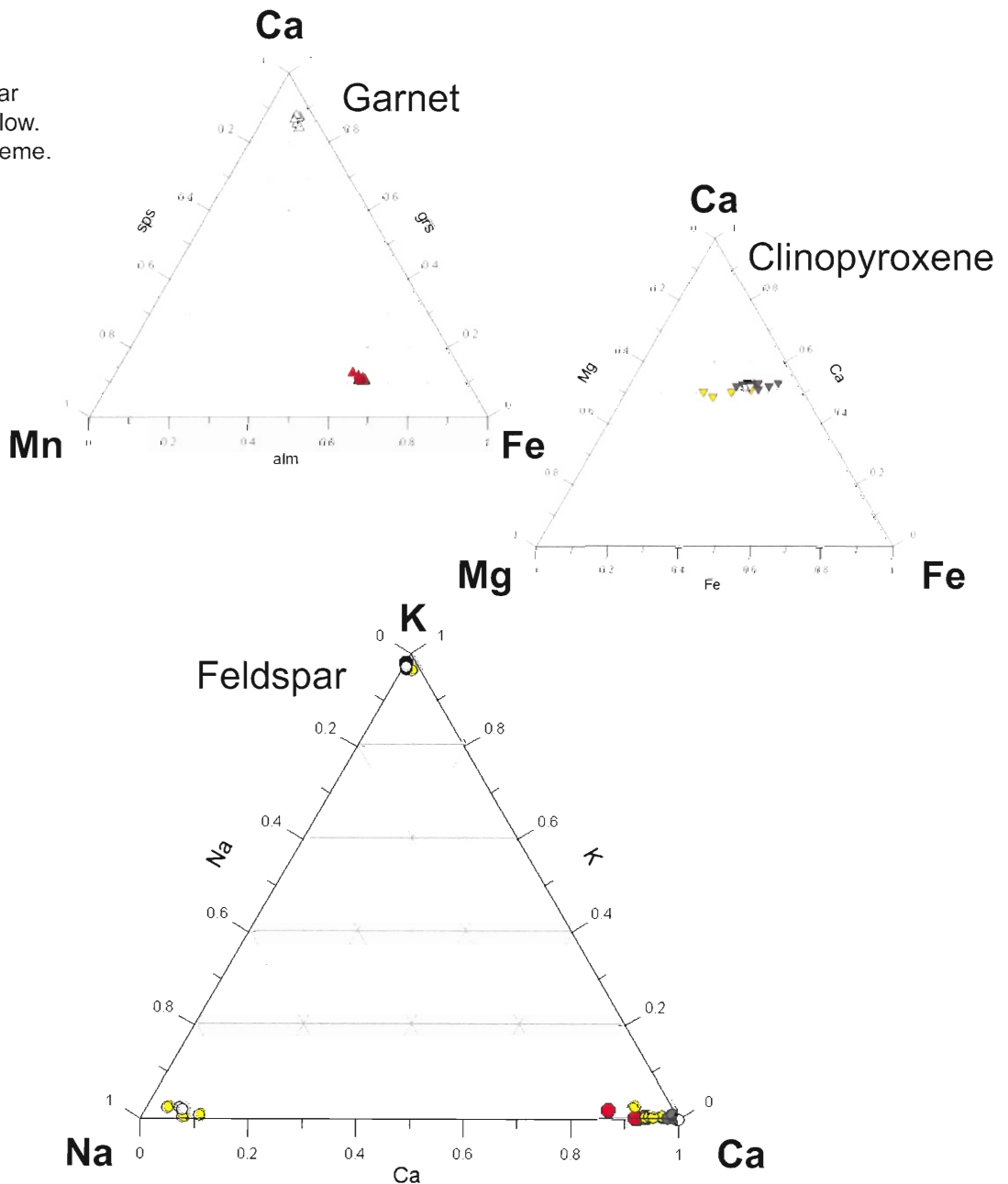
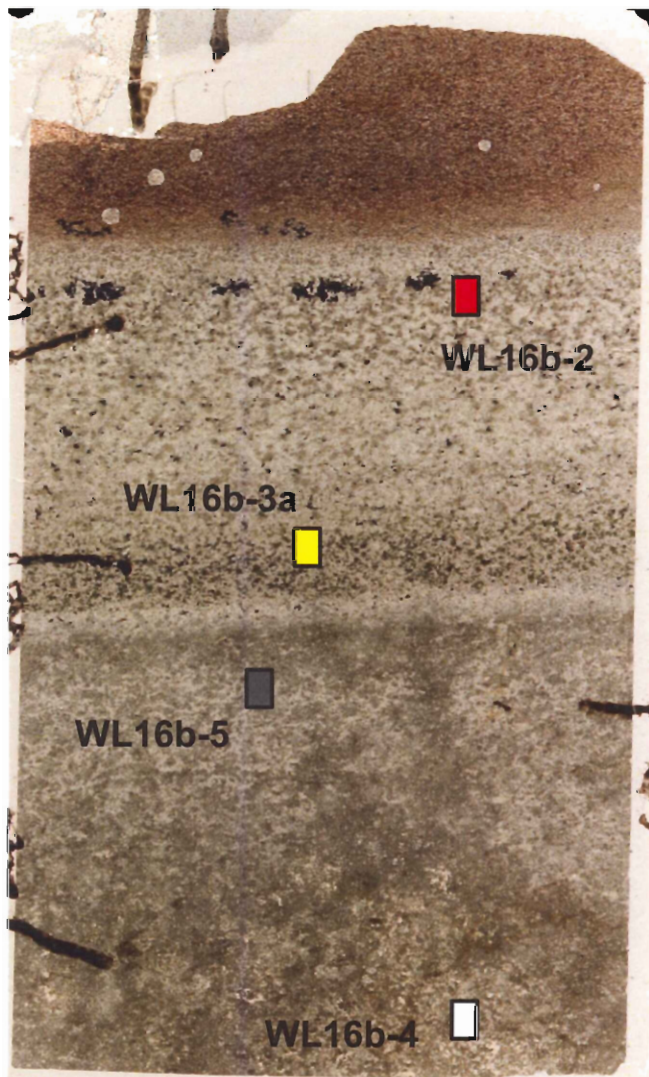
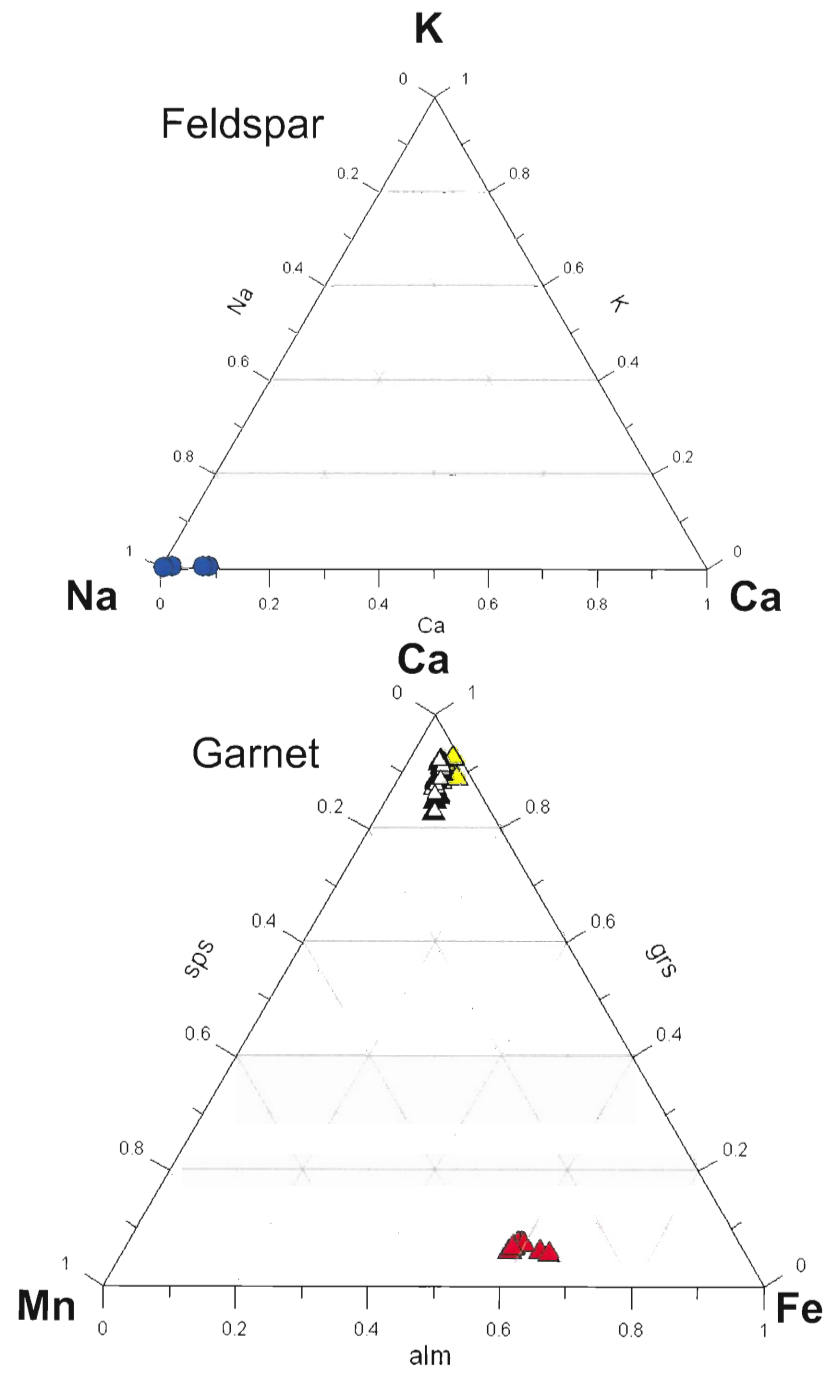
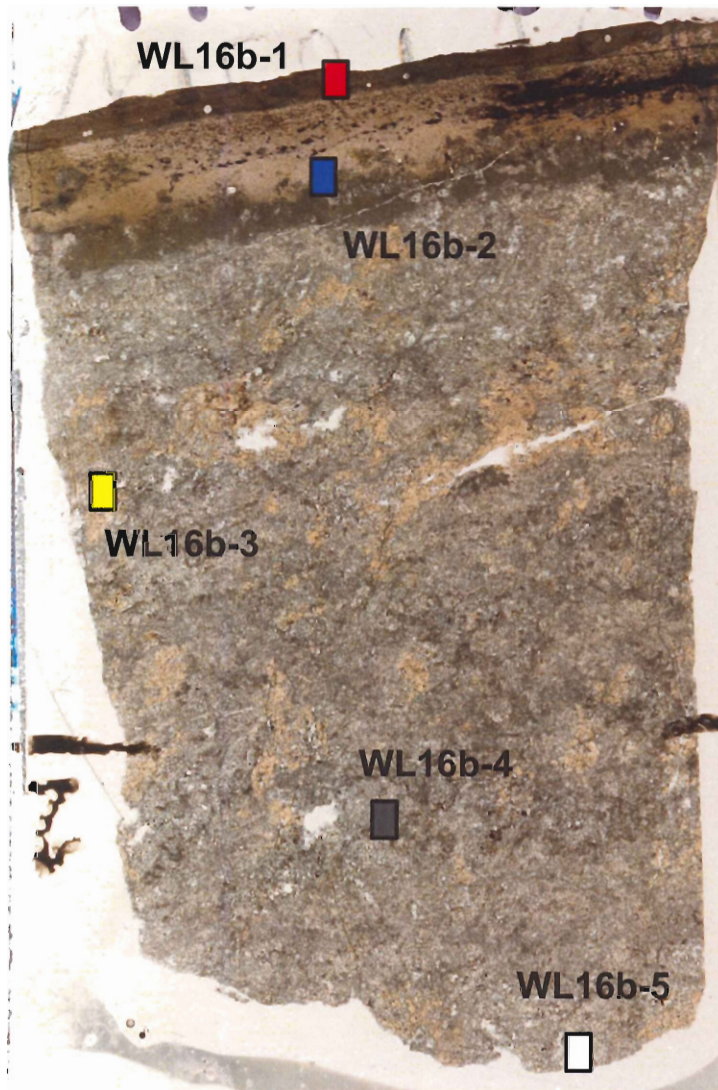


**Figure 4.9 WL-16b**

Standard polished section showing approximate analysis locations. EMP data for garnet is colour-coded to locations (coloured boxes) shown below. Area label corresponds to EMP data-point numbering scheme. (Appendix 1)



## Chapter 5

### PETROLOGY

#### **5.1 Introduction**

Metamorphic mineral assemblages are the product of geochemical reactions progressing toward thermodynamic equilibrium under given P-T conditions for a given bulk composition. The mineralogically zoned calcareous concretions of the Bluestone formation have developed contact metamorphic assemblages and textures primarily as a function of distance across an isobaric thermal gradient. In addition to temperature, the main factors controlling the mineral assemblages observed are bulk composition, chemical potential gradient (e.g. core-rim-boundary mineralogical zones), and fluid composition. Due to the limited size of the concretions, a working hypothesis assumes the H<sub>2</sub>O-rich pelitic host rock externally buffers calcareous and calc-silicate reactions, maintaining a X<sub>CO<sub>2</sub></sub> < 0.1. The program WinTWQ v. 2.36 (Berman, 2007), was used to calculate and plot potential equilibration reactions in P-T and T-X<sub>CO<sub>2</sub></sub> space based on observed mineral assemblages from each metamorphic grade. Only the core mineral assemblages are considered.

#### **5.2 Metamorphic Conditions**

The program WinTWQ calculates P-T and T-X plots for all possible equilibria reactions for a given mineral assemblage. P-T plots calculate reaction curves based on given X<sub>CO<sub>2</sub></sub>, generally 0. Similarly, T-X plots calculate reaction curves for a set pressure as a function of temperature and X<sub>CO<sub>2</sub></sub>. Thus, independent estimates of P-T-X conditions are necessary to infer reactions for the assemblage in question.

Mahoney (1996) estimated pressures of contact metamorphism ranging from 3.5 to 3.8 kb for the eastern margin of the South Mountain Batholith. Estimates for pressure used in this study follow Hart (2006), who estimated P-T conditions across the contact aureole in the Bluestone formation specifically associated with mineral isograds defined by the first appearance of biotite and andalusite at 3 kb. Hilchie & Jamieson (2008) applied a graphite geothermometer calibrated for the temperature-dependant change in Raman spectra of carbonaceous material to samples along a transect of the Halifax contact aureole. Isotherms derived from that study (fig. 5.1) parallel mineral isograds from Hart (2006)(fig. 1.1, 5.1). The 600°C isotherm runs 50 – 100 m above the andalusite-2 isograd, indicating peak T for all medium- to high-grade metamorphic assemblages in the study area lie close to or above 600°C. The 500°C isotherm runs parallel to and 300 m SW of the biotite-in isograd. All low-grade samples included in this study fall within the biotite-in isograd, close to and above the 500°C isotherm, indicating peak T of all low-grade metamorphic mineral assemblages is  $\geq 500^{\circ}\text{C}$ .

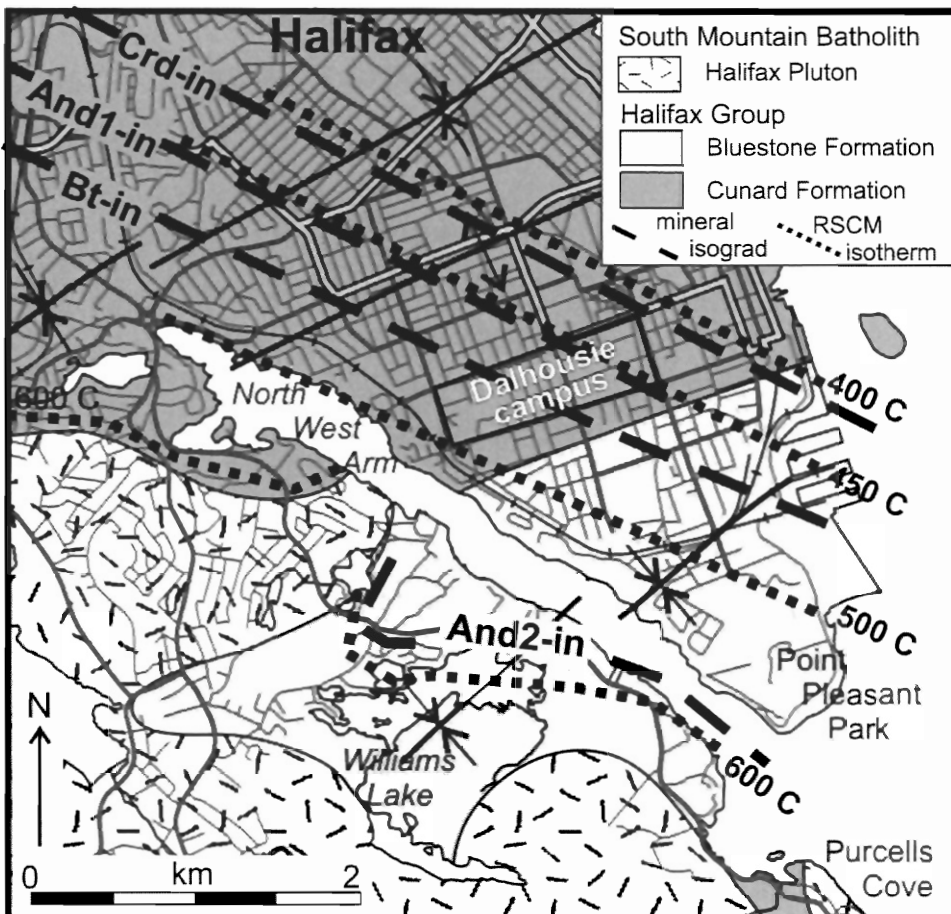


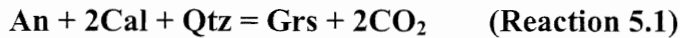
Figure 5.1 Geological map of Halifax showing metamorphic isograds formed during contact metamorphism of the Halifax Group, with isotherms determined by Raman spectroscopy of graphite (RSCM). (Jamieson et al., 2011)

### 5.3 Progressive Metamorphism

#### 5.3.1 Low-Grade

Samples collected from the eastern shore of Point Pleasant Park are defined by the assemblage An + Qtz + Cal + Grs, with rare clinopyroxene and epidote. Apatite, optically indistinguishable from the fine-grained matrix, is interpreted to be detrital, given the abundance of detrital apatite in the host metasandstone-siltstone.

Ca-rich garnet is largely an interstitial phase in low-grade assemblages, forming thin films between porphyroblastic anorthite and calcite. Garnet coarsens dramatically upgrade (westward across the study area) coinciding with the rapid disappearance of calcite, suggesting the reaction:



The T-X plot of reaction 5.1 (Fig. 5.2) shows the effect of high  $X_{\text{CO}_2}$  on the stability of grossular. All concretion samples included in this study lie above the bt-in isograd inferred from RCSM (Hilchie and Jamieson, 2008) to be  $\approx 450^\circ\text{C}$ , indicating equilibration of grossular at  $X_{\text{CO}_2} < 0.05$

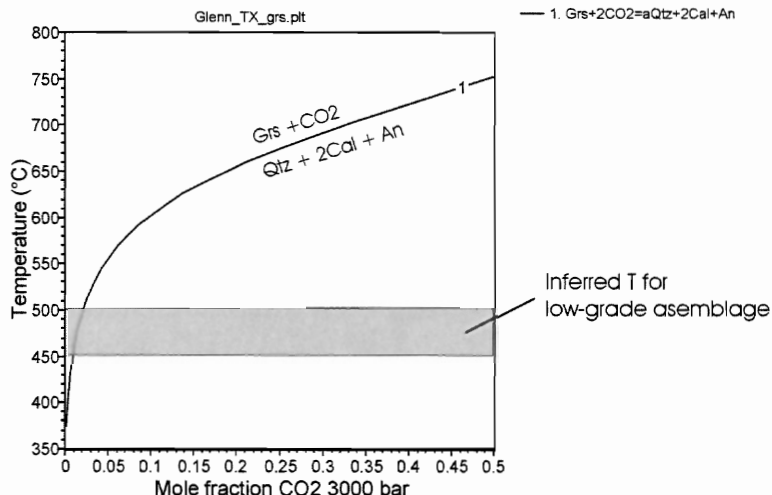


Figure 5.2 A T-X plot showing the stability of garnet in low grade assemblages as a function of temperature and  $X(\text{CO}_2)$ . Reaction calculated for 3 kb.

### 5.3.2 Medium-Grade

Sample PCR-23a, from the Bluestone Quarry, is anomalous for the lack of garnet, and predominance of clinopyroxene porphyroblasts. WinTWQ T-X plots for reactions involving the assemblage  $\text{Di} + \text{Grs} + \text{An} + \text{Clc}$  (Chlorite) +  $\text{Qtz}$  (calcite is assumed to be present in the pre-contact metamorphic assemblage) at 3kb (Fig. 5.2) demonstrate that

grossular is stable in higher T assemblages than clinopyroxene. Neither calcite or grossular are present in the assemblage at PCR-23a, likely reflecting a different, Al-poor bulk composition, or higher  $X_{CO_2}$ . If  $X_{CO_2}$  is in fact high enough, then the following reaction may be responsible for the assemblage at PCR-23a:

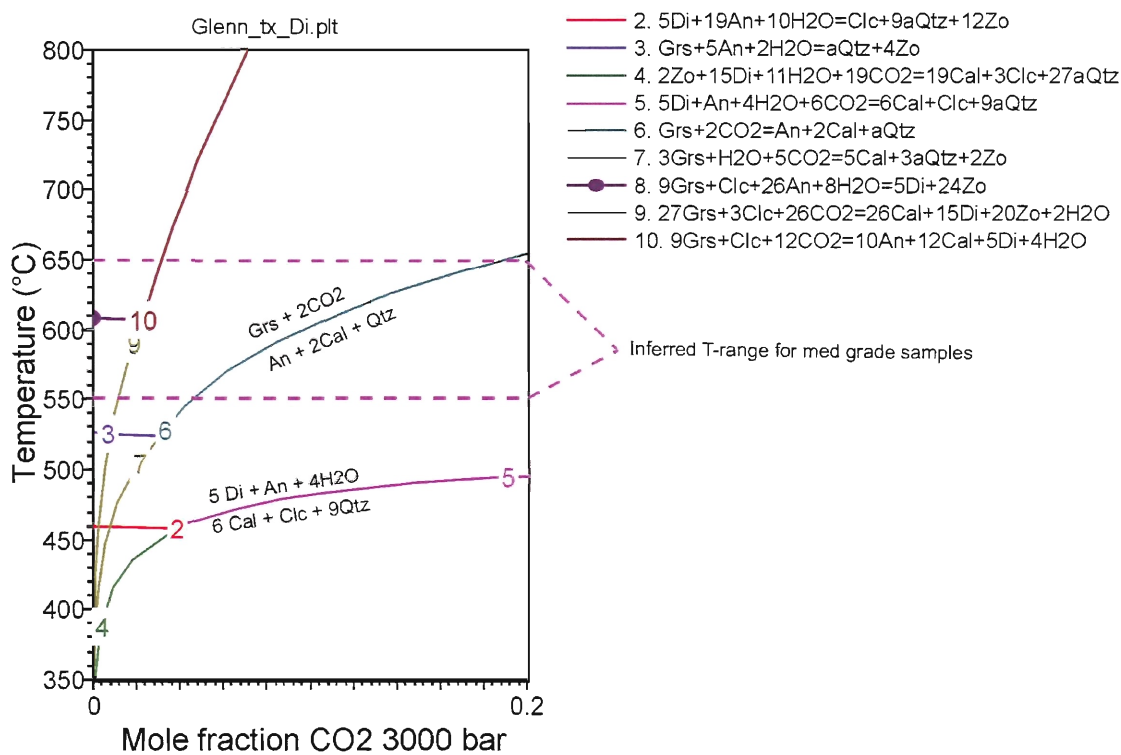


Figure 5.3 T-X plot showing potential reactions involving the medium-grade assemblage. Reactions for grossular are included to demonstrate disparity in thermal stability. Maximum  $X(CO_2) = 0.2$

Based on the reactions responsible for the generation of aluminum silicates, mica, and cordierite in pelitic host rocks, Hart (2006) estimated the equilibration temperature for the andalusite-in isograd in the Bluestone formation west of the Northwest Arm, to be 560°C at 3 kb. This is consistent with independent estimates for  $T \approx 600^\circ C$  near the contact (Hilchie and Jamieson, 2008).

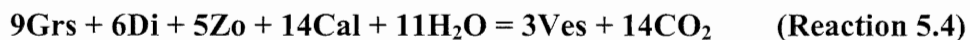
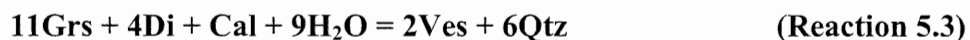
### 5.3.3 High-Grade

Calculations of P-T conditions based on mineral composition data from a given rock rely on the identification of an equilibrium assemblage. The use of low-grade concretion core assemblages is limited by the lack of distinct, identifiable equilibrium assemblages based on textural criteria and compositional heterogeneity discussed in chapters 3 and 4. Medium-grade assemblages show anomalous mineral assemblages, seemingly out of sequence from higher and lower grade assemblages. Despite this, the core of sample PCR-23a shows considerable progression toward compositional and mineralogical homogeneity. High-grade assemblages show considerable progress toward peak metamorphic equilibration. Mineralogically, samples WL-18b and PCR-11b contain higher temperature phases than PCR-23a. Texturally, however, these samples are very similar to PCR-23a, suggesting little difference in the relative rate or duration of metamorphism between these samples. The outcrops for samples PCR-23a, PCR-11b and WL-18b lie ~ 400 m, 170 m, and < 20 m from the contact respectively.

Sample WL-16b, by contrast, contains well-developed peak equilibration textures in garnet that are clearly visible despite a considerable degree of retrograde alteration and replacement. The simple, well-equilibrated peak mineral assemblage consists Grs + Ves + Qtz ± Ap, Ttn. Apatite appears to be detrital. Prehnite, present only in high-grade samples, is a retrograde phase.

Vesuvianite was integrated into the 2006 WinTWQ mineral database using thermodynamic properties taken from the multi-equilibrium calculation program Thermocalc (Holland and Powell, 1988) to calculate possible reactions to prehnite as

suggested by textural evidence. Vesuvianite is a common mineral in contact metamorphic zones in limestone and impure marble, and is commonly associated with grossular, hydrogrossular, diopside, wollastonite, and other moderate to high temperature calc-silicates (Deer et al., 1982). From thermodynamic equilibrium calculations in the CaO-MgO-Al<sub>2</sub>O<sub>3</sub>-SiO<sub>2</sub>-H<sub>2</sub>O-CO<sub>2</sub> system by Valley et al., (1982) two possible reactions for the formation of vesuvianite from the mineral assemblage identified in this study are:



A schematic T-X(H<sub>2</sub>O-CO<sub>2</sub>) plot of the CaO-MgO-AL<sub>2</sub>O<sub>3</sub>-SiO<sub>2</sub>-H<sub>2</sub>O-CO<sub>2</sub> system stability fields (Valley, 1982) illustrates the high H<sub>2</sub>O-dependence of vesuvianite stability. Reaction 5.2 and 5.3 correspond to curves 6 and 11, the latter terminating at invariant point IV, the highest X<sub>CO<sub>2</sub></sub> ( $\cong 0.11$ ) value at which vesuvianite is stable at pressures 1 - 4 kb. However, these calculations are based on vesuvianite stability in an Fe-free system. However, vesuvianite analyzed in this study contains average Fe/(Fe+Mg) = 0.56. Literature addressing the X<sub>CO<sub>2</sub></sub> stability of Fe-rich vesuvianite is sparse, though Labotka et al. (1988) suggested the association of Fe<sup>3+</sup>-rich grossular and Ti-rich vesuvianite may extend the stability field of vesuvianite to higher X<sub>CO<sub>2</sub></sub> beyond the  $\sim 0.11$  limit. Labotka et al. (1988) do not offer a range constituting “substantial” amounts of Fe<sup>3+</sup> and Ti, but the core assemblage of WL-16b contains vesuvianite with average wt % TiO<sub>2</sub> = 1.7, and grossular-garnet with average wt % FeO < 3.12 (fig. 4.8), roughly 50% and 75% lower than reported TiO<sub>2</sub> and FeO values from Labotka et al. (1988), respectively.

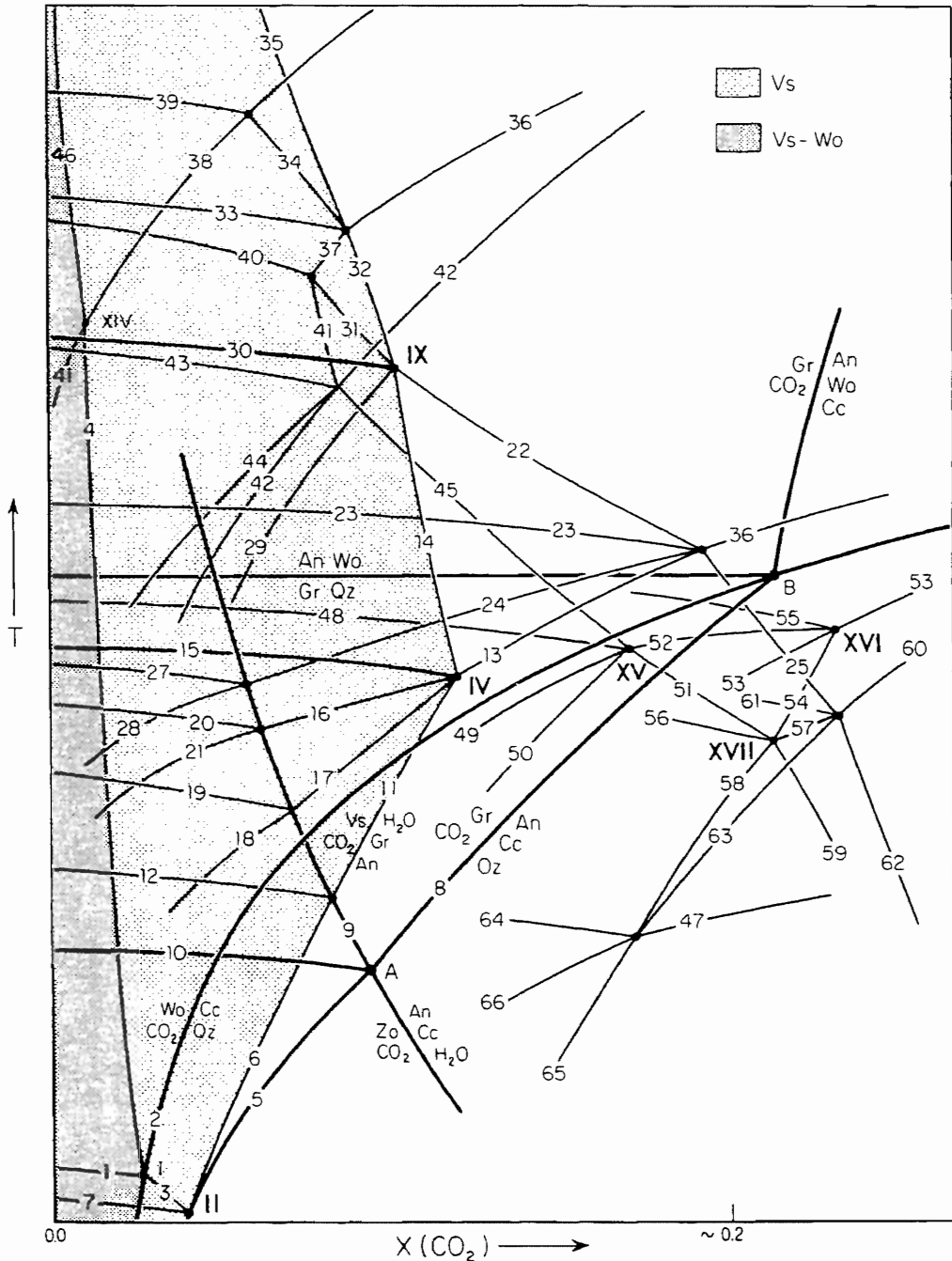
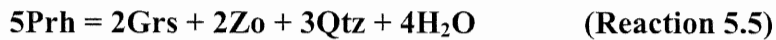


Figure 5.4 Schematic T-X( $\text{H}_2\text{O}-\text{CO}_2$ ) plots of equilibria in the system  $\text{CaO}-\text{MgO}-\text{Al}_2\text{O}_3-\text{SiO}_2-\text{CO}_2-\text{H}_2\text{O}$ . Light stipple corresponds to Mg-Ves Assemblage. Dark stipple corresponds to Mg-Ves + Wo assemblages. Plots 6 & 11 correspond to reactions 5.3 & 5.4, respectively. From Valley et al. (1985)

## **5.4      Retrograde Metamorphism**

Retrograde phases are difficult to identify optically at medium and low grade, given the fine-grained nature of the rock. The presence of prehnite in samples WL-16b and PCR-11b is a clear indication of retrograde reaction, an inference supported by textural relationships discussed in chapter 3. Retrogression is common in pelites near the contact, where it is inferred to result from fluid-rock interaction during cooling of the SMB.

Prehnite is a calcium-aluminum sheet silicate common in hydrothermally altered mafic volcanics and calcium metasomatized contact-altered impure limestones. The stability of prehnite is also highly sensitive to  $X_{CO_2}$  and generally limited to  $X_{CO_2} \leq 0.2$  (Deer et al., 1992). The upper limit of prehnite stability is probably given by the reaction:



which occurs at  $\sim 400^\circ C$  at 2-4 kb, and where  $X_{H_2O} = P_{\text{fluid}}$ . (Deer et al., 1992)

## **5.5      Metasomatism and Mineralogical Zonation**

This chapter focuses on core-region mineral assemblages exclusively, to assess progressive mineralogical assemblages with proximity to the South Mountain Batholith contact. The development of core and rim mineralogical assemblages or mineralogical zonation of concretions also indicates progressive degrees of metasomatism.

Metasomatism is defined as any process involving a change of the bulk chemical composition of the mineral assemblage (Purves, 1974). Whole-rock geochemical analyses of core and rim compositions were not performed on these samples, however textural evidence and EMP mineral chemistry data clearly demonstrate the presence of

concretion margin-parallel mineralogical and compositional zones, consistent with chemical mobility across a reaction potential gradient perpendicular to the margin. Previous studies by Purves (1974), and Mitchell (2006) argue for the formation of concentric, margin-parallel mineral and chemical zones in calcareous concretions during regional metamorphism. They argue increasing distinct and well-equilibrated mineralogical zones were the product of increasing regional metamorphic grade, correlated with progressive metamorphic grade of the host rocks from chlorite to sillimanite grade. Purves (1974) however, argued that the development of progressive, concentric zonation is an expression of increasingly efficient metasomatic diffusion between the original calcite dominated concretion and the semi-pelitic host. By contrast, all concretions sampled for this study occur in host rocks with pre-contact chlorite zone regional metamorphic assemblages. This strongly suggests that progressive mineralogical and chemical zonation observed in the Bluestone formation was facilitated, primarily, by progressively efficient diffusion of chemical components and equilibration reactions across the concretion-host margin as a function of the thermal gradient across the South Mountain Batholith contact aureole.

## 5.6 Summary

Assessments of equilibrium and peak metamorphic assemblage are hampered by the fine-grained nature of the calcareous and calc-silicate mineralogy at low and medium grades. Stability curves for inferred peak assemblages suggest  $X_{CO_2} \leq 0.1$  at all metamorphic grades. Software limitations prevent thorough assessment of stable reactions in calcareous and calc-silicate lithologies. Based on numerical models for Mg-vesuvianite stability (Valley et al., 1985), the presence of vesuvinite in the core-

assemblage indicates peak metamorphic  $X_{H2O} \cong P_{\text{fluid}}$  in the highest-grade metamorphic assemblage encompassed in this study. Previous studies on similar concretions in the Goldenville Group concluded that similar trends in mineralogical and chemical zonation correlated to and were a function progressive regional metamorphic grade. No progressive regional metamorphic grade is present in this study area however, and cannot account for mineralogical and chemical variations observed in concretions in the Bluestone formation.

### Crystallization sequence of concretion-core assemblage

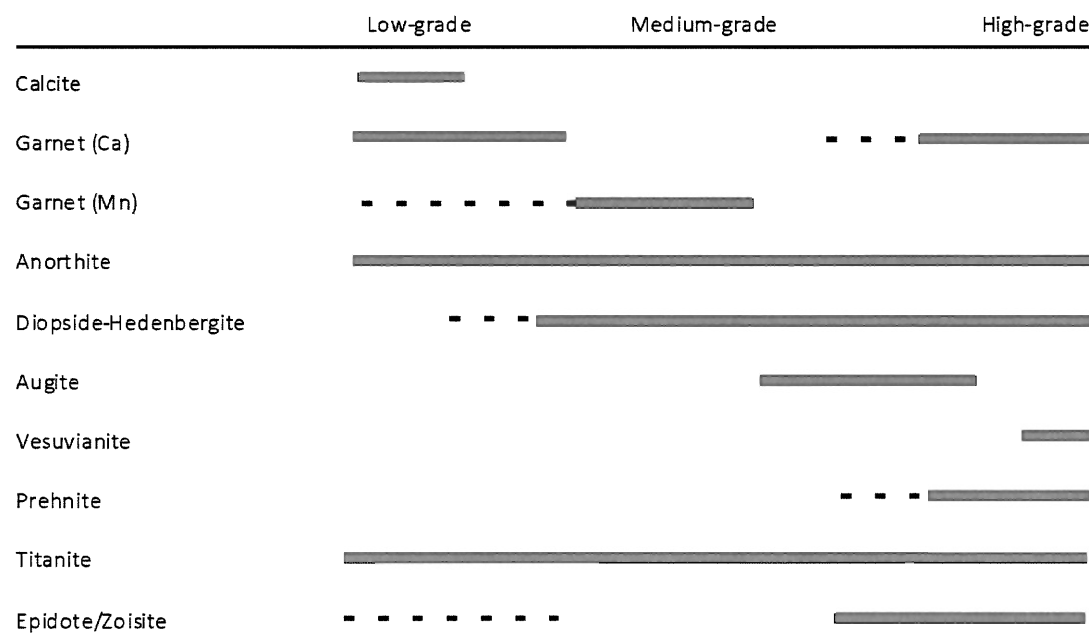


**Figure 5.5 Crystallization sequence of concretion core-region metamorphic minerals. The dashed lines represent minor phases or subordinate components.**

## Chapter 6

### SUMMARY AND CONCLUSIONS

#### 6.1 Discussion

Significant progress has been made to understand and document the characteristic features of the Bluestone formation since it was first differentiated from the Cunard formation in 2005. Mahoney (1996) studied the entire South Mountain Batholith aureole but failed to recognize the distinct isograd assemblages determined by Hart (2006). Tobey (2006) produced a general geological description of Point Pleasant Park, noting the presence of calcareous ‘nodules’, but did not investigate the features in great detail. Fraser (2010) produced a detailed measured-section from the Black Rock Beach member, noting the presence of concretions and horizons therein. Recent work by Waldron et al. (2011) and Jamieson et al. (2011) has established the lithological, structural, and stratigraphic basis for the subdivision of the Bluestone formation into the Point Pleasant member, the Black Rock Beach member, the Chain Rock member, and the Quarry Pond member.

This detailed study of calcareous concretions and horizons in all members of the Bluestone formation documents the texture, mineralogy, and composition of features that have largely been overlooked in previous work. The Cunard formation is a graphitic black slate, deposited in an anoxic deep marine basin. The Bluestone formation by contrast, records a shift to oxidizing condition, resulting in the deposition and mobilization of carbonate ions through a permeable substrate.

Stability curves for calc-silicate minerals in conjunction with previous estimates for local P-T conditions provide constraints on  $X_{(CO_2-H_2O)}$  conditions of both progressive

metamorphism and retrograde metamorphism-metasomatism where  $X_{CO_2} \leq 0.11$  and  $X_{H_2O} \approx P_{fluid}$  respectively. The identification of vesuvianite and prehnite in the Williams Lake area and Purcells Cove marks the first time these minerals have been observed in the study area. Additionally, a ~ 2 - 5 mm thick zone containing optically distinguishable ovoid to wheat-sheaf shaped aggregates of tabular radial chlorite has been identified along the rim of every concretion in the study area. This distinct chlorite morphology and restriction to the inner margin makes them key tracers for identifying concretion boundaries across metamorphic grade.

## 6.2 Conclusions

All calcareous concretions found in the Bluestone formation have enjoyed some degree of contact metamorphism within the South Mountain Batholith contact aureole. Mineralogically zoned concretions have developed metamorphic mineral assemblages, primarily as a function of distance from the contact along an isobaric thermal gradient, and bulk composition.

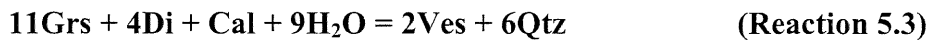
1. Calcareous concretions of the Bluestone formation contain distinct mineralogical and compositional zones that are gradational in low-grade samples and develop into more sharply defined, distinct compositional zones with increasing grade. Ion mobility resulting in the development of distinct mineralogical zoning appears to affect meta-siltstone and sandstone immediately adjacent these concretions which are cordierite-free relative to the host rock.
2. The development of poikiloblastic grossular after calcite and pure anorthite in low-grade assemblage requires exceptionally low  $X_{CO_2} < 0.05$  at 3kb, and is likely the product of the reaction:



3. The development of diopside porphyroblasts in medium-grade assemblages without grossular represents a change in bulk composition or  $X_{\text{CO}_2} > 0.2$ , possibly a stable product of the reaction:



4. The presence of vesuvianite in association with idioblastic, well-equilibrated grossular indicates peak metamorphic  $X_{\text{CO}_2} \leq 0.11$ , forming by either of two possible reactions:



Though textural evidence suggests significant retrograde alteration of vesuvianite to prehnite, no appropriate reactions have been found to account for this.

5. Prehnite found in two high-grade samples indicates significant retrograde metamorphism-metasomatism during cooling of the SMB, as the upper limit of prehnite stability is  $\sim 400^\circ\text{C}$  given by the reaction:



at 2-4 kb, and where  $X_{\text{CO}_2} \equiv P_{\text{fluid}}$ .

### **6.3 Suggestions for Further Work**

1. Preliminary XRF whole rock and trace element analysis indicates significant Fe-enrichment of concretion core assemblages. Thermodynamic data for Fe-end members of major minerals in calc-silicate assemblages are lacking or suspect. Further work regarding the effect of Fe & Ti content on the stability fields of calc-silicate minerals, particularly vesuvianite, for definitive inferences of  $X_{(CO_2-H_2O)}$  metamorphic conditions at the South Mountain Batholith contact.
2. The concretion sample population is limited by the dense urban infrastructure of south-end Halifax. Effort should be made to characterize the bulk composition of Bluestone formation members and determine if systematic variations in concretion compositions among members are present and meaningful.
3. Previous work on similar concretions in Goldenville Group formations in Liverpool, Nova Scotia, by Mitchell (2004) found scheelite as part of the core mineral assemblage. XRF data indicate core concentrations of tungsten up to 90 ppm in samples from Purcells Cove. If scheelite is present in the Bluestone formation, EMP analyses calibrated for W will be necessary.
4. Further work to understand the timing and mechanism of Ca-depletion from previously calcareous or calc-silicate compositions, as observed in sample PCR-26b.
5. New outcrops in the Williams Lake area representing high-grade lithologies should be found, given that sampling locations included in this study for this area are no longer accessible.
6. A quantitative assessment of the interaction between reaction and diffusion controls on mineralogical zonation at all metamorphic grades.

## References

- Clarke, D. B., Halliday, A. N. & Hamilton, P. J. (1988) Neodymium and strontium isotopic constraints on the origin of the peraluminous granitoids of the South Mountain Batholith, Nova Scotia, Canada. *Chemical Geology*, 73, 15-24.
- Clarke, D. B., MacDonald, M. A., Erdmann, S. (2004) Chemical variation in  $\text{Al}_2\text{O}_3$ - $\text{CaO}$ - $\text{Na}_2\text{O}$ - $\text{K}_2\text{O}$  space: controls on the peraluminosity of the South Mountain Batholith. *Canadian Journal of Earth Sciences* 41, 785-798
- Deer, W.A., Howie, R.A., Zussman, J. (1982) Rock Forming Minerals: Volume 1A, Orthosilicates. 2<sup>nd</sup> ed., Longman Group Limited
- Deer, W.A., Howie, R.A., Zussman, J. (1992). An Introduction to the Rock-Forming Minerals, Pearson-Prentice Hall
- Deer, W.A., Howie, R.A., Zussman, J. (1997) Rock Forming Minerals: Volume 2A, Single Chain Silicates. 2<sup>nd</sup> ed., The Geological Society, p. 294-398
- Erdmann, S., Jamieson, R.A., & MacDonald, M.A. (2009): Evaluating the origin of garnet, cordierite, and biotite in granitic rocks: a case study from the granitic South Mountain Batholith. *Journal of Petrology*, 50, 1477-1503.
- Fraser, J.A. (2010) Trends and Architecture of the Bluestone Formation Turbidites in Point Pleasant Park, Halifax, Nova Scotia. BSc. Honours Thesis, Dalhousie University, 71 pp.
- Fauer, G. (2008) Principles and Applications of Geochemistry. 2<sup>nd</sup> ed., Prentice Hall
- Hart, G. (2006) Andalusite in the South Mountain Batholith contact aureole, Halifax NS: A tale of two isograds. BSc. Honours Thesis, Dalhousie University, 121 pp.
- Hilchie, L.J., Jamieson, R.A. (2008) Graphite thermometry in the Halifax contact aureole. Atlantic Geoscience Society: Abstracts – 2008 Colloquium and Annual General Meeting, Dartmouth, Nova Scotia. *Atlantic Geology*, 44, 1-52
- Hicks, R.H., Jamieson, R.A. & Reynolds, P.H. (1999) Detrital and metamorphic  $^{40}\text{Ar}/^{39}\text{Ar}$  ages from muscovite and whole-rock samples, Meguma Supergroup, southern Nova Scotia. *Canadian Journal of Earth Sciences*, 36, 23-32.
- Horne, R.J., Culshaw, N. (2001) Flexural-slip folding in the Meguma Group, Halifax, Nova Scotia, Canada. *Journal of Structural Geology*, 22, 1631-1652
- Horne, R.J., Pelley, D. (2007). Geological Transect of the Meguma Terrane from Central Musquodoboit to Tangier: *in* Mineral Resources Branch, Report of Activities 2006, Nova Scotia Department of Natural Resources, Report ME 2007-1, p. 71-89
- Jamieson, R.A., Tobey, N. & ERT 3020 (2005) Contact metamorphism of the Halifax Formation on the southeastern margin of the Halifax Pluton, Halifax, Nova Scotia, GAC-MAC-CSPG-CSSS Joint Annual Meeting, Halifax, Abstracts, p. 95

Jamieson, R.A. (2008) Unpublished probe data, University of Calgary Laboratory for Electron Microprobe Analysis

Jamieson, R.A., Waldron, J.W.F. & White, C.E. (2011) Bluestone formation of the Halifax Group: metamorphosed slope and mass-transport deposits, Halifax Peninsula, Nova Scotia. Abstracts, Atlantic Geoscience Society Annual Meeting, Fredericton, February, 2011.

Labotka, T.C., Nabelek, P.I., Papika, J.J. (1988) Fluid infiltration through the Big Horse Limestone Member in the Notch Peak contact-metamorphic aureole, Utah. American Mineralogist. 73, 1302-1324

Mahoney, K.L. (1996) The contact aureole of the South Mountain Batholith, Nova Scotia. unpublished M.Sc. thesis, Acadia University, Wolfville, N.S., 156 p.

MacDonald, M.A. (2001) Geology of the South Mountain Batholith, Southwestern Nova Scotia. Nova Scotia Department of Natural Resources, Open File Report ME2001-2, 281 p.

MacDonald, M.A. & Clarke, D.B. (1985) The petrology, geochemistry, and economic potential of the Musquodoboit Batholith, Nova Scotia. Canadian Journal of Earth Sciences, 22, 1633-1642.

MacDonald, M. A. & Horne, R. J. (1988) Petrology of the zoned, peraluminous Halifax Pluton, South-Central Nova Scotia. Atlantic Geology, 24, 33-45.

Mitchell, F.M. (2006) Metamorphic petrology of calc-silicate nodules from chlorite to sillimanite grade, Liverpool-Pubnico area, Nova Scotia. B.Sc. Honours Thesis, Acadia University, Wolfville, Nova Scotia. 95 p.

O'Brien, B.H. (1988) A study of the Meguma Terrane in Lunenburg County, Nova Scotia. Geological Survey of Canada, Open File 1823, 139 p.

Purves, M.F. (1974) Metasomatism of calcareous concretions of the Goldenville Formation, Nova Scotia. B.Sc. Honours Thesis, Dalhousie University, Halifax, Nova Scotia. 61p.

Scallion, K.L., Jamieson, R.A., Barr, S.M., White, C.E. & Erdmann, S. (2011) Texture and composition of garnet as a guide to contamination of granitoid plutons: An example from the Governor Lake area, Meguma terrane, Nova Scotia. Canadian Mineralogist (in press).

Schenk, P.E. (1970) Regional variations of the flysch-like Meguma Group (lower Paleozoic) of Nova Scotia compared to recent sedimentation off the Scotian Shelf. In Flysch sedimentology in North America. Edited by J. Lajoie. Geological Association of Canada Special Paper 7, pp. 127-153.

Schenk, P.E. (1982). The Meguma Terrane of Nova Scotia – an aid in trans-Atlantic correlation. in Regional trends in the geology of the Appalachian-Caledonian-Hercynian-Mauritanide Orogen. Ed. P.E. Schenk. Reidel, Dordrecht, The Netherlands, 121-130

- Schenk, P.E. (1991) Events and sea-level changes on Gondwana's margin: The Meguma Zone (Cambrian to Devonian) of Nova Scotia, Canada. *Geological Society of America Bulletin* 103, 512-521
- Schenk, P.E. (1997) Sequence stratigraphy and provenance on Gondwana's margin: the Meguma Zone (Cambrian to Devonian) of Nova Scotia, Canada. *Geological Society of America Bulletin*, 109, pp. 395–409.
- Tobey, N. (2006) A geological description of Point Pleasant Park. B.Sc. honours thesis, Dalhousie University, Halifax, Nova Scotia
- Valley, J.W., Peacor, D.R., Bowman, J.R., Essene, E.J. (1985) Crystal chemistry and a Mg-vesuvianite and implications of phase equilibria in the system CaO-MgO-Al<sub>2</sub>O<sub>3</sub>-SiO<sub>2</sub>-H<sub>2</sub>O-CO<sub>2</sub>. *Journal of Metamorphic Geology*, 3, 137-153
- Waldron, J.W.F. (1992) The Goldenville–Halifax transition, Mahone Bay, Nova Scotia: relative sea-level change in the Meguma source terrane. *Canadian Journal of Earth Sciences*, 29, 1091–1105.
- Waldron, J.W.F., White, C.E., Barr, S.M., Simonetti, A. & Heaman, L.M. (2009) Provenance of the Meguma terrane, Nova Scotia: rifted margin of early Paleozoic Gondwana. *Canadian Journal of Earth Sciences*, 46, 1–8.
- Waldron, J.W.F., Jamieson, R.A. & White, C.E. (2011). Significance of a Meguma mass transport deposit in Halifax, Nova Scotia. Abstracts, Atlantic Geoscience Society Annual Meeting, Fredericton, February, 2011.
- White, C.E. (2010) Stratigraphy of the Lower Paleozoic Goldenville and Halifax groups in southwestern Nova Scotia. *Atlantic Geology* 46, 136–154.
- White, C.E., Bell, J.A., McLeish, D.F., MacDonald, M.A., Goodwin, T.A., MacNeil, J.D. (2008). Geology of the Halifax Regional Municipality, Central Nova Scotia. *in* Mineral Resources Branch, Report of Activities 2007, Nova Scotia Department of Natural Resources, Report ME 2008-1, p. 125-139

## Appendix I: Microprobe data

See figures 4.1-8 for areas of analysis on slides, appendix 2 for individual analysis locations, and figure 1.1 for outcrop locations.

**Table A.1 Concretion core: Garnet**

Sample	PPP30-3-1	PPP30-3-2	PPP30-3-3	PPP30-3-4	PPP30-3-6	PPP30-3-7	PPP30-3-11	PPP30-3-19	PPP30-3-20	PPP30-1-20	PPP30-1-21	PPP30-1-22
Probe #	8	9	10	11	13	14	18	26	27	80	81	82
<b>SiO<sub>2</sub></b>	38.59	38.09	38.20	37.77	38.35	38.20	38.50	37.87	37.58	36.84	37.68	37.60
<b>TiO<sub>2</sub></b>	0.31	0.08	0.21	0.24	0.34	0.33	0.43	0.71	0.72	1.04	0.77	0.73
<b>Al<sub>2</sub>O<sub>3</sub></b>	20.43	20.69	20.74	20.78	20.52	20.61	20.55	20.45	20.22	20.42	20.40	20.34
<b>Cr<sub>2</sub>O<sub>3</sub></b>	0.01	0.01	0.04	0.00	0.18	0.21	0.19	0.11	0.14	0.13	0.11	0.09
<b>FeO</b>	6.39	9.76	12.12	13.17	8.95	8.78	8.09	7.09	8.05	7.56	8.32	7.85
<b>MnO</b>	6.53	9.35	9.51	9.50	8.18	8.11	7.35	10.65	15.48	19.89	11.13	10.07
<b>MgO</b>	0.03	0.06	0.09	0.11	0.15	0.16	0.14	0.13	0.27	0.16	0.04	0.01
<b>CaO</b>	27.82	22.08	19.15	18.11	23.74	24.15	25.10	23.07	17.36	13.71	21.52	22.82
<b>Na<sub>2</sub>O</b>	0.02	0.01	0.01	0.02	0.08	0.08	0.06	0.06	0.08	0.02	0.01	0.00
<b>K<sub>2</sub>O</b>	0.02	0.03	0.03	0.04	0.04	0.03	0.03	0.03	0.03	0.02	0.03	0.03
<b>P<sub>2</sub>O<sub>5</sub></b>	0.00	0.02	0.01	0.02	0.02	0.02	0.02	0.02	0.02	0.01	0.01	0.01
<b>Total</b>	100.15	100.16	100.11	99.73	100.54	100.69	100.46	100.17	99.95	99.81	100.00	99.56
<b>Cations pfu based on 12 oxygen</b>												
<b>Si</b>	2.996	2.993	3.010	2.995	2.990	2.976	2.993	2.970	2.984	2.954	2.970	2.969
<b>Ti</b>	0.018	0.005	0.012	0.014	0.020	0.019	0.025	0.042	0.043	0.062	0.046	0.043
<b>Al</b>	1.870	1.916	1.926	1.943	1.886	1.892	1.883	1.890	1.892	1.931	1.896	1.894
<b>Cr</b>	0.000	0.001	0.002	0.000	0.011	0.013	0.012	0.006	0.008	0.008	0.006	0.006
<b>Fe</b>	0.415	0.641	0.798	0.874	0.584	0.572	0.526	0.464	0.534	0.508	0.548	0.518
<b>Mn</b>	0.430	0.622	0.635	0.638	0.541	0.535	0.484	0.707	1.042	1.351	0.743	0.674
<b>Mg</b>	0.004	0.007	0.011	0.013	0.018	0.018	0.017	0.016	0.031	0.019	0.004	0.001
<b>Ca</b>	2.315	1.859	1.616	1.540	1.984	2.016	2.090	1.938	1.477	1.177	1.817	1.931
<b>Na</b>	0.002	0.001	0.001	0.002	0.012	0.012	0.010	0.010	0.013	0.004	0.001	0.000
<b>K</b>	0.002	0.002	0.004	0.004	0.004	0.004	0.004	0.002	0.004	0.002	0.004	0.004
<b>P</b>	0.000	0.002	0.001	0.002	0.004	0.004	0.004	0.002	0.002	0.002	0.001	0.001
<b>Cation Total</b>	8.053	8.050	8.017	8.026	8.054	8.063	8.046	8.048	8.032	8.020	8.036	8.042
<b>x Almandine</b>	0.131	0.205	0.262	0.286	0.188	0.183	0.170	0.149	0.175	16.72	17.64	16.60
<b>x Grossular</b>	0.733	0.596	0.530	0.505	0.638	0.645	0.674	0.623	0.484	38.77	58.46	61.81
<b>x Spessartine</b>	0.136	0.199	0.208	0.209	0.174	0.171	0.156	0.227	0.341	44.51	23.90	21.59

Mol fraction: x Almandine = Fe/(Fe+Ca+Mn); x Grossular = Ca/(Fe+Ca+Mn); x Spessartine = Mn/(Fe+Ca+Mn)

Sample	PPP5c-1-20	PPP5c-1-24	PPP5c-1-25	PPP7c-1-12	PPP7c-1-13	PPP7c-1-15	PPP7c-1-16	PPP7c-1-17	PPP7c-1-18	PPP7c-1-20	PPP7c-1-21	PCR26b-1-1
Probe #	158	162	163	185	186	188	189	190	191	193	194	274
<b>SiO<sub>2</sub></b>	37.89	38.16	38.27	35.66	35.11	35.74	35.15	35.27	35.84	35.00	34.46	37.08
<b>TiO<sub>2</sub></b>	0.20	0.64	0.18	0.21	0.20	0.20	1.24	0.16	0.60	0.20	0.94	0.03
<b>Al<sub>2</sub>O<sub>3</sub></b>	21.10	20.91	21.07	20.34	20.07	20.25	19.47	19.81	19.72	20.29	19.17	21.35
<b>Cr<sub>2</sub>O<sub>3</sub></b>	0.17	0.26	0.24	0.19	0.17	0.19	0.17	0.18	0.09	0.07	0.31	0.00
<b>FeO</b>	10.48	5.69	10.55	11.50	12.50	11.67	9.99	10.87	8.77	9.11	7.65	24.20
<b>MnO</b>	10.46	11.08	10.43	12.27	13.30	12.71	21.97	11.21	15.31	19.25	21.06	14.76
<b>MgO</b>	0.08	0.07	0.07	0.14	0.23	0.18	0.34	0.11	0.17	0.27	0.29	1.33
<b>CaO</b>	19.70	23.15	19.74	17.18	14.89	15.89	9.14	18.03	16.55	11.94	11.61	1.52
<b>Na<sub>2</sub>O</b>	0.01	0.01	0.01	0.03	0.02	0.03	0.05	0.03	0.02	0.02	0.02	0.08
<b>K<sub>2</sub>O</b>	0.04	0.06	0.05	0.02	0.04	0.04	0.04	0.03	0.03	0.03	0.03	0.04
<b>P<sub>2</sub>O<sub>5</sub></b>	0.01	0.02	0.02	0.03	0.03	0.02	0.02	0.05	0.03	0.05	0.04	0.03
<b>Total</b>	100.13	100.05	100.62	97.57	96.55	96.91	97.57	95.74	97.12	96.25	95.59	100.42
<b>Cations pfu based on 12 oxygen</b>												
<b>Si</b>	2.982	2.980	2.995	2.920	2.920	2.942	2.927	2.934	2.947	2.926	2.915	2.998
<b>Ti</b>	0.012	0.037	0.011	0.013	0.012	0.013	0.078	0.010	0.037	0.012	0.060	0.001
<b>Al</b>	1.957	1.924	1.943	1.963	1.967	1.966	1.910	1.943	1.912	1.999	1.912	2.034
<b>Cr</b>	0.011	0.016	0.014	0.012	0.011	0.012	0.011	0.012	0.006	0.005	0.020	0.000
<b>Fe</b>	0.690	0.372	0.691	0.787	0.869	0.804	0.695	0.756	0.604	0.637	0.541	1.636
<b>Mn</b>	0.697	0.733	0.691	0.851	0.937	0.887	1.549	0.790	1.066	1.363	1.510	1.010
<b>Mg</b>	0.010	0.008	0.008	0.017	0.029	0.022	0.042	0.014	0.020	0.035	0.037	0.160
<b>Ca</b>	1.662	1.937	1.656	1.507	1.326	1.402	0.815	1.608	1.458	1.069	1.052	0.132
<b>Na</b>	0.001	0.001	0.001	0.005	0.002	0.005	0.007	0.005	0.004	0.002	0.004	0.013
<b>K</b>	0.004	0.006	0.006	0.002	0.004	0.005	0.005	0.002	0.004	0.002	0.004	0.005
<b>P</b>	0.000	0.001	0.001	0.002	0.002	0.001	0.001	0.004	0.002	0.004	0.004	0.002
<b>Cation Total</b>	8.027	8.016	8.020	8.080	8.078	8.059	8.041	8.078	8.060	8.054	8.058	7.991
<b>x Almandine</b>	0.226	0.122	0.227	0.250	0.277	0.260	0.227	0.240	0.193	0.208	0.174	0.589
<b>x Grossular</b>	0.545	0.637	0.545	0.479	0.423	0.453	0.266	0.510	0.466	0.348	0.339	0.048
<b>x Spessartine</b>	0.229	0.241	0.227	0.271	0.299	0.287	0.506	0.250	0.341	0.444	0.486	0.364

Mol fraction: x Almandine = Fe/(Fe+Ca+Mn); x Grossular = Ca/(Fe+Ca+Mn); x Spessartine = Mn/(Fe+Ca+Mn)

Sample	PCR26b-1-2	PCR26b-1-3	PCR26b-2-1	PCR26b-2-3	PCR26b-2-5	PCR11b-2-8	PCR11b-2-9	PCR11b-2-10	PCR11b-2-11	PCR11b-2-13	WL18b-4-1	WL18b-4-2
Probe #	275	276	305	307	309	542	543	544	545	547	36	37
<b>SiO<sub>2</sub></b>	36.83	36.77	37.58	37.40	37.08	38.21	38.82	38.26	37.92	38.50	39.02	39.10
<b>TiO<sub>2</sub></b>	0.05	0.05	0.09	0.01	0.13	0.00	0.24	0.20	0.48	0.82	0.91	0.87
<b>Al<sub>2</sub>O<sub>3</sub></b>	20.94	21.13	21.53	21.55	21.05	20.23	19.72	20.09	19.95	19.67	20.76	20.90
<b>Cr<sub>2</sub>O<sub>3</sub></b>	0.00	0.00	0.00	0.00	0.00	0.00	0.01	0.00	0.00	0.04	n/a	n/a
<b>FeO</b>	22.22	21.94	22.86	23.45	22.85	3.15	3.13	3.08	3.19	4.36	4.49	4.49
<b>MnO</b>	15.04	15.06	15.12	15.01	14.96	0.76	0.77	0.71	0.75	2.25	1.57	1.82
<b>MgO</b>	1.36	1.32	1.38	1.30	1.29	0.00	0.00	0.00	0.00	0.03	0.01	0.02
<b>CaO</b>	1.79	1.94	2.11	1.90	2.01	36.73	36.54	36.73	36.45	33.96	34.76	34.42
<b>Na<sub>2</sub>O</b>	0.00	0.00	0.02	0.02	0.06	0.00	0.00	0.00	0.01	0.02	-	-
<b>K<sub>2</sub>O</b>	0.03	0.04	0.03	0.04	0.01	0.02	0.04	0.03	0.01	0.02	0.01	0.00
<b>P<sub>2</sub>O<sub>5</sub></b>	0.03	0.03	0.03	0.03	0.00	0.00	0.00	0.01	0.03	0.04	n/a	n/a
<b>Total</b>	98.29	98.28	100.76	100.69	99.43	99.10	99.26	99.11	98.78	99.70	101.53	101.62
<b>Cations pfu based on 12 oxygen</b>												
<b>Si</b>	3.025	3.018	3.012	3.006	3.017	2.960	2.999	2.964	2.950	2.977	2.955	2.957
<b>Ti</b>	0.002	0.004	0.005	0.001	0.008	0.000	0.014	0.012	0.028	0.048	0.052	0.050
<b>Al</b>	2.027	2.044	2.034	2.041	2.018	1.848	1.795	1.834	1.829	1.793	1.853	1.863
<b>Cr</b>	0.000	0.000	0.000	0.000	0.000	0.000	0.001	0.000	0.000	0.002	n/a	n/a
<b>Fe</b>	1.526	1.506	1.532	1.576	1.554	0.204	0.202	0.199	0.208	0.282	0.284	0.284
<b>Mn</b>	1.046	1.048	1.027	1.021	1.031	0.050	0.050	0.047	0.049	0.148	0.101	0.116
<b>Mg</b>	0.167	0.162	0.166	0.155	0.156	0.000	0.000	0.000	0.000	0.004	0.001	0.002
<b>Ca</b>	0.157	0.170	0.181	0.163	0.175	3.050	3.024	3.049	3.037	2.814	2.821	2.790
<b>Na</b>	0.000	0.000	0.004	0.002	0.008	0.000	0.000	0.000	0.001	0.002	0.000	0.000
<b>K</b>	0.004	0.004	0.004	0.004	0.001	0.002	0.004	0.002	0.001	0.002	0.001	0.000
<b>P</b>	0.002	0.002	0.001	0.002	0.000	0.000	0.000	0.001	0.002	0.002	n/a	n/a
<b>Cation Total</b>	7.957	7.957	7.967	7.972	7.970	8.117	8.089	8.110	8.106	8.075	8.067	8.062
<b>x Almandine</b>	0.559	0.553	0.559	0.571	0.563	0.062	0.062	0.060	0.063	0.087	0.089	0.089
<b>x Grossular</b>	0.058	0.063	0.066	0.059	0.063	0.923	0.923	0.925	0.922	0.868	0.880	0.874
<b>x Spessartine</b>	0.383	0.385	0.375	0.370	0.373	0.015	0.015	0.014	0.015	0.046	0.031	0.036

Mol fraction: x Almandine = Fe/(Fe+Ca+Mn); x Grossular = Ca/(Fe+Ca+Mn); x Spessartine = Mn/(Fe+Ca+Mn)

Sample	WL18b-4-4	WL18b-4-5	WL18b-4-6	WL18b-4-7	WL16b-3-4	WL16b-3-5	WL16b-3-6	WL16b-3-7	WL16b-3-8	WL16b-3-9	WL16b-3-10	WL16b-3-11
Probe #	39	40	41	42	440	441	442	443	444	445	446	447
<b>SiO<sub>2</sub></b>	39.40	38.71	39.41	39.29	38.04	34.28	38.48	37.92	34.97	38.62	38.86	38.19
<b>TiO<sub>2</sub></b>	0.23	1.00	0.02	0.51	0.22	0.13	0.38	0.35	1.73	0.63	0.39	0.23
<b>Al<sub>2</sub>O<sub>3</sub></b>	21.56	20.58	21.74	20.13	21.19	19.39	20.83	20.88	17.10	20.65	20.86	20.77
<b>Cr<sub>2</sub>O<sub>3</sub></b>	n/a	n/a	n/a	n/a	0.01	0.02	0.02	0.02	0.02	0.04	0.03	0.03
<b>FeO</b>	4.03	4.62	4.06	5.37	2.85	3.11	3.27	3.03	3.14	3.44	2.68	3.63
<b>MnO</b>	1.89	2.63	2.49	2.49	2.49	1.43	2.29	2.97	0.48	1.63	1.26	2.94
<b>MgO</b>	0.02	0.05	0.01	0.03	0.04	0.08	0.06	0.04	1.44	0.10	0.00	0.00
<b>CaO</b>	34.94	33.80	34.27	34.12	34.08	34.82	34.19	33.58	35.84	34.85	35.14	33.23
<b>Na<sub>2</sub>O</b>	0.00	-	-	-	0.02	0.02	0.00	0.01	0.02	0.00	0.00	0.00
<b>K<sub>2</sub>O</b>	0.00	0.00	-	0.00	0.03	0.04	0.04	0.03	0.03	0.02	0.03	0.02
<b>P<sub>2</sub>O<sub>5</sub></b>	n/a	n/a	n/a	n/a	0.00	0.00	0.00	0.00	0.00	0.00	0.00	0.00
<b>Total</b>	102.08	101.39	102.00	101.94	98.97	93.31	99.55	98.82	94.78	99.98	99.24	99.02
<b>Cations pfu based on 12 oxygen</b>												
<b>Si</b>	2.960	2.946	2.965	2.982	2.946	2.850	2.964	2.947	2.866	2.962	2.986	2.964
<b>Ti</b>	0.013	0.057	0.001	0.029	0.013	0.008	0.022	0.020	0.107	0.036	0.023	0.013
<b>Al</b>	1.910	1.846	1.928	1.800	1.933	1.901	1.891	1.913	1.652	1.866	1.889	1.900
<b>Cr</b>	n/a	n/a	n/a	n/a	0.001	0.001	0.001	0.001	0.001	0.002	0.001	0.002
<b>Fe</b>	0.253	0.294	0.256	0.341	0.185	0.216	0.210	0.197	0.215	0.221	0.173	0.235
<b>Mn</b>	0.120	0.170	0.159	0.160	0.163	0.101	0.149	0.196	0.034	0.106	0.082	0.193
<b>Mg</b>	0.002	0.006	0.001	0.003	0.005	0.011	0.006	0.005	0.176	0.011	0.000	0.000
<b>Ca</b>	2.813	2.756	2.762	2.774	2.827	3.102	2.822	2.796	3.148	2.863	2.893	2.764
<b>Na</b>	0.000	0.000	0.000	0.000	0.002	0.002	0.000	0.001	0.004	0.000	0.000	0.000
<b>K</b>	0.000	0.000	0.000	0.000	0.002	0.004	0.004	0.004	0.004	0.002	0.002	0.001
<b>P</b>	n/a	n/a	n/a	n/a	0.000	0.000	0.000	0.000	0.000	0.000	0.000	0.000
<b>Cation Total</b>	8.072	8.074	8.071	8.089	8.078	8.196	8.070	8.081	8.207	8.070	8.048	8.072
<b>x Almandine</b>	0.079	0.091	0.080	0.104	0.058	0.063	0.066	0.062	0.063	0.069	0.055	0.074
<b>x Grossular</b>	0.882	0.855	0.869	0.846	0.890	0.907	0.887	0.877	0.927	0.898	0.919	0.866
<b>x Spessartine</b>	0.038	0.053	0.050	0.049	0.051	0.029	0.047	0.061	0.010	0.033	0.026	0.061

Mol fraction: x Almandine = Fe/(Fe+Ca+Mn); x Grossular = Ca/(Fe+Ca+Mn); x Spessartine = Mn/(Fe+Ca+Mn)

Sample	WL16b-3-12	WL16b-3-13	WL16b-4-1	WL16b-4-2	WL16b-4-3	WL16b-4-4	WL16b-4-5	WL16b-4-6	WL16b-4-7	WL16b-4-8	WL16b-5-6	WL16b-5-7
Probe #	448	449	464	465	466	467	468	469	470	471	489	490
<b>SiO<sub>2</sub></b>	35.60	35.65	38.61	38.32	37.38	38.36	38.26	38.63	38.04	38.49	38.52	37.97
<b>TiO<sub>2</sub></b>	1.45	1.87	0.30	0.07	0.37	0.27	0.21	0.15	0.24	0.23	0.23	0.42
<b>Al<sub>2</sub>O<sub>3</sub></b>	16.46	16.16	21.05	21.24	20.72	21.08	20.63	21.06	20.46	20.84	21.24	20.66
<b>Cr<sub>2</sub>O<sub>3</sub></b>	0.02	0.06	0.03	0.06	0.06	0.06	0.05	0.03	0.05	0.02	0.07	0.08
<b>FeO</b>	3.13	4.35	2.28	2.93	3.62	2.36	4.05	2.71	3.73	2.97	2.27	3.28
<b>MnO</b>	0.36	0.97	1.36	2.56	3.53	1.53	4.10	1.57	3.04	1.84	1.50	2.84
<b>MgO</b>	0.32	1.34	0.11	0.08	0.06	0.15	0.07	0.12	0.07	0.11	0.11	0.04
<b>CaO</b>	35.69	35.14	35.56	34.10	32.53	35.13	32.14	35.07	33.08	34.69	35.65	33.55
<b>Na<sub>2</sub>O</b>	0.00	0.01	0.06	0.05	0.07	0.06	0.09	0.06	0.05	0.06	0.02	0.02
<b>K<sub>2</sub>O</b>	0.04	0.03	0.04	0.03	0.04	0.03	0.03	0.02	0.03	0.03	0.04	0.04
<b>P<sub>2</sub>O<sub>5</sub></b>	0.01	0.00	0.00	0.00	0.00	0.00	0.00	0.00	0.00	0.00	0.02	0.02
<b>Total</b>	93.08	95.59	99.41	99.44	98.39	99.02	99.62	99.42	98.78	99.27	99.67	98.92
<b>Cations pfu based on 12 oxygen</b>												
<b>Si</b>	2.963	2.912	2.963	2.953	2.930	2.957	2.964	2.968	2.965	2.968	2.951	2.951
<b>Ti</b>	0.091	0.115	0.018	0.004	0.022	0.016	0.012	0.008	0.014	0.013	0.013	0.025
<b>Al</b>	1.614	1.556	1.904	1.930	1.915	1.915	1.884	1.907	1.879	1.894	1.918	1.891
<b>Cr</b>	0.001	0.004	0.001	0.004	0.004	0.004	0.004	0.002	0.002	0.001	0.004	0.005
<b>Fe</b>	0.217	0.298	0.146	0.188	0.238	0.152	0.263	0.174	0.244	0.192	0.145	0.212
<b>Mn</b>	0.025	0.067	0.089	0.167	0.235	0.100	0.269	0.102	0.200	0.120	0.097	0.187
<b>Mg</b>	0.040	0.163	0.013	0.008	0.007	0.017	0.007	0.013	0.007	0.012	0.012	0.005
<b>Ca</b>	3.182	3.076	2.924	2.815	2.732	2.902	2.669	2.887	2.762	2.867	2.927	2.794
<b>Na</b>	0.000	0.001	0.010	0.008	0.011	0.008	0.013	0.008	0.007	0.010	0.004	0.002
<b>K</b>	0.004	0.004	0.004	0.004	0.004	0.002	0.002	0.002	0.004	0.002	0.005	0.005
<b>P</b>	0.001	0.000	0.000	0.000	0.000	0.000	0.000	0.000	0.000	0.000	0.001	0.001
<b>Cation Total</b>	8.140	8.196	8.072	8.081	8.099	8.074	8.087	8.074	8.086	8.078	8.076	8.080
<b>x Almandine</b>	0.063	0.087	0.046	0.059	0.074	0.048	0.082	0.055	0.076	0.060	0.046	0.067
<b>x Grossular</b>	0.929	0.894	0.926	0.888	0.852	0.920	0.834	0.913	0.862	0.902	0.924	0.875
<b>x Spessartine</b>	0.007	0.020	0.028	0.053	0.073	0.032	0.084	0.032	0.063	0.038	0.031	0.059

Mol fraction: x Almandine = Fe/(Fe+Ca+Mn); x Grossular = Ca/(Fe+Ca+Mn); x Spessartine = Mn/(Fe+Ca+Mn)

Sample	WL16b-5-8	WL16b-5-9	WL16b-5-10	WL16b-5-11	WL16b-5-12	WL16b-5-13	WL16b-5-14
Probe #	491	492	493	494	495	496	497
<b>SiO<sub>2</sub></b>	38.09	38.59	37.78	38.67	38.53	38.66	37.75
<b>TiO<sub>2</sub></b>	0.25	0.40	0.35	0.32	0.14	0.30	0.34
<b>Al<sub>2</sub>O<sub>3</sub></b>	20.82	20.84	20.80	20.89	20.87	21.17	20.75
<b>Cr<sub>2</sub>O<sub>3</sub></b>	0.10	0.11	0.09	0.07	0.09	0.03	0.11
<b>FeO</b>	4.08	2.96	3.08	2.78	3.13	2.26	3.33
<b>MnO</b>	4.01	1.61	2.75	1.48	2.22	1.53	3.24
<b>MgO</b>	0.03	0.11	0.06	0.07	0.03	0.10	0.03
<b>CaO</b>	32.11	35.16	33.66	35.34	34.28	35.46	33.15
<b>Na<sub>2</sub>O</b>	0.00	0.02	0.01	0.02	0.02	0.02	0.02
<b>K<sub>2</sub>O</b>	0.04	0.04	0.05	0.05	0.05	0.06	0.05
<b>P<sub>2</sub>O<sub>5</sub></b>	0.01	0.02	0.04	0.02	0.02	0.01	0.04
<b>Total</b>	99.54	99.84	98.66	99.71	99.38	99.59	98.81
<b>Cations pfu based on 12 oxygen</b>							
<b>Si</b>	2.953	2.959	2.941	2.965	2.971	2.962	2.940
<b>Ti</b>	0.014	0.023	0.020	0.018	0.008	0.017	0.019
<b>Al</b>	1.902	1.883	1.908	1.888	1.897	1.912	1.906
<b>Cr</b>	0.006	0.006	0.005	0.005	0.005	0.001	0.007
<b>Fe</b>	0.264	0.190	0.200	0.179	0.202	0.145	0.217
<b>Mn</b>	0.263	0.104	0.181	0.096	0.145	0.100	0.214
<b>Mg</b>	0.004	0.012	0.007	0.008	0.004	0.011	0.004
<b>Ca</b>	2.666	2.888	2.808	2.904	2.832	2.911	2.767
<b>Na</b>	0.000	0.002	0.001	0.002	0.002	0.002	0.002
<b>K</b>	0.004	0.005	0.005	0.005	0.005	0.006	0.005
<b>P</b>	0.001	0.001	0.002	0.001	0.001	0.001	0.002
<b>Cation Total</b>	8.078	8.075	8.080	8.072	8.072	8.068	8.084
<b>x Almandine</b>	0.083	0.060	0.063	0.056	0.063	0.046	0.068
<b>x Grossular</b>	0.835	0.908	0.880	0.914	0.891	0.922	0.865
<b>x Spessartine</b>	0.082	0.033	0.057	0.030	0.046	0.032	0.067

Mol fraction: x Almandine = Fe/(Fe+Ca+Mn); x Grossular = Ca/(Fe+Ca+Mn); x Spessartine = Mn/(Fe+Ca+Mn)

**Table A.2** Concretion core: Clinopyroxene

Sample	PPP30-3-9	PPP30-3-15	PPP5c-1-15	PPP5c-1-21	PPP5c-1-22	PPP5c-1-27	PCR23a-3-1	PCR23a-3-2	PCR23a-3-3	PCR23a-3-6	PCR23a-3-7	PCR23a-3-8
Probe #	16	22	153	159	160	165	645	646	647	650	651	652
<b>SiO<sub>2</sub></b>	49.99	50.15	49.16	49.22	49.35	49.31	48.98	48.76	49.33	49.49	50.69	51.44
<b>TiO<sub>2</sub></b>	0.08	0.13	0.10	0.07	0.06	0.06	0.01	0.03	0.05	0.00	0.06	0.01
<b>Al<sub>2</sub>O<sub>3</sub></b>	0.31	0.23	0.08	0.15	0.10	0.19	0.16	0.37	0.22	0.26	0.75	0.13
<b>Cr<sub>2</sub>O<sub>3</sub></b>	0.14	0.09	0.12	0.11	0.14	0.16	0.00	0.00	0.02	0.01	0.00	0.00
<b>FeO</b>	19.09	19.22	18.34	20.27	18.54	18.15	22.26	23.18	22.22	21.44	14.77	13.25
<b>MnO</b>	1.92	1.88	4.87	3.37	4.25	4.53	1.31	1.28	1.46	1.13	1.36	1.91
<b>MgO</b>	4.73	4.74	3.42	3.16	3.62	3.80	2.86	2.25	2.66	3.77	8.56	9.15
<b>CaO</b>	23.91	23.64	23.01	23.14	22.91	23.03	23.25	23.36	23.33	23.60	23.26	23.58
<b>Na<sub>2</sub>O</b>	0.11	0.08	0.02	0.04	0.04	0.07	0.00	0.03	0.01	0.03	0.08	0.03
<b>K<sub>2</sub>O</b>	0.05	0.04	0.03	0.05	0.04	0.04	0.02	0.01	0.05	0.01	0.01	0.01
<b>P<sub>2</sub>O<sub>5</sub></b>	0.02	0.02	0.02	0.01	0.02	0.06	0.01	0.01	0.01	0.00	0.00	0.02
<b>Total</b>	100.34	100.22	99.15	99.59	99.07	99.41	98.88	99.27	99.36	99.74	99.52	99.53
<b>Cations pfu based on 6 oxygen</b>												
<b>Si</b>	1.984	1.990	1.993	1.991	1.996	1.988	1.996	1.988	2.000	1.989	1.974	1.994
<b>Ti</b>	0.002	0.004	0.003	0.002	0.002	0.002	0.001	0.001	0.002	0.000	0.002	0.000
<b>Al</b>	0.014	0.011	0.004	0.007	0.005	0.009	0.008	0.017	0.010	0.012	0.034	0.006
<b>Cr</b>	0.004	0.003	0.004	0.004	0.004	0.005	0.000	0.000	0.001	0.000	0.000	0.000
<b>Fe</b>	0.634	0.638	0.622	0.686	0.627	0.612	0.759	0.791	0.754	0.721	0.481	0.430
<b>Mn</b>	0.065	0.063	0.167	0.115	0.146	0.155	0.045	0.044	0.050	0.038	0.045	0.063
<b>Mg</b>	0.280	0.281	0.206	0.191	0.218	0.229	0.174	0.137	0.161	0.226	0.497	0.529
<b>Ca</b>	1.016	1.005	0.999	1.003	0.993	0.995	1.015	1.021	1.013	1.016	0.971	0.979
<b>Na</b>	0.008	0.007	0.001	0.003	0.003	0.005	0.000	0.002	0.001	0.002	0.006	0.002
<b>K</b>	0.002	0.002	0.002	0.002	0.002	0.002	0.001	0.001	0.002	0.001	0.000	0.001
<b>P</b>	0.001	0.002	0.001	0.001	0.001	0.002	0.001	0.000	0.000	0.000	0.000	0.001
<b>Cation Total</b>	4.011	4.005	4.002	4.004	3.997	4.004	4.000	4.003	3.994	4.005	4.010	4.004
<b>Mg/(Mg+Fe+Ca)</b>	0.145	0.146	0.113	0.102	0.119	0.125	0.089	0.070	0.083	0.115	0.255	0.273
<b>Fe/(Mg+Fe+Ca)</b>	0.328	0.332	0.340	0.365	0.341	0.333	0.390	0.406	0.391	0.367	0.247	0.222
<b>Ca/(Mg+Fe+Ca)</b>	0.527	0.522	0.547	0.534	0.540	0.542	0.521	0.524	0.526	0.518	0.498	0.505

Sample	PCR23a-3-9	PCR23a-3-10	PCR23a-3-11	PCR23a-3-12	PCR23a-3-13	PCR11b-2-1	PCR11b-2-2	PCR11b-2-3	PCR11b-2-5	PCR11b-2-6	PCR11b-2-12	PCR11b-3-1
Probe #	653	654	655	656	657	535	536	537	539	540	546	560
<b>SiO<sub>2</sub></b>	50.43	51.65	49.47	49.75	51.13	49.985	49.808	49.755	49.818	50.685	49.707	51.23
<b>TiO<sub>2</sub></b>	0.04	0.01	0.02	0.06	0.01	0.048	0.027	0.050	0.055	0.005	0.022	0.03
<b>Al<sub>2</sub>O<sub>3</sub></b>	0.83	0.13	0.26	0.30	0.30	0.242	0.084	0.149	0.361	0.147	0.110	0.23
<b>Cr<sub>2</sub>O<sub>3</sub></b>	0.00	0.00	0.00	0.00	0.03	0.052	0.089	0.079	0.023	0.030	0.075	0.10
<b>FeO</b>	16.29	12.15	19.82	20.24	13.30	18.601	18.769	19.579	19.708	15.730	19.683	13.50
<b>MnO</b>	1.44	1.87	1.10	1.14	1.89	2.486	3.098	2.475	2.367	3.120	2.442	2.71
<b>MgO</b>	6.99	9.84	4.59	4.51	8.86	4.725	4.244	3.872	4.027	6.197	3.828	8.94
<b>CaO</b>	23.83	23.94	23.35	23.75	23.27	23.693	23.278	23.821	23.470	24.050	23.629	22.96
<b>Na<sub>2</sub>O</b>	0.06	0.04	0.02	0.03	0.06	0.013	0.015	0.005	0.010	0.009	0.038	0.06
<b>K<sub>2</sub>O</b>	0.01	0.01	0.01	0.02	0.02	0.035	0.039	0.029	0.027	0.027	0.024	0.03
<b>P<sub>2</sub>O<sub>5</sub></b>	0.00	0.00	0.02	0.02	0.02	0.000	0.030	0.014	0.000	0.000	0.050	0.02
<b>Total</b>	99.93	99.64	98.66	99.80	98.88	99.879	99.481	99.828	99.865	100.001	99.609	99.83
<b>Cations pfu based on 6 oxygen</b>												
<b>Si</b>	1.975	1.991	1.994	1.987	1.994	1.991	1.997	1.993	1.992	1.994	1.996	1.987
<b>Ti</b>	0.001	0.001	0.001	0.002	0.001	0.001	0.001	0.002	0.002	0.000	0.001	0.001
<b>Al</b>	0.038	0.006	0.013	0.014	0.014	0.011	0.004	0.007	0.017	0.007	0.005	0.010
<b>Cr</b>	0.000	0.000	0.000	0.000	0.001	0.002	0.003	0.002	0.001	0.001	0.002	0.003
<b>Fe</b>	0.533	0.392	0.668	0.676	0.434	0.620	0.629	0.656	0.659	0.518	0.661	0.438
<b>Mn</b>	0.047	0.061	0.038	0.038	0.062	0.084	0.105	0.084	0.080	0.104	0.083	0.089
<b>Mg</b>	0.408	0.565	0.276	0.268	0.515	0.281	0.254	0.231	0.240	0.364	0.229	0.517
<b>Ca</b>	1.000	0.989	1.008	1.016	0.973	1.011	1.000	1.022	1.006	1.014	1.016	0.955
<b>Na</b>	0.005	0.003	0.002	0.002	0.005	0.001	0.001	0.001	0.001	0.001	0.003	0.005
<b>K</b>	0.001	0.000	0.001	0.001	0.001	0.002	0.002	0.001	0.001	0.001	0.001	0.002
<b>P</b>	0.000	0.000	0.001	0.001	0.001	0.000	0.001	0.001	0.000	0.000	0.002	0.001
<b>Cation Total</b>	4.008	4.008	4.001	4.005	4.001	4.004	3.998	4.001	3.998	4.003	4.000	4.008
<b>Mg/(Mg+Fe+Ca)</b>	0.210	0.290	0.141	0.137	0.268	0.147	0.135	0.121	0.126	0.192	0.120	0.271
<b>Fe/(Mg+Fe+Ca)</b>	0.275	0.201	0.342	0.345	0.226	0.324	0.334	0.343	0.346	0.273	0.347	0.229
<b>Ca/(Mg+Fe+Ca)</b>	0.515	0.508	0.516	0.519	0.506	0.529	0.531	0.536	0.528	0.535	0.533	0.500

Sample	PCR11b-3-2	PCR11b-3-3	PCR11b-3-5	PCR11b-3-6	PCR11b-3-7	PCR11b-3-8	PCR11b-3-9	PCR11b-3-15	PCR11b-4-1	PCR11b-4-2	PCR11b-4-3	PCR11b-4-4
Probe #	561	562	564	565	566	567	568	574	587	588	589	590
<b>SiO<sub>2</sub></b>	50.69	51.04	51.28	49.24	49.40	51.31	51.01	51.27	52.15	51.80	51.63	51.83
<b>TiO<sub>2</sub></b>	0.04	0.03	0.05	0.18	0.18	0.04	0.06	0.01	0.15	0.21	0.26	0.26
<b>Al<sub>2</sub>O<sub>3</sub></b>	0.30	0.24	0.29	1.51	1.67	0.31	0.32	0.20	2.73	3.37	3.37	3.01
<b>Cr<sub>2</sub>O<sub>3</sub></b>	0.07	0.08	0.12	0.08	0.10	0.08	0.02	0.06	0.05	0.06	0.07	0.06
<b>FeO</b>	16.76	13.50	13.26	16.78	16.92	14.09	13.90	13.55	14.72	15.01	14.60	14.53
<b>MnO</b>	1.97	1.90	1.91	1.74	1.60	2.62	2.55	2.33	1.25	1.38	1.41	1.21
<b>MgO</b>	7.15	9.49	9.39	6.22	6.12	8.56	8.85	8.84	13.57	13.27	13.54	13.34
<b>CaO</b>	23.14	23.08	22.99	22.88	23.17	22.82	22.43	23.29	11.79	11.67	11.47	11.65
<b>Na<sub>2</sub>O</b>	0.07	0.07	0.07	0.12	0.10	0.08	0.08	0.07	0.17	0.22	0.25	0.24
<b>K<sub>2</sub>O</b>	0.03	0.02	0.02	0.02	0.03	0.02	0.03	0.03	0.10	0.15	0.15	0.15
<b>P<sub>2</sub>O<sub>5</sub></b>	0.00	0.04	0.00	0.04	0.04	0.03	0.00	0.03	0.01	0.00	0.02	0.00
<b>Total</b>	100.23	99.49	99.36	98.81	99.35	99.97	99.24	99.68	96.70	97.13	96.76	96.28
<b>Cations pfu based on 6 oxygen</b>												
<b>Si</b>	1.984	1.981	1.989	1.956	1.952	1.990	1.990	2.007	1.989	1.987	2.002	
<b>Ti</b>	0.001	0.001	0.001	0.005	0.005	0.001	0.002	0.001	0.004	0.006	0.007	0.008
<b>Al</b>	0.014	0.011	0.013	0.071	0.078	0.014	0.015	0.009	0.124	0.152	0.153	0.137
<b>Cr</b>	0.002	0.002	0.004	0.002	0.003	0.002	0.001	0.002	0.001	0.002	0.002	0.002
<b>Fe</b>	0.549	0.438	0.430	0.557	0.559	0.457	0.454	0.440	0.474	0.482	0.470	0.469
<b>Mn</b>	0.065	0.062	0.063	0.059	0.053	0.086	0.084	0.077	0.041	0.045	0.046	0.040
<b>Mg</b>	0.418	0.549	0.543	0.368	0.361	0.495	0.515	0.511	0.779	0.760	0.776	0.769
<b>Ca</b>	0.970	0.960	0.956	0.974	0.981	0.948	0.937	0.969	0.486	0.480	0.473	0.482
<b>Na</b>	0.005	0.005	0.005	0.009	0.008	0.006	0.006	0.005	0.013	0.016	0.019	0.018
<b>K</b>	0.001	0.001	0.001	0.001	0.001	0.001	0.001	0.001	0.005	0.007	0.007	0.008
<b>P</b>	0.000	0.001	0.000	0.001	0.001	0.001	0.000	0.001	0.001	0.000	0.001	0.000
<b>Cation Total</b>	4.010	4.012	4.005	4.004	4.003	4.003	4.005	4.006	3.935	3.939	3.940	3.935
<b>Mg/(Mg+Fe+Ca)</b>	0.271	0.271	0.271	0.271	0.271	0.271	0.271	0.271	0.448	0.441	0.452	0.447
<b>Fe/(Mg+Fe+Ca)</b>	0.229	0.229	0.229	0.229	0.229	0.229	0.229	0.229	0.273	0.280	0.273	0.273
<b>Ca/(Mg+Fe+Ca)</b>	0.500	0.500	0.500	0.500	0.500	0.500	0.500	0.500	0.280	0.279	0.275	0.280

Sample	PCR11b-4-7	WL18b-5-1	WL18b-5-2	WL18b-5-3	WL18b-5-4	WL18b-5-6	WL18b-5-7	WL18b-5-13	WL18b-5-25	WL18b-5-26	WL18b-5-27	WL18b-5-30	WL18b-5-31
Probe #	593	2	3	4	5	7	8	14	26	27	31	30	32
<b>SiO<sub>2</sub></b>	51.08	50.65	50.54	50.99	50.97	50.22	51.03	50.76	51.20	50.47	50.63	51.06	-
<b>TiO<sub>2</sub></b>	0.22	-	-	0.14	0.00	0.12	0.16	-	0.01	-	-	-	-
<b>Al<sub>2</sub>O<sub>3</sub></b>	3.37	0.16	0.11	0.88	0.18	0.23	0.73	0.14	0.15	0.26	0.18	0.18	0.18
<b>Cr<sub>2</sub>O<sub>3</sub></b>	0.12	n/a	n/a	n/a	n/a	n/a	n/a						
<b>FeO</b>	15.16	18.73	20.22	18.22	19.21	23.65	18.80	22.02	19.24	23.33	20.48	19.97	-
<b>MnO</b>	1.34	4.35	4.09	2.41	4.03	3.62	2.83	1.77	4.54	2.58	4.04	2.76	-
<b>MgO</b>	12.72	4.40	3.73	6.03	4.44	1.84	5.28	4.13	4.38	2.94	3.65	4.71	-
<b>CaO</b>	11.43	23.79	23.21	24.26	23.83	23.43	24.18	23.63	23.88	23.94	23.59	23.65	-
<b>Na<sub>2</sub>O</b>	0.23	0.01	0.01	0.04	0.02	0.01	0.02	-	-	0.02	0.01	0.01	0.01
<b>K<sub>2</sub>O</b>	0.15	-	0.00	0.02	0.01	0.01	0.02	0.02	-	0.01	-	-	-
<b>P<sub>2</sub>O<sub>5</sub></b>	0.01	n/a	n/a	n/a	n/a	n/a	n/a						
<b>Total</b>	95.82	102.09	101.91	102.98	102.69	103.11	103.04	102.45	103.41	103.54	102.58	102.34	-
<b>Cations pfu based on 6 oxygen</b>													
<b>Si</b>	1.991	1.986	1.994	1.960	1.987	1.986	1.969	1.989	1.985	1.977	1.987	1.991	-
<b>Ti</b>	0.007	0.000	0.000	0.004	0.000	0.003	0.005	0.000	0.000	0.000	0.000	0.000	0.000
<b>Al</b>	0.155	0.007	0.005	0.040	0.008	0.011	0.033	0.006	0.007	0.012	0.009	0.008	-
<b>Cr</b>	0.004	n/a	n/a	n/a	n/a	n/a	n/a						
<b>Fe</b>	0.494	0.614	0.667	0.586	0.626	0.782	0.607	0.722	0.624	0.764	0.672	0.651	-
<b>Mn</b>	0.044	0.144	0.137	0.079	0.133	0.121	0.093	0.059	0.149	0.086	0.134	0.091	-
<b>Mg</b>	0.739	0.257	0.219	0.346	0.258	0.109	0.304	0.241	0.253	0.172	0.213	0.274	-
<b>Ca</b>	0.477	1.000	0.981	0.999	0.995	0.993	1.000	0.992	0.992	1.005	0.992	0.988	-
<b>Na</b>	0.017	0.001	0.001	0.003	0.002	0.001	0.001	0.000	0.000	0.002	0.000	0.001	-
<b>K</b>	0.008	0.000	0.000	0.001	0.000	0.000	0.001	0.001	0.000	0.000	0.000	0.000	-
<b>P</b>	0.001	n/a	n/a	n/a	n/a	n/a	-						
<b>Cation Total</b>	3.937	4.010	4.004	4.017	4.010	4.006	4.011	4.009	4.011	4.018	4.009	4.005	-
<b>Mg/(Mg+Fe+Ca)</b>	0.432	0.137	0.117	0.179	0.137	0.058	0.159	0.123	0.135	0.088	0.114	0.143	-
<b>Fe/(Mg+Fe+Ca)</b>	0.289	0.328	0.357	0.303	0.333	0.415	0.318	0.369	0.334	0.394	0.358	0.340	-
<b>Ca/(Mg+Fe+Ca)</b>	0.279	0.534	0.525	0.518	0.530	0.527	0.524	0.507	0.531	0.518	0.528	0.516	-

**Table A.3** **Concretion core: Feldspar**

Sample	PPP30-3-23	PPP30-3-24	PPP30-3-25	PPP30-1-1	PPP30-1-2	PPP30-1-3	PPP30-1-4	PPP30-1-5	PPP30-1-6	PPP30-1-7	PPP30-1-13	PPP5c-1-5
Probe #	30	31	32	61	62	63	64	65	66	67	73	143
<b>SiO<sub>2</sub></b>	43.08	43.15	43.51	42.70	42.92	43.33	43.45	43.25	43.40	42.99	44.13	43.25
<b>TiO<sub>2</sub></b>	0.05	0.00	0.00	0.00	0.01	0.00	0.01	0.03	0.00	0.01	0.00	0.00
<b>Al<sub>2</sub>O<sub>3</sub></b>	36.16	37.09	37.04	36.59	36.33	35.97	36.48	36.61	36.31	36.30	36.27	36.18
<b>Cr<sub>2</sub>O<sub>3</sub></b>	0.00	0.00	0.00	0.00	0.01	0.00	0.00	0.00	0.00	0.00	0.00	0.01
<b>FeO</b>	0.43	0.11	0.12	0.09	0.09	0.07	0.08	0.12	0.06	0.15	0.19	0.12
<b>MnO</b>	0.06	0.00	0.01	0.02	0.03	0.01	0.03	0.01	0.00	0.12	0.03	0.02
<b>MgO</b>	0.27	0.00	0.00	0.00	0.00	0.00	0.00	0.00	0.03	0.00	0.13	0.00
<b>CaO</b>	19.68	20.30	19.97	20.08	20.10	19.58	19.91	20.12	19.83	20.02	16.31	19.94
<b>Na<sub>2</sub>O</b>	0.35	0.15	0.31	0.13	0.15	0.40	0.27	0.25	0.26	0.22	0.42	0.19
<b>K<sub>2</sub>O</b>	0.01	0.02	0.03	0.04	0.02	0.03	0.02	0.02	0.06	0.03	1.38	0.06
<b>P<sub>2</sub>O<sub>5</sub></b>	0.02	0.02	0.01	0.01	0.00	0.00	0.00	0.00	0.00	0.00	0.00	0.01
<b>Total</b>	100.12	100.83	101.00	99.65	99.67	99.39	100.26	100.42	99.95	99.83	98.86	99.78
<b>Cations pfu based on 8 oxygen</b>												
<b>Si</b>	1.998	1.986	1.997	1.988	1.998	2.019	2.008	1.998	2.011	1.998	2.058	2.009
<b>Ti</b>	0.002	0.000	0.000	0.000	0.000	0.000	0.001	0.001	0.000	0.000	0.000	0.000
<b>Al</b>	1.978	2.011	2.004	2.008	1.993	1.975	1.987	1.993	1.983	1.989	1.994	1.981
<b>Cr</b>	0.000	0.000	0.000	0.000	0.001	0.000	0.000	0.000	0.000	0.000	0.000	0.001
<b>Fe</b>	0.017	0.004	0.005	0.003	0.003	0.003	0.003	0.005	0.002	0.006	0.007	0.005
<b>Mn</b>	0.002	0.000	0.000	0.001	0.001	0.001	0.001	0.001	0.000	0.005	0.002	0.001
<b>Mg</b>	0.019	0.000	0.000	0.000	0.000	0.000	0.000	0.000	0.002	0.000	0.009	0.000
<b>Ca</b>	0.978	1.001	0.982	1.002	1.002	0.978	0.986	0.996	0.985	0.998	0.815	0.992
<b>Na</b>	0.032	0.014	0.027	0.012	0.014	0.036	0.025	0.022	0.023	0.020	0.038	0.017
<b>K</b>	0.001	0.001	0.002	0.002	0.002	0.002	0.002	0.001	0.004	0.002	0.082	0.003
<b>P</b>	0.002	0.002	0.002	0.001	0.000	0.000	0.000	0.000	0.000	0.000	0.000	0.000
<b>Cation Total</b>	5.029	5.018	5.018	5.017	5.013	5.014	5.012	5.016	5.010	5.017	5.005	5.008
<b>x anorthite</b>	0.968	0.986	0.971	0.986	0.985	0.963	0.974	0.977	0.973	0.979	0.872	0.980
<b>x albite</b>	0.032	0.013	0.027	0.012	0.013	0.035	0.025	0.022	0.023	0.020	0.041	0.017
<b>x orthoclase</b>	0.001	0.001	0.002	0.002	0.002	0.002	0.002	0.001	0.004	0.002	0.087	0.003

Mole fraction xAn = Ca/(Ca+Na+K); xAb = Na/(Ca+Na+K); xOr = K/(Ca+Na+K)

Sample	PPP5c-1-7	PPP5c-1-8	PPP7c-1-1	PPP7c-1-2	PPP7c-1-3	PPP7c-2-9	PCR26b-1-22	PCR26b-2-2	PCR26b-2-6	PCR23a-3-15	PCR23a-3-16	PCR23a-3-17
Probe #	145	146	174	175	176	207	295	306	310	659	660	661
<b>SiO<sub>2</sub></b>	42.80	42.95	40.27	41.14	39.98	43.22	43.00	43.98	59.44	43.37	43.64	43.28
<b>TiO<sub>2</sub></b>	0.02	0.01	0.00	0.03	0.00	0.11	0.00	0.00	0.00	0.00	0.00	0.00
<b>Al<sub>2</sub>O<sub>3</sub></b>	35.92	35.92	35.52	35.83	35.94	35.89	34.69	35.42	26.24	35.76	34.98	35.71
<b>Cr<sub>2</sub>O<sub>3</sub></b>	0.03	0.02	0.00	0.00	0.00	0.07	0.00	0.00	0.00	0.00	0.00	0.00
<b>FeO</b>	0.19	0.28	0.04	0.14	0.10	0.19	0.51	0.61	0.90	0.09	0.14	0.00
<b>MnO</b>	0.03	0.05	0.00	0.04	0.01	0.11	0.30	0.37	0.26	0.00	0.00	0.00
<b>MgO</b>	0.00	0.00	0.00	0.00	0.00	0.11	0.00	0.01	0.34	0.01	0.01	0.01
<b>CaO</b>	20.09	20.20	20.26	20.03	20.18	20.36	18.94	19.31	1.44	19.88	19.41	20.27
<b>Na<sub>2</sub>O</b>	0.11	0.13	0.36	0.26	0.15	0.32	0.47	0.48	6.38	0.29	0.50	0.17
<b>K<sub>2</sub>O</b>	0.06	0.05	0.01	0.02	0.01	0.02	0.02	0.01	3.72	0.01	0.04	0.01
<b>P<sub>2</sub>O<sub>5</sub></b>	0.00	0.00	0.02	0.00	0.00	0.07	0.02	0.01	0.00	0.00	0.00	0.00
<b>Total</b>	99.23	99.60	96.48	97.49	96.38	100.48	97.96	100.20	98.72	99.41	98.71	99.45
<b>Cations pfu based on 8 oxygen</b>												
<b>Si</b>	2.002	2.003	1.9464	1.964	1.934	2.000	2.038	2.038	2.689	2.022	2.047	2.018
<b>Ti</b>	0.001	0.001	0	0.001	0.000	0.004	0.000	0.000	0.000	0.000	0.000	0.000
<b>Al</b>	1.981	1.975	2.024	2.017	2.049	1.958	1.938	1.935	1.399	1.965	1.934	1.962
<b>Cr</b>	0.001	0.001	0	0.000	0.000	0.002	0.000	0.000	0.000	0.000	0.000	0.000
<b>Fe</b>	0.007	0.011	0.0016	0.006	0.004	0.007	0.020	0.024	0.034	0.004	0.006	0.000
<b>Mn</b>	0.001	0.002	0	0.002	0.000	0.005	0.012	0.014	0.010	0.000	0.000	0.000
<b>Mg</b>	0.000	0.000	0	0.000	0.000	0.008	0.000	0.001	0.022	0.001	0.001	0.001
<b>Ca</b>	1.007	1.010	1.0496	1.025	1.046	1.010	0.962	0.959	0.070	0.993	0.975	1.013
<b>Na</b>	0.010	0.012	0.0336	0.024	0.014	0.029	0.043	0.043	0.560	0.026	0.045	0.015
<b>K</b>	0.003	0.002	0.0008	0.002	0.001	0.001	0.002	0.001	0.214	0.001	0.002	0.001
<b>P</b>	0.000	0.000	0.0008	0.000	0.000	0.002	0.001	0.000	0.000	0.000	0.000	0.000
<b>Cation Total</b>	5.013	5.017	5.0568	5.039	5.050	5.026	5.015	5.016	4.999	5.011	5.010	5.010
<b>x anorthite</b>	0.987	0.986	0.968	0.976	0.986	0.972	0.955	0.956	0.082	0.974	0.954	0.984
<b>x albite</b>	0.009	0.012	0.031	0.023	0.014	0.001	0.043	0.043	0.664	0.025	0.044	0.015
<b>x orthoclase</b>	0.003	0.002	0.001	0.002	0.001	0.028	0.002	0.001	0.254	0.001	0.002	0.001

Mole fraction xAn = Ca/(Ca+Na+K); xAb = Na/(Ca+Na+K); xOr = K/(Ca+Na+K)

Sample	PCR23a-3-18	PCR11b-4-8	PCR11b-4-10	PCR11b-4-11	PCR11b-4-9	WL18b-4-17	WL18b-4-10	WL18b-4-15	WL18b-4-18
Probe #	662	594	596	597	595	52	45	50	53
<b>SiO<sub>2</sub></b>	43.11	44.60	45.25	45.02	64.96	39.33	67.68	68.28	64.50
<b>TiO<sub>2</sub></b>	0.00	0.00	0.00	0.02	0.00	0.05	0.01	0.00	0.00
<b>Al<sub>2</sub>O<sub>3</sub></b>	35.72	34.81	34.42	34.74	18.21	29.66	20.80	20.92	19.23
<b>Cr<sub>2</sub>O<sub>3</sub></b>	0.00	0.00	0.00	0.00	0.00	n/a	n/a	n/a	n/a
<b>FeO</b>	0.06	0.03	0.09	0.04	0.07	5.78	0.50	0.14	0.19
<b>MnO</b>	0.00	0.00	0.00	0.00	0.00	0.50	0.06	0.02	0.01
<b>MgO</b>	0.01	0.00	0.00	0.00	0.00	0.07	0.39	0.01	0.00
<b>CaO</b>	19.86	18.94	18.25	18.88	0.00	24.29	1.06	0.91	0.13
<b>Na<sub>2</sub>O</b>	0.18	0.78	1.18	0.88	0.04	0.00	8.68	6.77	0.24
<b>K<sub>2</sub>O</b>	0.02	0.02	0.03	0.01	16.14	0.01	0.35	0.23	16.00
<b>P<sub>2</sub>O<sub>5</sub></b>	0.00	0.01	0.00	0.00	0.00	n/a	n/a	n/a	n/a
<b>Total</b>	98.95	99.19	99.22	99.59	99.43	99.69	99.53	97.27	100.29
<b>Cations pfu based on 8 oxygen</b>									
<b>Si</b>	2.018	2.076	2.102	2.086	3.012	1.935	2.959	3.012	2.970
<b>Ti</b>	0.000	0.000	0.000	0.001	0.000	0.002	0.000	0.000	0.000
<b>Al</b>	1.971	1.910	1.886	1.898	0.996	1.720	1.072	1.088	1.044
<b>Cr</b>	0.000	0.000	0.000	0.000	0.000	n/a	n/a	n/a	n/a
<b>Fe</b>	0.002	0.002	0.003	0.002	0.002	0.238	0.018	0.005	0.007
<b>Mn</b>	0.000	0.000	0.000	0.000	0.000	0.021	0.002	0.001	0.000
<b>Mg</b>	0.000	0.000	0.000	0.000	0.000	0.005	0.025	0.001	0.000
<b>Ca</b>	0.996	0.945	0.909	0.938	0.000	1.281	0.050	0.043	0.006
<b>Na</b>	0.016	0.070	0.106	0.079	0.003	0.000	0.736	0.579	0.022
<b>K</b>	0.002	0.002	0.002	0.001	0.955	0.001	0.019	0.013	0.940
<b>P</b>	0.000	0.000	0.000	0.000	0.000	n/a	n/a	n/a	n/a
<b>Cation Total</b>	5.006	5.005	5.009	5.004	4.970	5.203	4.882	4.740	4.989
<b>x anorthite</b>	0.983	0.929	0.894	0.921	0.000	1.000	0.061	0.068	0.006
<b>x albite</b>	0.016	0.069	0.105	0.078	0.003	0.000	0.914	0.912	0.022
<b>x orthoclase</b>	0.002	0.002	0.002	0.001	0.997	0.000	0.024	0.021	0.971

Mole fraction xAn = Ca/(Ca+Na+K); xAb = Na/(Ca+Na+K); xOr = K/(Ca+Na+K)

**Table A.4 Concretion core: Chlorite**

Sample	PPP30-3-10	PPP30-3-13	PPP30-3-14	PPP30-1-15	PPP30-1-16	PPP5c-1-17	PPP5c-1-19	PPP7c-1-7	PPP7c-1-8	PPP7c-1-9	PPP7c-1-10	PPP7c-1-23
Probe #	17	20	21	75	76	155	157	180	181	182	183	196
<b>SiO<sub>2</sub></b>	24.85	28.74	27.59	31.00	29.51	24.70	24.50	24.28	24.72	23.90	23.69	28.46
<b>TiO<sub>2</sub></b>	0.08	0.09	0.06	0.05	0.03	0.27	0.09	0.07	0.59	0.05	0.04	0.02
<b>Al<sub>2</sub>O<sub>3</sub></b>	21.70	14.56	15.49	17.72	16.17	20.21	19.52	19.73	20.39	18.88	19.58	17.21
<b>Cr<sub>2</sub>O<sub>3</sub></b>	0.05	0.06	0.07	0.05	0.05	0.09	0.09	0.04	0.02	0.07	0.03	0.03
<b>FeO</b>	26.72	25.58	25.86	24.81	24.13	32.59	32.35	28.36	25.96	28.16	28.11	18.64
<b>MnO</b>	3.39	0.86	1.55	2.00	0.66	2.85	2.98	1.50	1.59	1.45	1.51	1.56
<b>MgO</b>	9.03	13.98	12.42	10.40	15.92	6.61	6.89	10.94	12.53	11.13	11.36	18.84
<b>CaO</b>	0.73	1.75	2.74	1.51	0.38	0.28	0.25	0.12	0.47	0.11	0.16	0.23
<b>Na<sub>2</sub>O</b>	0.06	0.08	0.06	0.00	0.04	0.00	0.00	0.00	0.02	0.01	0.02	0.23
<b>K<sub>2</sub>O</b>	0.02	0.03	0.03	0.04	0.05	0.05	0.06	0.03	0.03	0.03	0.02	0.05
<b>P<sub>2</sub>O<sub>5</sub></b>	0.01	0.01	0.01	0.00	0.01	0.02	0.02	0.00	0.01	0.04	0.00	0.01
<b>Total</b>	86.64	85.72	85.90	87.57	86.94	87.6725	86.7479	85.07	86.35	83.83	84.52	85.29
<b>Cations pfu based on 18 oxygen</b>												
<b>Si</b>	3.501	4.030	3.902	4.194	4.005	3.541	3.559	3.496	3.458	3.499	3.438	3.854
<b>Ti</b>	0.007	0.009	0.007	0.005	0.002	0.029	0.011	0.007	0.061	0.005	0.004	0.002
<b>Al</b>	3.604	2.407	2.583	2.826	2.587	3.416	3.341	3.348	3.361	3.258	3.350	2.747
<b>Cr</b>	0.005	0.007	0.007	0.005	0.005	0.011	0.011	0.005	0.002	0.007	0.004	0.004
<b>Fe</b>	3.148	3.001	3.060	2.806	2.738	3.908	3.929	3.413	3.037	3.449	3.411	2.111
<b>Mn</b>	0.403	0.103	0.185	0.229	0.076	0.346	0.367	0.182	0.189	0.180	0.185	0.180
<b>Mg</b>	1.895	2.921	2.621	2.099	3.220	1.413	1.492	2.347	2.612	2.428	2.457	3.802
<b>Ca</b>	0.110	0.263	0.416	0.220	0.054	0.043	0.038	0.018	0.072	0.018	0.025	0.034
<b>Na</b>	0.016	0.020	0.016	0.000	0.009	0.002	0.000	0.002	0.005	0.004	0.004	0.059
<b>K</b>	0.004	0.005	0.005	0.007	0.009	0.009	0.011	0.005	0.005	0.005	0.005	0.009
<b>P</b>	0.002	0.002	0.004	0.000	0.002	0.002	0.002	0.000	0.002	0.005	0.000	0.002
<b>Cation Total</b>	12.697	12.769	12.809	12.393	12.708	12.721	12.760	12.823	12.803	12.861	12.884	12.805
<b>Mg/(Mg+Mn+Fe)</b>	0.348	0.485	0.447	0.409	0.534	0.249	0.258	0.395	0.447	0.401	0.406	0.624

Sample	PPP7c-1-24	PPP7c-1-25	PPP7c-2-10	PPP7c-2-20	PPP7c-2-22	PCR26b-1-15	PCR26b-1-16	PCR26b-1-18	PCR26b-1-19	PCR26b-1-20	PCR26b-1-21	PCR23a-3-4
Probe #	197	198	208	218	220	288	289	291	292	293	294	648
<b>SiO<sub>2</sub></b>	26.70	24.87	27.26	25.55	26.45	24.81	24.93	24.77	23.73	25.56	25.51	24.46
<b>TiO<sub>2</sub></b>	0.05	0.04	0.13	0.30	0.14	0.00	0.00	0.00	0.00	0.00	0.04	0.03
<b>Al<sub>2</sub>O<sub>3</sub></b>	19.95	21.94	24.66	19.76	19.55	23.05	21.97	22.06	22.52	22.26	20.88	19.84
<b>Cr<sub>2</sub>O<sub>3</sub></b>	0.01	0.03	0.04	0.13	0.13	0.00	0.00	0.00	0.00	0.00	0.00	0.00
<b>FeO</b>	20.20	20.35	18.75	28.30	28.56	29.50	29.19	29.52	29.50	27.55	25.08	33.09
<b>MnO</b>	1.80	2.02	1.84	1.61	1.49	0.51	0.46	0.50	0.46	0.42	0.44	0.88
<b>MgO</b>	16.64	15.13	16.70	11.81	12.21	8.54	9.86	9.23	8.30	9.62	11.44	7.45
<b>CaO</b>	0.14	0.03	0.04	0.18	0.10	0.08	0.06	0.06	0.44	0.15	0.03	0.13
<b>Na<sub>2</sub>O</b>	1.29	0.02	0.14	0.27	0.15	0.00	0.00	0.00	0.00	0.00	0.01	0.00
<b>K<sub>2</sub>O</b>	0.05	0.02	0.03	0.04	0.03	0.04	0.04	0.04	0.03	0.05	0.14	0.01
<b>P<sub>2</sub>O<sub>5</sub></b>	0.01	0.00	0.06	0.10	0.08	0.08	0.07	0.02	0.02	0.02	0.02	0.00
<b>Total</b>	86.85	84.46	89.65	88.05	88.88	86.60	86.57	86.20	85.01	85.64	83.60	85.89
<b>Cations pfu based on 18 oxygen</b>												
<b>Si</b>	3.602	3.443	3.4848	3.5388	3.618	3.476	3.494	3.496	3.409	3.582	3.627	3.559
<b>Ti</b>	0.005	0.004	0.0126	0.0324	0.0144	0.000	0.000	0.000	0.000	0.000	0.005	0.004
<b>Al</b>	3.172	3.582	3.7152	3.2256	3.1518	3.805	3.629	3.670	3.814	3.676	3.499	3.402
<b>Cr</b>	0.002	0.004	0.0036	0.0144	0.0144	0.000	0.000	0.000	0.000	0.000	0.000	0.000
<b>Fe</b>	2.279	2.356	2.0052	3.2778	3.267	3.456	3.422	3.485	3.546	3.229	2.983	4.027
<b>Mn</b>	0.205	0.238	0.1998	0.189	0.1728	0.061	0.054	0.059	0.056	0.050	0.052	0.108
<b>Mg</b>	3.346	3.123	3.1824	2.4372	2.4894	1.784	2.061	1.942	1.778	2.011	2.425	1.615
<b>Ca</b>	0.022	0.005	0.0054	0.027	0.0144	0.013	0.009	0.009	0.068	0.023	0.005	0.022
<b>Na</b>	0.337	0.004	0.036	0.072	0.0378	0.000	0.000	0.000	0.000	0.000	0.004	0.000
<b>K</b>	0.009	0.004	0.0054	0.0072	0.0054	0.007	0.007	0.007	0.007	0.009	0.025	0.002
<b>P</b>	0.000	0.000	0.0072	0.0126	0.009	0.011	0.007	0.002	0.004	0.002	0.002	0.000
<b>Cation Total</b>	12.980	12.762	12.6594	12.8358	12.7962	12.614	12.685	12.670	12.685	12.584	12.629	12.739
<b>Mg/(Mg+Mn+Fe)</b>	0.574	0.546	0.591	0.413	0.420	0.337	0.372	0.354	0.331	0.380	0.444	0.281

Sample	PCR23a-3- 5 649	WL18b-4- 13 48	WL18b-5- 12 13
Probe #			
<b>SiO<sub>2</sub></b>	23.78	33.28	24.66
<b>TiO<sub>2</sub></b>	0.00	0.00	0.01
<b>Al<sub>2</sub>O<sub>3</sub></b>	19.86	16.31	21.61
<b>Cr<sub>2</sub>O<sub>3</sub></b>	0.00	n/a	n/a
<b>FeO</b>	34.11	15.07	38.18
<b>MnO</b>	0.85	0.93	1.48
<b>MgO</b>	6.41	21.49	6.08
<b>CaO</b>	0.10	1.32	0.18
<b>Na<sub>2</sub>O</b>	0.00	0.00	-
<b>K<sub>2</sub>O</b>	0.02	0.01	0.02
<b>P<sub>2</sub>O<sub>5</sub></b>	0.02	n/a	n/a
<b>Total</b>	85.15	88.40	92.21
<b>Cations pfu based on 18 oxygen</b>			
<b>Si</b>	3.519	4.211	3.145
<b>Ti</b>	0.000	0.000	0.001
<b>Al</b>	3.463	2.433	3.537
<b>Cr</b>	0.000	n/a	n/a
<b>Fe</b>	4.221	1.595	4.421
<b>Mn</b>	0.106	0.100	0.174
<b>Mg</b>	1.415	4.054	1.255
<b>Ca</b>	0.016	0.178	0.027
<b>Na</b>	0.000	0.000	0.000
<b>K</b>	0.004	0.002	0.003
<b>P</b>	0.002	n/a	n/a
<b>Cation Total</b>	12.748	12.573	
<b>Mg/(Mg+Mn+Fe)</b>	0.246	0.705	12.822

**Table A.5** Concretion core: Vesuvianite

Sample	WL16b-6-1	WL16b-6-2	WL16b-6-3	WL16b-6-4	WL16b-6-5	WL16b-6-6	WL16b-6-7	WL16b-6-8	WL16b-6-9	WL16b-6-10
Probe #	1	2	3	4	5	6	7	8	9	10
<b>SiO<sub>2</sub></b>	36.123	36.2585	35.8976	35.9757	35.9292	36.6744	36.6026	36.2179	36.2217	35.6485
<b>TiO<sub>2</sub></b>	1.7469	1.6923	1.7959	1.7003	1.6054	1.7806	1.8123	1.6966	1.7239	1.8587
<b>Al<sub>2</sub>O<sub>3</sub></b>	15.9103	15.9283	15.8893	16.0034	15.8097	15.6617	16.3366	16.2072	15.7319	15.7847
<b>Cr<sub>2</sub>O<sub>3</sub></b>	0.0217	0.0366	0.0191	0.0098	0.0243	0.0161	0.0208	0	0.0719	0.0125
<b>FeO</b>	3.9765	3.9043	3.9094	3.9275	3.8191	3.7201	2.4765	2.5775	4.2507	4.0468
<b>MnO</b>	0.9974	1.0402	1.0206	0.9571	0.9349	0.9088	0.316	0.3654	0.9361	0.9428
<b>MgO</b>	1.4919	1.4542	1.4848	1.4939	1.535	1.5628	1.9242	1.9429	1.4182	1.4297
<b>CaO</b>	35.2997	35.5585	35.2735	35.4654	35.3242	35.2976	36.1059	35.9529	35.2415	35.3911
<b>Na<sub>2</sub>O</b>	0.0149	0.0294	0.0269	0.0174	0.0145	0.0269	0.0167	0.0065	0.0188	0.0158
<b>K<sub>2</sub>O</b>	0.0136	0.0068	0.0104	0.0116	0.0231	0.0216	0.0293	0.0361	0.0257	0.022
<b>P<sub>2</sub>O<sub>5</sub></b>	n/a									
<b>Total</b>	95.596	95.9091	95.3275	95.5622	95.0195	95.6707	95.641	95.0031	95.6405	95.1526
<b>Cations pfu based on 74 oxygen</b>										
<b>Si</b>	18.1522	18.167	18.1004	18.093	18.1596	18.3594	18.204	18.1596	18.2114	18.0338
<b>Ti</b>	0.6586	0.6364	0.6808	0.6438	0.6068	0.6734	0.6808	0.6364	0.6512	0.7104
<b>Al</b>	9.4202	9.4054	9.4424	9.4868	9.4202	9.2426	9.5756	9.583	9.324	9.4128
<b>Cr</b>	0.0074	0.0148	0.0074	0.0074	0.0074	0.0074	0.0074	0	0.0296	0.0074
<b>Fe</b>	1.6724	1.6354	1.6502	1.6502	1.6132	1.554	1.0286	1.0804	1.7908	1.7094
<b>Mn</b>	0.4218	0.444	0.4366	0.407	0.3996	0.3848	0.1332	0.1554	0.3996	0.407
<b>Mg</b>	1.1174	1.0878	1.1174	1.1174	1.1544	1.1692	1.4282	1.4504	1.0656	1.0804
<b>Ca</b>	19.0032	19.0846	19.055	19.1068	19.129	18.9366	19.2474	19.3214	18.981	19.1808
<b>Na</b>	0.0148	0.0296	0.0296	0.0148	0.0148	0.0296	0.0148	0.0074	0.0148	0.0148
<b>K</b>	0.0074	0.0074	0.0074	0.0074	0.0148	0.0148	0.0222	0.0222	0.0148	0.0148
<b>P</b>	n/a									
<b>Cation Total</b>	50.4754	50.5198	50.5346	50.542	50.5272	50.3718	50.3496	50.4236	50.4828	50.579
<b>Fe/(Fe+Mg)</b>	0.60	0.60	0.60	0.60	0.58	0.57	0.42	0.43	0.63	0.61
<b>Mg/(Fe+Mg)</b>	0.40	0.40	0.40	0.40	0.42	0.43	0.58	0.57	0.37	0.39

**Table A.6 Concretion core: Prehnite**

Sample	PCR11b-2-18	PCR11b-2-19	PCR11b-2-20	PCR11b-2-21	PCR11b-2-22	PCR11b-3-19	PCR11b-3-20	PCR11b-3-21
Probe #	552	553	554	555	556	578	579	580
<b>SiO<sub>2</sub></b>	43.689	43.694	43.341	43.771	43.383	43.100	43.134	45.294
<b>TiO<sub>2</sub></b>	0.000	0.000	0.000	0.000	0.000	0.000	0.000	0.000
<b>Al<sub>2</sub>O<sub>3</sub></b>	23.769	23.710	23.558	23.622	23.632	23.516	23.761	25.676
<b>Cr<sub>2</sub>O<sub>3</sub></b>	0.000	0.000	0.000	0.000	0.000	0.000	0.000	0.000
<b>FeO</b>	0.122	0.247	0.122	0.238	0.327	0.583	0.489	0.255
<b>MnO</b>	0.052	0.083	0.053	0.093	0.083	0.066	0.268	0.223
<b>MgO</b>	0.000	0.007	0.000	0.121	0.000	0.006	0.020	0.012
<b>CaO</b>	25.992	25.909	25.999	25.954	26.412	26.375	26.004	22.770
<b>Na<sub>2</sub>O</b>	0.105	0.091	0.099	0.092	0.065	0.025	0.034	0.338
<b>K<sub>2</sub>O</b>	0.013	0.016	0.074	0.066	0.015	0.015	0.025	1.233
<b>P<sub>2</sub>O<sub>5</sub></b>	0.040	0.040	0.027	0.046	0.008	0.028	0.017	0.019
<b>Total</b>	93.782	93.798	93.274	94.001	93.925	93.713	93.751	95.819
<b>Cations pfu based on 24 oxygen</b>								
<b>Si</b>	6.653	6.655	6.646	6.658	6.619	6.602	6.598	6.713
<b>Ti</b>	0.000	0.000	0.000	0.000	0.000	0.000	0.000	0.000
<b>Al</b>	4.267	4.258	4.258	4.234	4.250	4.246	4.284	4.486
<b>Cr</b>	0.000	0.000	0.000	0.000	0.000	0.000	0.000	0.000
<b>Fe</b>	0.014	0.031	0.017	0.031	0.041	0.074	0.062	0.031
<b>Mn</b>	0.007	0.010	0.007	0.012	0.010	0.010	0.034	0.029
<b>Mg</b>	0.000	0.002	0.000	0.026	0.000	0.002	0.005	0.002
<b>Ca</b>	4.241	4.229	4.272	4.229	4.318	4.330	4.262	3.614
<b>Na</b>	0.031	0.026	0.029	0.026	0.019	0.007	0.010	0.096
<b>K</b>	0.002	0.002	0.014	0.012	0.002	0.002	0.005	0.233
<b>P</b>	0.005	0.005	0.002	0.005	0.000	0.002	0.002	0.002
<b>Cation Total</b>	15.221	15.218	15.247	15.233	15.262	15.278	15.264	15.209

**Table B.1** Concretion rim: Garnet

Sample	PPP5c-2-16	PPP5c-2-17	PPP5c-2-18	PPP5c-2-19	PPP5c-2-20	PPP5c-2-21	PPP5c-2-22	PPP5c-3-15	PPP5c-3-16	PPP7c-3-12	PPP7c-3-14	PPP7c-3-17
Probe #	98	99	100	101	102	103	104	131	132	237	239	242
<b>SiO<sub>2</sub></b>	36.92	36.97	36.68	37.24	37.16	37.01	36.95	36.96	36.90	38.66	38.69	38.57
<b>TiO<sub>2</sub></b>	0.12	0.85	0.23	0.13	0.72	0.98	0.24	0.20	0.10	0.78	0.25	0.37
<b>Al<sub>2</sub>O<sub>3</sub></b>	21.50	20.19	21.45	21.67	20.46	20.27	21.39	21.53	21.90	18.87	20.66	20.11
<b>Cr<sub>2</sub>O<sub>3</sub></b>	0.15	0.04	0.04	0.04	0.04	0.03	0.14	0.11	0.05	0.92	0.14	0.14
<b>FeO</b>	15.91	10.11	15.69	16.42	10.27	10.10	15.55	18.17	17.97	5.77	5.85	7.29
<b>MnO</b>	19.44	17.11	20.20	18.78	17.31	16.59	19.16	19.13	20.41	4.10	7.99	4.61
<b>MgO</b>	1.36	0.17	1.19	1.40	0.15	0.15	1.27	1.25	1.06	0.04	0.06	0.04
<b>CaO</b>	3.73	13.61	3.73	4.01	13.36	14.55	4.28	2.52	2.00	30.83	26.67	29.16
<b>Na<sub>2</sub>O</b>	0.06	0.02	0.03	0.00	0.02	0.02	0.02	0.01	0.00	0.03	0.04	0.02
<b>K<sub>2</sub>O</b>	0.04	0.03	0.04	0.03	0.04	0.04	0.04	0.04	0.03	0.03	0.06	0.04
<b>P<sub>2</sub>O<sub>5</sub></b>	0.00	0.00	0.00	0.00	0.00	0.00	0.00	0.04	0.04	0.04	0.04	0.06
<b>Total</b>	99.22	99.11	99.29	99.72	99.52	99.73	99.04	99.96	100.46	100.06	100.43	100.42
<b>Cations pfu based on 12 oxygen</b>												
<b>Si</b>	2.992	2.982	2.980	2.998	2.983	2.966	2.995	2.987	2.975	3.004	2.996	2.988
<b>Ti</b>	0.007	0.052	0.014	0.008	0.043	0.059	0.014	0.012	0.006	0.046	0.014	0.022
<b>Al</b>	2.053	1.919	2.053	2.057	1.937	1.914	2.044	2.051	2.081	1.728	1.886	1.836
<b>Cr</b>	0.010	0.002	0.002	0.002	0.002	0.002	0.008	0.007	0.004	0.056	0.008	0.008
<b>Fe</b>	1.079	0.682	1.066	1.105	0.690	0.677	1.055	1.228	1.212	0.376	0.379	0.473
<b>Mn</b>	1.334	1.169	1.390	1.280	1.177	1.127	1.316	1.309	1.393	0.270	0.524	0.302
<b>Mg</b>	0.164	0.020	0.144	0.168	0.018	0.018	0.154	0.151	0.127	0.005	0.006	0.004
<b>Ca</b>	0.324	1.176	0.325	0.346	1.150	1.249	0.372	0.218	0.173	2.567	2.214	2.420
<b>Na</b>	0.010	0.004	0.004	0.000	0.002	0.002	0.004	0.001	0.001	0.004	0.006	0.004
<b>K</b>	0.004	0.004	0.004	0.002	0.004	0.005	0.004	0.005	0.004	0.002	0.006	0.005
<b>P</b>	0.000	0.000	0.000	0.000	0.000	0.000	0.000	0.002	0.002	0.002	0.002	0.004
<b>Cation Total</b>	7.978	8.010	7.981	7.968	8.008	8.020	7.966	7.972	7.978	8.059	8.044	8.066
<b>x Almandine</b>	0.394	0.225	0.383	0.405	0.229	0.222	0.385	0.446	0.436	0.117	0.122	0.148
<b>x Grossular</b>	0.118	0.389	0.117	0.127	0.381	0.409	0.136	0.079	0.062	0.799	0.710	0.757
<b>x Spessartine</b>	0.488	0.386	0.500	0.469	0.390	0.369	0.480	0.475	0.502	0.084	0.168	0.095

Mol fraction: x Almandine = Fe/(Fe+Ca+Mn); x Grossular = Ca/(Fe+Ca+Mn); x Spessartine = Mn/(Fe+Ca+Mn)

Sample	PPP7c-3-18	PPP7c-3-19	PPP7c-3-21	PPP7c-4-1	PPP7c-4-2	PPP7c-4-3	PPP7c-4-4	PPP7c-4-5	PPP7c-4-6	WL18b-2-28	WL18b-2-29	WL18b-2-30
Probe #	243	244	246	251	252	253	254	255	256	47	48	49
<b>SiO<sub>2</sub></b>	38.02	38.43	38.29	37.47	38.52	37.05	38.31	36.99	38.19	36.73	36.80	36.55
<b>TiO<sub>2</sub></b>	0.34	0.38	0.02	0.87	0.42	0.69	0.20	0.74	0.10	n/a	n/a	n/a
<b>Al<sub>2</sub>O<sub>3</sub></b>	20.72	20.41	27.02	19.92	20.16	20.25	20.40	20.22	20.72	20.36	20.40	20.06
<b>Cr<sub>2</sub>O<sub>3</sub></b>	0.08	0.09	0.07	0.19	0.11	0.00	0.00	0.00	0.00	n/a	n/a	n/a
<b>FeO</b>	12.92	6.61	7.62	8.35	7.48	7.74	7.95	7.82	8.89	26.65	27.06	26.15
<b>MnO</b>	9.49	7.69	0.35	18.68	7.87	21.99	9.26	22.27	10.17	11.41	11.08	10.65
<b>MgO</b>	0.08	0.06	0.02	0.38	0.05	0.34	0.05	0.35	0.09	0.94	1.02	1.03
<b>CaO</b>	18.63	26.96	24.02	13.65	25.01	11.04	23.28	10.78	21.21	3.67	3.61	3.53
<b>Na<sub>2</sub>O</b>	0.06	0.03	0.03	0.03	0.02	0.02	0.04	0.02	0.02	n/a	n/a	n/a
<b>K<sub>2</sub>O</b>	0.04	0.05	0.03	0.03	0.02	0.03	0.03	0.04	0.04	n/a	n/a	n/a
<b>P<sub>2</sub>O<sub>5</sub></b>	0.04	0.06	0.12	0.00	0.00	0.00	0.00	0.00	0.00	n/a	n/a	n/a
<b>Total</b>	100.42	100.77	97.58	99.58	99.68	99.15	99.53	99.23	99.43	99.77	99.97	97.97
<b>Cations pfu based on 12 oxygen</b>												
<b>Si</b>	2.994	2.978	2.923	3.002	3.016	2.995	3.013	2.992	3.012	3.004	3.003	3.030
<b>Ti</b>	0.020	0.022	0.001	0.053	0.025	0.042	0.012	0.046	0.006	n/a	n/a	n/a
<b>Al</b>	1.924	1.865	2.431	1.882	1.860	1.930	1.891	1.927	1.927	1.963	1.962	1.960
<b>Cr</b>	0.005	0.006	0.004	0.012	0.007	0.000	0.000	0.000	0.000	n/a	n/a	n/a
<b>Fe</b>	0.851	0.428	0.486	0.559	0.490	0.523	0.523	0.529	0.587	1.822	1.846	1.813
<b>Mn</b>	0.632	0.505	0.023	1.268	0.522	1.506	0.617	1.526	0.679	0.790	0.765	0.748
<b>Mg</b>	0.008	0.007	0.001	0.046	0.006	0.041	0.006	0.043	0.011	0.115	0.125	0.127
<b>Ca</b>	1.572	2.239	1.966	1.172	2.099	0.956	1.962	0.934	1.793	0.322	0.316	0.313
<b>Na</b>	0.008	0.005	0.005	0.005	0.004	0.004	0.006	0.004	0.002	n/a	n/a	n/a
<b>K</b>	0.004	0.005	0.002	0.002	0.001	0.004	0.004	0.004	0.004	n/a	n/a	n/a
<b>P</b>	0.002	0.004	0.007	0.000	0.000	0.000	0.000	0.000	0.000	n/a	n/a	n/a
<b>Cation Total</b>	8.021	8.065	7.849	8.003	8.029	8.002	8.035	8.005	8.021	8.015	8.016	7.990
<b>x Almandine</b>	0.278	0.135	0.196	0.186	0.157	0.175	0.169	0.177	0.192	0.621	0.631	0.631
<b>x Grossular</b>	0.515	0.706	0.794	0.391	0.675	0.320	0.632	0.312	0.586	0.110	0.108	0.109
<b>x Spessartine</b>	0.207	0.159	0.009	0.423	0.168	0.504	0.199	0.511	0.222	0.269	0.261	0.260

Mol fraction: x Almandine = Fe/(Fe+Ca+Mn); x Grossular = Ca/(Fe+Ca+Mn); x Spessartine = Mn/(Fe+Ca+Mn)

Sample	WL18b-2-31	WL18b-2-33	WL18b-2-34	WL18b-2-35	WL18b-2-37	WL18b-2-38	WL18b-2-39	WL18b-2-40
Probe #	50	52	53	54	56	57	58	59
SiO <sub>2</sub>	37.00	36.77	36.99	37.03	37.08	36.97	37.02	37.09
TiO <sub>2</sub>	n/a							
Al <sub>2</sub> O <sub>3</sub>	20.43	20.41	20.56	20.31	20.54	20.60	20.45	20.37
Cr <sub>2</sub> O <sub>3</sub>	n/a							
FeO	27.10	27.28	27.28	27.12	26.82	26.60	26.24	25.63
MnO	10.60	10.84	10.69	10.60	10.71	11.22	11.06	11.52
MgO	1.13	1.08	1.04	1.10	1.10	0.96	0.95	0.80
CaO	3.69	3.65	3.73	3.73	3.89	3.71	4.10	4.40
Na <sub>2</sub> O	n/a							
K <sub>2</sub> O	n/a							
P <sub>2</sub> O <sub>5</sub>	n/a							
Total	99.95	100.03	100.30	99.88	100.14	100.05	99.82	99.81
<b>Cations pfu based on 12 oxygen</b>								
Si	3.012	2.999	3.004	3.018	3.011	3.008	3.015	3.022
Ti	n/a							
Al	1.960	1.962	1.968	1.950	1.966	1.975	1.964	1.956
Cr	n/a							
Fe	1.845	1.861	1.853	1.848	1.822	1.810	1.788	1.746
Mn	0.731	0.749	0.735	0.732	0.736	0.773	0.763	0.795
Mg	0.138	0.131	0.126	0.134	0.133	0.116	0.115	0.097
Ca	0.322	0.319	0.325	0.325	0.339	0.323	0.358	0.384
Na	n/a							
K	n/a							
P	n/a							
Cation Total	8.008	8.021	8.012	8.007	8.006	8.005	8.003	8.000
x Almandine	0.637	0.635	0.636	0.636	0.629	0.623	0.615	0.597
x Grossular	0.111	0.109	0.112	0.112	0.117	0.111	0.123	0.131
x Spessartine	0.252	0.256	0.252	0.252	0.254	0.266	0.262	0.272

Mol fraction: x Almandine = Fe/(Fe+Ca+Mn); x Grossular = Ca/(Fe+Ca+Mn); x Spessartine = Mn/(Fe+Ca+Mn)

**Table B.2** Concretion rim: Clinopyroxene

Sample	PPP30-2-18	PPP30-2-19	PCR23a-1-9	PCR23a-1-10	PCR23a-1-12	PCR23a-1-13	PCR23a-2-2	PCR23a-2-3	PCR23a-2-7	PCR23a-2-9	PCR23a-2-10	PCR23a-2-13
Probe #	50	51	611	612	614	615	626	627	631	633	634	637
<b>SiO<sub>2</sub></b>	50.06	50.71	50.88	51.19	50.23	51.30	50.86	52.40	51.71	51.35	50.76	50.86
<b>TiO<sub>2</sub></b>	0.03	0.01	0.00	0.00	0.00	0.00	0.00	0.00	0.00	0.01	0.03	0.02
<b>Al<sub>2</sub>O<sub>3</sub></b>	0.35	0.47	1.31	0.95	0.34	0.47	0.29	2.50	0.30	0.51	0.59	0.57
<b>Cr<sub>2</sub>O<sub>3</sub></b>	0.00	0.00	0.00	0.00	0.00	0.00	0.00	0.00	0.00	0.04	0.00	0.02
<b>FeO</b>	14.54	13.20	14.08	14.48	19.05	14.41	15.53	15.08	12.74	13.69	15.75	16.45
<b>MnO</b>	1.86	1.62	1.03	1.14	1.13	1.05	0.98	0.86	1.69	1.58	1.42	1.37
<b>MgO</b>	7.43	8.59	8.82	8.55	5.38	8.90	7.58	13.24	9.98	9.47	7.37	7.01
<b>CaO</b>	23.87	23.87	23.39	23.34	23.40	23.67	23.89	12.14	22.99	23.12	23.81	23.53
<b>Na<sub>2</sub>O</b>	0.05	0.07	0.10	0.07	0.02	0.05	0.04	0.25	0.07	0.09	0.05	0.04
<b>K<sub>2</sub>O</b>	0.02	0.04	0.00	0.00	0.00	0.00	0.00	0.06	0.00	0.01	0.02	0.01
<b>P<sub>2</sub>O<sub>5</sub></b>	0.00	0.00	0.00	0.00	0.02	0.00	0.00	0.00	0.00	0.03	0.04	0.02
<b>Total</b>	98.22	98.57	99.61	99.71	99.57	99.86	99.18	96.52	99.49	99.90	99.84	99.89
<b>Cations pfu based on 6 oxygen</b>												
<b>Si</b>	1.986	1.987	1.969	1.982	1.994	1.985	1.994	2.021	1.994	1.981	1.982	1.989
<b>Ti</b>	0.001	0.000	0.000	0.000	0.000	0.000	0.000	0.000	0.000	0.001	0.001	0.001
<b>Al</b>	0.016	0.022	0.060	0.043	0.016	0.021	0.014	0.113	0.013	0.023	0.027	0.026
<b>Cr</b>	0.000	0.000	0.000	0.000	0.000	0.000	0.000	0.000	0.000	0.001	0.000	0.001
<b>Fe</b>	0.482	0.433	0.456	0.469	0.632	0.466	0.509	0.487	0.411	0.442	0.514	0.538
<b>Mn</b>	0.062	0.053	0.034	0.037	0.038	0.034	0.032	0.028	0.055	0.052	0.047	0.045
<b>Mg</b>	0.439	0.502	0.509	0.493	0.319	0.514	0.443	0.761	0.574	0.545	0.429	0.409
<b>Ca</b>	1.015	1.002	0.970	0.968	0.995	0.982	1.004	0.502	0.950	0.956	0.997	0.986
<b>Na</b>	0.004	0.005	0.007	0.005	0.001	0.004	0.003	0.019	0.005	0.007	0.004	0.003
<b>K</b>	0.001	0.002	0.000	0.000	0.000	0.000	0.000	0.003	0.000	0.000	0.001	0.001
<b>P</b>	0.000	0.000	0.000	0.000	0.001	0.000	0.000	0.000	0.000	0.001	0.001	0.001
<b>Cation Total</b>	4.007	4.005	4.005	3.998	3.997	4.006	4.000	3.934	4.003	4.007	4.004	3.999
<b>Mg/(Mg+Fe+Ca)</b>	0.227	0.259	0.263	0.256	0.164	0.262	0.226	0.435	0.297	0.281	0.221	0.211
<b>Fe/(Mg+Fe+Ca)</b>	0.249	0.223	0.236	0.243	0.325	0.238	0.260	0.278	0.212	0.227	0.265	0.278
<b>Ca/(Mg+Fe+Ca)</b>	0.524	0.518	0.501	0.502	0.511	0.500	0.513	0.287	0.491	0.492	0.514	0.510

Sample	PCR23a-2-2	PCR23a-2-3	PCR23a-2-7	PCR23a-2-9	PCR23a-2-10	PCR23a-2-13	WL18b-3a-1	WL18b-3a-2	WL18b-3a-3	WL18b-3a-7	WL18b-3a-8	WL18b-3a-11
<b>Probe #</b>	626	627	631	633	634	637	56	57	58	62	63	66
<b>SiO<sub>2</sub></b>	50.86	52.40	51.71	51.35	50.76	50.86	51.67	50.59	50.43	50.24	51.19	51.63
<b>TiO<sub>2</sub></b>	0.00	0.00	0.00	0.01	0.03	0.02	-	0.01	0.01	0.00	0.07	0.00
<b>Al<sub>2</sub>O<sub>3</sub></b>	0.29	2.50	0.30	0.51	0.59	0.57	0.18	0.89	0.12	0.31	0.58	0.37
<b>Cr<sub>2</sub>O<sub>3</sub></b>	0.00	0.00	0.00	0.04	0.00	0.02	n/a	n/a	n/a	n/a	n/a	n/a
<b>FeO</b>	15.53	15.08	12.74	13.69	15.75	16.45	19.44	20.15	20.10	20.08	13.30	17.92
<b>MnO</b>	0.98	0.86	1.69	1.58	1.42	1.37	3.64	2.98	3.10	2.63	1.99	1.77
<b>MgO</b>	7.58	13.24	9.98	9.47	7.37	7.01	4.83	4.62	4.63	4.70	9.47	6.86
<b>CaO</b>	23.89	12.14	22.99	23.12	23.81	23.53	23.77	23.40	23.43	22.81	23.49	23.50
<b>Na<sub>2</sub>O</b>	0.04	0.25	0.07	0.09	0.05	0.04	0.00	0.03	0.02	0.04	0.06	0.05
<b>K<sub>2</sub>O</b>	0.00	0.06	0.00	0.01	0.02	0.01	-	0.00	0.01	0.02	-	-
<b>P<sub>2</sub>O<sub>5</sub></b>	0.00	0.00	0.00	0.03	0.04	0.02	n/a	n/a	n/a	n/a	n/a	n/a
<b>Total</b>	99.18	96.52	99.49	99.90	99.84	99.89	103.52	102.66	101.83	100.82	100.15	102.09
<b>Cations pfu based on 6 oxygen</b>												
<b>Si</b>	1.994	2.021	1.994	1.981	1.982	1.989	1.991	1.970	1.983	1.989	1.973	1.988
<b>Ti</b>	0.000	0.000	0.000	0.001	0.001	0.001	0.008	0.041	0.006	0.014	0.026	0.017
<b>Al</b>	0.014	0.113	0.013	0.023	0.027	0.026	0.000	0.000	0.000	0.000	0.002	0.000
<b>Cr</b>	0.000	0.000	0.000	0.001	0.000	0.001	n/a	n/a	n/a	n/a	n/a	n/a
<b>Fe</b>	0.509	0.487	0.411	0.442	0.514	0.538	0.627	0.656	0.661	0.665	0.429	0.577
<b>Mn</b>	0.032	0.028	0.055	0.052	0.047	0.045	0.119	0.098	0.103	0.088	0.065	0.058
<b>Mg</b>	0.443	0.761	0.574	0.545	0.429	0.409	0.278	0.268	0.272	0.277	0.544	0.394
<b>Ca</b>	1.004	0.502	0.950	0.956	0.997	0.986	0.982	0.976	0.987	0.968	0.970	0.969
<b>Na</b>	0.003	0.019	0.005	0.007	0.004	0.003	0.000	0.002	0.001	0.003	0.004	0.004
<b>K</b>	0.000	0.003	0.000	0.000	0.001	0.001	0.000	0.000	0.000	0.001	0.000	0.000
<b>P</b>	0.000	0.000	0.000	0.001	0.001	0.001	n/a	n/a	n/a	n/a	n/a	n/a
<b>Cation Total</b>	4.000	3.934	4.003	4.007	4.004	3.999	4.005	4.011	4.014	4.006	4.014	4.006
<b>Mg/(Mg+Fe+Ca)</b>	0.226	0.435	0.297	0.281	0.221	0.211	0.147	0.141	0.141	0.145	0.280	0.203
<b>Fe/(Mg+Fe+Ca)</b>	0.260	0.278	0.212	0.227	0.265	0.278	0.332	0.345	0.344	0.348	0.221	0.297
<b>Ca/(Mg+Fe+Ca)</b>	0.513	0.287	0.491	0.492	0.514	0.510	0.521	0.514	0.514	0.507	0.499	0.500

**Table B.3** Concretion rim: Feldspar

Sample	PPP30-2-11	PPP30-2-12	PPP30-2-16	PPP30-2-20	PPP30-2-21	PPP5c-2-1	PPP5c-2-2	PPP5c-2-3	PPP5c-2-4	PPP5c-3-4	PPP5c-3-5	PPP5c-3-6
Probe #	43	44	48	52	53	83	84	85	86	120	121	122
<b>SiO<sub>2</sub></b>	43.42	42.95	43.50	42.76	43.67	44.914	46.658	45.566	45.906	46.393	48.128	56.535
<b>TiO<sub>2</sub></b>	0.00	0.00	0.00	0.00	0.00	0.000	0.000	0.000	0.000	0.000	0.000	0.000
<b>Al<sub>2</sub>O<sub>3</sub></b>	36.28	36.63	36.39	36.73	36.40	34.662	33.545	34.182	33.669	33.980	33.126	27.472
<b>Cr<sub>2</sub>O<sub>3</sub></b>	0.00	0.00	0.00	0.00	0.00	0.000	0.000	0.000	0.008	0.000	0.000	0.000
<b>FeO</b>	0.10	0.15	0.20	0.12	0.31	0.052	0.087	0.063	0.060	0.040	0.009	0.066
<b>MnO</b>	0.00	0.00	0.00	0.00	0.00	0.018	0.010	0.021	0.010	0.000	0.002	0.000
<b>MgO</b>	0.01	0.03	0.02	0.03	0.01	0.000	0.000	0.000	0.016	0.028	0.000	0.000
<b>CaO</b>	19.40	19.78	19.70	20.27	19.51	18.180	16.702	17.564	17.176	16.957	16.134	8.993
<b>Na<sub>2</sub>O</b>	0.58	0.27	0.38	0.21	0.58	1.157	2.020	1.563	1.708	1.943	2.725	6.585
<b>K<sub>2</sub>O</b>	0.01	0.01	0.02	0.02	0.01	0.028	0.047	0.035	0.031	0.035	0.041	0.088
<b>P<sub>2</sub>O<sub>5</sub></b>	0.00	0.00	0.00	0.00	0.00	0.000	0.001	0.000	0.000	0.000	0.002	0.000
<b>Total</b>	99.81	99.82	100.21	100.14	100.49	99.011	99.069	98.994	98.584	99.375	100.166	99.739
<b>Cations pfu based on 8 oxygen</b>												
<b>Si</b>	2.014	1.994	2.011	1.982	2.014	2.091	2.162	2.119	2.142	2.145	2.202	2.544
<b>Ti</b>	0.000	0.000	0.000	0.000	0.000	0.000	0.000	0.000	0.000	0.000	0.000	0.000
<b>Al</b>	1.984	2.005	1.983	2.007	1.979	1.902	1.833	1.874	1.851	1.852	1.787	1.457
<b>Cr</b>	0.000	0.000	0.000	0.000	0.000	0.000	0.000	0.000	0.000	0.000	0.000	0.000
<b>Fe</b>	0.004	0.006	0.008	0.005	0.012	0.002	0.003	0.002	0.002	0.002	0.000	0.002
<b>Mn</b>	0.000	0.000	0.000	0.000	0.000	0.001	0.000	0.001	0.000	0.000	0.000	0.000
<b>Mg</b>	0.001	0.002	0.002	0.002	0.001	0.000	0.000	0.000	0.001	0.002	0.000	0.000
<b>Ca</b>	0.965	0.984	0.976	1.007	0.965	0.907	0.830	0.875	0.858	0.840	0.791	0.434
<b>Na</b>	0.052	0.024	0.034	0.019	0.052	0.105	0.182	0.141	0.154	0.174	0.242	0.574
<b>K</b>	0.001	0.000	0.001	0.001	0.000	0.002	0.002	0.002	0.002	0.002	0.002	0.005
<b>P</b>	0.000	0.000	0.000	0.000	0.000	0.000	0.000	0.000	0.000	0.000	0.000	0.000
<b>Cation Total</b>	5.022	5.015	5.016	5.024	5.024	5.010	5.013	5.015	5.010	5.017	5.025	5.016
<b>x anorthite</b>	0.948	0.976	0.965	0.981	0.949	0.895	0.818	0.859	0.846	0.826	0.764	0.428
<b>x albite</b>	0.051	0.024	0.034	0.019	0.051	0.103	0.179	0.138	0.152	0.172	0.233	0.567
<b>x orthoclase</b>	0.001	0.000	0.001	0.001	0.000	0.002	0.002	0.002	0.002	0.002	0.002	0.005

Mole fraction xAn = Ca/(Ca+Na+K); xAb = Na/(Ca+Na+K); xOr = K/(Ca+Na+K)

Sample	PPP5c-3-7	PPP5c-3-8	PPP7c-3-4	PPP7c-3-5	PPP7c-3-6	PPP7c-3-7	PPP7c-3-8	PPP7c-3-22	PPP7c-3-23	PPP7c-4-14	PPP7c-4-15	PPP7c-4-16
Probe #	123	124	230	231	232	233	250	247	248	264	265	266
<b>SiO<sub>2</sub></b>	59.703	47.470	43.32	43.45	42.99	42.95	43.37	43.33	43.13	44.21	43.63	43.82
<b>TiO<sub>2</sub></b>	0.000	0.000	0.00	0.00	0.00	0.00	0.00	0.00	0.00	0.00	0.00	0.00
<b>Al<sub>2</sub>O<sub>3</sub></b>	25.247	33.942	36.26	35.82	36.28	34.15	36.09	36.49	36.11	34.54	35.47	35.32
<b>Cr<sub>2</sub>O<sub>3</sub></b>	0.000	0.000	0.00	0.00	0.00	0.00	0.00	0.00	0.00	0.00	0.00	0.00
<b>FeO</b>	0.042	0.096	0.26	0.55	0.71	0.76	0.25	0.56	0.18	0.01	0.02	0.14
<b>MnO</b>	0.000	0.000	0.01	0.00	0.00	0.06	0.01	0.00	0.00	0.00	0.00	0.07
<b>MgO</b>	0.000	0.000	0.00	0.05	0.00	0.48	0.01	0.01	0.00	0.00	0.00	0.00
<b>CaO</b>	6.203	16.304	20.47	19.89	20.27	18.42	20.39	20.50	20.41	19.44	20.15	19.93
<b>Na<sub>2</sub>O</b>	8.134	2.229	0.25	0.39	0.19	0.43	0.17	0.17	0.15	0.78	0.35	0.39
<b>K<sub>2</sub>O</b>	0.088	0.048	0.04	0.03	0.02	0.05	0.03	0.03	0.02	0.02	0.02	0.02
<b>P<sub>2</sub>O<sub>5</sub></b>	0.000	0.000	0.03	0.00	0.00	0.04	0.02	0.03	0.02	0.00	0.00	0.00
<b>Total</b>	99.418	100.088	100.62	100.18	100.47	97.34	100.35	101.11	100.03	98.99	99.65	99.69
<b>Cations pfu based on 8 oxygen</b>												
<b>Si</b>	2.674	2.174	2.001	2.015	1.992	2.046	2.007	1.994	2.002	2.067	2.030	2.038
<b>Ti</b>	0.000	0.000	0.000	0.000	0.000	0.000	0.000	0.000	0.000	0.000	0.000	0.000
<b>Al</b>	1.333	1.832	1.974	1.958	1.982	1.918	1.969	1.979	1.976	1.904	1.946	1.936
<b>Cr</b>	0.000	0.000	0.000	0.000	0.000	0.000	0.000	0.000	0.000	0.000	0.000	0.000
<b>Fe</b>	0.002	0.004	0.010	0.022	0.028	0.030	0.010	0.022	0.007	0.001	0.001	0.006
<b>Mn</b>	0.000	0.000	0.000	0.000	0.000	0.002	0.000	0.000	0.000	0.000	0.000	0.002
<b>Mg</b>	0.000	0.000	0.000	0.004	0.000	0.034	0.001	0.001	0.000	0.000	0.000	0.000
<b>Ca</b>	0.298	0.800	1.013	0.989	1.006	0.940	1.011	1.010	1.015	0.974	1.005	0.994
<b>Na</b>	0.706	0.198	0.022	0.035	0.017	0.040	0.015	0.015	0.014	0.070	0.031	0.035
<b>K</b>	0.005	0.003	0.002	0.002	0.002	0.003	0.002	0.002	0.002	0.001	0.002	0.001
<b>P</b>	0.000	0.000	0.001	0.000	0.000	0.002	0.001	0.001	0.001	0.000	0.000	0.000
<b>Cation Total</b>	5.017	5.011	5.022	5.025	5.026	5.015	5.016	5.024	5.017	5.018	5.015	5.012
<b>x anorthite</b>	0.295	0.799	0.977	0.964	0.982	0.956	0.984	0.984	0.985	0.932	0.968	0.965
<b>x albite</b>	0.700	0.197	0.002	0.002	0.002	0.003	0.002	0.002	0.002	0.067	0.030	0.034
<b>x orthoclase</b>	0.005	0.003	0.021	0.034	0.016	0.041	0.015	0.015	0.013	0.001	0.002	0.001

Mole fraction xAn = Ca/(Ca+Na+K); xAb = Na/(Ca+Na+K); xOr = K/(Ca+Na+K)

Sample	PPP7c-4-19	PCR26b-5-11	PCR26b-5-14	PCR26b-5-18	PCR26b-5-22	PCR26b-5-24	PCR23a-1-15	PCR23a-1-16	PCR23a-1-17	PCR23a-1-18	PCR23a-2-5	PCR23a-2-15
Probe #	269	388	391	395	399	401	617	618	619	620	629	639
<b>SiO<sub>2</sub></b>	44.05	61.15	59.96	64.18	63.31	62.58	43.77	43.66	43.45	43.84	43.33	43.27
<b>TiO<sub>2</sub></b>	0.00	0.00	0.00	0.00	0.00	0.00	0.00	0.00	0.00	0.00	0.00	0.00
<b>Al<sub>2</sub>O<sub>3</sub></b>	35.32	20.77	22.08	22.69	23.04	23.67	35.67	35.76	35.86	35.55	35.75	36.08
<b>Cr<sub>2</sub>O<sub>3</sub></b>	0.00	0.00	0.00	0.00	0.00	0.00	0.00	0.00	0.00	0.00	0.00	0.00
<b>FeO</b>	0.00	0.29	0.00	0.00	0.05	0.13	0.00	0.17	0.01	0.00	0.23	0.04
<b>MnO</b>	0.00	0.00	0.00	0.00	0.00	0.00	0.00	0.00	0.00	0.00	0.00	0.00
<b>MgO</b>	0.00	0.03	0.00	0.00	0.00	0.00	0.00	0.00	0.00	0.00	0.00	0.00
<b>CaO</b>	19.63	2.89	4.69	3.62	4.05	4.72	19.64	19.70	19.89	19.53	19.93	19.95
<b>Na<sub>2</sub>O</b>	0.51	9.68	9.14	10.08	9.68	9.36	0.45	0.31	0.26	0.41	0.22	0.18
<b>K<sub>2</sub>O</b>	0.02	0.17	0.15	0.12	0.12	0.12	0.00	0.04	0.00	0.00	0.00	0.01
<b>P<sub>2</sub>O<sub>5</sub></b>	0.00	0.00	0.00	0.01	0.02	0.03	0.00	0.01	0.00	0.00	0.00	0.00
<b>Total</b>	99.53	94.98	96.01	100.70	100.27	100.61	99.54	99.65	99.47	99.34	99.48	99.54
<b>Cations pfu based on 8 oxygen</b>												
<b>Si</b>	2.048	2.846	2.774	2.818	2.794	2.760	2.034	2.029	2.022	2.041	2.020	2.014
<b>Ti</b>	0.000	0.000	0.000	0.000	0.000	0.000	0.000	0.000	0.000	0.000	0.000	0.000
<b>Al</b>	1.935	1.139	1.204	1.174	1.199	1.230	1.954	1.959	1.967	1.950	1.964	1.979
<b>Cr</b>	0.000	0.000	0.000	0.000	0.000	0.000	0.000	0.000	0.000	0.000	0.000	0.000
<b>Fe</b>	0.000	0.011	0.000	0.000	0.002	0.005	0.000	0.006	0.000	0.000	0.009	0.002
<b>Mn</b>	0.000	0.000	0.000	0.000	0.000	0.000	0.000	0.000	0.000	0.000	0.000	0.000
<b>Mg</b>	0.000	0.002	0.000	0.000	0.000	0.000	0.000	0.000	0.000	0.000	0.000	0.000
<b>Ca</b>	0.978	0.144	0.233	0.170	0.192	0.223	0.978	0.981	0.992	0.974	0.995	0.994
<b>Na</b>	0.046	0.874	0.820	0.858	0.829	0.800	0.041	0.028	0.023	0.038	0.020	0.017
<b>K</b>	0.001	0.010	0.009	0.006	0.007	0.007	0.000	0.002	0.000	0.000	0.000	0.001
<b>P</b>	0.000	0.000	0.000	0.001	0.001	0.001	0.000	0.001	0.000	0.000	0.000	0.000
<b>Cation Total</b>	5.009	5.026	5.039	5.028	5.024	5.027	5.008	5.007	5.005	5.004	5.008	5.007
<b>x anorthite</b>	0.954	0.140	0.219	0.165	0.187	0.217	0.960	0.970	0.977	0.963	0.980	0.983
<b>x albite</b>	0.045	0.850	0.772	0.829	0.806	0.776	0.040	0.028	0.023	0.037	0.020	0.017
<b>x orthoclase</b>	0.001	0.009	0.008	0.006	0.007	0.007	0.000	0.002	0.000	0.000	0.000	0.001

Mole fraction xAn = Ca/(Ca+Na+K); xAb = Na/(Ca+Na+K); xOr = K/(Ca+Na+K)

Sample	PCR23a-2-16	PCR11b-1-12	PCR11b-1-13	PCR11b-1-14	PCR11b-1-15	WL18b-2-8	WL18b-2-9	WL18b-2-16	WL18b-2-21	WL18b-3a-4	WL18b-3a-6	WL18b-3a-9
Probe #	640	526	527	528	529	113	114	121	126	59	61	64
<b>SiO<sub>2</sub></b>	43.68	64.10	63.89	45.91	45.34	45.89	45.01	45.43	45.63	44.24	43.89	45.37
<b>TiO<sub>2</sub></b>	0.00	0.04	0.00	0.00	0.00	0.05	-	-	0.03	-	0.05	-
<b>Al<sub>2</sub>O<sub>3</sub></b>	35.58	18.68	18.42	33.86	34.48	37.30	37.00	36.42	36.87	37.19	35.90	36.43
<b>Cr<sub>2</sub>O<sub>3</sub></b>	0.00	0.00	0.00	0.00	0.00	n/a	n/a	n/a	n/a	n/a	n/a	n/a
<b>FeO</b>	0.24	0.07	0.54	0.19	0.12	1.09	0.19	0.58	0.54	0.37	0.38	0.26
<b>MnO</b>	0.00	0.00	0.00	0.00	0.00	0.09	0.01	0.06	0.03	0.03	0.02	0.03
<b>MgO</b>	0.00	0.00	0.00	0.00	0.00	0.12	-	0.03	0.00	0.04	-	0.00
<b>CaO</b>	19.62	0.00	0.00	17.71	18.28	19.06	18.70	18.62	18.50	19.98	18.93	19.07
<b>Na<sub>2</sub>O</b>	0.41	0.09	0.07	1.52	1.23	0.72	0.90	0.75	0.96	0.19	0.38	0.73
<b>K<sub>2</sub>O</b>	0.00	14.63	15.87	0.05	0.04	0.02	0.01	0.02	0.01	0.03	0.03	0.02
<b>P<sub>2</sub>O<sub>5</sub></b>	0.00	0.00	0.00	0.00	0.00	n/a	n/a	n/a	n/a	n/a	n/a	n/a
<b>Total</b>	99.53	97.60	98.79	99.23	99.50	104.32	101.82	101.91	102.55	102.07	99.59	101.91
<b>Cations pfu based on 8 oxygen</b>												
<b>Si</b>	2.033	3.003	2.990	2.131	2.102	2.039	2.040	2.059	2.054	2.008	2.038	2.056
<b>Ti</b>	0.000	0.002	0.000	0.000	0.000	0.002	0.000	0.000	0.001	0.000	0.002	0.000
<b>Al</b>	1.952	1.032	1.015	1.853	1.884	1.953	1.976	1.946	1.956	1.990	1.964	1.946
<b>Cr</b>	0.000	0.000	0.000	0.000	0.000	n/a	n/a	n/a	n/a	n/a	n/a	n/a
<b>Fe</b>	0.010	0.003	0.021	0.007	0.005	0.040	0.007	0.022	0.020	0.014	0.015	0.010
<b>Mn</b>	0.000	0.000	0.000	0.000	0.000	0.003	0.000	0.002	0.001	0.001	0.001	0.001
<b>Mg</b>	0.000	0.000	0.000	0.000	0.000	0.008	0.000	0.002	0.000	0.003	0.000	0.000
<b>Ca</b>	0.978	0.000	0.000	0.881	0.908	0.907	0.908	0.904	0.892	0.972	0.942	0.926
<b>Na</b>	0.038	0.008	0.006	0.137	0.110	0.062	0.079	0.066	0.084	0.017	0.034	0.064
<b>K</b>	0.000	0.874	0.947	0.002	0.002	0.001	0.001	0.001	0.000	0.002	0.002	0.001
<b>P</b>	0.000	0.000	0.000	0.000	0.000	n/a	n/a	n/a	n/a	n/a	n/a	n/a
<b>Cation Total</b>	5.011	4.923	4.979	5.012	5.011	5.015	5.012	5.002	5.009	5.006	4.997	5.004
<b>x anorthite</b>	0.963	0.000	0.000	0.864	0.889	0.935	0.919	0.931	0.914	0.981	0.963	0.934
<b>x albite</b>	0.037	0.009	0.007	0.134	0.108	0.064	0.080	0.068	0.086	0.017	0.035	0.065
<b>x orthoclase</b>	0.000	0.991	0.993	0.002	0.002	0.001	0.001	0.001	0.000	0.002	0.002	0.001

Mole fraction xAn = Ca/(Ca+Na+K); xAb = Na/(Ca+Na+K); xOr = K/(Ca+Na+K)

Sample	WL18b-3a-15	WL18b-3a-13	WL16b-2-19	WL16b-2-20	WL16b-2-21	WL16b-2-22
Probe #	70	68	432	433	434	435
<b>SiO<sub>2</sub></b>	44.69	68.15	63.82	64.75	65.20	66.89
<b>TiO<sub>2</sub></b>	-	-	0.00	0.02	0.00	0.00
<b>Al<sub>2</sub>O<sub>3</sub></b>	37.05	20.66	20.31	18.47	20.49	19.26
<b>Cr<sub>2</sub>O<sub>3</sub></b>	n/a	n/a	0.00	0.00	0.00	0.00
<b>FeO</b>	0.25	0.31	0.06	0.07	0.09	0.00
<b>MnO</b>	0.02	0.03	0.02	0.00	0.00	0.00
<b>MgO</b>	0.02	0.02	0.00	0.00	0.00	0.00
<b>CaO</b>	19.64	1.34	1.63	0.34	1.58	0.10
<b>Na<sub>2</sub>O</b>	0.40	8.88	9.74	9.94	10.81	11.35
<b>K<sub>2</sub>O</b>	0.02	0.06	0.08	0.05	0.07	0.03
<b>P<sub>2</sub>O<sub>5</sub></b>	n/a	n/a	0.00	0.00	0.00	0.00
<b>Total</b>	102.09	99.45	95.67	93.63	98.24	97.63
<b>Cations pfu based on 8 oxygen</b>						
<b>Si</b>	2.025	2.976	2.920	3.007	2.915	2.990
<b>Ti</b>	0.000	0.000	0.000	0.001	0.000	0.000
<b>Al</b>	1.978	1.063	1.095	1.010	1.080	1.014
<b>Cr</b>	n/a	n/a	0.000	0.000	0.000	0.000
<b>Fe</b>	0.009	0.011	0.002	0.002	0.003	0.000
<b>Mn</b>	0.001	0.001	0.001	0.000	0.000	0.000
<b>Mg</b>	0.001	0.001	0.000	0.000	0.000	0.000
<b>Ca</b>	0.953	0.063	0.080	0.017	0.076	0.005
<b>Na</b>	0.035	0.752	0.864	0.895	0.937	0.983
<b>K</b>	0.001	0.003	0.005	0.003	0.004	0.002
<b>P</b>	n/a	n/a	0.000	0.000	0.000	0.000
<b>Cation Total</b>	5.004	4.871	4.967	4.936	5.016	4.995
<b>x anorthite</b>	0.963	0.077	0.084	0.018	0.075	0.005
<b>x albite</b>	0.036	0.919	0.911	0.978	0.921	0.994
<b>x orthoclase</b>	0.001	0.004	0.005	0.003	0.004	0.002

Mole fraction xAn = Ca/(Ca+Na+K); xAb = Na/(Ca+Na+K); xOr = K/(Ca+Na+K)

**Table B.4 Concretion rim: Chlorite**

Sample	PPP30-2-1	PPP30-2-2	PPP30-2-3	PPP30-2-5	PPP30-2-13	PPP30-2-14	PPP30-2-22	PPP30-2-23	PPP30-2-24	PPP30-2-25	PPP5c-2-5	PPP5c-2-6
Probe #	33	34	35	37	45	46	54	55	56	57	87	88
<b>SiO<sub>2</sub></b>	24.42	24.38	23.38	29.98	24.92	30.09	30.57	28.64	27.57	23.85	32.32	32.93
<b>TiO<sub>2</sub></b>	0.02	0.00	0.00	0.00	0.00	0.00	0.05	0.12	0.13	0.04	0.22	1.20
<b>Al<sub>2</sub>O<sub>3</sub></b>	20.30	20.13	19.68	16.54	19.83	16.83	17.29	18.38	16.04	19.96	16.08	16.46
<b>Cr<sub>2</sub>O<sub>3</sub></b>	0.00	0.02	0.00	0.00	0.00	0.00	0.03	0.00	0.00	0.08	0.08	0.15
<b>FeO</b>	31.26	30.67	31.94	22.98	30.38	22.44	23.04	23.63	23.28	32.02	24.04	18.45
<b>MnO</b>	2.25	2.06	1.98	0.50	2.08	0.51	0.54	2.01	0.50	1.98	1.71	0.78
<b>MgO</b>	7.73	7.97	6.78	15.63	8.24	16.16	15.19	13.14	13.79	7.16	12.45	14.14
<b>CaO</b>	0.30	0.38	0.41	0.59	0.21	0.27	0.45	0.42	3.18	0.31	0.50	0.22
<b>Na<sub>2</sub>O</b>	0.01	0.02	0.05	0.03	0.06	0.30	0.12	0.04	0.06	0.08	0.01	0.03
<b>K<sub>2</sub>O</b>	0.04	0.02	0.03	0.02	0.03	0.03	0.05	0.03	0.03	0.04	0.04	4.00
<b>P<sub>2</sub>O<sub>5</sub></b>	0.01	0.00	0.01	0.00	0.00	0.01	0.00	0.00	0.00	0.01	0.01	0.00
<b>Total</b>	86.33	85.66	84.25	86.27	85.76	86.63	87.32	86.42	84.57	85.53	87.46	88.36
<b>Cations pfu based on 18 oxygen</b>												
<b>Si</b>	3.526	3.537	3.490	4.063	3.598	4.048	4.082	3.920	3.888	3.497	4.336	4.329
<b>Ti</b>	0.002	0.000	0.000	0.000	0.000	0.000	0.005	0.013	0.014	0.004	0.022	0.119
<b>Al</b>	3.454	3.442	3.465	2.642	3.375	2.668	2.722	2.965	2.666	3.452	2.542	2.551
<b>Cr</b>	0.000	0.002	0.000	0.000	0.000	0.000	0.004	0.000	0.000	0.009	0.009	0.016
<b>Fe</b>	3.775	3.721	3.989	2.605	3.668	2.524	2.572	2.705	2.747	3.928	2.698	2.029
<b>Mn</b>	0.275	0.254	0.250	0.058	0.254	0.058	0.061	0.232	0.059	0.247	0.194	0.086
<b>Mg</b>	1.663	1.723	1.508	3.159	1.773	3.240	3.024	2.682	2.900	1.566	2.489	2.772
<b>Ca</b>	0.047	0.059	0.067	0.086	0.032	0.040	0.063	0.061	0.481	0.049	0.072	0.031
<b>Na</b>	0.004	0.007	0.014	0.007	0.018	0.077	0.031	0.011	0.016	0.023	0.004	0.007
<b>K</b>	0.007	0.004	0.005	0.004	0.005	0.005	0.007	0.005	0.005	0.007	0.007	0.670
<b>P</b>	0.004	0.000	0.004	0.000	0.000	0.004	0.000	0.000	0.000	0.002	0.002	0.000
<b>Cation Total</b>	12.757	12.748	12.793	12.623	12.726	12.663	12.571	12.596	12.778	12.785	12.377	12.611
<b>Mg/(Mg+Mn+Fe)</b>	0.291	0.302	0.262	0.543	0.311	0.557	0.535	0.477	0.508	0.273	0.463	0.567

Sample	PPP5c-2-7	PPP5c-2-9	PPP5c-2-10	PPP5c-2-11	PPP5c-2-12	PPP5c-2-13	PPP5c-2-14	PPP7c-3-1	PPP7c-3-2	PPP7c-3-3	PPP7c-3-9	PPP7c-3-10
Probe #	89	91	92	93	94	95	96	227	228	229	234	235
<b>SiO<sub>2</sub></b>	28.27	33.11	33.32	35.66	29.36	32.21	34.70	26.38	26.68	29.95	27.79	29.67
<b>TiO<sub>2</sub></b>	0.06	0.05	1.30	1.77	0.82	1.42	1.57	0.00	0.03	0.00	0.00	0.02
<b>Al<sub>2</sub>O<sub>3</sub></b>	19.98	15.99	16.32	16.16	18.37	17.17	16.47	22.84	22.97	18.94	20.25	20.25
<b>Cr<sub>2</sub>O<sub>3</sub></b>	0.10	0.07	0.14	0.11	0.14	0.18	0.00	0.00	0.00	0.00	0.02	0.02
<b>FeO</b>	27.23	23.02	18.86	15.38	21.79	19.11	16.58	20.81	19.16	19.19	21.88	20.89
<b>MnO</b>	1.66	1.33	0.91	0.55	1.07	0.91	0.68	2.08	1.86	1.65	1.79	1.74
<b>MgO</b>	9.23	12.95	13.38	13.42	13.66	12.62	14.38	14.56	15.32	17.60	16.05	16.42
<b>CaO</b>	0.25	0.72	0.27	0.08	0.19	0.10	0.16	0.05	0.07	0.16	0.11	0.17
<b>Na<sub>2</sub>O</b>	0.00	0.00	0.04	0.10	0.04	0.04	0.06	0.02	0.02	0.06	0.03	0.24
<b>K<sub>2</sub>O</b>	0.05	0.05	4.30	6.86	1.07	4.26	5.39	0.02	0.03	0.04	0.06	0.05
<b>P<sub>2</sub>O<sub>5</sub></b>	0.00	0.02	0.00	0.00	0.00	0.00	0.00	0.01	0.01	0.02	0.00	0.00
<b>Total</b>	86.84	87.32	88.85	90.11	86.51	88.02	89.98	86.78	86.14	87.62	87.98	89.48
<b>Cations pfu based on 18 oxygen</b>												
<b>Si</b>	3.906	4.410	4.372	4.565	3.973	4.277	4.448	3.541	3.569	3.924	3.697	3.839
<b>Ti</b>	0.005	0.005	0.128	0.171	0.085	0.142	0.151	0.000	0.002	0.000	0.000	0.002
<b>Al</b>	3.253	2.511	2.525	2.439	2.930	2.687	2.489	3.613	3.622	2.925	3.173	3.089
<b>Cr</b>	0.011	0.007	0.014	0.011	0.016	0.020	0.000	0.000	0.000	0.000	0.002	0.002
<b>Fe</b>	3.146	2.563	2.070	1.647	2.466	2.122	1.777	2.336	2.142	2.104	2.434	2.261
<b>Mn</b>	0.194	0.149	0.101	0.059	0.122	0.103	0.074	0.236	0.211	0.184	0.202	0.191
<b>Mg</b>	1.901	2.572	2.617	2.561	2.756	2.497	2.749	2.914	3.055	3.438	3.182	3.168
<b>Ca</b>	0.038	0.103	0.038	0.011	0.027	0.014	0.022	0.007	0.009	0.022	0.016	0.023
<b>Na</b>	0.000	0.002	0.009	0.025	0.009	0.011	0.014	0.005	0.004	0.016	0.007	0.061
<b>K</b>	0.009	0.009	0.720	1.121	0.184	0.722	0.882	0.004	0.005	0.007	0.009	0.007
<b>P</b>	0.000	0.005	0.000	0.000	0.000	0.000	0.000	0.002	0.002	0.002	0.000	0.000
<b>Cation Total</b>	12.463	12.337	12.596	12.613	12.568	12.596	12.605	12.659	12.622	12.623	12.722	12.643
<b>Mg/(Mg+Mn+Fe)</b>	0.363	0.487	0.547	0.600	0.516	0.529	0.598	0.531	0.565	0.600	0.547	0.564

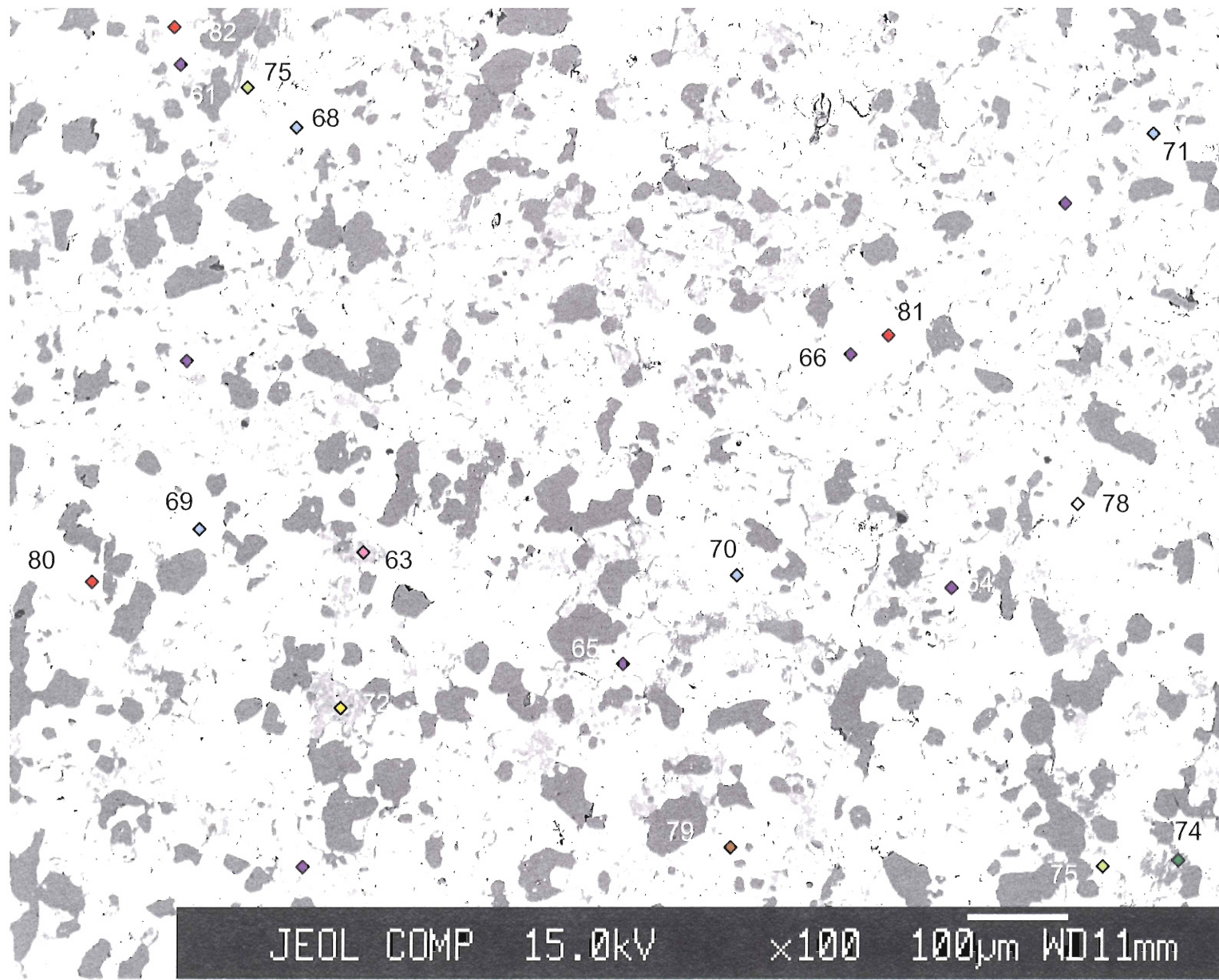
Sample	PPP7c-3-11	PPP7c-4-11	PPP7c-4-12	PPP7c-4-13	PCR26b-3-3	PCR26b-3-4	PCR26b-3-6	PCR26b-3-8	PCR26b-3-9	PCR26b-3-12	PCR26b-3-13	PCR26b-3-17
Probe #	236	261	262	263	330	331	333	335	336	339	340	344
<b>SiO<sub>2</sub></b>	26.87	26.67	26.30	27.56	24.62	28.12	23.53	26.35	25.22	23.82	24.20	27.25
<b>TiO<sub>2</sub></b>	0.00	0.00	0.00	0.00	0.75	1.73	5.54	1.06	1.13	0.56	1.14	1.09
<b>Al<sub>2</sub>O<sub>3</sub></b>	24.35	23.71	22.87	22.18	18.15	16.57	16.39	18.80	17.87	18.97	17.93	17.14
<b>Cr<sub>2</sub>O<sub>3</sub></b>	0.00	0.00	0.00	0.00	0.22	0.22	0.34	0.11	0.16	0.14	0.14	0.03
<b>FeO</b>	19.78	19.49	21.29	21.30	25.27	21.92	23.97	23.57	25.09	26.89	25.73	23.63
<b>MnO</b>	2.04	1.87	2.04	2.06	0.38	0.45	0.42	0.41	0.43	0.40	0.42	0.42
<b>MgO</b>	14.48	14.77	14.06	15.20	9.52	9.35	9.06	9.77	9.89	9.18	9.67	9.81
<b>CaO</b>	0.07	0.10	0.19	0.21	0.01	0.02	0.04	0.00	0.00	0.10	0.03	0.00
<b>Na<sub>2</sub>O</b>	0.06	0.01	0.04	0.08	0.01	0.03	0.02	0.06	0.08	0.00	0.02	0.04
<b>K<sub>2</sub>O</b>	0.03	0.01	0.02	0.02	0.62	3.99	0.69	1.56	1.27	0.39	0.61	3.02
<b>P<sub>2</sub>O<sub>5</sub></b>	0.01	0.00	0.00	0.00	0.04	0.00	0.04	0.01	0.00	0.06	0.00	0.00
<b>Total</b>	87.71	86.64	86.80	88.62	79.58	82.39	80.04	81.70	81.14	80.52	79.89	82.43
<b>Cations pfu based on 18 oxygen</b>												
<b>Si</b>	3.550	3.539	3.623	3.550	3.728	4.093	3.551	3.845	3.755	3.598	3.670	3.982
<b>Ti</b>	0.000	0.000	0.000	0.000	0.085	0.189	0.628	0.115	0.126	0.063	0.130	0.119
<b>Al</b>	3.717	3.627	3.438	3.717	3.240	2.844	2.916	3.233	3.136	3.377	3.204	2.952
<b>Cr</b>	0.000	0.000	0.000	0.000	0.027	0.025	0.041	0.013	0.018	0.016	0.016	0.004
<b>Fe</b>	2.169	2.396	2.344	2.169	3.200	2.669	3.026	2.876	3.123	3.397	3.263	2.887
<b>Mn</b>	0.211	0.232	0.230	0.211	0.049	0.056	0.054	0.050	0.054	0.052	0.054	0.052
<b>Mg</b>	2.930	2.821	2.981	2.930	2.149	2.029	2.038	2.124	2.194	2.066	2.185	2.137
<b>Ca</b>	0.014	0.027	0.031	0.014	0.002	0.004	0.005	0.000	0.000	0.016	0.005	0.000
<b>Na</b>	0.002	0.011	0.022	0.002	0.004	0.009	0.007	0.018	0.023	0.000	0.005	0.011
<b>K</b>	0.002	0.004	0.004	0.002	0.119	0.742	0.133	0.292	0.241	0.076	0.119	0.563
<b>P</b>	0.000	0.000	0.000	0.000	0.005	0.000	0.005	0.002	0.000	0.007	0.000	0.000
<b>Cation Total</b>	12.596	12.656	12.674	12.596	12.609	12.661	12.406	12.569	12.672	12.670	12.654	12.708
<b>Mg/(Mg+Mn+Fe)</b>	0.552	0.518	0.537	0.552	0.398	0.427	0.398	0.421	0.409	0.375	0.397	0.421

Sample	PCR26b-3-18	PCR26b-3-19	PCR26b-3-21	PCR26b-4-1	PCR26b-4-2	PCR26b-4-3	PCR26b-4-4	PCR26b-4-6	PCR26b-4-7	PCR26b-4-8	PCR26b-4-11	PCR11b-1-2
Probe #	345	346	348	355	356	357	358	360	361	362	365	516
<b>SiO<sub>2</sub></b>	24.80	24.65	23.73	25.75	28.13	25.14	25.10	24.28	23.72	26.37	25.53	25.67
<b>TiO<sub>2</sub></b>	1.93	1.79	0.43	1.08	1.69	0.94	0.83	0.70	1.37	1.02	0.92	0.03
<b>Al<sub>2</sub>O<sub>3</sub></b>	18.02	17.87	19.48	19.07	18.03	19.64	19.27	19.31	19.25	18.73	19.62	20.09
<b>Cr<sub>2</sub>O<sub>3</sub></b>	0.02	0.03	0.06	0.05	0.03	0.06	0.01	0.04	0.10	0.13	0.04	0.00
<b>FeO</b>	25.66	24.94	27.10	25.22	23.68	25.64	24.61	24.59	25.66	24.47	25.55	25.51
<b>MnO</b>	0.45	0.43	0.45	0.47	0.51	0.42	0.42	0.45	0.36	0.48	0.45	1.06
<b>MgO</b>	9.59	9.49	8.58	9.05	8.48	8.83	8.69	8.70	8.36	9.10	9.29	13.25
<b>CaO</b>	0.04	0.01	0.00	0.06	0.05	0.06	0.04	0.07	0.12	0.07	0.11	0.07
<b>Na<sub>2</sub>O</b>	0.00	0.02	0.00	0.04	0.07	0.01	0.02	0.04	0.03	0.05	0.01	0.00
<b>K<sub>2</sub>O</b>	0.58	0.65	0.31	1.99	4.35	1.64	1.58	1.09	0.60	2.38	1.20	0.03
<b>P<sub>2</sub>O<sub>5</sub></b>	0.02	0.03	0.03	0.03	0.05	0.03	0.04	0.04	0.04	0.07	0.00	0.00
<b>Total</b>	81.12	79.89	80.16	82.81	85.07	82.40	80.63	79.30	79.61	82.86	82.69	85.71
<b>Cations pfu based on 18 oxygen</b>												
<b>Si</b>	3.690	3.713	3.598	3.758	4.000	3.690	3.746	3.685	3.604	3.836	3.717	3.582
<b>Ti</b>	0.216	0.203	0.049	0.119	0.180	0.104	0.094	0.081	0.157	0.112	0.101	0.004
<b>Al</b>	3.159	3.173	3.481	3.280	3.022	3.398	3.391	3.454	3.447	3.211	3.366	3.305
<b>Cr</b>	0.002	0.004	0.007	0.005	0.004	0.007	0.002	0.004	0.011	0.014	0.004	0.000
<b>Fe</b>	3.193	3.143	3.436	3.078	2.817	3.148	3.071	3.121	3.260	2.977	3.110	2.977
<b>Mn</b>	0.058	0.054	0.058	0.059	0.061	0.052	0.054	0.058	0.047	0.059	0.056	0.124
<b>Mg</b>	2.128	2.129	1.939	1.969	1.798	1.931	1.935	1.969	1.892	1.973	2.014	2.758
<b>Ca</b>	0.005	0.000	0.000	0.009	0.007	0.009	0.007	0.011	0.020	0.011	0.016	0.011
<b>Na</b>	0.002	0.004	0.000	0.011	0.020	0.004	0.005	0.011	0.007	0.014	0.004	0.000
<b>K</b>	0.110	0.124	0.059	0.371	0.788	0.306	0.302	0.212	0.117	0.443	0.221	0.005
<b>P</b>	0.002	0.004	0.004	0.004	0.005	0.004	0.005	0.005	0.005	0.009	0.000	0.000
<b>Cation Total</b>	12.566	12.553	12.631	12.663	12.703	12.654	12.614	12.611	12.566	12.661	12.609	12.767
<b>Mg/(Mg+Mn+Fe)</b>	0.396	0.400	0.357	0.386	0.385	0.376	0.382	0.383	0.364	0.394	0.389	0.471

Sample	PCR11b-1-3	PCR11b-1-8	PCR11b-1-10	WL18b-2-5	WL18b-2-6	WL18b-2-15	WL18b-2-20	WL18b-2-22	WL18b-2-25	WL18b-2-26	WL16b-2-13
Probe #	517	522	524	110	111	120	125	127	130	131	426
<b>SiO<sub>2</sub></b>	30.57	25.34	25.81	28.75	26.89	27.68	26.24	27.00	26.17	26.22	27.26
<b>TiO<sub>2</sub></b>	0.89	0.05	0.02	-	0.00	0.04	0.18	0.08	0.07	0.10	0.08
<b>Al<sub>2</sub>O<sub>3</sub></b>	16.56	20.74	20.33	19.89	20.25	19.28	19.90	20.02	20.43	19.93	20.73
<b>Cr<sub>2</sub>O<sub>3</sub></b>	0.11	0.01	0.04	n/a	n/a	n/a	n/a	n/a	n/a	n/a	0.00
<b>FeO</b>	22.20	28.00	25.95	24.50	33.71	33.00	32.27	32.83	32.27	31.18	20.93
<b>MnO</b>	0.62	0.77	1.17	1.11	0.88	0.80	0.72	0.74	0.70	0.73	0.96
<b>MgO</b>	15.15	12.16	13.55	16.10	10.00	10.08	10.28	10.57	10.51	10.63	15.90
<b>CaO</b>	0.22	0.04	0.09	0.11	0.12	0.29	0.26	0.09	0.10	0.09	0.11
<b>Na<sub>2</sub>O</b>	0.02	0.00	0.00	0.02	0.01	0.00	0.02	-	-	0.00	0.01
<b>K<sub>2</sub>O</b>	1.91	0.05	0.03	0.01	0.00	-	0.05	0.06	0.01	0.02	0.03
<b>P<sub>2</sub>O<sub>5</sub></b>	0.00	0.00	0.00	n/a	n/a	n/a	n/a	n/a	n/a	n/a	0.00
<b>Total</b>	88.26	87.16	87.00	90.49	91.85	91.18	89.91	91.39	90.25	88.91	86.03
<b>Cations pfu based on 18 oxygen</b>											
<b>Si</b>	4.075	3.517	3.555	3.744	3.624	3.743	3.601	3.641	3.571	3.617	3.6774
<b>Ti</b>	0.088	0.005	0.002	0.000	0.000	0.004	0.019	0.008	0.007	0.010	0.009
<b>Al</b>	2.601	3.393	3.301	3.053	3.216	3.073	3.218	3.182	3.285	3.241	3.294
<b>Cr</b>	0.011	0.002	0.005	n/a	n/a	n/a	n/a	n/a	n/a	n/a	0.000
<b>Fe</b>	2.475	3.249	2.990	2.668	3.800	3.731	3.703	3.702	3.683	3.597	2.360
<b>Mn</b>	0.070	0.090	0.137	0.123	0.101	0.092	0.084	0.084	0.081	0.085	0.110
<b>Mg</b>	3.011	2.515	2.783	3.125	2.009	2.031	2.103	2.125	2.137	2.186	3.197
<b>Ca</b>	0.032	0.007	0.013	0.015	0.017	0.043	0.038	0.013	0.015	0.013	0.016
<b>Na</b>	0.005	0.000	0.000	0.004	0.002	0.001	0.004	0.000	0.000	0.000	0.004
<b>K</b>	0.326	0.009	0.005	0.002	0.001	0.000	0.008	0.010	0.001	0.004	0.005
<b>P</b>	0.000	0.000	0.000	n/a	n/a	n/a	n/a	n/a	n/a	n/a	0.000
<b>Cation Total</b>	12.697	12.787	12.793	12.733	12.769	12.717	12.777	12.765	12.781	12.754	12.672
<b>Mg/(Mg+Mn+Fe)</b>	0.542	0.430	0.471	0.528	0.340	0.347	0.357	0.359	0.362	0.373	0.564

Appendix II.  
EBS images with EMP analysis locations

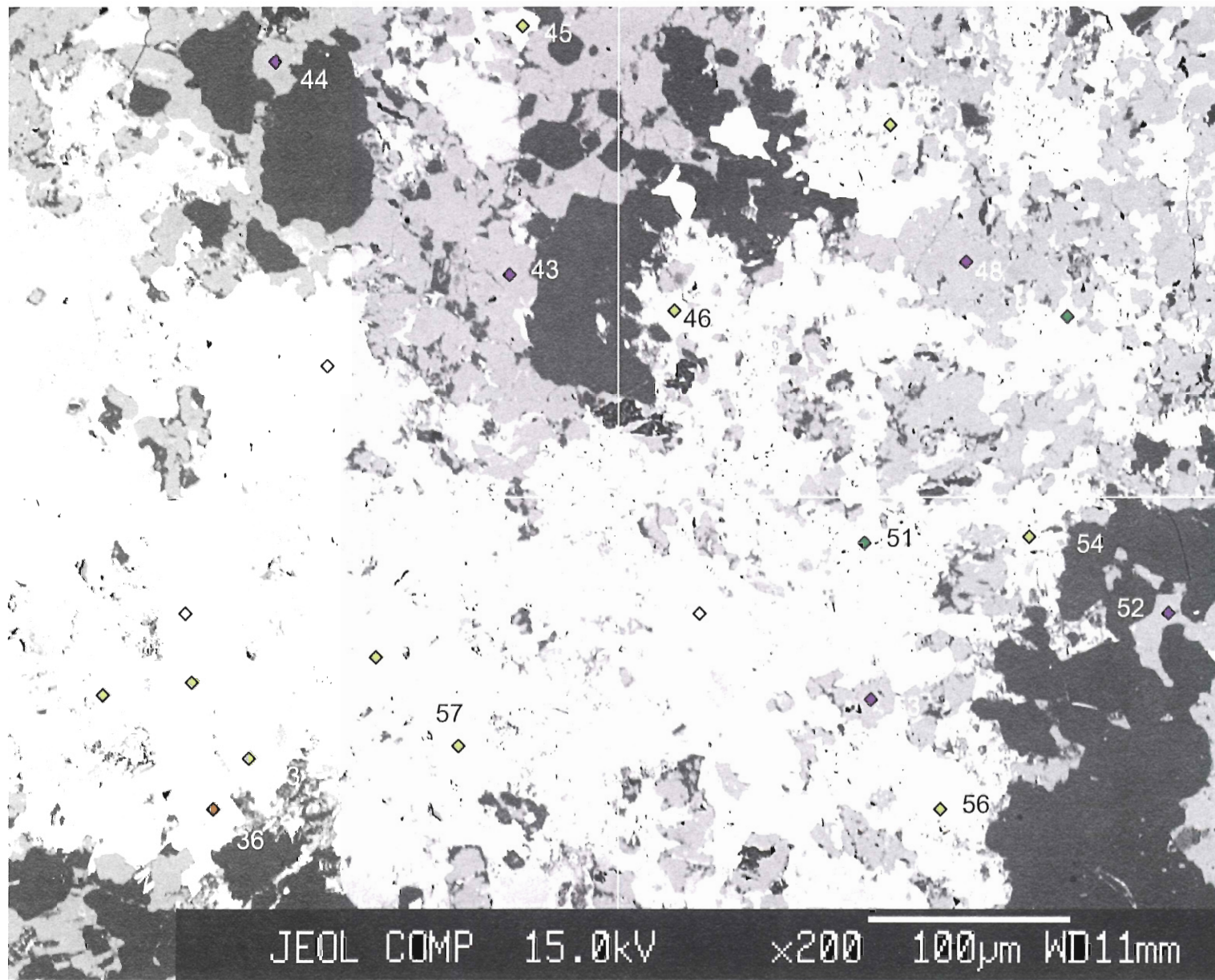
**PPP-30 area 1**



**Mineral key**

- ◊ Apatite
- ◆ Amphibole ?
- ♦ Titanite
- ◊ Muscovite
- ♦ Garnet
- ◊ Calcite
- ◊ Chlorite
- Plagioclase
- ◊ An<sub><90</sub>
- ◊ An<sub>>90</sub>

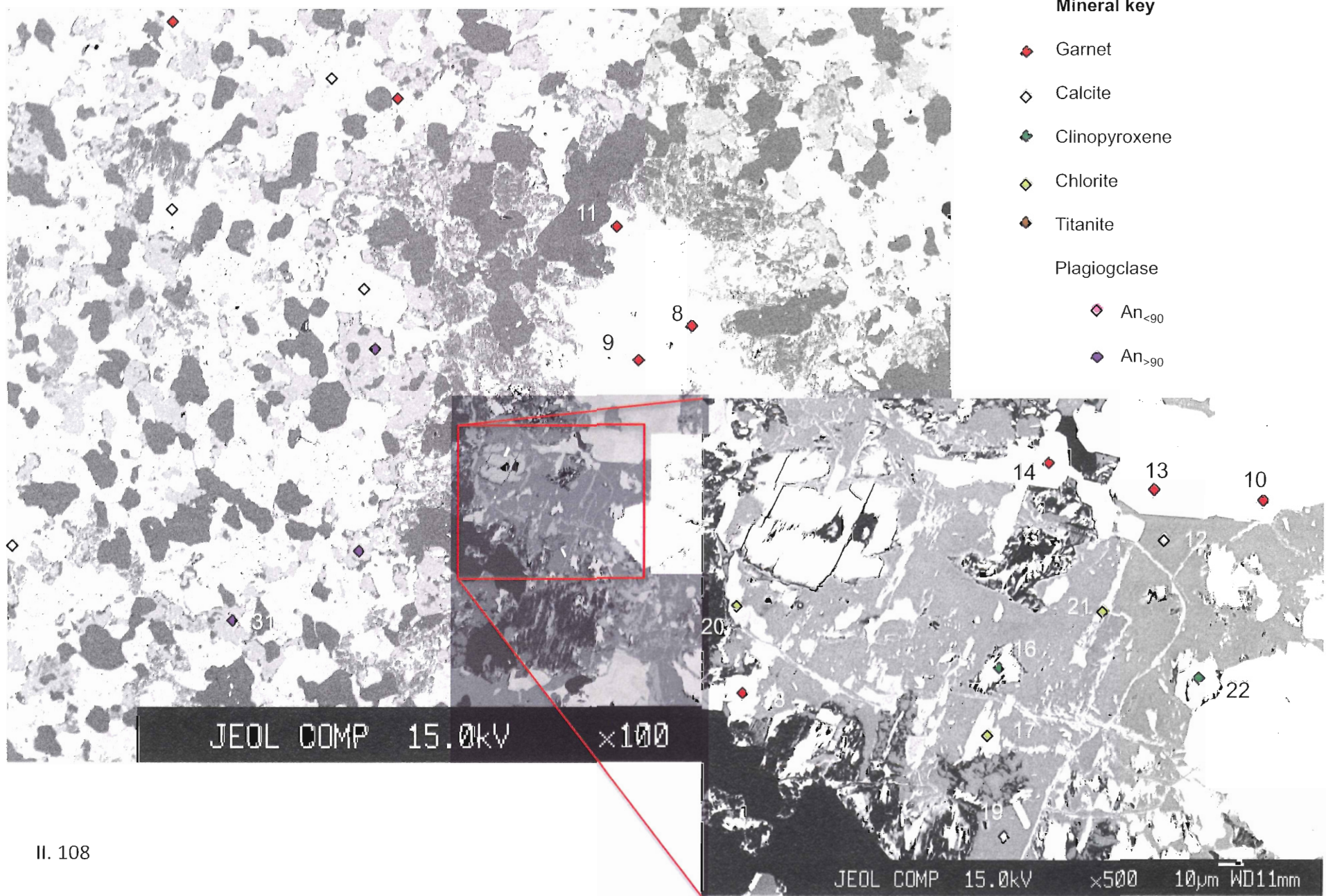
## PPP-30 area 2



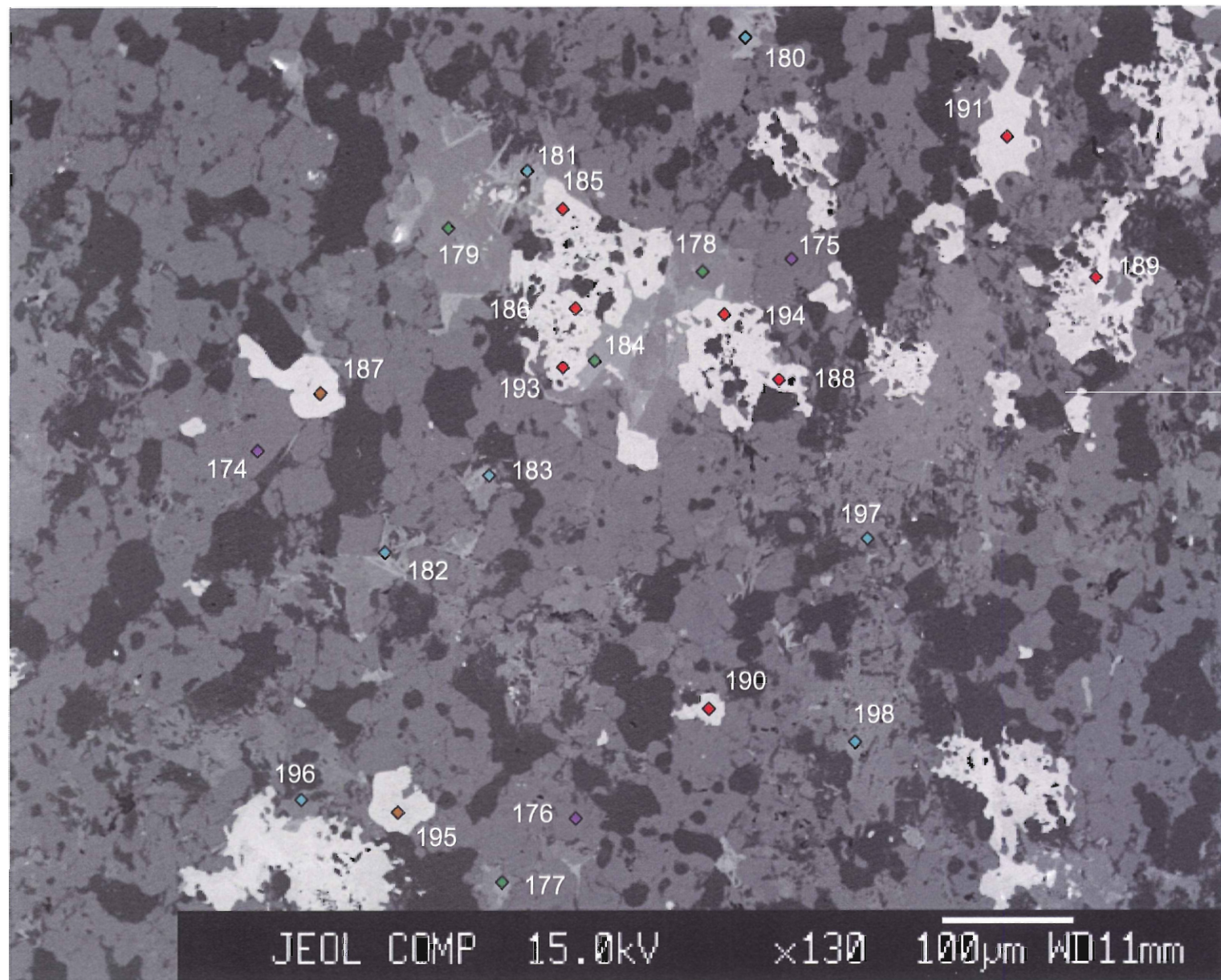
**Mineral key**

- ◆ Titanite
- ◇ Calcite
- ◆ Clinopyroxene
- ◆ Chlorite
- Plagioclase
  - ◆  $An_{<90}$
  - ◆  $An_{>90}$

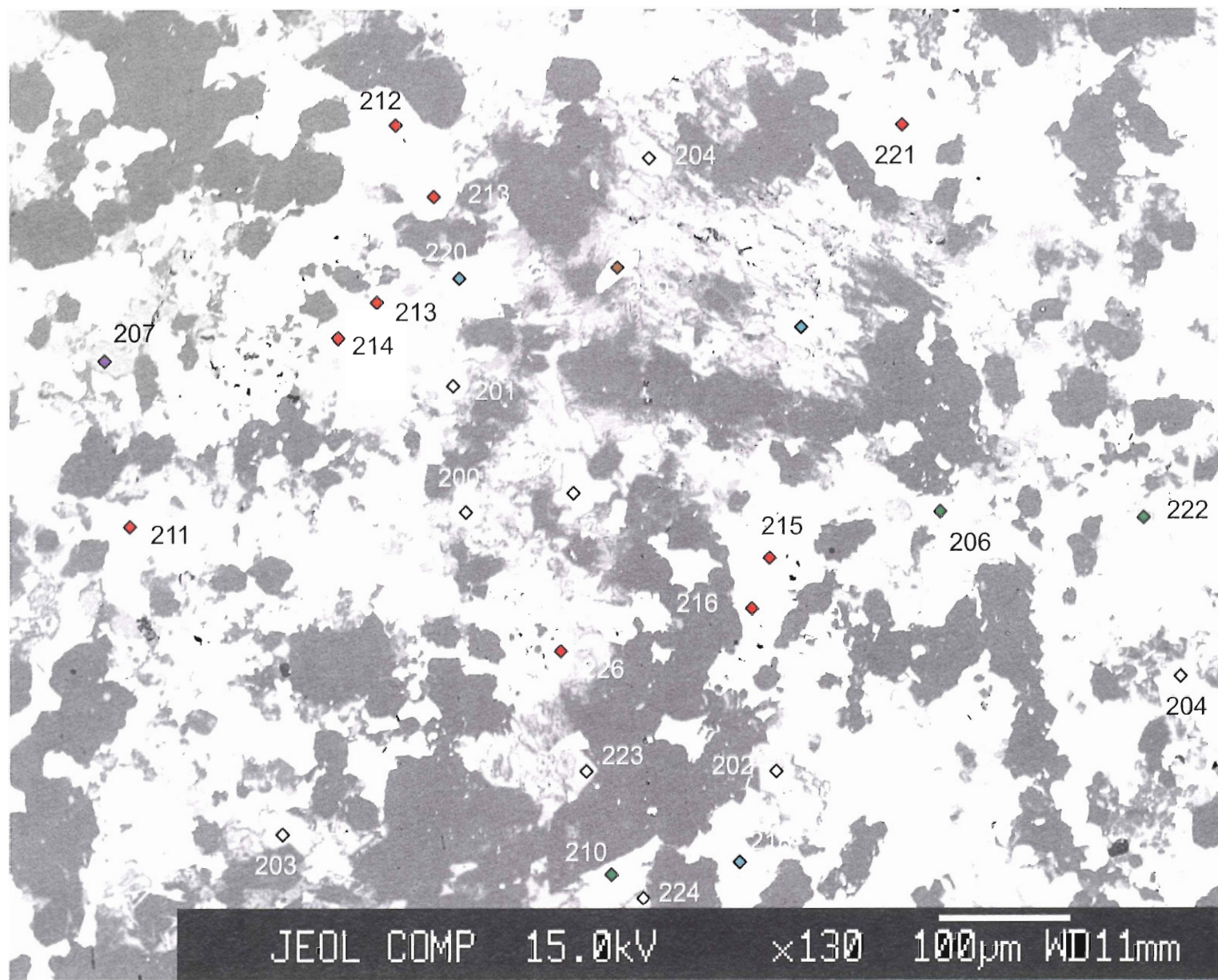
## PPP-30 area 3



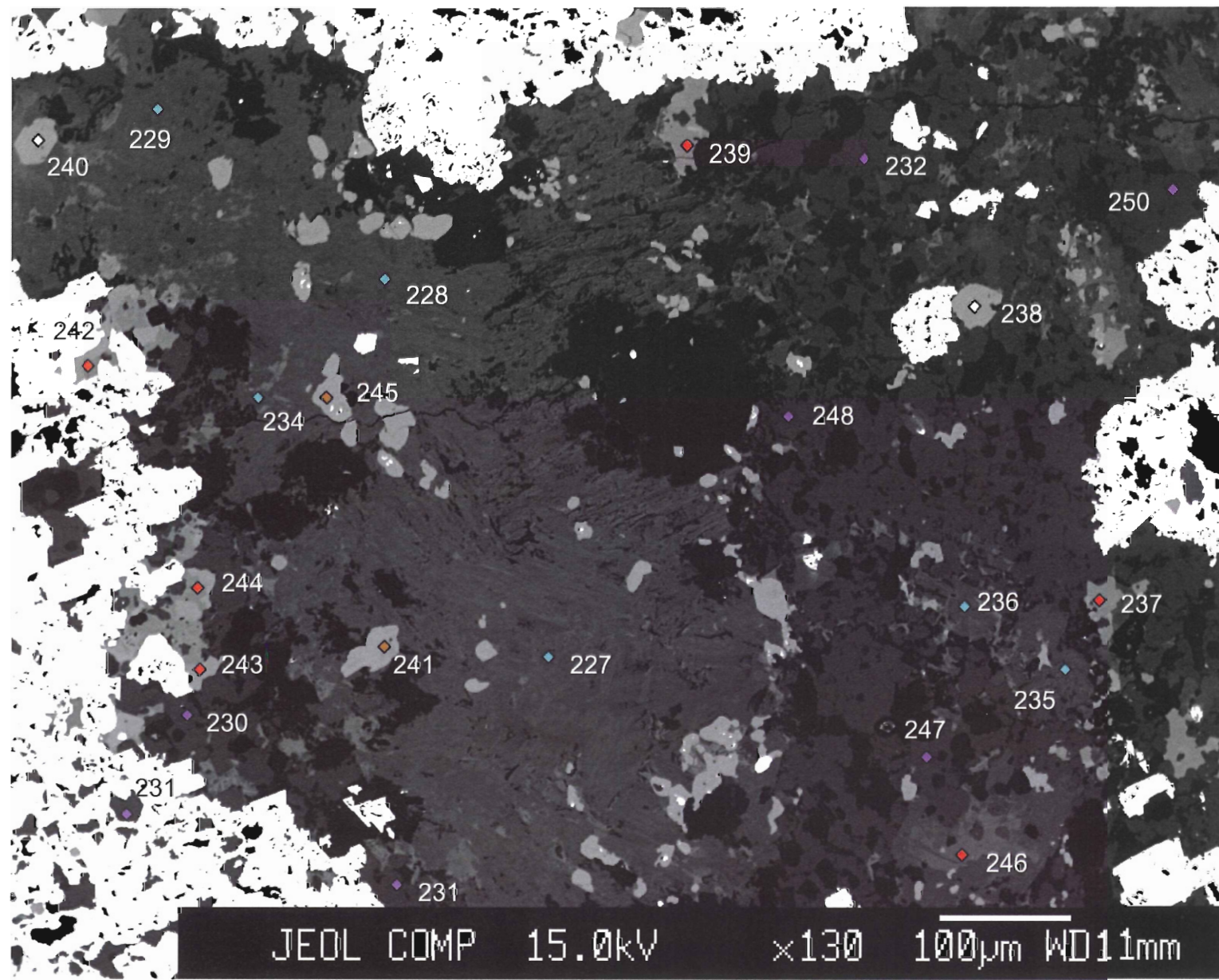
## PPP-7c area 1



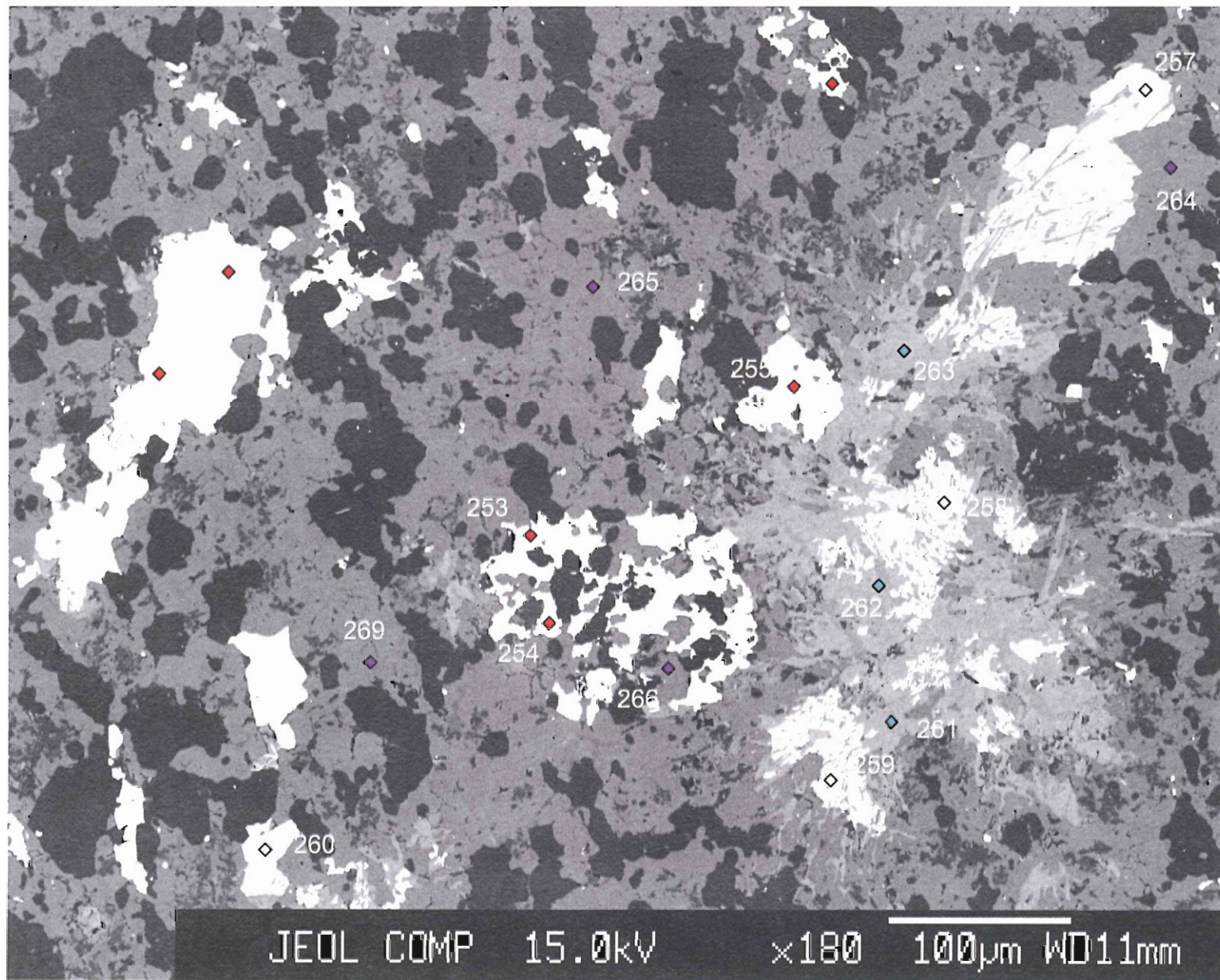
## PPP-7c area 2



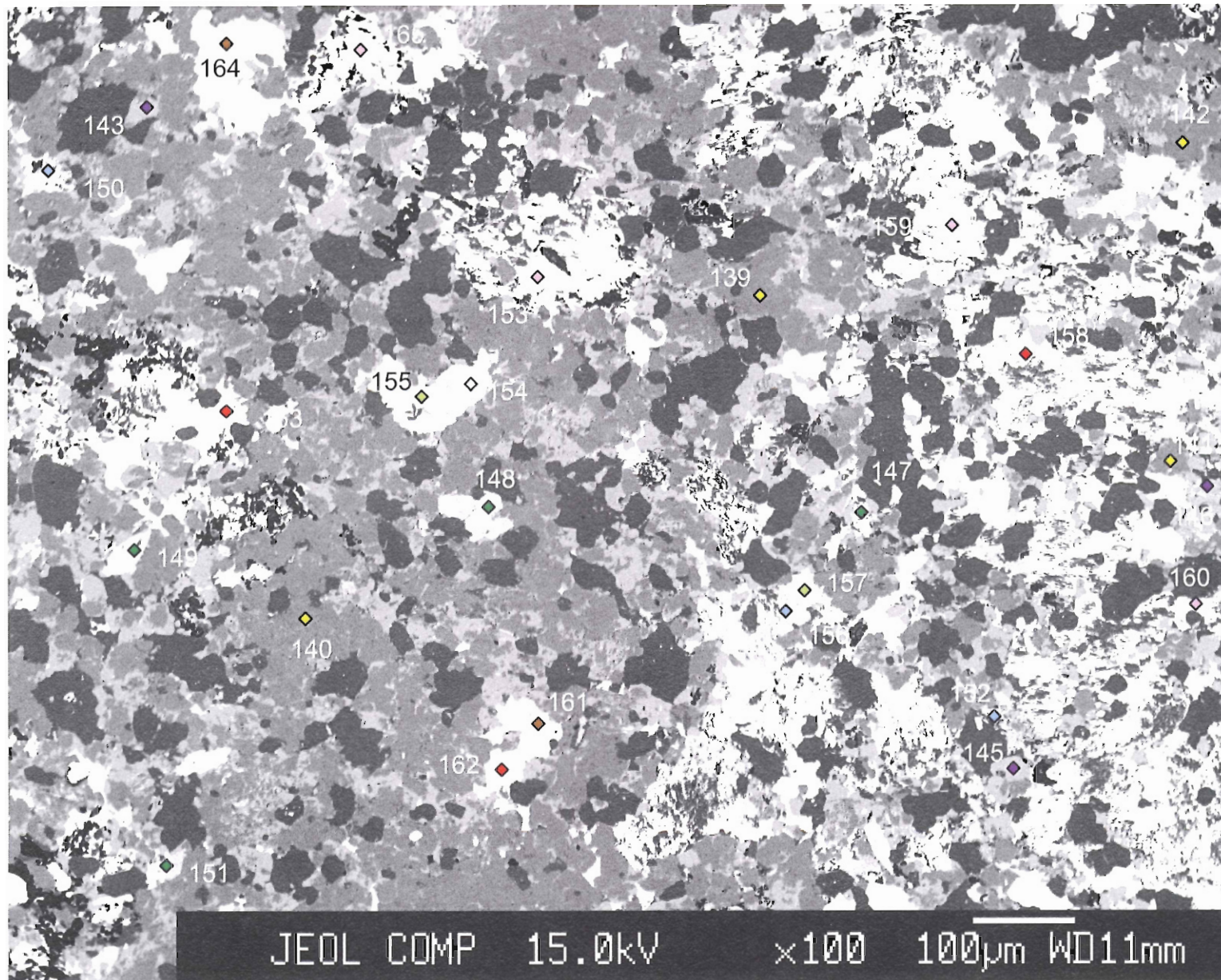
## PPP-7c area 3



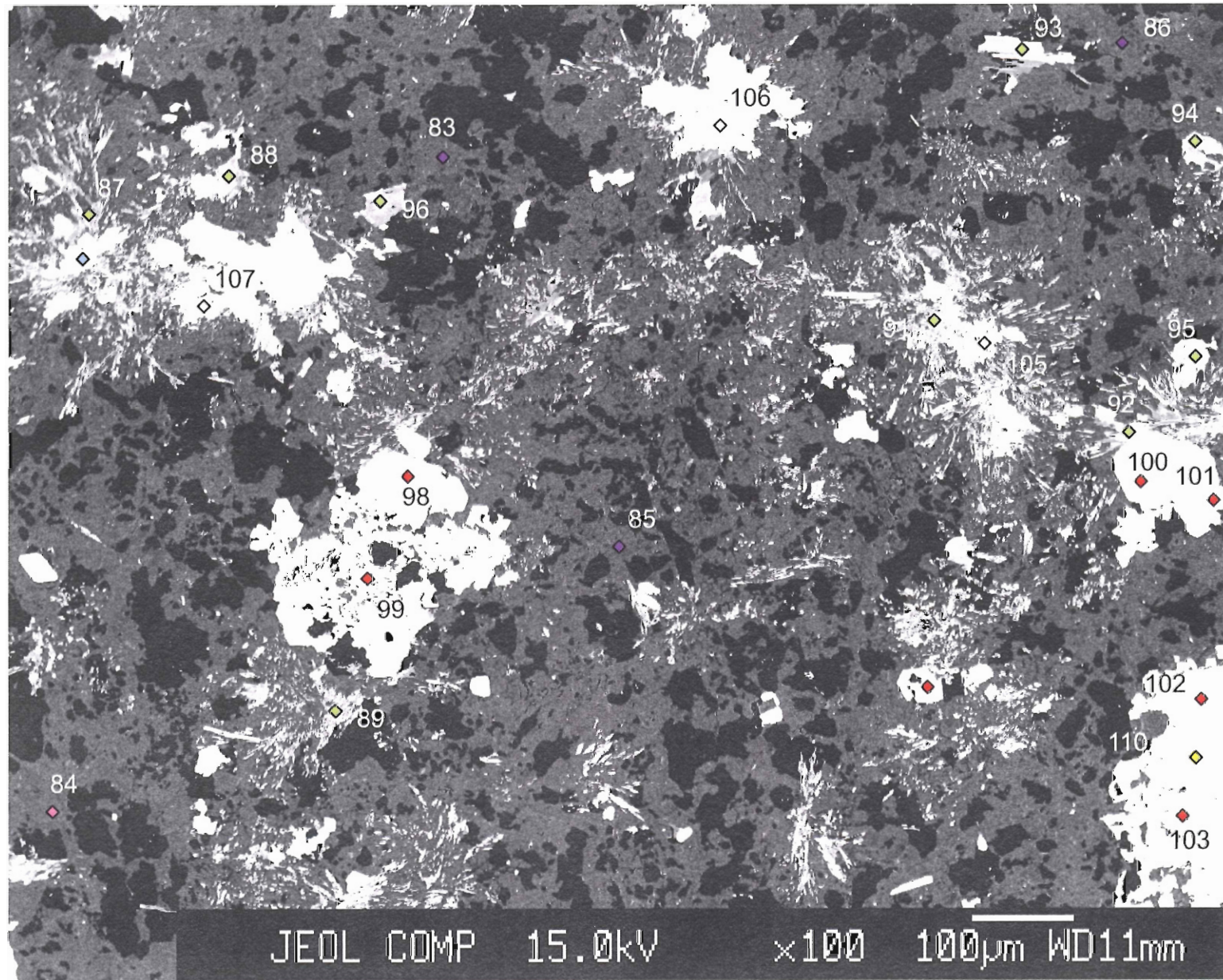
## PPP-7c area 4



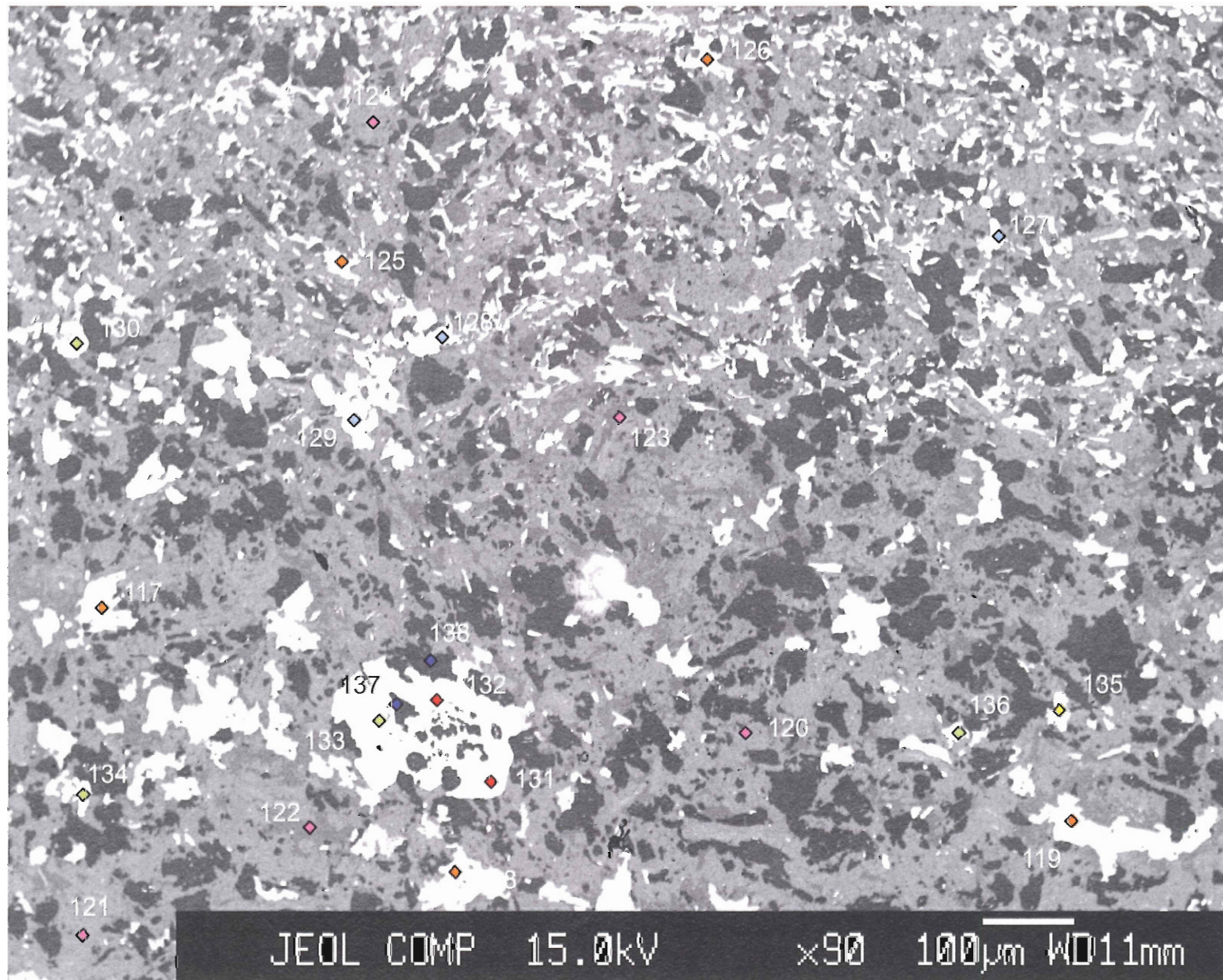
## PPP-5c area 1



## PPP-5c area 2



## PPP-5c area 2



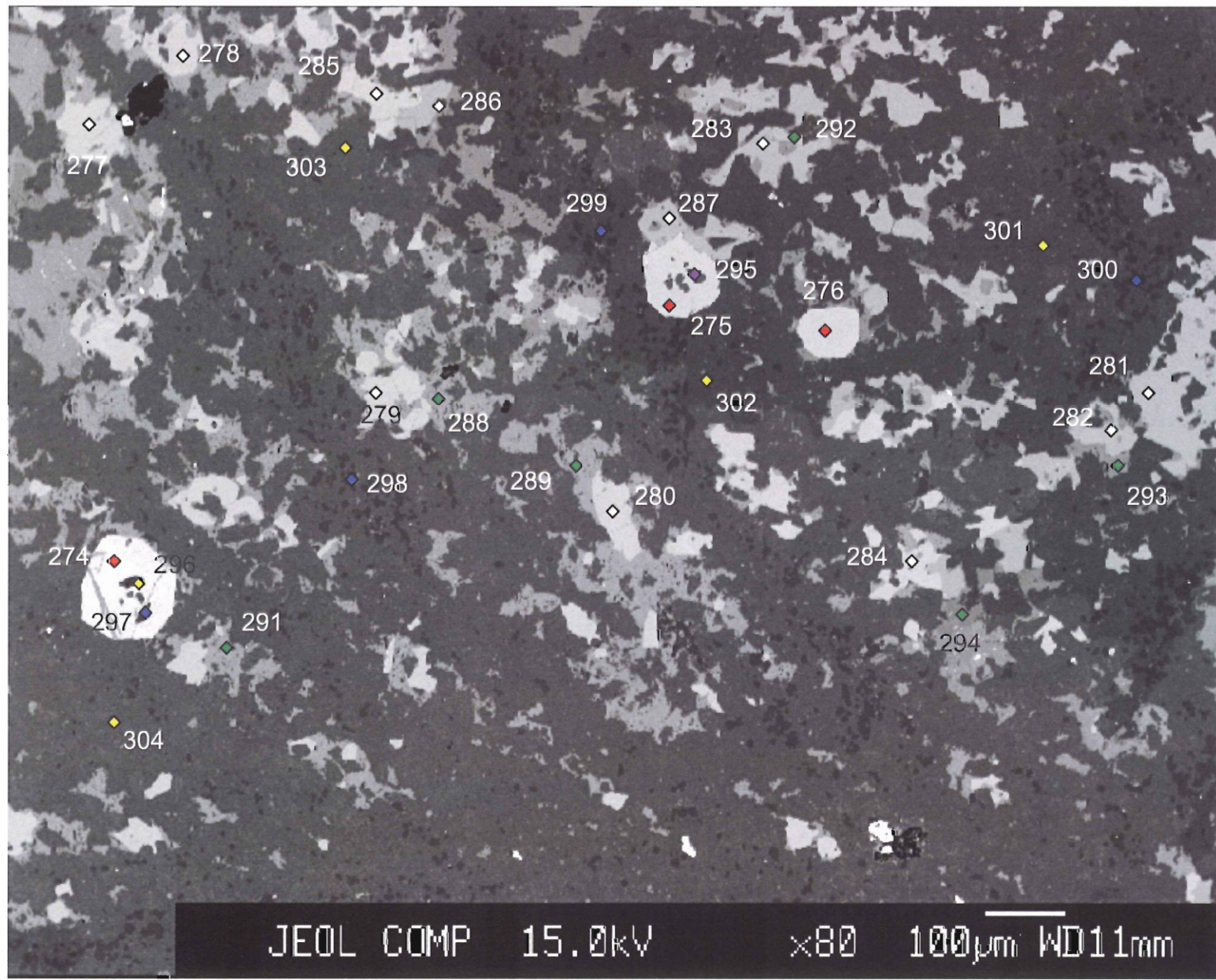
**Mineral key**

- Garnet
- Biotite
- Ilmenite
- Fe-sulph
- Allanite ?
- Quartz
- Plagioclase

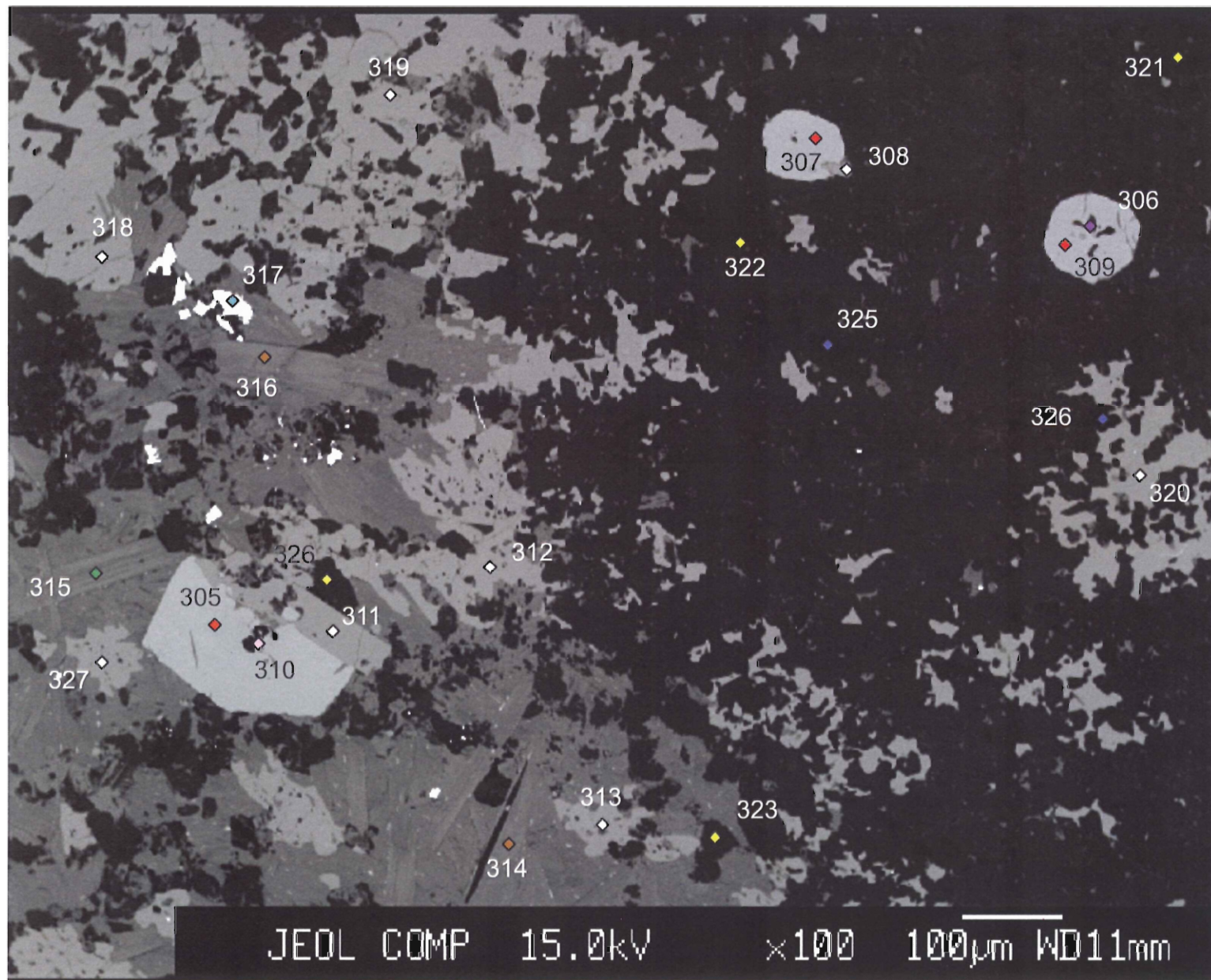
An<sub><90</sub>

An<sub>>90</sub>

## PCR-26b area 1



## PCR-26b area 2



Mineral key	
◊	Apatite
◆	Chlorite
♦	Biotite
◊	Muscovite
◊	Fe-sulphide
◊	Quartz
Plagioclase	
◊	An <sub>&lt;90</sub>
◊	An <sub>&gt;90</sub>
◊	K-feldspar
◊	Garnet

JEOL COMP

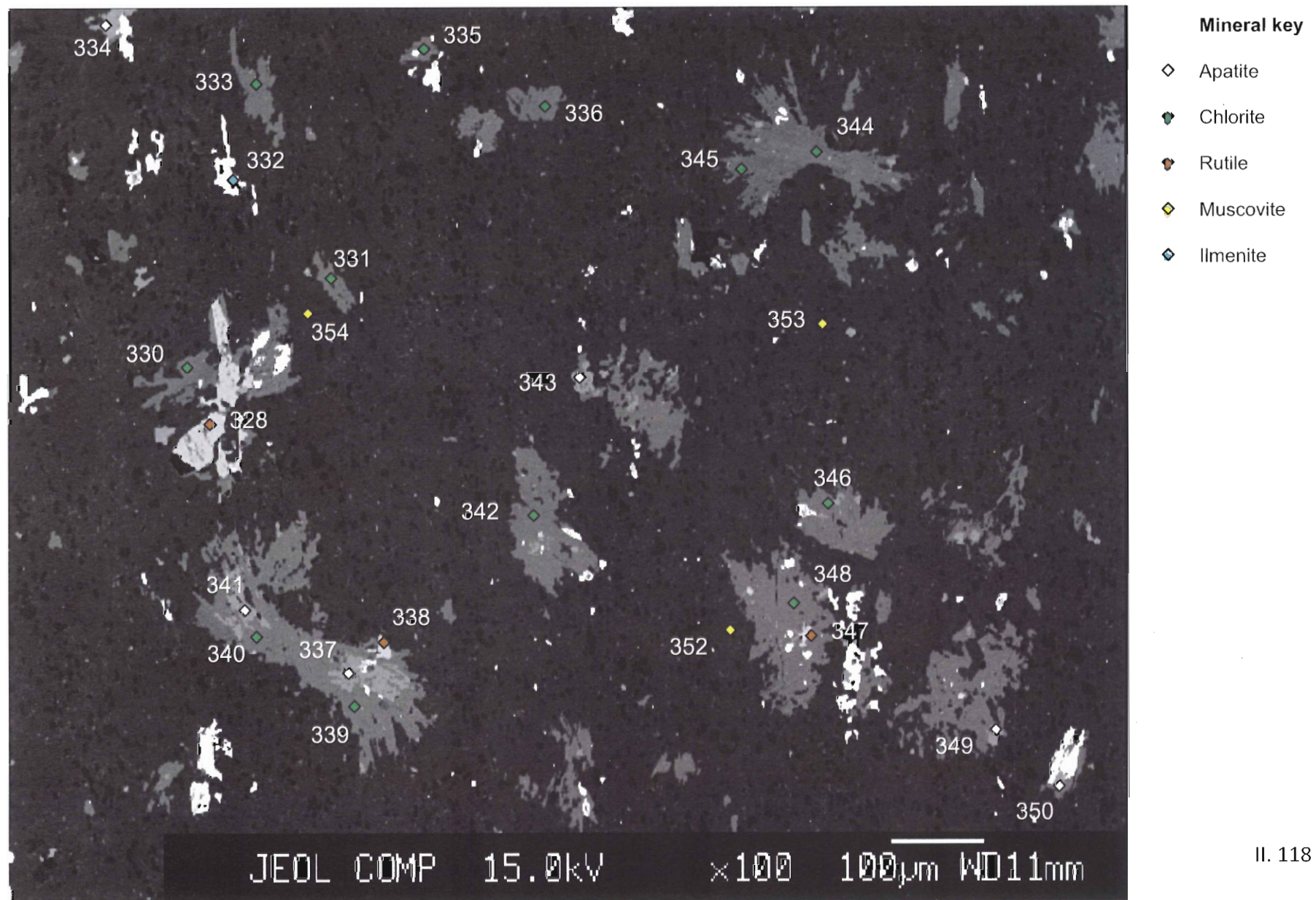
15.0kV

×100

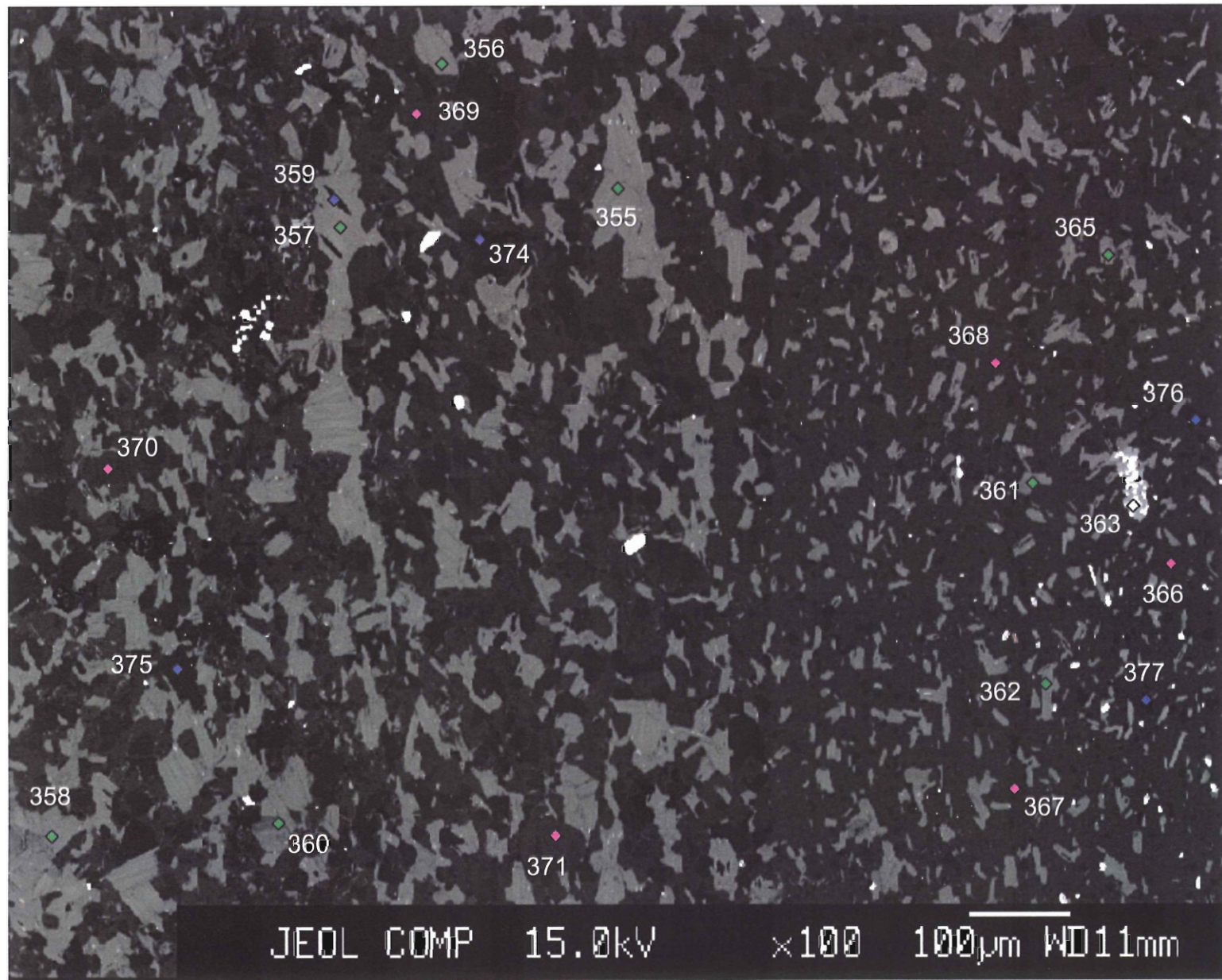
100µm WD11mm

II. 117

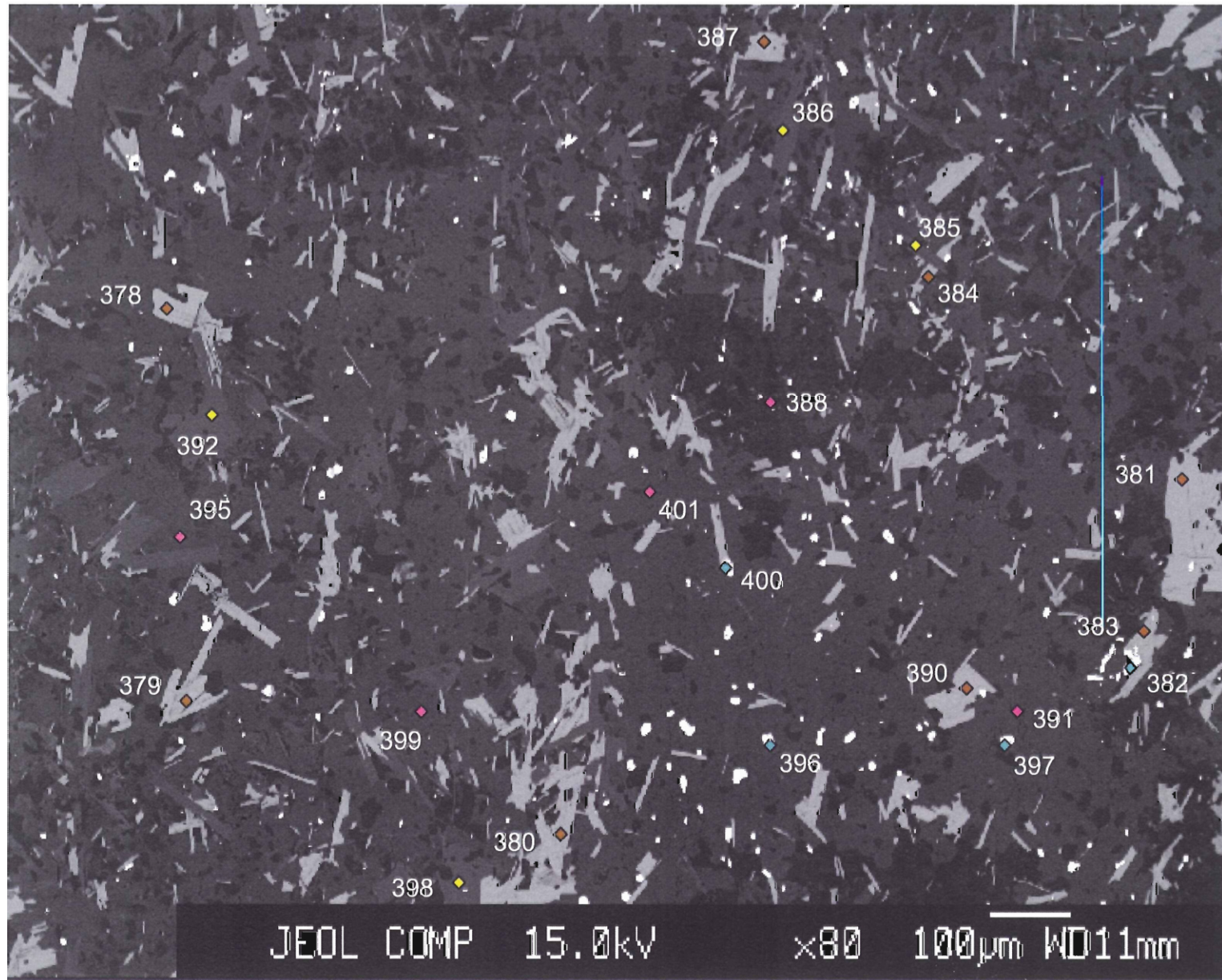
## PCR-26b area 3



## PCR-26b area 4

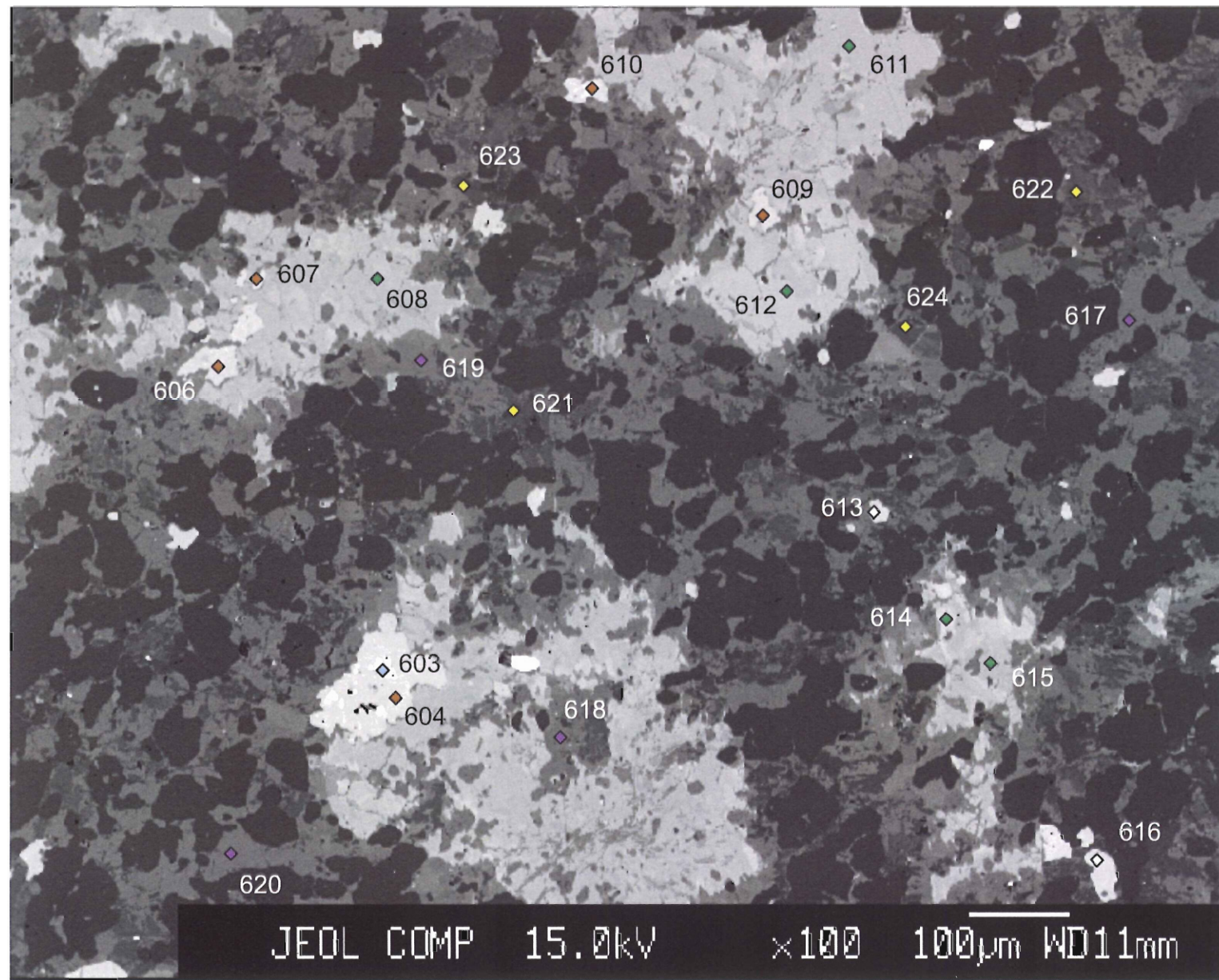


## PCR-26b area 5



II. 120

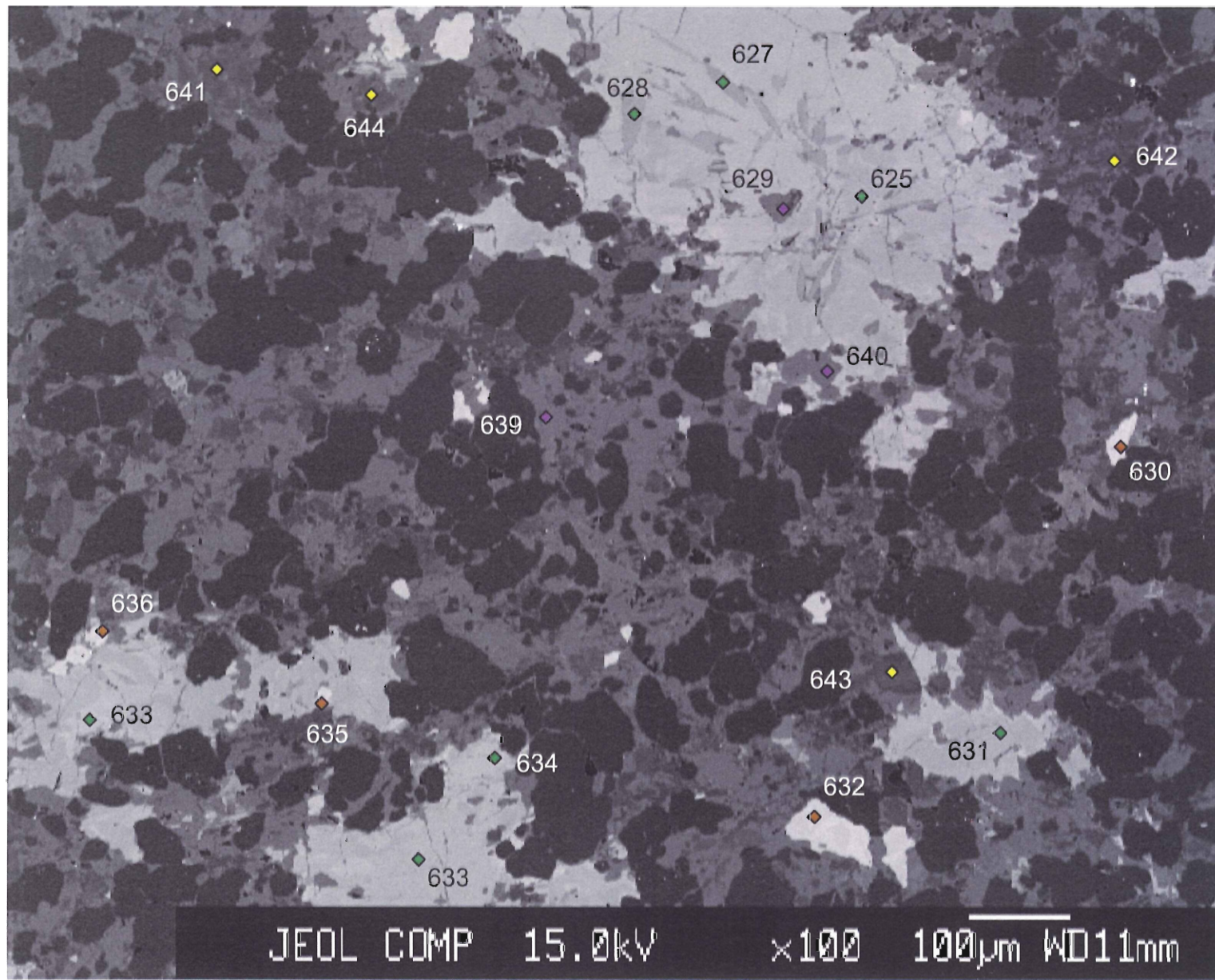
## PCR-23a area 1



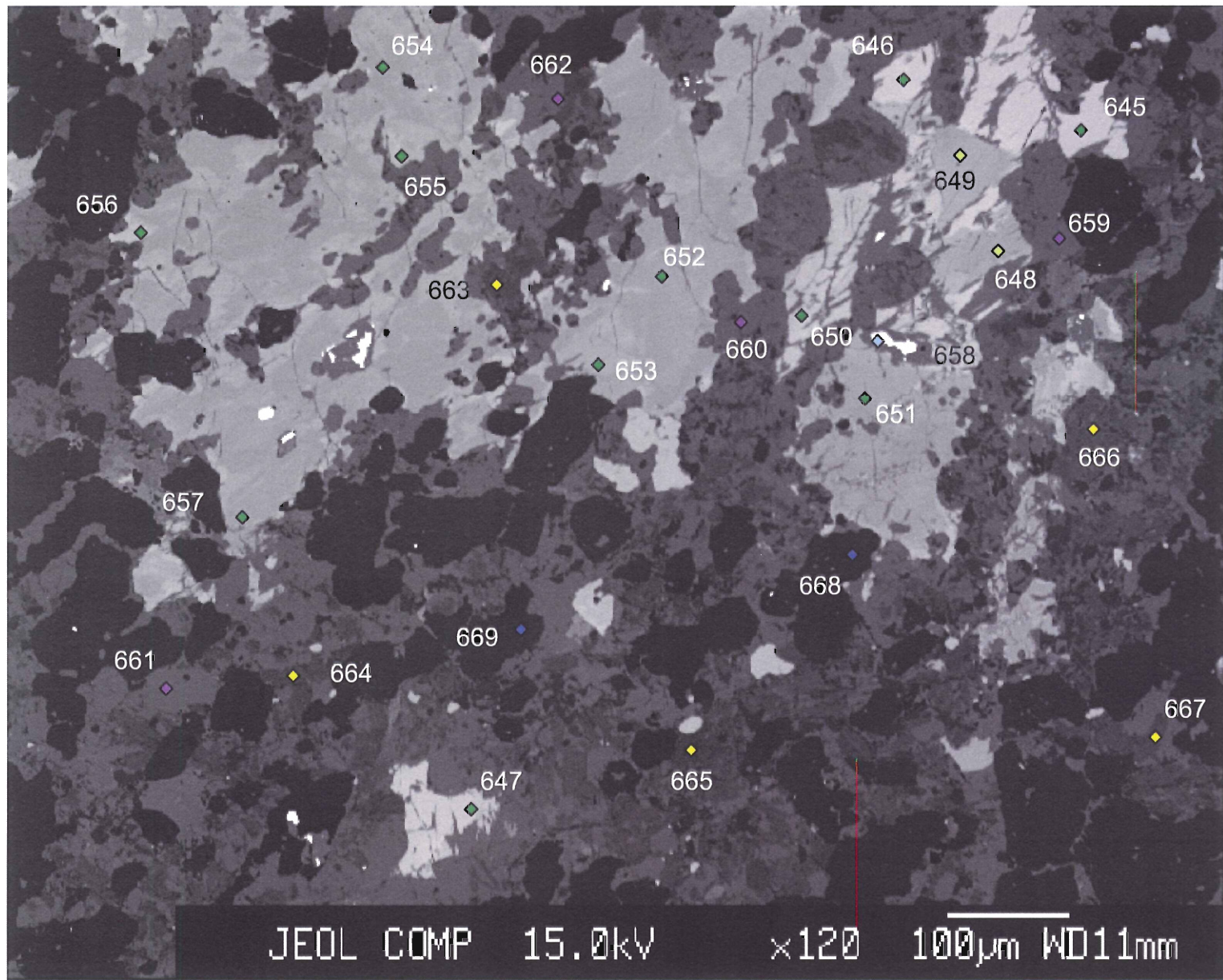
**Mineral key**

- ◊ Apatite
- ◆ Clinopyroxene
- ◆ Titanite
- ◆ Muscovite
- ◆ Ilmenite
- Plagioclase
  - ◆ An<sub><90</sub>
  - ◆ An<sub>>90</sub>

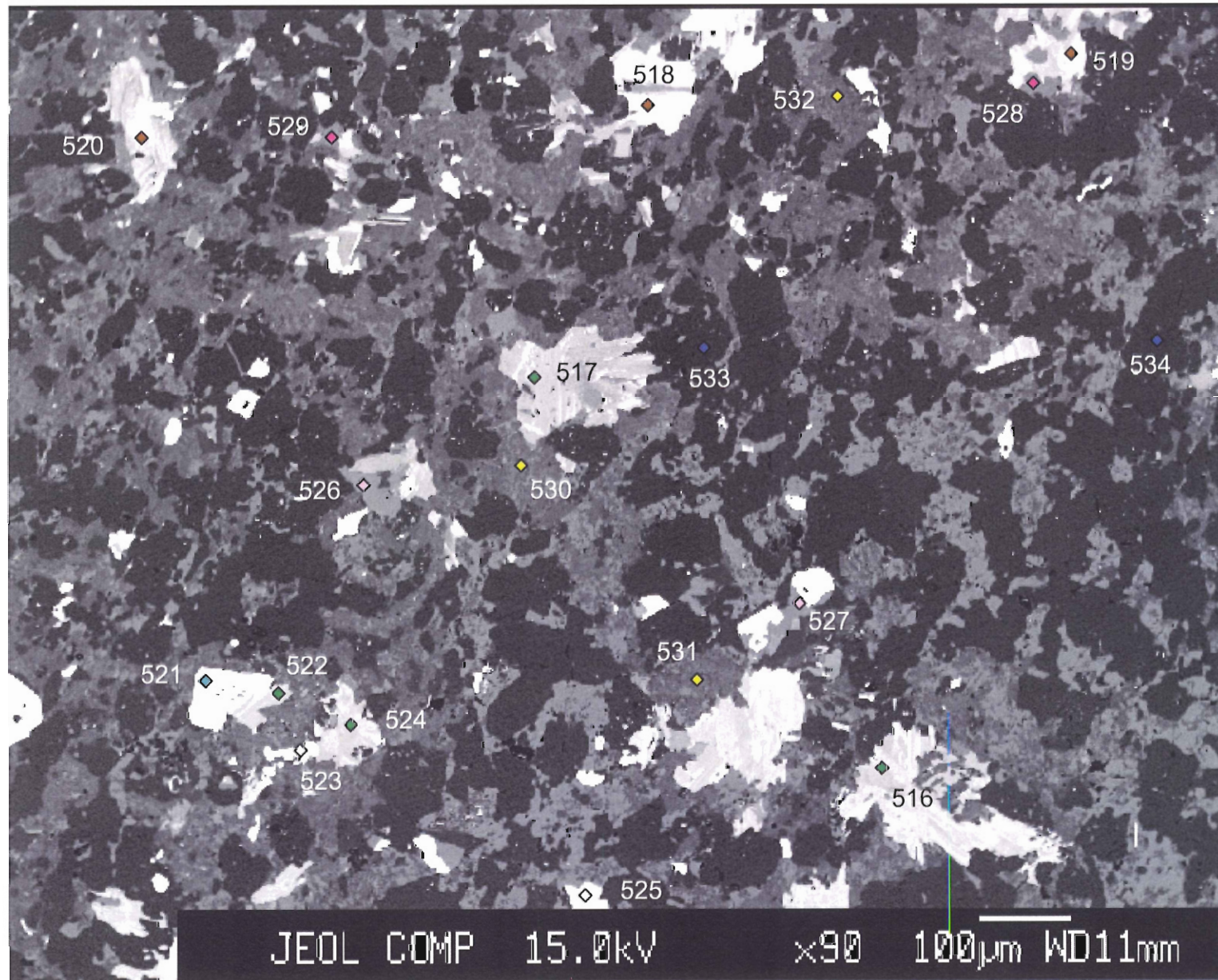
## PCR-23a area 2



## PCR-23a area 2

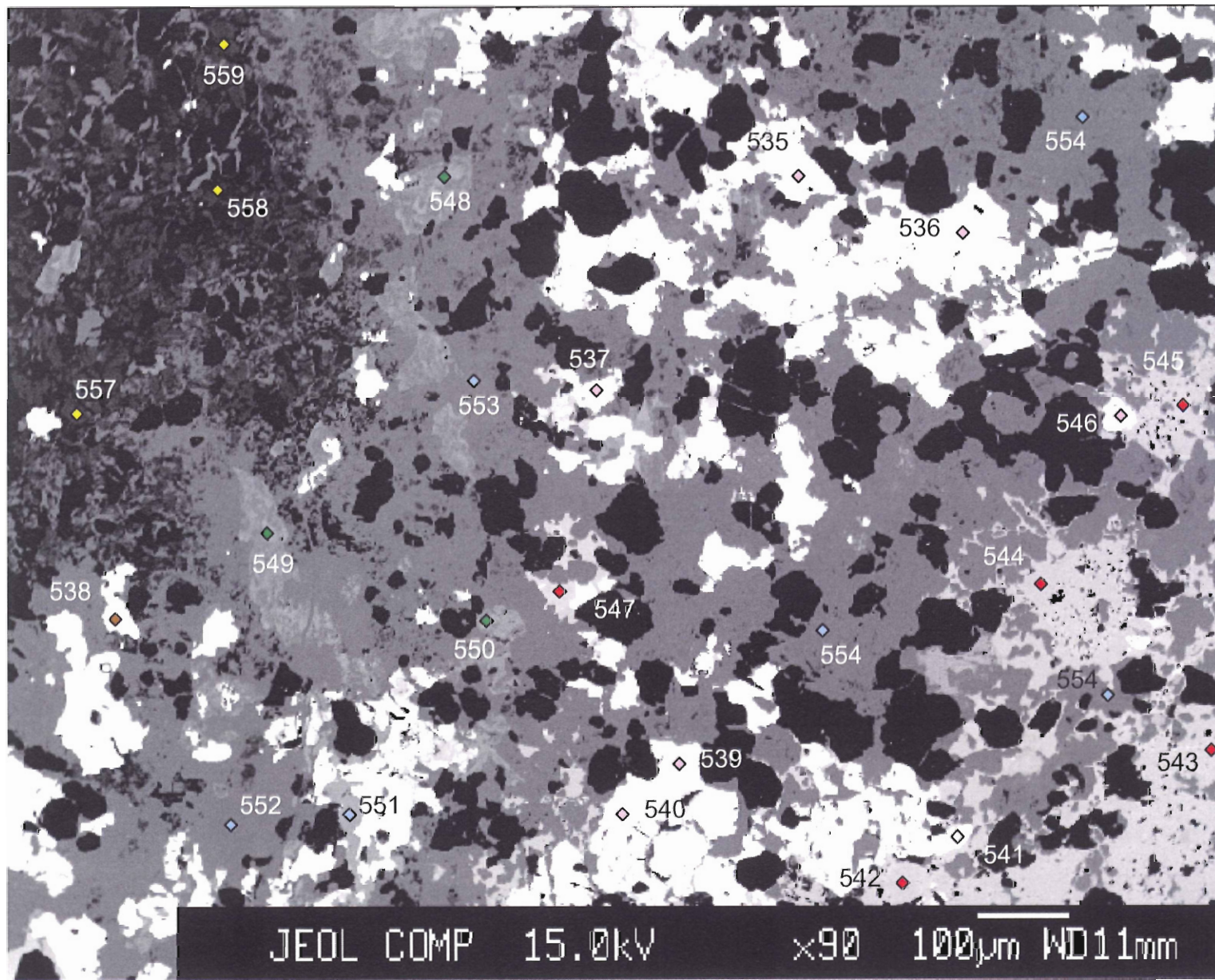


## PCR-11b area 1



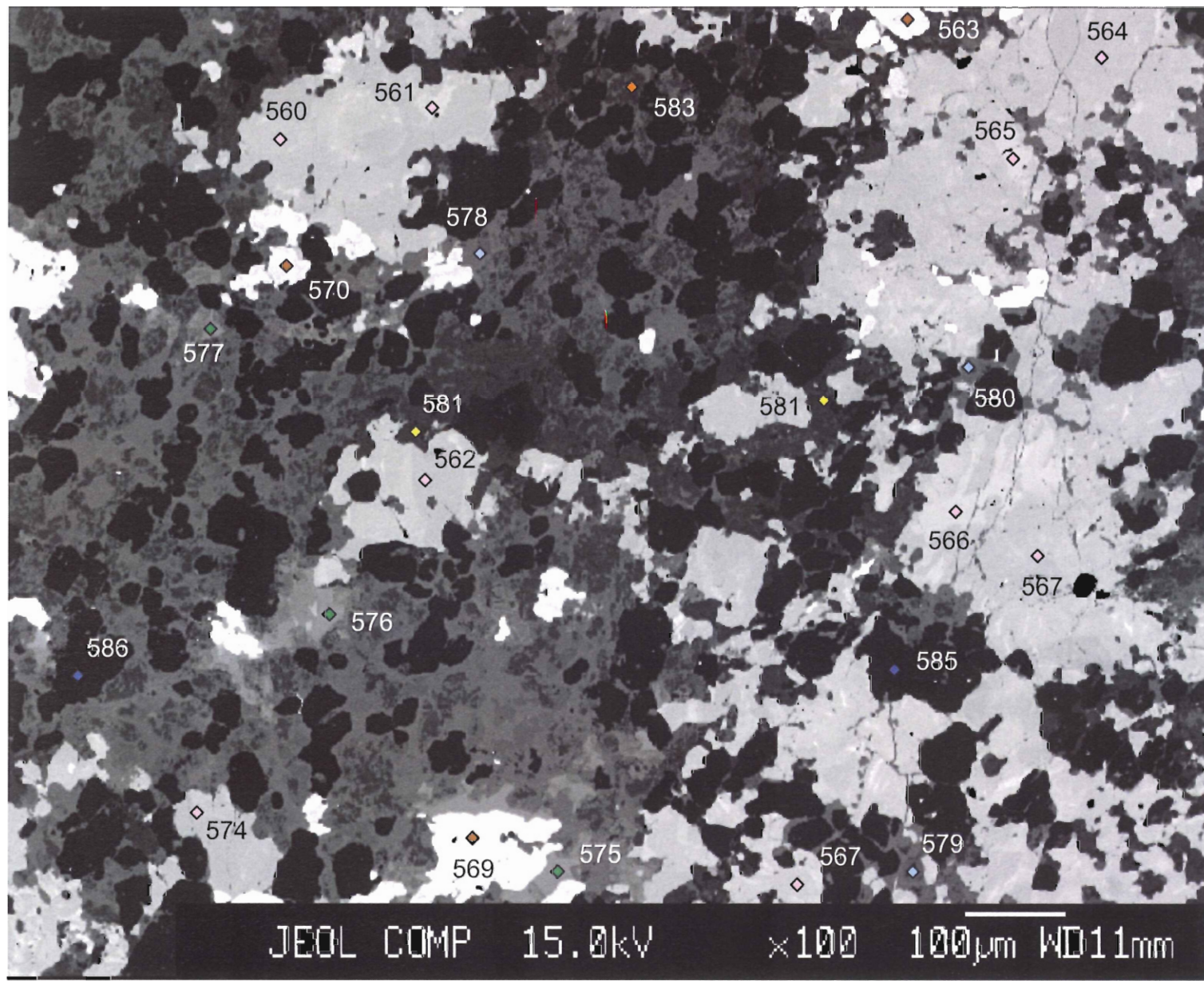
Mineral key	
◊	Apatite
◆	Chlorite
◆	Biotite
◆	Muscovite
◆	Fe-sulphide
◆	Quartz
Plagioclase	
◆	$\text{An}_{<90}$
◆	$\text{An}_{>90}$
◊	K-feldspar

## PCR-11b area 2



II. 125

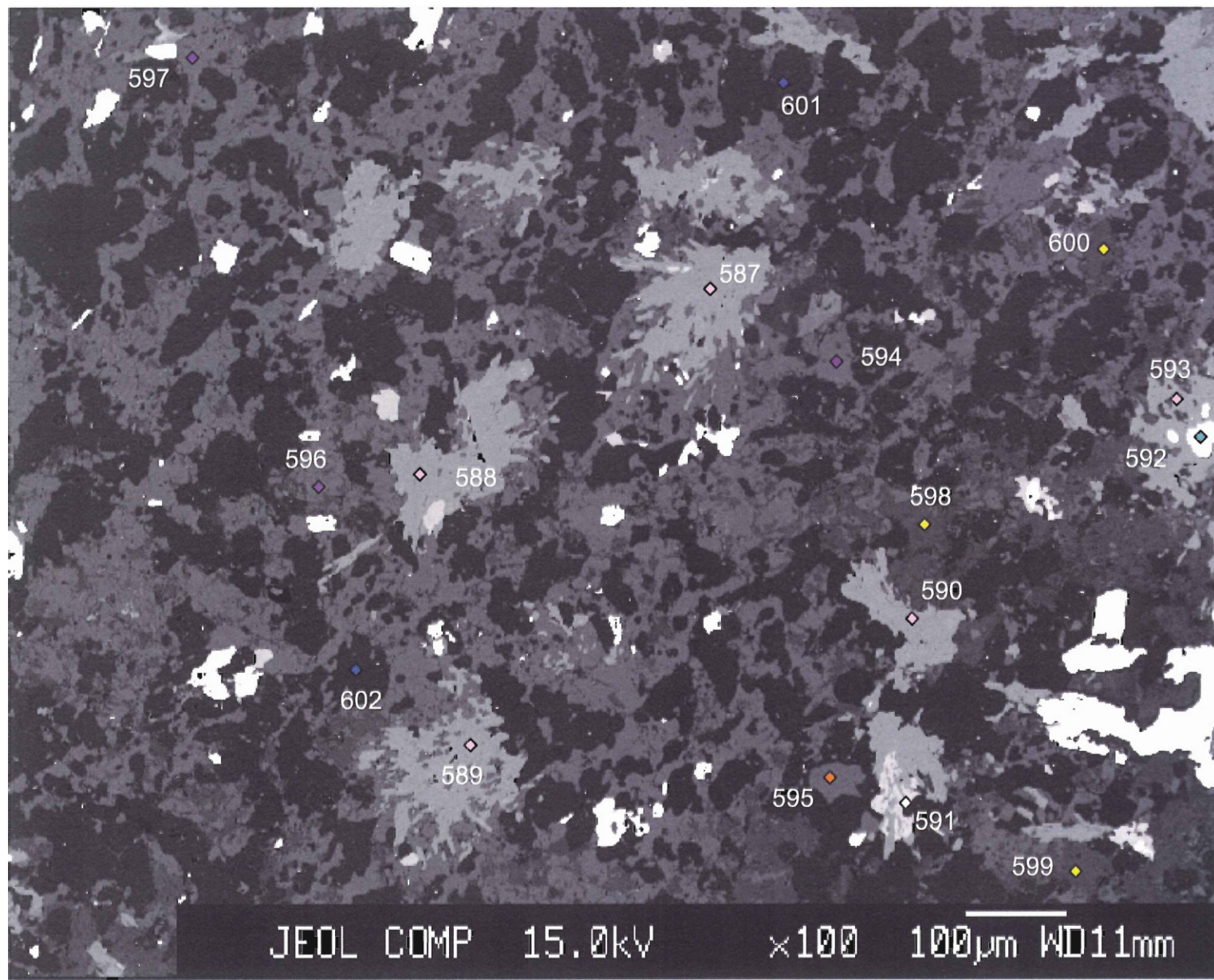
## PCR-11b area 3



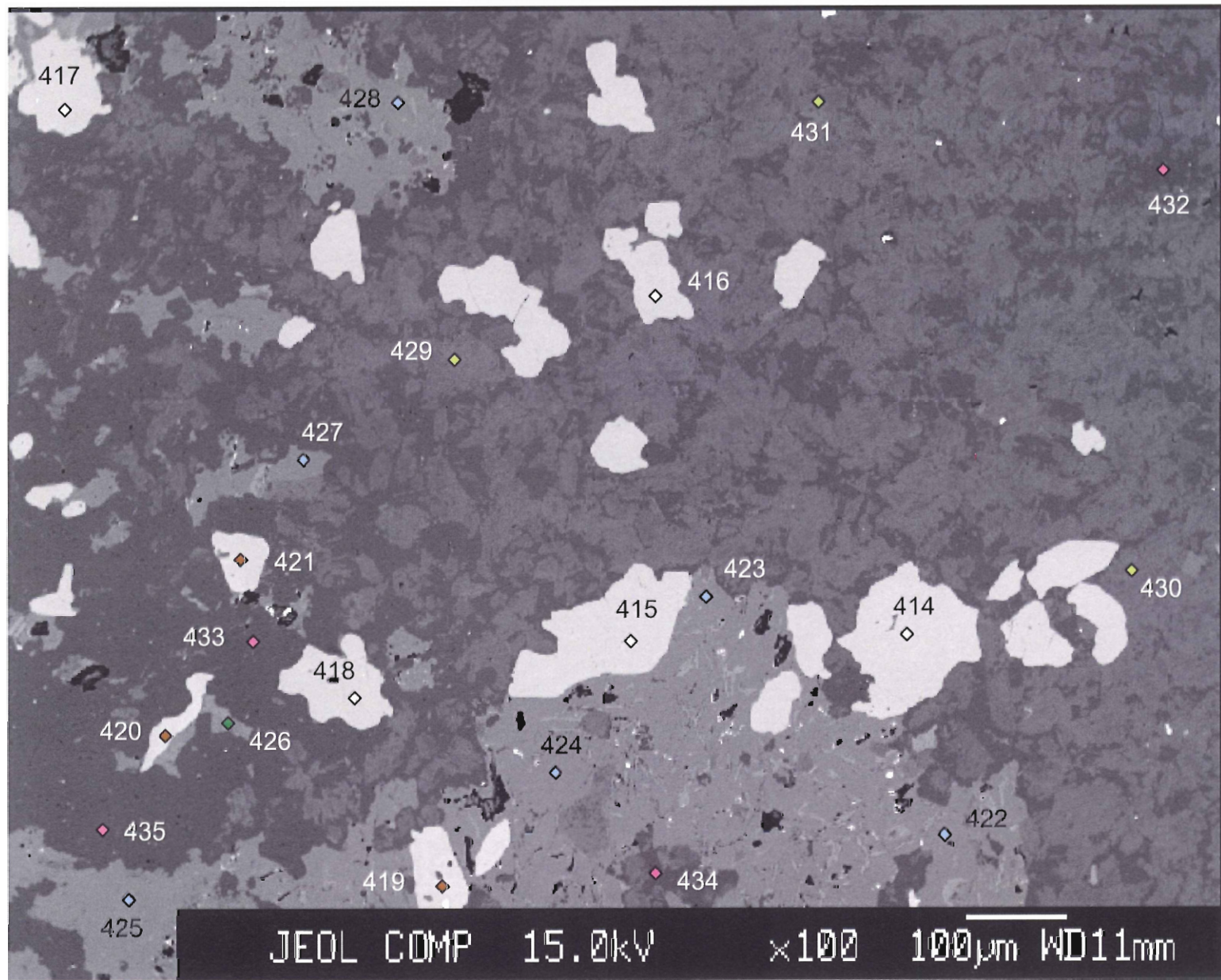
II. 126

JEOL COMP 15.0kV ×100 100µm WD11mm

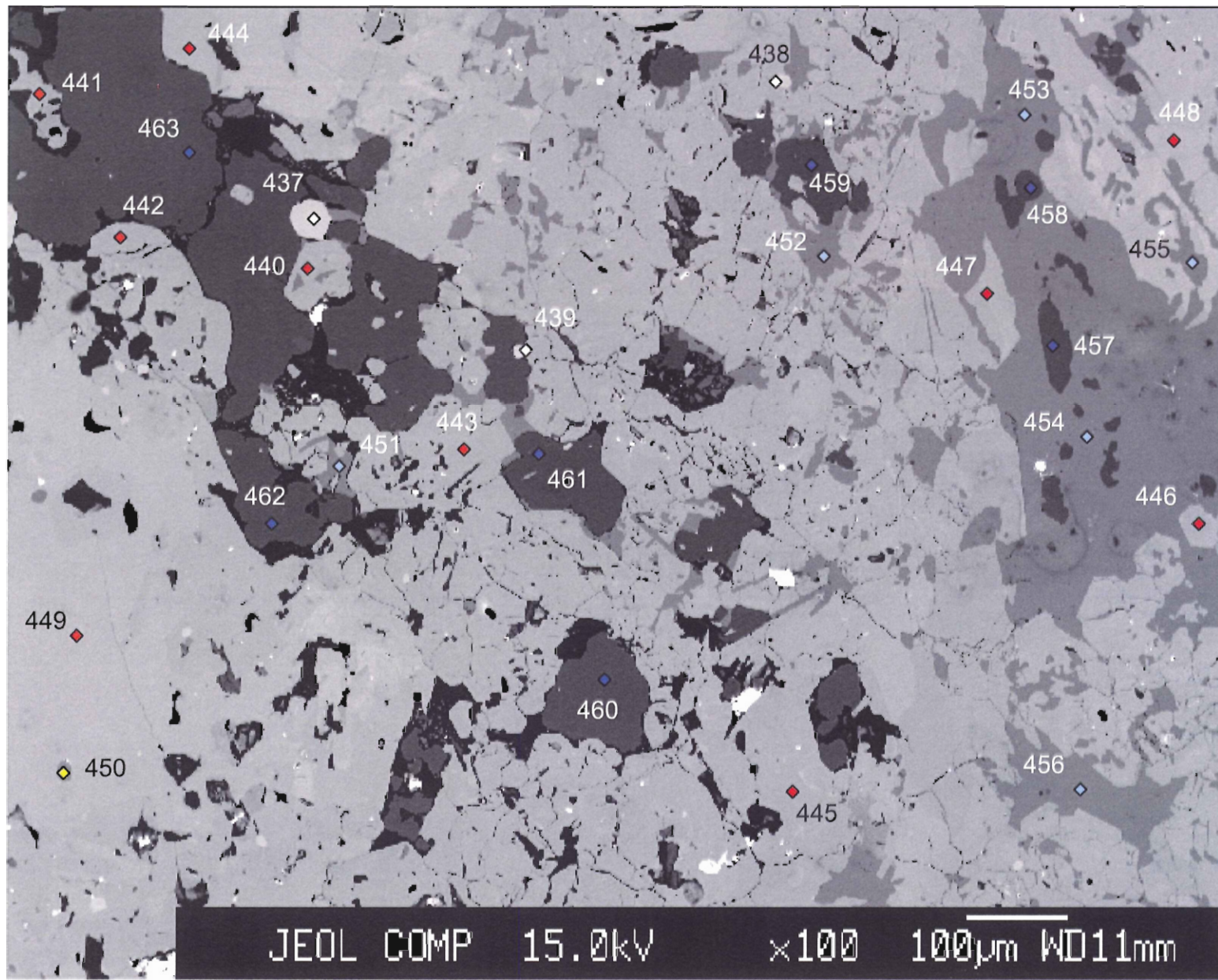
## PCR-11b area 4



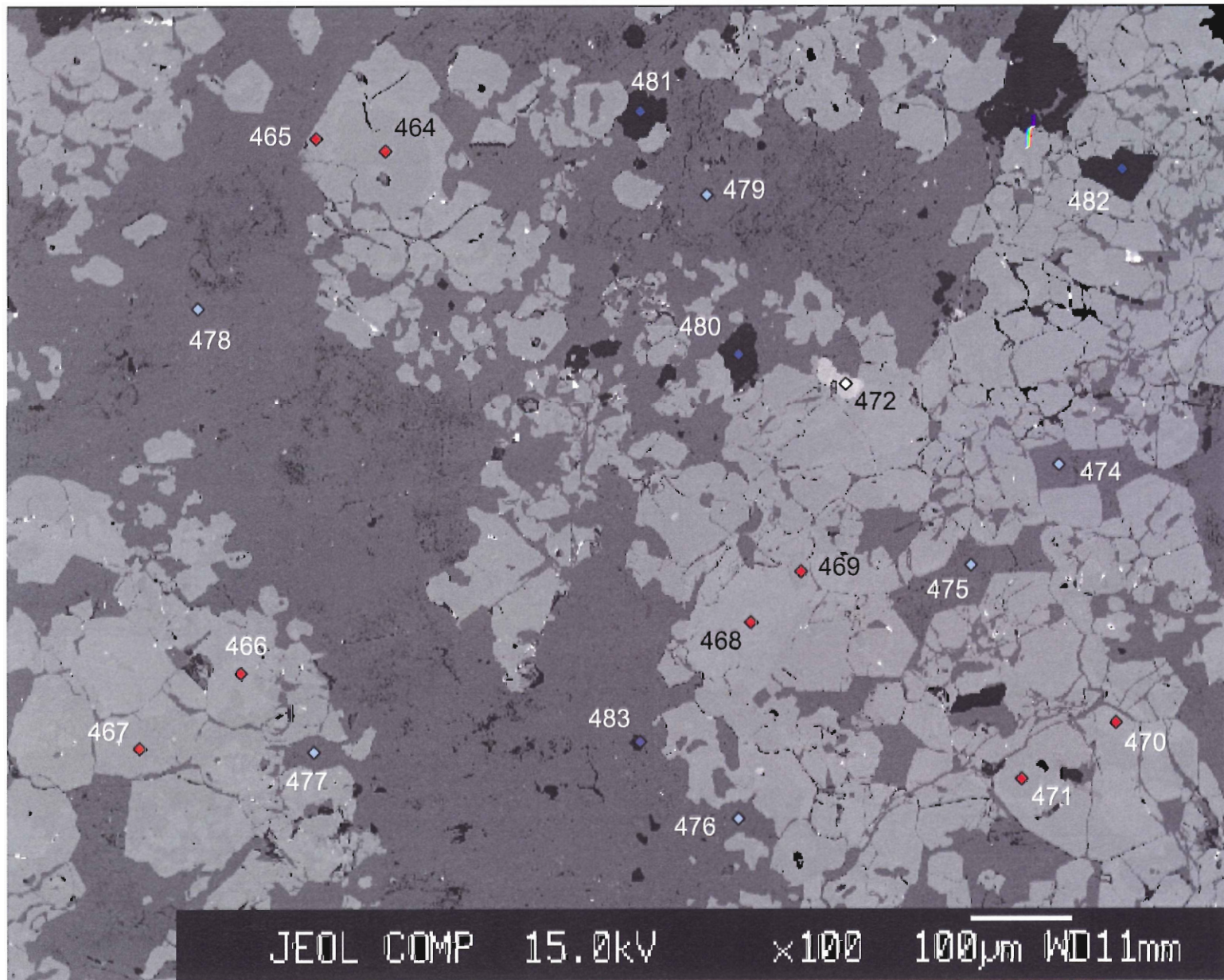
WL-16b-2



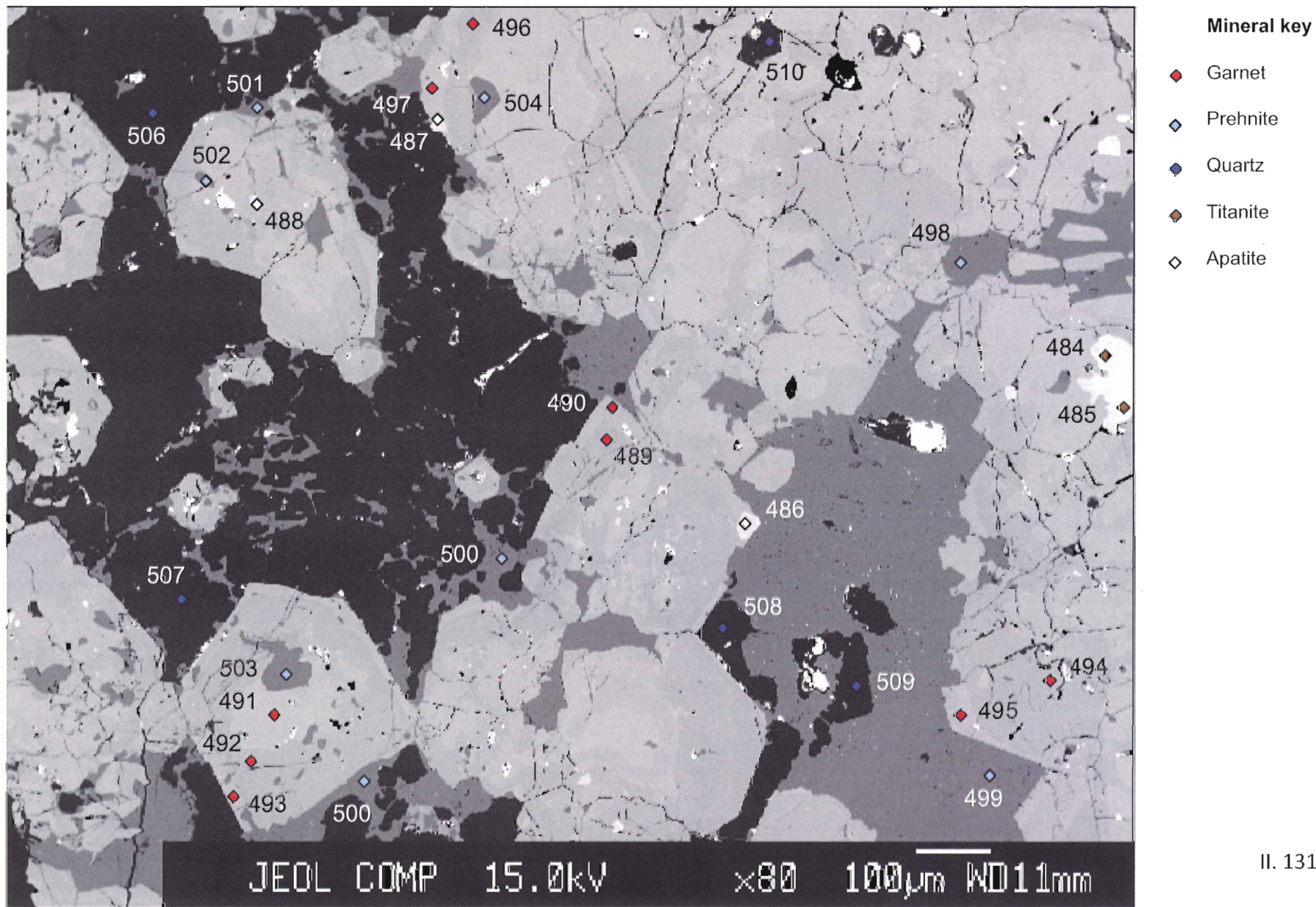
WL-16b-3



WL-16b-4



WL-16b-5



---

#### Appendix IV

Sample	Easting	Northing
PPP-30	455307	4941333
PPP-7c	455343	4940942
PPP-5c	455231	4940951
PCR- 26b	454523	4940469
PCR-23	454346	4940423
PCR-11b	454718	4941099
WL-16b	451682	4941183
WL-18b	451609	4941203

Table C.1

UTM coordinates of outcrops with concretions or horizons sampled for this study

## Appendix IV

## Raw XRF data

Date	Field 1	Field 2	P	S	Cl	K	Ca	Ti	V	Cr
03/14/11										
03/14/11	D12-W11-229-s1		ND	3923	275	14401	230	4489	77	98
03/14/11	D12-W11-229-s12		288	2603	412	16950	184	5329	93	109
03/14/11	D12-W11-229-sst1		ND	17900	593	19311	ND	4515	74	53
03/14/11	D12-W11-229-sst2		ND	12629	342	21059	ND	4426	85	57
03/14/11	D12-W11-229-sst3							4284	326	60
03/14/11	D12-W11-229-sst3							4383	287	61
03/14/11	D12-W11-229-sst3		ND	6292	851	16667	ND	4722	88	96
03/14/11	PCR07-18-1	dark band	4	1325	1486	20771	74714	4155	157	117
03/14/11	PCR07-18-2	v. dark band	3984	1209	2065	39190	105826	4775	277	107
03/14/11	PCR07-18-3	outer core	158	1603	2815	14878	193427	3691	146	100
03/14/11	PCR07-18-4	inner core	1172	1112	2701	7871	226037	3186	86	108
03/14/11	PCR07-18-5	outer core 2	1003	1525	2669	8758	242952	3523	100	84
03/14/11	PCR07-18-6	dk band	ND	10552	1512	16769	68322	3775	142	97
03/14/11	PCR07-18-7	pelitic	478	590	1757	20197	19280	3609	90	65
03/14/11	PCR07-26B-1	pelitic	ND	1068	1324	35248	4723	4991	106	75
03/14/11	PCR07-26B-2	pelitic smaller	ND	712	1862	39693	6873	4939	103	83
03/14/11	PCR07-26B-3	pink layer	ND	1584	2288	29428	8177	4297	86	86
03/14/11	PCR07-26B-4	dark layer	2790	3471	1806	36927	20202	6252	118	117
03/14/11	PCR07-26B-5	bt band	1333	19414	2280	51327	7826	5313	307	86
03/14/11	PCR07-26B-6	bt band	4635	12409	1975	54395	8079	2241	134	66
03/14/11	PCR07-07-11- calc- core		613	1455	1057	11853	130059	2648	53	64
03/14/11										
03/14/11	PCR07-07-11- calc- rim 1		ND	1118	382	22998	89220	3968	75	59
03/14/11	PCR07-07-11- calc- rim 2		6169	5906	327	8616	86599	2217	43	47
03/14/11	PCR07-07-11- pelite		1331	6232	1651	18271	27900	4798	127	92
03/14/11	PPP-7C-1	calc core	1549	1845	3293	988	111876	3361	78	132
03/14/11	PPP-7C-2	calc outer	ND	1715	1570	2773	118763	2389	27	51
03/14/11	PPP-7C-3	elite	1081	11608	1963	16354	34658	6901	100	122
03/14/11	PPP-07-28-1	pelitic layer	ND	371	1106	41566	1130	5144	121	92
03/14/11	PPP-07-28-2	grey silt	1760	4841	991	27474	962	4783	77	51
03/14/11	PPP-07-28-3	grey silt	600	1155	1342	36776	2782	4604	101	76
03/14/11	WL07-20B-1	calc-1	ND	957	2414	14964	92969	2270	58	65
03/14/11	WL07-20B-2	calc-2	2851	2230	2302	21689	97326	3184	57	41
03/14/11	WL07-20B-3	calc-3	2243	537	1517	18294	75780	3417	81	87

## Appendix IV

## Raw XRF data

Date	Field 1	Field 2	P	S	Cl	K	Ca	Ti	V	Cr
03/14/11										
03/14/11	D12-W11-229-s1		ND	3923	275	14401	230	4489	77	98
03/14/11	D12-W11-229-s12		288	2603	412	16950	184	5329	93	109
03/14/11	D12-W11-229-sst1		ND	17900	593	19311	ND	4515	74	53
03/14/11	D12-W11-229-sst2		ND	12629	342	21059	ND	4426	85	57
03/14/11	D12-W11-229-sst3							4284	326	60
03/14/11	D12-W11-229-sst3							4383	287	61
03/14/11	D12-W11-229-sst3		ND	6292	851	16667	ND	4722	88	96
03/14/11	PCR07-18-1	dark band	4	1325	1486	20771	74714	4155	157	117
03/14/11	PCR07-18-2	v. dark band	3984	1209	2065	39190	105826	4775	277	107
03/14/11	PCR07-18-3	outer core	158	1603	2815	14878	193427	3691	146	100
03/14/11	PCR07-18-4	inner core	1172	1112	2701	7871	226037	3186	86	108
03/14/11	PCR07-18-5	outer core 2	1003	1525	2669	8758	242952	3523	100	84
03/14/11	PCR07-18-6	dk band	ND	10552	1512	16769	68322	3775	142	97
03/14/11	PCR07-18-7	pelitic	478	590	1757	20197	19280	3609	90	65
03/14/11	PCR07-26B-1	pelitic	ND	1068	1324	35248	4723	4991	106	75
03/14/11	PCR07-26B-2	pelitic smaller	ND	712	1862	39693	6873	4939	103	83
03/14/11	PCR07-26B-3	pink layer	ND	1584	2288	29428	8177	4297	86	86
03/14/11	PCR07-26B-4	dark layer	2790	3471	1806	36927	20202	6252	118	117
03/14/11	PCR07-26B-5	bt band	1333	19414	2280	51327	7826	5313	307	86
03/14/11	PCR07-26B-6	bt band	4635	12409	1975	54395	8079	2241	134	66
03/14/11	PCR07-07-11- calc- core		613	1455	1057	11853	130059	2648	53	64
03/14/11										
03/14/11	PCR07-07-11- calc- rim 1		ND	1118	382	22998	89220	3968	75	59
03/14/11	PCR07-07-11- calc- rim 2		6169	5906	327	8616	86599	2217	43	47
03/14/11	PCR07-07-11- pelite		1331	6232	1651	18271	27900	4798	127	92
03/14/11	PPP-7C-1	calc core	1549	1845	3293	988	111876	3361	78	132
03/14/11	PPP-7C-2	calc outer	ND	1715	1570	2773	118763	2389	27	51
03/14/11	PPP-7C-3	pelite	1081	11608	1963	16354	34658	6901	100	122
03/14/11	PPP-07-28-1	pelitic layer	ND	371	1106	41566	1130	5144	121	92
03/14/11	PPP-07-28-2	grey silt	1760	4841	991	27474	962	4783	77	51
03/14/11	PPP-07-28-3	grey silt	600	1155	1342	36776	2782	4604	101	76
03/14/11	WL07-20B-1	calc-1	ND	957	2414	14964	92969	2270	58	65
03/14/11	WL07-20B-2	calc-2	2851	2230	2302	21689	97326	3184	57	41
03/14/11	WL07-20B-3	calc-3	2243	537	1517	18294	75780	3417	81	87

Mn	Fe	Co	Ni	Cu	Zn	As	Se	Rb	Sr	Y
288	16568	7	ND	2	26	1	ND	73	195	32
297	17974	7	ND	8	27	2	ND	80	213	25
238	18940	6	ND	12	25	1	0	96	183	20
134	18947	6	ND	15	11	5	0	106	220	28
136	28305	11	ND	15	14	3	0	82	207	30
116	28350	11	ND	12	14	4	ND	82	207	28
157	28052	12	ND	15	10	2	0	83	203	30
3711	47046	9	ND	18	41	1	0	104	515	34
5415	51003	13	ND	7	76	5	1	174	552	53
8780	67567	15	ND	8	116	5	ND	62	441	56
9921	68587	15	ND	9	98	5	1	27	275	53
9003	61494	13	ND	10	95	8	1	37	291	46
2467	43722	14	ND	153	56	6	1	81	463	26
1180	49031	18	ND	12	59	3	1	187	320	9
815	39788	15	ND	18	39	8	0	145	268	35
831	53309	19	ND	14	84	6	1	188	264	28
1099	65724	26	ND	26	74	3	0	169	247	26
1265	46715	16	ND	44	39	3	ND	144	262	30
2515	58211	19	ND	550	6	5	1	144	344	55
689	52725	19	ND	66	13	8	1	199	157	47
3453	29025	8	ND	13	56	6	0	43	620	29
2765	17472	5	ND	15	19	5	0	95	521	49
1114	12309	4	7	20	10	7	1	26	560	47
1276	46562	19	ND	54	84	ND	1	129	347	46
13911	91752	13	ND	17	31	15	0	5	322	36
5616	39462	7	ND	13	111	5	1	13	371	28
1742	55275	21	ND	42	99	7	1	119	331	29
662	32298	12	ND	7	64	3	ND	185	115	37
468	31693	13	ND	23	65	6	ND	153	94	55
666	36273	13	ND	7	67	3	0	190	111	34
9150	67459	12	ND	3	97	8	0	72	166	21
10013	59397	10	ND	6	314	9	ND	98	210	21
7674	45687	9	ND	5	183	9	ND	91	211	30

Zr	Nb	Mo	Ag	Cd	Sn	Sb	Ba	La	Ce	Pr
81	14	8	ND	2	5	0	481	25	115	ND
101	16	14	ND	1	ND	ND	544	50	82	ND
419	16	8	6	ND	2	1	685	ND	21	ND
399	13	10	12	1	5	3	715	ND	42	ND
211	16	11	ND	0	5	ND	551	79	93	ND
214	15	12	7	ND	5	3	561	17	108	ND
213	15	11	2	0	9	ND	558	65	107	ND
108	15	ND	40	ND	12	ND	1852	85	112	ND
99	20	1	68	ND	20	1	2866	34	214	ND
88	21	3	25	ND	24	ND	1126	81	236	ND
90	19	ND	8	0	18	1	354	106	152	ND
93	19	1	17	4	22	ND	659	86	180	ND
167	14	ND	25	ND	17	ND	1416	35	146	ND
129	11	1	17	0	11	ND	926	90	67	ND
152	20	ND	13	ND	15	2	843	ND	118	ND
136	19	ND	20	ND	13	4	719	43	6	ND
124	19	1	15	ND	13	1	409	25	67	ND
117	24	ND	27	3	14	4	1229	83	70	ND
58	32	1	98	ND	23	ND	3585	48	91	ND
52	10	2	34	1	10	ND	1406	19	62	ND
157	19	ND	4	ND	18	2	73	46	97	ND
240	37	2	7	0	16	ND	332	36	142	ND
224	24	1	1	ND	14	ND	163	49	177	ND
239	17	ND	21	ND	13	1	1199	36	114	ND
88	24	1	ND	ND	17	6	ND	156	228	15
67	18	0	9	0	12	ND	66	44	ND	ND
275	20	ND	6	1	9	1	462	37	112	ND
121	22	0	22	3	11	ND	1075	37	76	ND
684	19	1	22	ND	10	ND	711	ND	52	ND
128	20	0	25	1	13	1	939	ND	ND	ND
229	15	ND	ND	0	42	5	278	75	140	ND
287	19	2	16	2	43	ND	538	86	129	ND
234	19	1	4	3	27	ND	377	78	233	ND

Nd	Sm	W	Hg	Pb	Bi	Th	U
142	12	2	3	1	2	46	4
84	17	0	3	2	7	68	4
ND	ND	ND	5	14	2	59	4
71	14	1	4	16	ND	35	4
77	19	ND	5	3	ND	63	4
326	1	0	5	2	ND	53	3
59	ND	6	3	2	1	75	4
568	ND	7	12	3	ND	82	ND
617	ND	23	14	ND	ND	66	ND
440	ND	90	32	ND	5	60	ND
20	ND	41	33	ND	11	86	ND
71	ND	25	35	ND	13	76	ND
268	5	8	11	15	ND	74	ND
383	16	12	5	3	ND	55	ND
156	ND	8	9	31	7	102	4
285	ND	4	9	31	4	72	3
105	ND	8	6	17	4	82	1
344	ND	15	8	10	5	90	1
766	ND	39	15	ND	12	85	ND
214	1	10	11	ND	2	45	ND
85	ND	9	13	ND	ND	105	ND
26	8	10	13	ND	ND	140	ND
ND	32	7	12	ND	ND	78	ND
287	ND	ND	12	16	4	89	ND
326	21	31	38	34	7	83	ND
ND	ND	14	18	90	ND	62	ND
108	ND	10	13	34	ND	123	1
273	ND	6	8	15	2	91	2
ND	ND	4	7	11	ND	168	6
303	0	9	6	9	3	72	2
19	ND	22	18	ND	10	70	2
241	ND	19	18	ND	11	44	ND
ND	13	25	14	ND	ND	132	3